Control strategies for genetic feedback loops

Lucie Chambon

UNIVERSITÉ CÔTE D'AZUR

ÉCOLE DOCTORALE
SCIENCES ET TECHNOLOGIES DE L'INFORMATION ET DE LA COMMUNICATION

THÈSE DE DOCTORAT

Stratégies de contrôle pour des boucles de rétroaction génétiques

Control strategies for genetic feedback loops

Lucie CHAMBON

Institut national de recherche en sciences et technologies du numérique (Inria) Équipe Projet BIOCORE

Présentée en vue de l'obtention du grade de docteur en Automatique, Traitement du Signal et des Images **d'**Université Côte d'Azur
Dirigée par: Jean-Luc Gouzé
Soutenue le: 10 septembre 2020

Devant le jury, composé de:
Sylvain Bénito, Cofondateur et Directeur Scientifique d'ExactCure
Franck Delaunay, Professeur, Université Côte d'Azur
Mario Di Bernardo, Professeur, University of Bristol
Roderick Edwards, Professeur, University of Victoria
Jacques-Alexandre Sepulchre, Maître de Conférence, Université Côte d'Azur

RÉGION SUD PROVENCE ALPES CÔTE D'AZUR
SIGNALIFE
Inria
AGENCE NATIONALE DE LA RECHERCHE ANR

Stratégies de contrôle pour des boucles de rétroaction génétiques

Control strategies for genetic feedback loops

Jury:

Président du jury

Franck Delaunay, Professeur, Université Côte d'Azur (France)

Rapporteurs

Mario Di Bernardo, Professeur, University of Bristol (Royaume-Uni)
Roderick Edwards, Professeur, University of Victoria (Canada)

Examinateurs

Sylvain Bénito, Cofondateur et Directeur Scientifique d'ExactCure (France)
Franck Delaunay, Professeur, Université Côte d'Azur (France)
Jean-Luc Gouzé, Directeur de recherche, Inria (France)
Jacques-Alexandre Sepulchre, Maître de Conférences, Université Côte d'Azur (France)

Résumé et mots clés

Les boucles de rétroaction positives et négatives sont les deux motifs principaux et essentiels de régulation génétique, respectivement responsables de la différenciation cellulaire ainsi que de l'homéostasie et des oscillations biologiques. Elles sont couramment modélisées par des systèmes d'équations différentielles ordinaires non-linéaires dont la dynamique reproduit fidèlement leurs comportements biologiques: la bistabilité pour la boucle positive, et la convergence globale vers une orbite périodique ou un unique point d'équilibre pour la boucle négative. Cette thèse propose plusieurs stratégies mathématiques pour contrôler ces deux motifs avec deux objectifs principaux: la stabilisation globale de points d'équilibre instables et la déstabilisation de points d'équilibre stables pour l'émergence d'oscillations soutenues. Ces deux objectifs semblent intéressants et prometteurs d'un point de vue biologique, notamment pour la mise en place de nouvelles thérapies: pour la boucle négative, ils pourraient permettre une compréhension plus aboutie de certaines maladies liées à la dérégulation de l'homéostasie ou d'horloges biologiques, tandis que pour la boucle positive, ces stratégies pourraient aider à concevoir des processus de dédifférenciation cellulaire. Pour répondre à ces attentes, les différentes lois de contrôle sont adaptées petit à petit afin de respecter plusieurs contraintes expérimentales, dont la nature qualitative et incertaine des données biologiques fournies par les appareils de mesures. Pour cela, plusieurs stratégies de contrôle sont présentées dans ce manuscrit: des contrôles linéaires, des contrôles saturés, des contrôles incertains constants par morceaux, ainsi que des modifications intrinsèques des réseaux. Par conséquent, les systèmes dynamiques étudiés sont non-linéaires et de grande dimension, et certains présentent même des discontinuités dans leur champ de vecteurs pouvant générer des comportements particuliers comme les modes glissants, et pour lesquels la théorie classique sur les systèmes dynamiques monotones et la théorie du contrôle ne s'appliquent pas. Pour cette raison, de nouvelles méthodologies qualitatives, se basant sur la construction de régions répulsives et invariantes, sont présentées et permettent d'établir des résultats de convergence globale et de stabilité au sens de Lyapunov. Ces résultats théoriques sont appuyés par quelques exemples biologiques, dont le Repressilator, le Toggle Switch, la boucle p53-Mdm2 et l'horloge circadienne.

Mots clés: systèmes non-linéaires, boucles de rétroaction, réseaux de régulation génétique, théorie du contrôle, contrôle qualitatif, mesures discrètes, équations différentielles ordinaires.

Abstract and keywords

Positive and negative genetic feedback loops are two main and essential gene regulatory motifs, respectively responsible for cell differentiation, and the emergence of both homeostasis and biological oscillations. They are accurately modeled by highly non-linear ordinary differential equations whose dynamics properly capture their biological behaviors: bistability for the positive loop, and global convergence towards either a periodic orbit or a unique steady state for the negative loop. This manuscript proposes different mathematical strategies for the control of both loops with two main objectives: the global stabilization of unstable steady states and the destabilization of stable steady states for the emergence of sustained oscillations. From a biological point of view, both objectives seem promising regarding disease treatments and conception of new therapies: for the negative loop, such a control objective may allow to better understand and cure diseases induced by a dyshomeostasis or a disrupted clock, while for the positive loop, these strategies may help in grasping and conceiving cell dedifferentiation processes. With these biological applications in mind, the control strategies have been successively improved in order to comply with biological implementations and to take into account more and more biological constraints, including qualitative and uncertain information provided by biological measurement techniques. To reflect this progression, different strategies are introduced in this manuscript: affine control laws, saturated control laws, qualitative and uncertain switched control laws, as well as intrinsic synthetic modifications of networks. This results in the analysis of non-linear and high-dimensional dynamical systems, as well as systems with discontinuous right-hand sides for which non-classical behaviors such as sliding modes may emerge, and classical theories on control and monotone dynamical systems do not apply. In order to prove global convergence and Lyapunov stability for these non-trivial systems, original, general, and qualitative methodologies based on the construction of successive repelling and invariant regions are developed. These results are supported and illustrated with a few biological examples such as the Toggle Switch, the Repressilator, the p53-Mdm2 loop or the circadian clock.

Keywords: non-linear systems, feedback loops, gene regulatory networks, control theory, qualitative control, discrete measurements, ordinary differential equations.

Acknowledgments

Je tiens tout d'abord à remercier mon directeur de thèse, Jean-Luc Gouzé. Son expérience et ses connaissances m'ont permis d'avancer sans m'éparpiller. Je le remercie d'avoir cru en moi et de la confiance qu'il m'a accordée pendant ces trois années. Je tiens ensuite à remercier Etienne Farcot et Jacques-Alexandre Sepulchre pour avoir suivi mon travail pendant trois ans et pour les précieux conseils qu'ils m'ont donnés. I would also like to thank Mario Di Bernardo and Roderick Edwards for accepting and taking the time to carefully read my manuscript. Je remercie aussi Franck Delaunay pour les discussions que nous avons eues, pour les conseils et les pistes qu'il m'a donnés en biologie, et aussi pour sa gentillesse. Un grand merci à Sylvain Bénito pour s'être intéressé à mon travail, ainsi qu'à Frédéric Dayan et toute l'équipe d'ExactCure pour m'accueillir et m'offrir la chance de travailler avec eux. Special thanks also to Stephen Coombes and the whole teaching staff members of the MMB MSc of the University of Nottingham, who inspired me and made me want to explore further this amazing field of mathematics and biology. Merci aussi à Valérie François, Martine Olivi et toute l'équipe de MASTIC qui m'ont permis de participer à des événements de médiations scientifiques. Je remercie Jean-Baptiste Caillau et Laetitia Giraldi pour leur aide et la confiance qu'ils m'ont accordée lors de mes enseignements à l'école Polytech Sophia. Plus généralement, je remercie Laetitia pour son soutien et son amitié lors de ces trois années. Un grand merci aussi à Marie-Line Meirinho dont je n'oublierai pas la gentillesse et la précieuse aide dans toutes mes démarches administratives. Merci Frédéric, Madalena, Valentina, Olivier et Suzanne pour m'avoir si bien accueillie dans l'équipe Biocore.

Je remercie et je n'oublierai jamais les amis rencontrés à l'Inria, qui ont apporté bonne humeur et rigolade pendant ces trois ans: Marjorie, Natacha, PO, Nicolas, David, Carlos, Elena, Lamberto, Agustín, Claudia, Ouassim, Ignacio, Clotilde, Walid, Yves, Israël, Sofia, Diego, Côme, Samuel, Christos, Konstantinos, Adam, Yacine, Clément, Sébastien, Marielle, Bruno, Nicolas, Jean-Baptiste, Luís, Victor, Léna, Luis, Sophie. Merci pour tous ces moments passés ensemble autour d'un café et d'un carreau de chocolat, d'une bière, ou d'un calcul. Je n'oublierai pas non plus Biocours et ses performances au marathon Nice-Cannes. Un merci spécial à Florence et Carine qui ont réussi à me rendre zen tous les mardis midi pendant trois ans. Un grand merci à Juliette aussi, et à ses belles photos souvenirs. Je remercie évidemment mes amis intemporels : Elow, Léa, Arthur, Gaëlle, Clara, Antoine, Malou, Alice, et surtout ma chère Pauline qui me nourrissait de frites dans les moments difficiles. Je remercie la famille Mourard, et tout particulièrement Denis qui m'a soutenue et m'a donné de bons conseils lors de l'écriture de mon manuscrit.

Une pensée particulière à mes parents Jacques et Marie Germaine, et à mon frère ThomThom qui m'ont supportée, soutenue et motivée depuis toujours. Maman, tes Stollen ont été d'une grande aide dans les moments les plus difficiles. Merci aussi à Mousse, qui m'a donné de bonnes histoires à raconter à la pause-café, et qui n'a pas arrêté de m'encourager à sa manière. Je finis bien sûr par Colin, qui a toujours cru en moi, surtout dans les périodes de doutes. Merci pour ton sourire, tes taquineries et tes grimaces qui m'ont accompagnée quotidiennement.

Funding

This work was supported by Région PACA, by the French Government (National Research Agency, ANR) through the "Investments for the Future" LABEX SIGNALIFE (program reference ANR-11-LABX-0028-01) and by ANR project Maximic (ANR-17-CE40-0024-01).

List of publications

1. L. Chambon, J. L. Gouzé. A new qualitative control strategy for the genetic Toggle Switch. *IFAC-PapersOnLine*, 52:532-537, 2019. Presented at the 12th IFAC conference on Dynamics and Control of Process Systems, including Biosystems (DYCOPS), Florianòpolis, April 23rd-26th, 2019. This article received the Young Author Award.

2. L. Chambon, J. L. Gouzé. Global stabilization of a genetic positive feedback loop via the design of a synthetic auto-repression. *IFAC-PapersOnLine*, 52:143-148, 2019. Presented at the 8th IFAC conference on Foundations of Systems Biology in Engineering (FOSBE), València, October 15th-18th, 2019.

3. L. Chambon, J. L. Gouzé. Global asymptotic stability of a genetic negative feedback loop with an affine control. Presented at the 58th IEEE conference on Decision and Control (CDC), Nice, December, 11th-13th, 2019.

4. L. Chambon, I. Belgacem, J. L. Gouzé. Qualitative control of undesired oscillations in a genetic negative feedback loop with uncertain measurements. *Automatica*, 112, 2020.

5. L. Chambon, J. L. Gouzé. Control strategies for sustained oscillations in a disrupted biological clock. Presented at the 21st IFAC World Congress, Berlin, July, 12th-17th, 2020.

The content of paper 3 can be found in chapter 4, papers 1 and 4 in chapters 6 and 7, paper 2 in Chapter 8 and paper 5 in chapter 9.

The content of chapters 6 and 7 has also been presented at the 11th European Conference on Mathematical and Theoretical Biology (ECMTB), Lisbon, July, 23rd-27th, 2018.

Contents

Résumé et mots clés **1**

Abstract and keywords **2**

Acknowledgments **3**

Fundings **4**

List of publications **5**

1 Motivations and organization of the manuscript **9**

2 Biological context **12**
2.1 Gene regulatory networks . . . 12
2.2 Genetic feedback loops . . . 14
2.3 Importance of understanding and controlling these loops . . . 15
2.4 Biological design and control tools . . . 17
2.5 Conclusion . . . 20

3 Mathematical modeling of genetic feedback loops **21**
3.1 The deterministic and ordinary differential equation framework . . . 21
3.2 Non-linear ordinary differential systems . . . 22
3.2.1 Modeling transcription and translation . . . 22
3.2.2 ODE model for genetic feedback loops in dimension N . . . 24
3.2.3 Steady states . . . 28
3.2.4 Local Stability . . . 29
3.2.5 Monotone dynamical systems . . . 31
3.2.6 Monotone cyclic feedback systems . . . 33
3.2.7 Numerical illustrations . . . 33
3.3 Piecewise affine differential systems . . . 33
3.4 Boolean systems . . . 37
3.5 Conclusion . . . 39

4 Classical control strategy **40**
4.1 Introduction . . . 40
4.2 The controlled model . . . 41
4.3 A new methodology for global results . . . 42
4.4 Schwarzian derivatives . . . 47
4.5 Conditions on α . . . 48
4.6 Numerical illustrations . . . 51
4.7 Conclusion . . . 53

5 Saturated control strategy **55**
5.1 Introduction . . . 55
5.2 The controlled model . . . 55
5.3 Global asymptotic stability . . . 56
5.4 Conclusion . . . 58

6 Piecewise constant control strategy **61**
6.1 Introduction . . . 61
6.2 The controlled model . . . 62
6.3 Global convergence . . . 63
6.3.1 Global convergence for the negative loop . . . 63
6.3.2 Global convergence for the positive loop . . . 66
6.4 Global stability . . . 70
6.4.1 Global stability for the negative loop . . . 71
6.4.2 Global stability for the positive loop . . . 74
6.5 The PWC control inside Hill functions: an illustration . . . 77
6.5.1 The controlled Toggle Switch model . . . 78
6.5.2 Global results . . . 79
6.6 A trade-off between speed of convergence and strength of inputs . . . 84
6.7 Conclusion . . . 88

7 Piecewise constant control strategy with uncertain measurements **90**
7.1 Introduction . . . 90
7.2 The controlled model . . . 90
7.3 Global convergence . . . 91
7.3.1 Global convergence for the negative loop . . . 91
7.3.2 Global convergence for the positive loop . . . 94
7.4 A synthetic example: the Repressilator . . . 100
7.5 A biological example: the p53-Mdm2 negative loop . . . 101
7.6 The PWC control with uncertainties inside Hill functions: an illustration . . . 104
7.6.1 The controlled Toggle Switch model . . . 104
7.6.2 Global results . . . 104
7.7 Conclusion . . . 106

8 Design of synthetic modifications **108**
8.1 Introduction . . . 108
8.2 The controlled model . . . 108
8.3 Global asymptotic stability . . . 110
8.4 Global convergence towards an undifferentiated region for the positive loop . . . 111
8.5 Conclusion . . . 116

9 A new problematic: the emergence of oscillations **118**
9.1 Introduction . . . 118
9.2 A biological motivation: the circadian clock . . . 118
9.2.1 A reduced circadian clock model . . . 119
9.3 A synthetic modification of the loop . . . 120
9.4 A PWC control strategy . . . 124
9.5 Application to the circadian clock . . . 125
9.6 Conclusion . . . 126

10 Conclusions and perspectives **128**

A Supplementary material of chapter 3 **136**
A.1 Schwarzian derivative . . . 136
A.2 Proof of proposition 3.2.8 . . . 136
A.3 Proof of proposition 3.2.9 . . . 137

B Supplementary material of chapter 4 **138**
B.1 Proof of proposition 4.3.2 . . . 138
B.2 Proof of proposition 4.3.3 . . . 139
B.3 Proof of proposition 4.3.4 . . . 140
B.4 Proof of proposition 4.3.7 . . . 141
B.5 Proof of proposition 4.3.8 . . . 143
B.6 Proof of proposition 4.4.1 . . . 145

C Supplementary material of chapter 6 **146**
C.1 Proof of proposition 6.4.1 . . . 146
C.2 Proof of lemma 6.4.1 . . . 147
C.3 Proof of proposition 6.4.3 . . . 148
C.4 Proof of lemma 6.4.3 . . . 149

D Supplementary material of chapter 8 **151**
D.1 Proof of lemma 8.3.1 . . . 151

E Supplementary material of chapter 9 **155**
E.1 Proof of lemma 9.3.1 . . . 155

Chapter 1

Motivations and organization of the manuscript

Despite the complexity of gene regulatory networks, two recurrent and small patterns have been identified as essential for several vital functions: the positive and negative genetic feedback loops. While the first motif is largely responsible for cell decision making and cell differentiation, the second is important for both homeostasis and biological clocks. These key roles also explain their implication in many diseases and disorders, such as dyshomeostasis or arrhythmic clocks for the negative loop, and abnormal cell proliferation for the positive loop. These realities provide evidence that a deep understanding and ways of controlling both motifs is promising for the improvement of insight into diseases and pharmacological treatments. In this context, this manuscript uses the theory of dynamical systems in order to design different biologically relevant strategies for controlling mathematical models of both a positive and a negative genetic feedback loop.

In order to provide a meaningful biological context to this mathematical work, chapter 2 presents the structure and the roles of genetic feedback loops, as well as precise motivations for their control. Moreover, this chapter introduces the concrete techniques and constraints that emerge from real biological experiments, that will be carefully considered in the mathematical framework throughout the whole manuscript.

The dynamical models for the canonical form of both the positive and negative feedback loop are introduced in chapter 3. These systems are shown to accurately reproduce the behaviors observed in biology. The bistability of the positive dynamical system with two stable and an unstable steady states appropriately imitate a cell differentiation process, while the unique steady state of the negative dynamical model replicates properly homeostasis in case of local stability, and biological clocks with the emergence of periodic orbits in case of local instability.

From chapters 4 to 8, this manuscript proposes different mathematical strategies for the global stabilization of the unstable steady state of both loops. From a biological point of view, this objective may allow to better understand and cure diseases induced by a dyshomeostasis in a disrupted negative loop that display undesired sustained oscillations, while for the positive loop, this goal may help in grasping and conceiving cell dedifferentiation processes. With these biological applications in mind, the control strategies are successively improved in the different chapters in order to comply with biological implementations and take into account more and more biological constraints.

A first naive classical affine control strategy is presented in chapter 4 and is shown to be able to stabilize the unstable steady state of both the negative and positive feedback loop in their canonical form. For biological purpose, this control is designed as simple as possible in order to reduce the use of devices and the complexity of the biological set-up. For this reason, the control law only

depends on the measurement of a unique gene and only acts on its own expression. Due to the complexity of this controlled dynamical system, a new methodology, based on the construction of successive hyperrectangles of the state space that act as Lyapunov function level-sets, is proposed in order to prove global convergence and global stability results. Despite its apparent simplicity, this affine control law is shown to globally stabilize the feedback loop system.

However, this affine control strategy usually well adapted for engineering control problems may be hard to implement in biology. Indeed, this control law may take either high positive or negative values, hard to interpret from a biological point of view, especially if the control inputs are doses of inducer molecules for example. This situation is avoided in chapter 5 by saturating the control law. With appropriate conditions on the up and bottom saturated values, the unstable steady state of both loops is shown to be globally asymptotically stable. Interestingly, this non-trivial problem is easily solved thanks to the methodology developed in chapter 4.

Both the classical control strategy developed in chapter 4 and the saturated control strategy presented in chapter 5 depend on precise knowledge of the system state. However, biological measurement techniques do not provide a precise and quantitative knowledge of the system. Instead, only partial and qualitative information are available. For this reason, in chapter 6 the control law is chosen piecewise constant and dependent on specific regions of the state space. Under appropriate conditions on the control inputs, global convergence towards the unstable steady state is achieved for both loops through successive repulsive regions of the state space and a final sliding mode. Moreover, the asymptotic stability property is shown, which guarantees robustness of the resulting system. These results are adapted for the control of the synthetic Toggle Switch.

This piecewise constant strategy is further improved in chapter 7, in which biological device inaccuracies are taken into account, leading to the hypothesis of uncertain measurements. In the mathematical framework, this hypothesis generates regions in which the control law is undefined. Under appropriate conditions on the control inputs, successive repelling regions of the state space are determined in order to prove the global convergence of the system towards an adjustable zone around the unstable steady state. These results are illustrated with the Toggle Switch, the synthetic Repressilator, and the p53-Mdm2 genetic feedback loop.

In order to simplify further biological experiments, chapter 8 shows that the synthetic design of a simple self-inhibition of one gene in both the positive and negative loop is able to globally stabilize the unstable steady state of the network. Compared to the different control strategies developed in the previous chapters, this synthetic modification of the circuit prevents the use of any input and measurement devices, reducing greatly the complexity of the biological set-up. Once again, the global results are proved thanks to the methodology developed in chapter 4, supporting the idea that this methodology is well adapted for many different control problems. Furthermore, in order to take into account inherent biological uncertainties for the positive feedback loop, the cell undifferentiated state is later considered as a region of the state space around the unstable steady state and is shown to be globally attractive with the same simple synthetic modification of the loop. Some conditions are given such that all the possible steady states of the circuit are confined in the undifferentiated region and the global results are proved with the theory of monotone dynamical systems.

Finally, the control strategies developed in this manuscript for the global stabilization of the unstable steady state of a negative feedback loop, are extended in chapter 9 for the reverse objective: generate sustained oscillations in a disrupted clock that shows arrhythmic behavior. In this chapter, the unique steady state of the canonical form of a genetic negative feedback loop is supposed to be stable, reproducing accurately the damped oscillations observed in a damaged oscillator. A simple synthetic modification of the network is proved to generate sustained oscillations and allow to recover a functional clock. The desired periodic trajectories are obtained by destabilizing the steady state $\bar{x}^-$ of the model and monotone properties are applied for global results. In a limit case, this modification of the loop is shown to be equivalent to an external piecewise constant control

law, supporting the conjecture that simple qualitative control strategies may be able to guarantee sustained oscillations. From the perspective of a biological implementation, this result is promising as these types of control are well adapted to experimental constraints. To support this theoretical work, the methods are applied to the disrupted circadian clock observed in human cancer cells.

Chapter 2

Biological context

2.1 Gene regulatory networks

A gene is a functional unit composed of bases of DNA (Deoxyribonucleic Acid) that encodes any type of information determining the phenotype of a living organism (see figure 2.1.1). This information is transmitted to the organism through a process called "gene expression", mainly composed of two steps: transcription and translation [6].

The transcription step describes the process by which the sequence of DNA composing a gene is copied into mRNA (messenger Ribonucleic Acid) by a specific enzyme called RNA polymerase that binds to the starting point of the DNA branch, called promoter, and slides along the gene up to a terminal point called the untranslated region, in order to scan and produce a copy of the information. The mRNA is then decoded by a macromolecule called Ribosome that synthesizes a long chain of amino acids forming a protein: this step is the translation (see figure 2.1.1). In a naive way, it will be considered that one gene codes for one protein through this gene expression machinery. In fact, the reality may be much more complex: a single gene often codes for different proteins depending on the splicing process during which some parts of mRNA are removed before translation. However, this

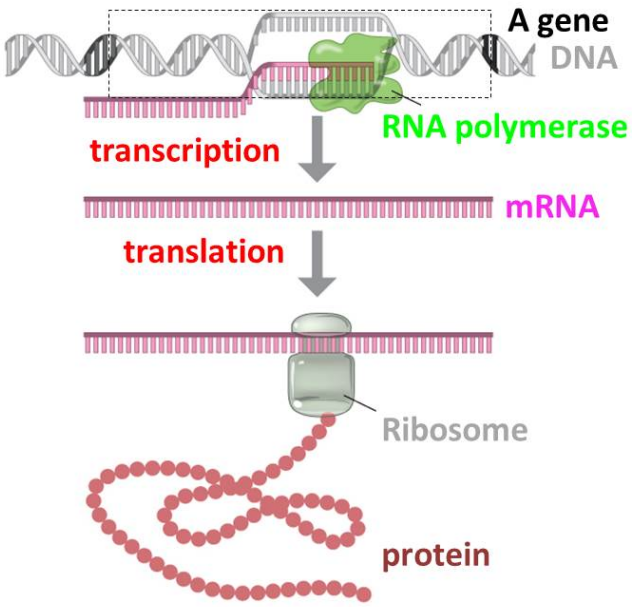

Figure 2.1.1: Illustration of gene expression (picture modified from [1]).

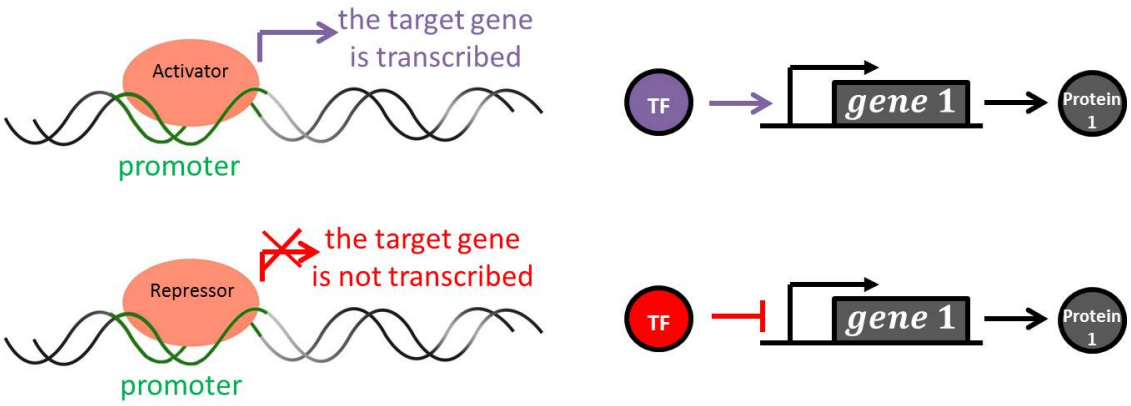

Figure 2.1.2: Left: illustration of the two types of transcription factors (TF), namely repressor and activator (picture modified from [2]). Right: corresponding schematic representations that will be used in the rest of the manuscript.

phenomenon goes far beyond the scope of this manuscript. More information about gene expression can be found in [6].

Proteins are essential for living organisms as they perform most cellular functions. These macromolecules are indeed involved in transport and storage (such as Hemoglobin that carries oxygen throughout the whole organism), in structures (such as Actin that forms microfilaments for cell shape), in body defense (such as Antibodies that bind and neutralize specific pathogens), in chemical reactions (such as enzymes that bind to substrates to convert them into different molecules of interest) and in communication (such as hormones that transmit signals between organs), to name but a few. This manuscript will focus on a specific group of proteins involved in gene expression regulation, called transcription factors (TF).

Transcription factors are proteins able to control the rate of transcription of a specific gene in order to ensure that it is expressed at the right place, at the right time and in the right amount within the organism. They are often divided in two groups: the activators that boost the transcription of one gene, and repressors that instead decrease the transcription of one gene. Usually, the transcription factor induces the regulation by binding to a specific region of the gene under control, called binding site or promoter (see figure 2.1.2). Once bound, an activator is able to increase the likelihood of transcription of the gene by taping itself to RNA polymerase with strong protein-protein interactions and thus helping its recruitement. Conversely, the repressors either prevent physically the RNA polymerase to bind to the promoter of the gene and transcribe it into mRNA (called DNA-binding repression), or prevent the translation of mRNA into protein by binding to the mRNA directly (called RNA-binding repression) (see [6] for more details).

A transcription factor is not always specific to a unique gene. It may even be sometimes both activator or inhibitor, depending on the cellular context and on the other transcription factors or proteins that may bind to the same binding site, called associated co-factors [6]. It follows that a unique gene is most of the time controlled by multiple simultaneous transcription factors leading to a combinatorial regulation of transcription, and determining whether the gene is up or down-regulated is a hard task.

Usually, all these interactions between genes, mRNA and proteins at the level of a reaction, of a cell, of an organ or of a whole organism, form a large network called “gene regulatory network”. These networks are composed of nodes and edges, where nodes represent proteins or genes and the edges summarize regulatory relationships between these nodes and may either be direct or

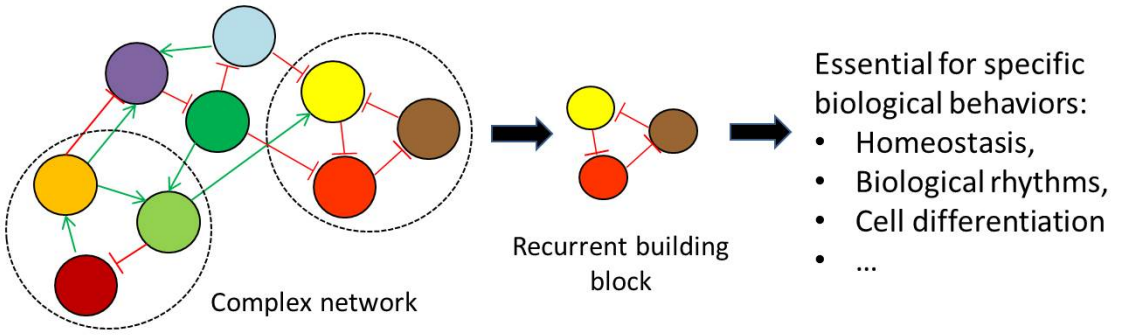

Figure 2.1.3: Illustration of complex gene regulatory networks composed of recurrent building blocks, essential and responsible for different biological functions.

indirect, activations or repressions [9] (see figure 2.1.3). Studying gene regulatory networks allow to explain and understand how the genotype shapes physiological and phenotypic observations. However, when considering that the number of human genes has been estimated between 20000 and 25000, and the number of transcription factors is approximately 2600, it is easy to imagine how large and how complex these regulatory networks may become. To circumvent this problem, it has been observed that these complex networks display abundant recurrent and repetitive motifs composed of a small number of genes highly interconnected, called building blocks (see figure 2.1.3). Indeed, several types of motifs were found to happen more often in gene regulatory networks than in randomly generated networks that share the same topological properties [90]. These different recurrent patterns often play central roles in biological functions, and this manuscript will focus on one particular essential motif called "feedback loops".

2.2 Genetic feedback loops

Genetic feedback loops have the topology of a ring: the expression of each gene in the network is regulated by one previous gene and regulates the expression of a following gene, so that the genes in the network are coupled successively and form a directed cycle (see figure 2.2.1). Two main groups of feedback loops exist depending on the number of repressions within the network. If the number of repressions is even, the loop is called "positive feedback loop". In this case, one gene indirectly activates its own expression via the activations and the even number of repressions within the cycle. Conversely, if the number of repressions is odd, the loop is called "negative feedback loop" and in this case a gene indirectly represses its own expression [114] (see figure 2.2.1).

Negative feedback loops have been shown to be essential for two different mechanisms: homeostasis and biological oscillations. Homeostasis is a vital function that allows to maintain relatively constant the biological internal operating conditions despite environmental or molecular fluctuations. A lot of common and popular features are under the control of homeostatic mechanisms in the human body, such as the body temperature, blood pressure, blood sugar level [106], or ATP (Adenosine triphosphate) that plays a central role in providing energy for many processes in living cells [68]... Negative loops are also responsible for the emergence of self-sustained oscillations and endogenous biological clocks that coordinate periodically different biological functions [40]. From the macro-scale to the micro-scale, oscillatory behaviors can be observed everywhere. For example, the circadian clock allows organisms to anticipate and adapt to environmental changes by generating 24-hours self-sustained oscillations coupled to day-night cycles in a wide variety of genes, molecules and internal parameters such as the sleep-wake cycle or the body temperature [7, 104]. Similarly, the cell cycle is composed of different phases during which a single cell goes through the duplication of its genetic material in order to divide and seems synchronized with the circadian clock with a period of 24 hours [6, 46]. As a last example, the female menstrual cycle is also a complicated

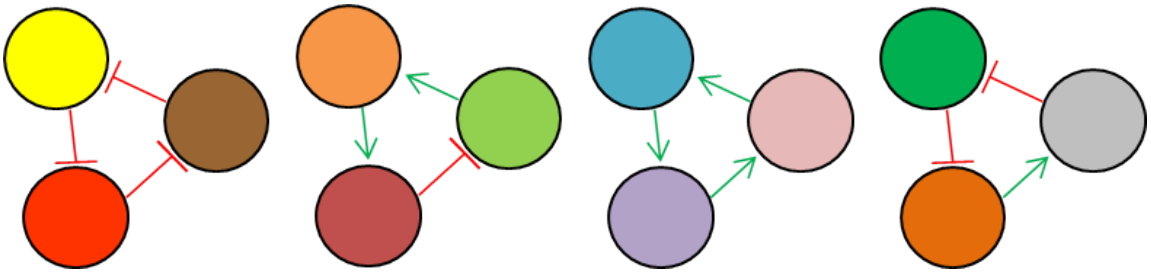

Figure 2.2.1: All possible feedback loops composed of three genes. The two on the left are negative loops with 1 or 3 inhibitions, and the two on the right are positive loops with 0 or 2 inhibitions.

oscillator that controls the reproductive system through different hormones that vary with a period of approximately 28 days [106]. All these phenomena can emerge through an underlying genetic regulation composed of negative loops. Interestingly, some systems highlight both the homeostatic and oscillatory behaviour, depending on internal conditions. This is the case for the regulation of a protein called p53. This protein has been discovered in 1979 and it is now clear that it plays an essential role in living organisms: p53 is indeed involved in tumor suppression, apoptosis, DNA repair and acts as a transcription factor that regulates a huge amount of genetic pathways (see for example [73] for a complete review). In healthy organisms and unstressed conditions, this protein is kept at low levels thanks to tight homeostatic control mechanisms [21]. In various stress conditions however, such as the presence of malignant cells or in case of DNA damage, it has been observed that the concentration of p53 starts to oscillate [78, 85, 23]. These sustained oscillations have been interpreted as essential for DNA repair or tumor suppression [122]. These two main dynamical behaviors have been partly explained through a negative regulation of p53 by another protein called Mdm2.

While negative feedback loops tend to reduce the effect of a small disturbance, positive feedback loops have an inverse effect and exacerbate perturbations. For this reason, they have been shown to be responsible for multi-stability, leading to differentiation processes or cell decision making [114]. Cell differentiation allows undifferentiated cells, called stem cells, to differentiate into any specialized cells with specific functions and is a life-long process, from development stages to repair phases (see the left sketch in figure 2.3.1). This multi-stability property also allows drastically different fates and decisions from one cell to another, even in the case of daughter cells in similar genetic and molecular environments [6]. A famous and essential example of cell decision making is apoptosis, a process during which an old or damaged cell dies. It has been interestingly observed that sister cells do not always respond similarly to various apoptosis signals: some of them indeed go through the apoptotic phases and die while others do not react. This difference in decision is partly explained by an auto-activation of a family of enzymes called Caspases that become activated when cell death is programmed [6].

2.3 Importance of understanding and controlling these loops

As highlighted in the previous sections, gene regulatory feedback loops govern a large amount of vital biological functions. For this reason, a better understanding of their underlying mechanisms as well as new strategies for the control of their dynamics would lead to an improvement regarding insight into diseases and pharmacological treatments [110].

Disrupted negative feedback loops have now been identified in many diseases. For example, an homeostasis disruption, called a dyshomeostasis, may result in the emergence of undesirable sustained oscillations with sometimes dramatic consequences for the organism. For instance, due to its important role in apoptosis, the protein p53 introduced in the previous section has been shown to be tightly regulated in healthy organisms in order to prevent extreme expression levels. Indeed,

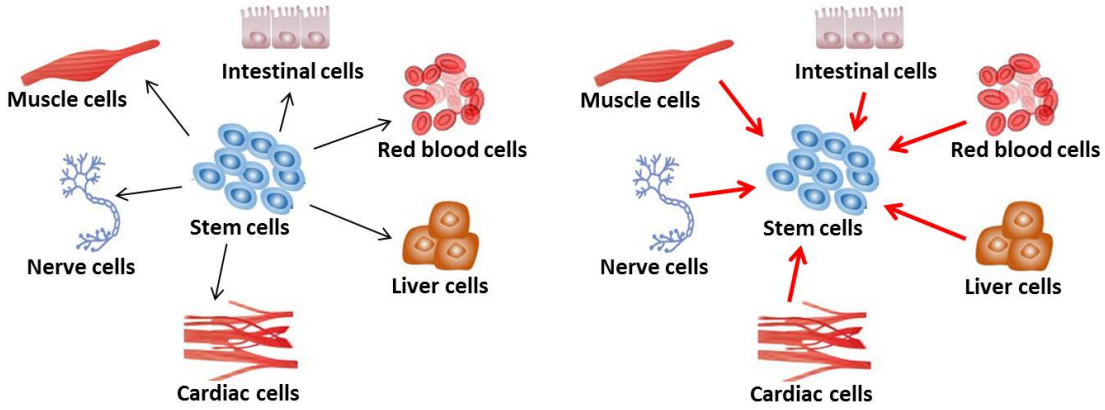

Figure 2.3.1: Left: a stem cell is able to differentiate into different specialized cells through the process of cell differentiation (picture modified from [3]). Right: the dedifferentiation process is when a specialized cell is able to dedifferentiate into a stem cell (picture modified from [3]).

inappropriate activity of p53 with too high or too low concentrations can lead to various diseases, such as neurodegenerative disorders characterized by a neuronal loss like Alzheimer [113], or early embryonic lethality [21]. These types of disruptions are not restricted to the genetic scale: at the neuron scale for example, periodic firing patterns with under- and over-stimulation are known to be involved in various kinds of cerebral damage [65, 51]. Due to the underlying role of genetic networks, it seems likely that homeostatic behaviors at any scale may often hide a genetic homeostatic control. For example, in [53], it has been shown that the coenzyme PLP (Pyridoxal phosphate: a catalyst derived from a vitamin) is tightly regulated through a genetic cascade in order to guarantee homeostasis of neurotransmitters. In case of extreme PLP activities, the consequent dyshomeostasis of neurotransmitters (such as serotonin or dopamine) has been shown to provoke epileptic attacks.

The reverse scenario, namely the disruption of a biological oscillator, seems also involved in many disorders. For example, it has been observed that many diseases such as cancers [76] or neurodegenerative disorders [91] are susceptible to cause a disruption of the circadian clock. Alternatively, the synthetic generation of circadian rhythms in disrupted organisms has been proved to be effective for the slowdown of disease progression [76]. For these reasons, the circadian clock is now considered as a promising tool for therapeutic progress, and especially for cancer treatments. All these examples support the high interest of finding new strategies for the control of biological negative feedback loops.

Similarly, the control of biological positive feedback loops opens up vast biotechnological applications and opportunities. For example, it has been shown recently that cell differentiation is a reversible process [24]: scientists have indeed been able to turn a differentiated cell back into an undifferentiated stem cell. However, this phenomenon called “dedifferentiation” is not yet well understood (see the right sketch in figure 2.3.1). Being able to control and understand dedifferentiation processes may allow to produce and store a large amount of stem cells. These non-specialized cells are helpful in many domains. For example, cancers are often induced by an abnormal cell growth and division that invade and spread widely throughout the organism, and the control and understanding of differentiation processes may reveal how and why such diseases start and develop. Furthermore, these cells are more and more used in cancer treatments as they are able to replace any damaged cell. Indeed, chemotherapy or radiotherapy that are responsible for the destruction of cancer cells do not make the distinction with healthy cells. In order to restore a normal amount of healthy cells, patients with typical diseases such as Leukemia for example, can receive stem cell transplants. Finally, the control of positive feedback loops can also be useful for programmed cell differentiation in order to force a cell to differentiate into any particular cell type. This may be

interesting in the context of tissue regeneration for example, where a great amount of specialized cells is needed.

2.4 Biological design and control tools

Synthetic biology has made significant progress over the past few years and has offered multiple tools for the design and the control of genetic motifs [103].

The idea of synthetic biology emerged at the end of the 20th century, but the first synthetic circuits were really engineered at the beginning of the 21st century. This recent multidisciplinary field derived from genetics, biophysics but also computer and control engineering, in order to create, redesign, control and program fully artificial biological systems. Most of the time, some DNA building blocks or sequences are stitched and assembled artificially together thanks to different enzymes that are able to both cleave and facilitate the joining of DNA strands, and these new modules are then inserted in living organisms for different purposes. Thanks to synthetic modification of DNA, a lot of transcriptional and translational parameters may be tuned: for example, by changing the promoter of a gene, its transcription rate may be modified, whereas its degradation rate may be impacted by a modification of its stop codon.

A famous and extensively used application of synthetic biology concerns gene expression measurement. Indeed, understanding and studying a genetic motif often induces the investigation of genetic expression changes. In 2008, the three chemists Osamu Shimomura, Roger Tsien and Martin Chalfie received the Nobel Prize for their study on bioluminescent jellyfish. He discovered a protein called GFP (green fluorescent protein) that exhibits green fluorescence after exposure to blue light. Nowadays, this protein or other similar fluorescent proteins such as YFP, RFP, CFP (for respectively Yellow, Red and Cyan fluorescent protein) are widely used as reporter genes for the measurement of gene expression. One way to do this in practice is to fuse the coding sequence of the reporter gene downstream or upstream of the coding sequence of the gene of interest. In this way, both genes are expressed to the same extent (see figure 2.4.1): a chimeric protein is produced and recapitulates the expression level of the gene of interest. The expression of the reporter gene can be quantified thanks to fluorescence microscopy. As the light is proportional to the abundance of protein expression, the intensity of fluorescence leads to a partial estimation of the temporal and spatial gene expression level within the cell. In this way, gene expression can be evaluated by quantifying levels of the gene product, which usually consists in the corresponding coding proteins.

Synthetic biology is also a useful tool for the design of simplified and minimal genetic circuits that reproduce the characteristics of bigger and more complex real biological networks. For both the

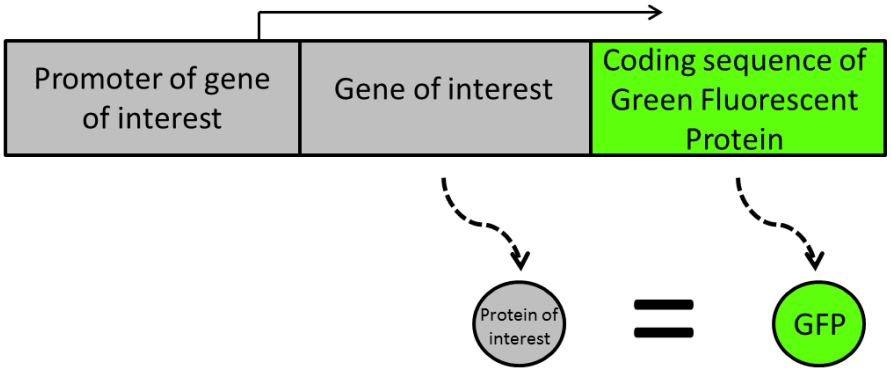

Figure 2.4.1: Synthetic modification of a gene for the measurement of its expression through a fluorescent protein.

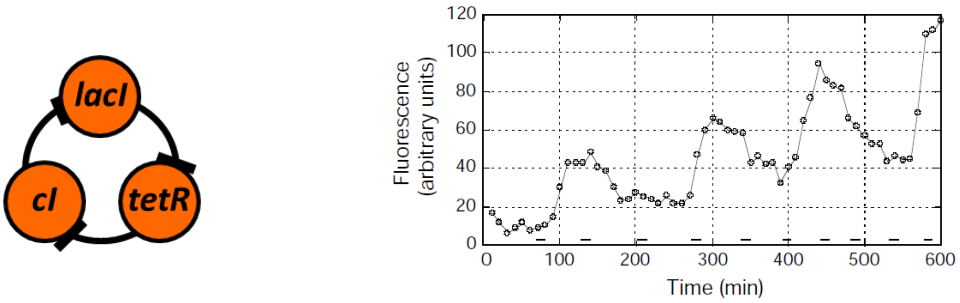

Figure 2.4.2: Left: the three genes that compose the Repressilator. Right: oscillations produced by the Repressilator (figure from [40]).

negative and positive genetic feedback loops, two breakthrough synthetic circuits were designed at the beginning of the 21st century in order to understand and illustrate the possible behaviors of these loops, and are still extensively used nowadays.

The first synthetic genetic negative feedback loop, called the Repressilator, was designed by Michael Elowitz and Stanislas Leibler in 2000 [40], and was implemented in the organism *Escherichia Coli*. The aim of this work was to generate a synthetic gene regulatory network mimicking a biological oscillator. Three genes were assembled in a negative feedback loop as illustrated in the left sketch of figure 2.4.2. The first protein LacI expressed by the first gene *lacI* represses the expression of the second gene *tetR*. Its protein product TetR is in turn responsible for the inhibition of a third gene *cI*. Lastly, the third resulting protein CI represses the first gene *lacI*. Thanks to a green fluorescence protein, sustained oscillations were measured (see figure 2.4.2). Similarly, Attila Becskei and Luis Serrano investigated at the same period the role of autoregulation in gene networks by designing a synthetic negative feedback system, and demonstrated its ability to provide stability [18]. Since then, other synthetic oscillators have been designed, and the major ones can be found in the review by [103].

The same year, Timothy Gardner, Charles Cantor and James Collins synthetically constructed the first genetic positive feedback loop, also known as Toggle Switch, in the organism *Escherichia Coli* [54]. This motif was composed of two genes *lacI* and *tetR* that mutually repressed each other through the proteins LacI and TetR for which they code. The circuit was designed in order to measure the expression of both genes: the red fluorescent protein RFP was added to *lacI* and the green fluorescent protein GFP was added to *tetR*, so that LacI could be measured with levels of red fluorescence and TetR with levels of green fluorescence (see the left sketch in figure 2.4.3). During the experiments, it was observed that this small motif is able to reproduce a cell differentiation process, emerging from the underlying genetic positive feedback loop. Indeed, from an initial orange fluorescent state for which both *tetR* and *lacI* are expressed, each cell was able to differentiate either into a red fluorescent state for which *lacI* is expressed and *tetR* is off, or into a green fluorescent state for which *tetR* is expressed and *lacI* is off (see the right picture in figure 2.4.3).

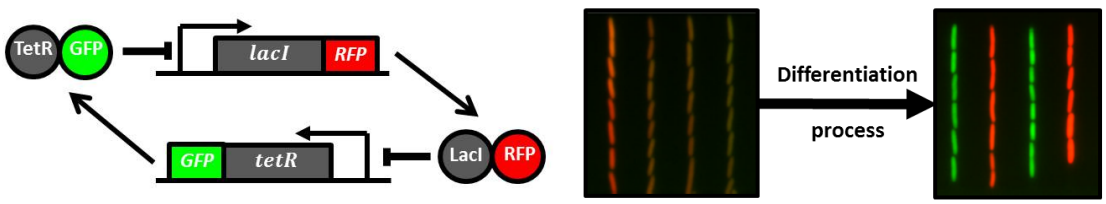

Figure 2.4.3: Left: the genetic circuit composing the Toggle Switch. Right: differentiation process produced by the Toggle Switch (figure from [80]).

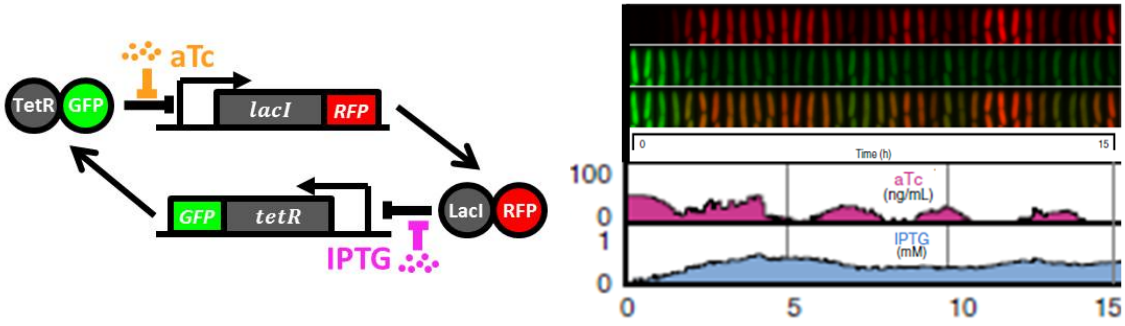

Figure 2.4.4: Left: the genetic circuit composing the Toggle Switch with synthetic modification that allows IPTG and aTc to control genes interactions. Right: dedifferentiation process produced by the introduction of aTc and IPTG on the Toggle Switch (figure from [80]). The fluorescence of a single cell is tracked for 15 hours. It is possible to observe that both *tetR* and *lacI* are expressed.

Besides the synthetic design of motifs, a lot of external control methods have been created in order to perturb the natural behavior of a genetic network. For example, the introduction of specific inducer molecules has been proved to be effective in interfering with some genes and proteins of interest [87, 49, 50, 69]. With these techniques, a recent successful dedifferentiation process control strategy has been implemented in [80] for the genetic circuit of the Toggle Switch. In this experiment, the goal was to maintain cell lines near the undifferentiated orange fluorescent state. For this purpose, the motif was modified in order to perturb the original circuit with the introduction of two inducer molecules, namely aTc and IPTG. In this new network, aTc inhibits the inhibition of TetR on *lacI*, while IPTG inhibits the inhibition of LacI on *tetR* (see the left sketch in figure 2.4.4). It was observed that even if a cell starts in a green or red fluorescent differentiated state, the introduction of the two inducer molecules is able to block the cell in an undifferentiated state where both *tetR* and *lacI* are expressed (see figure 2.4.4). For a fine tuning of inducer molecule inputs, microfluidic devices have been used. These devices are composed of chambers in which cells can grow, and two syringes that contain the two inducer molecules. In principle, the inducer molecules are introduced dynamically and precisely in really small amounts by varying the difference in hydrostatic pressure between the two syringes, and this allows to switch the growth medium. Similarly, the modification of environmental conditions such as the temperature or the osmotic pressure within a cell [120] may allow control of gene expression.

A more recent technique based on light pulses, called optogenetics, has been emerging [89, 116, 88, 27]. Traditionally, this technique has been used in the brain to control neuronal activity, but is more and more developed for other types of cells. This approach has the advantage of being less invasive and more targeted. Indeed, in order to control a target gene expression, its promoter is appropriately modified to make it responsive to a specific wavelength. This type of control acts as an on-off switch: the system is controlled when the light is turned on, and uncontrolled when the light is turned off. As a concrete example, optogenetic processes are often convenient when the expression of the target gene is under the control of a transcription factor that first needs to be phosphorylated or methylated in order to bind to the promoter of the gene and activate its transcription (phosphorylation is the attachment of a phosphoryl group to a molecule, and methylation the attachment of a methyl group). As done in [27] or [88], optogenetics may control this phosphorylation or methylation process, and then indirectly control transcription (see figure 2.4.5). Similarly, other studies such as [116] or [89] use light pulses in order to induce or block interactions between two different molecules. Finally, compared to inducer molecule techniques that are only able to control cell populations, optogenetics has always the advantage to be adapted for the control of a biological system both at the population and the single cell level.

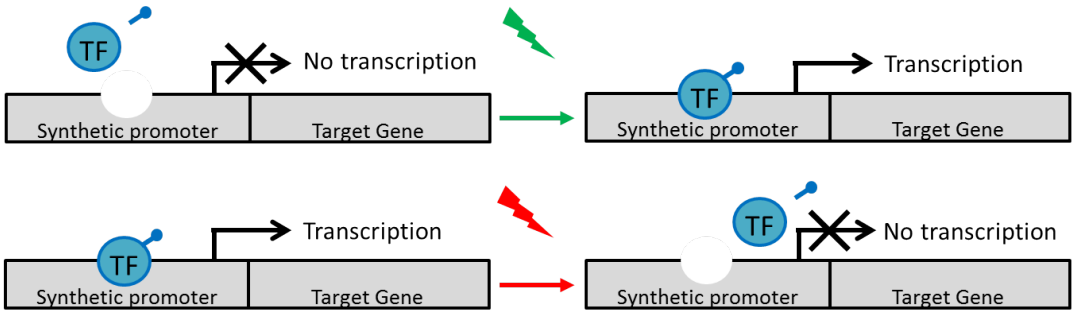

Figure 2.4.5: Example of an optogenetics process when the expression of a gene is under the control of a transcription factor TF that first needs to be phosphorylated or methylated in order to activate transcription. Under green light, the TF gets phosphorylated and is able to transcribe the gene of interest, and under red light, the transcription is blocked by dephosphorylation of the TF.

2.5 Conclusion

All these synthetic techniques often lead to tedious, time-consuming, numerous and expensive biological trials partly due to the high precision and quality devices required. For example, most of the experiments presented in the previous sections used cloning of genes or segments of DNA. For this purpose, several techniques exist and need more or less expensive materials: one way to do this in practice is to clone genes with PCR (polymerase chain reaction) techniques for which the systems cost a few thousands of dollars, insert these copies into plasmids (circular pieces of DNA), and insert these plasmids into bacteria [6]. All the processes can cost a few hundreds of dollars and take a few hours. Similarly, the devices that are used for the monitoring of gene expression in single cells, such as fluorescence microscopes introduced in section 2.4, of flow cytometer instruments (with this technique, the cells pass through a laser, are given a positive or a negative charge depending on their fluorescence, and are then sorted by an electric field) can cost a few thousands of dollars [6]. For all these reasons, the use of mathematical modeling and the theory of dynamical systems and control may provide a good insight in order to help designing the first draft of a control strategy. For this purpose, the mathematical modeling of genetic feedback loops is introduced in next chapter.

Chapter 3

Mathematical modeling of genetic feedback loops

3.1 The deterministic and ordinary framework

Depending on the objectives and hypothesis, different modeling approaches exist in order to describe and analyze gene regulatory networks. In this manuscript, the models used are limited to deterministic and ordinary differential systems for which dynamical and convergence results may be analytically proved.

If the number of molecules in the biological system is considered to be small, such as transcription factors or mRNA for example that often appear in scarce and low copy numbers, then deterministic and continuous approaches are not sufficient to reproduce and describe the biological system dynamics. Indeed, in this case, as soon as two molecules need to interact, a time-delay and a meeting probability must be taken into account. These hypotheses may lead to the construction and analysis of random dynamical systems such as stochastic differential equations (also called master equation for chemical reactions), or continuous time discrete-state Markov processes, where states of the system and its evolution are described in probabilistic term. It is important to keep in mind that these types of systems exist, especially for extending and validating the results found, but this framework has not been treated in this manuscript. Instead, it has been considered that the biological components are in high concentration and well mixed, so that deterministic models can be used. This hypothesis is well adapted for the biological examples that will be used in the manuscript and allows to state analytical results that may be extended later in the case of stochastic systems.

Similarly, it may be assumed that molecules are not homogeneous within the biological system of interest and these inhomogeneity phenomena may happen at different scales. For example, the transcription of a gene into mRNA takes place inside the nucleus of a cell, but the mRNA must leave the nucleus and reach the ribosomes in the cytoplasm for the translation. As a second example, spatial properties are essential during development phases where some genes are intentionally on or off depending on the location in the embryo for the development of particular organs. More generally, as soon as a molecule diffuses within a cell or an organ, diffusive terms must be included in the model and an ordinary differential equation approach is not sufficient. In this case, spatial components must be taken into account, leading to the analysis of partial differential equations, such as reaction-diffusion equations that have been extensively used in biology to explain pattern formation with the theory of Turing in particular. Again, this manuscript will only focus on small genetic feedback loops for which spatial dependence do not have to be considered.

A lot more details about non deterministic and non ordinary differential equation models for gene regulatory networks can be found in the complete review by [36].

3.2 Non-linear ordinary differential systems

3.2.1 Modeling transcription and translation

For the modeling of gene regulatory networks, the different biological steps explained in chapter 2 for gene expression are mathematically described (more details can be found in chapter 2 of [26] and for a textbook on non-linear systems see [75]). For the transcription, the binding of n similar transcription factors to the free promoter of the gene of interest is described by the following chemical reaction:

$$nTF + P_{free} \underset{k_2}{\overset{k_1}{\rightleftharpoons}} P_{bound}$$

where TF is the concentration of transcription factor, P_{free} is the concentration of free promoter of the gene of interest and P_{bound} is the concentration of the complex formed by the promoter of the gene and the n transcription factors that bind to it to enhance or repress the transcription of the gene. The two parameters k_1 and k_2 are rate constants, and may be seen as the number of reactions per unit of time. The ordinary differential equation (ODE) for this type of chemical reaction is derived by the law of mass action:

$$\begin{cases} \dot{P}_{free} = k_2 P_{bound} - k_1 TF^n P_{free} \\ \dot{P}_{bound} = k_1 TF^n P_{free} - k_2 P_{bound} = -\dot{P}_{free}. \end{cases}$$

This formalism may be seen as the limit of an infinite number of molecules in stochastic models. For example, the production of P_{bound} is conditioned by the likelihood that n transcription factors and a free promoter meet, inducing the term $TF^n P_{free}$ in the ODE.

DNA molecules are often present in fixed numbers in biological systems, and can be considered constant in the ODE. The DNA molecules are the sum of the free promoters and the bound ones, leading to $P_{free} + P_{bound} = P_{total}$ where P_{total} is constant. This hypothesis of conservation of mass is easily verified in the ODE as $\dot{P}_{free} + \dot{P}_{bound} = 0$.

It is important to consider that the gene expression machinery has several timescales. Indeed, the time for the binding and unbinding of transcription factors to DNA is of the order of magnitude of 1 second, whereas for the transcription and translation process, the order of magnitude is 1 minute [9]. In this context, the Quasi Steady State Approximation (QSSA) is used in the previous ODE, and considers that the bound and unbound promoter concentration reaches a steady state almost instantaneously (see for example [107] for the application of QSSA methodology):

$$\begin{cases} \dot{P}_{free} = 0 \\ \dot{P}_{bound} = 0. \end{cases}$$

With the conservation of mass $P_{free} = P_{total} - P_{bound}$, the concentration of P_{free} and P_{bound} becomes:

$$\begin{cases} P_{free} = P_{total} \dfrac{\theta^n}{\theta^n + TF^n} \\ P_{bound} = P_{total} \dfrac{TF^n}{\theta^n + TF^n} \end{cases}$$

where $\theta = (k_2/k_1)^{1/n}$. Now that the model for the transcription factor binding has been stated, the transcription process can be derived. It will be considered that mRNA degrades with time, and is both produced from the transcription of a gene with and without transcription factors, leading to the following chemical reactions:

$$\begin{cases} P_{free} \xrightarrow[\alpha_1]{} M_{RNA} \\ P_{bound} \xrightarrow[\alpha_2]{} M_{RNA} \\ M_{RNA} \xrightarrow[\gamma_m]{} \emptyset \end{cases}$$

where M_{RNA} is the concentration of mRNA. Again, with the law of mass action, and by considering that all processes are independent, the concentration of mRNA obeys the following differential equation:

$$\dot{M}_{RNA} = \alpha_1 P_{free} + \alpha_2 P_{bound} - \gamma_m M_{RNA}.$$

With the expression for P_{free} and P_{bound}, the equation becomes:

$$\dot{M}_{RNA} = P_{total}\left[\alpha_1 \frac{\theta^n}{\theta^n + TF^n} + \alpha_2 \frac{TF^n}{\theta^n + TF^n}\right] - \gamma_m M_{RNA}.$$

Two cases can be distinguished depending on the nature of the transcription factor. If the transcription of the gene is increased by an activator, the production of mRNA is mainly due to bound promoters, and in this case $\alpha_1 \ll \alpha_2$, leading to:

$$\begin{aligned} \dot{M}_{RNA} &= P_{total}\left[\alpha_1\left(1 - \frac{TF^n}{\theta^n + TF^n}\right) + \alpha_2 \frac{TF^n}{\theta^n + TF^n}\right] - \gamma_m M_{RNA} \\ &= P_{total}\alpha_1 + (\alpha_2 - \alpha_1)\frac{TF^n}{\theta^n + TF^n} - \gamma_m M_{RNA} \\ &= \beta_1 + \beta_2 \frac{TF^n}{\theta^n + TF^n} - \gamma_m M_{RNA} \end{aligned}$$

where $\beta_1 = P_{total}\alpha_1$ and $\beta_2 = \alpha_2 - \alpha_1$.

Conversely, if the transcription of the gene is decreased by a repressor, the production of mRNA is mainly due to free promoters, and in this case $\alpha_2 \ll \alpha_1$, leading to:

$$\begin{aligned} \dot{M}_{RNA} &= P_{total}\left[\alpha_1 \frac{\theta^n}{\theta^n + TF^n} + \alpha_2\left(1 - \frac{\theta^n}{\theta^n + TF^n}\right)\right] - \gamma_m M_{RNA} \\ &= P_{total}\alpha_2 + (\alpha_1 - \alpha_2)\frac{\theta^n}{\theta^n + TF^n} - \gamma_m M_{RNA} \\ &= \beta_1 + \beta_2 \frac{\theta^n}{\theta^n + TF^n} - \gamma_m M_{RNA} \end{aligned}$$

where $\beta_1 = P_{total}\alpha_2$ and $\beta_2 = \alpha_1 - \alpha_2$.

The last translation step for the production of the corresponding protein is modeled by assuming that each protein is produced by mRNA and can degrade, leading to:

$$\begin{cases} M_{RNA} \xrightarrow[\rho_1]{} P \\ P \xrightarrow[\gamma_p]{} \emptyset \end{cases}$$

where P is the concentration of the protein. With the law of mass action, P evolves according the following differential equation:

$$\dot{P} = \rho_1 M_{RNA} - \gamma_p P.$$

Again, different timescales emerge during these processes: the degradation of mRNA is of the order of magnitude of 1 minute whereas for the degradation of a protein, the order of magnitude is 1 hour [9], leading to $\gamma_p \ll \gamma_m$. The differential system can be rewritten:

$$\begin{cases} \dfrac{\mathrm{d}M_{RNA}}{\gamma_p \mathrm{d}t} = \dfrac{\beta_1}{\gamma_p} + \dfrac{\beta_2}{\gamma_p}\mathrm{f}(TF) - \dfrac{\gamma_m}{\gamma_p} M_{RNA} \\ \dfrac{\mathrm{d}P}{\gamma_p \mathrm{d}t} = \dfrac{\rho_1}{\gamma_p} M_{RNA} - P \end{cases}$$

where $\mathrm{f}(TF)$ is either $TF^n/(\theta^n + TF^n)$ or $\theta^n/(\theta^n + TF^n)$. With the change of timescale $\tau = \gamma_p t$, and $\epsilon = \gamma_p/\gamma_m \ll 1$, the differential equation becomes:

$$\begin{cases} \epsilon \dfrac{\mathrm{d}M_{RNA}}{\mathrm{d}\tau} = \dfrac{\beta_1}{\gamma_m} + \dfrac{\beta_2}{\gamma_m}\mathrm{f}(TF) - M_{RNA} \\ \dfrac{\mathrm{d}P}{\mathrm{d}\tau} = \dfrac{\rho_1}{\gamma_p} M_{RNA} - P. \end{cases}$$

The system is then separated into a fast variable M_{RNA} and a slow variable P, as $\dot{M}_{RNA}$ evolves very rapidly compared to $\dot{P}$. Under appropriate conditions that will not be discussed here, the theorem of Tikhonov can be applied (see for example [75] for more details): basically, it states that the fast variable M_{RNA} reaches a quasi steady state M^*_{RNA} solution of $(\beta_1/\gamma_m)+(\beta_2/\gamma_m)\mathrm{f}(TF)-M^*_{RNA} = 0$, and the new differential system reduced to the unique variable P has essentially the same dynamical behavior as the complete system.

By substituting $M_{RNA} = M^*_{RNA} = (\beta_1/\gamma_m) + (\beta_2/\gamma_m)\,\mathrm{f}(TF)$ in the equation for P, the system becomes:

$$\dot{P} = \kappa_0 + \kappa \mathrm{f}(TF) - \gamma_p P$$

where $\kappa_0 = \rho_1\beta_1/\gamma_m$ can be interpreted as a basal rate, and $\kappa = \rho_1\beta_2/\gamma_m$. With this equation, the dynamical behavior of a protein is directly related to the concentration of its transcription factor. To summarize, if the transcription factor is an activator, then

$$\dot{P} = \kappa_0 + \kappa \mathrm{h}^+(TF, \theta, n) - \gamma_p P$$

while if the transcription factor is a repressor:

$$\dot{P} = \kappa_0 + \kappa \mathrm{h}^-(TF, \theta, n) - \gamma_p P$$

where $\mathrm{h}^+(TF, \theta, n) = TF^n/(\theta^n + TF^n) \in [0, 1[$ and $\mathrm{h}^-(TF, \theta, n) = \theta^n/(\theta^n + TF^n) \in]0, 1]$. For $n = 1$, these functions are known as Michaelis-Menten functions, historically introduced to describe the kinetics of enzyme catalysis. For $n \geq 2$, they are sigmoid functions known as Hill functions, and are a generalization of Michaelis-Menten dynamics for cooperative bindings, extensively used to model activation and repression. Their inflection point is reached at $\theta\left((n-1)/(n+1)\right)^{1/n}$ and the half expression is reached at θ. For n large, as it is often the case for gene regulatory networks, the inflection point and the half expression are reached approximately at θ and the maximum slope is proportional to n. Hence, θ can be interpreted as a threshold below (resp. above) which the regulation of the transcription factor is low (resp. strong), and n can be interpreted as the effectiveness of this regulation. These functions and their properties are illustrated in figure 3.2.1.

3.2.2 ODE model for genetic feedback loops in dimension N

As explained in chapter 2, genetic feedback loops have the topology of a ring and are classified in two families: positive loops with an even number of inhibitions, and negative loops with an odd number of inhibitions. In the rest of the manuscript, a loop with no inhibition will be considered as the canonical form of positive feedback loops and a loop with only one inhibition will be considered as the canonical form of negative feedback loops. Each loop is supposed to be composed of N proteins that act as transcription factors for the coding genes within the network. The variable x_i $\forall\ i \in \{1, ..., N\}$ represents the concentration of the protein i. From what has been explained in

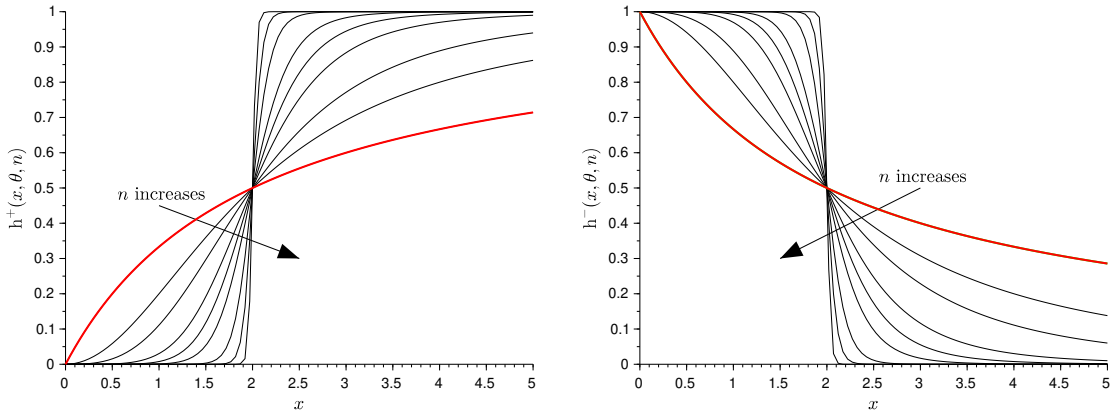

Figure 3.2.1: Effect of increasing n on Hill functions with $\theta = 2$ and $n \in \{2, 3, 5, 7, 10, 20, 40, 100\}$. The red curve is the Michaelis-Menten function with $n = 1$.

section 3.2.1, the dynamical equation for the concentration of each protein is directly linked to the concentration of its transcription factor through a Hill function. From the topological property of genetic loops, each protein i is regulated by only one protein in order to form a ring structure. It follows that the system is modeled by the following non-linear ordinary differential equation:

$$\begin{cases} \dot{x}_1(x_1, x_N) = \kappa_{01} + \kappa_1 \mathrm{h}^*(x_N, \theta_N, n_N) - \gamma_1 x_1, \\ \dot{x}_i(x_i, x_{i-1}) = \kappa_{0i} + \kappa_i \mathrm{h}^+(x_{i-1}, \theta_{i-1}, n_{i-1}) - \gamma_i x_i \quad \forall\ i \in \{2, ..., N\} \end{cases} \tag{3.2.1}$$

where $\mathrm{h}^*(x_N, \theta_N, n_N) = \mathrm{h}^+(x_N, \theta_N, n_N)$ for the canonical positive loop, and $\mathrm{h}^*(x_N, \theta_N, n_N) = \mathrm{h}^-(x_N, \theta_N, n_N)$ for the canonical negative loop. Each protein is produced with a basal rate κ_{0i}, degraded with a rate γ_i, and experiences regulation with intensity κ_i. For biological consistency, all these parameters are considered positive. More precisely, $\kappa_i > 0$, $\gamma_i > 0$ and $\theta_i > 0$ for both loops. Moreover, for the negative loop $\kappa_{0i} \geq 0$. For the positive loop however, it will be assumed that $\kappa_{0i} \geq 0\ \forall\ i \in \{1, ..., N\}$ and that there is at least one $j \in \{1, ..., N\}$ such that $\kappa_{0j} > 0$. This condition for the positive loop will be detailed later in this section, but seems reasonable as transcription and translation are leaky processes such that always a few proteins are expressed even in absence of activators or presence of repressors. Furthermore, the integer n appears to be large in most genetic regulations as discussed in the previous section. For this reason, it will be assumed that $n_i \geq 2$. Finally, $\forall\ i \in \{2, ..., N\}$, the production of protein i is activated by protein $i - 1$, and for the positive loop, the production of protein 1 is activated by protein N, while inhibited for the negative loop.

Remark 3.2.1. *For the sake of simplicity, it will always be understood that $i - 1 = N$ for $i = 1$ throughout the whole manuscript.*
For example, the notation " $\dot{x}_i(x_i, x_{i-1}) = \kappa_{0i} + \kappa_i h^+(x_{i-1}, \theta_{i-1}, n_{i-1}) - \gamma_i x_i\ \forall\ i \in \{1, ..., N\}$ " will also include $\dot{x}_1(x_1, x_N) = \kappa_{01} + \kappa_1 h^+(x_N, \theta_N, n_N) - \gamma_1 x_1$.

The structure of these networks is conveniently summarized in a directed graph where nodes represent proteins and edges represent their regulation. The graph of these two canonical loops are illustrated in figure 3.2.2.

As already indicated, system (3.2.1) is considered as the canonical form of genetic feedback loops. Indeed it is possible to show that any loop composed of an odd number of inhibitions is fully equivalent to the canonical negative loop and any loop composed of an even number of inhibitions is fully equivalent to the positive loop, through a simple change of variable of type $y_i = -x_i$ for appropriately chosen indices $i \in \{1, ..., N\}$ [83]. For example, with the change of variable $y_2 = -x_2$, the following three dimensional negative loop composed of three inhibitions

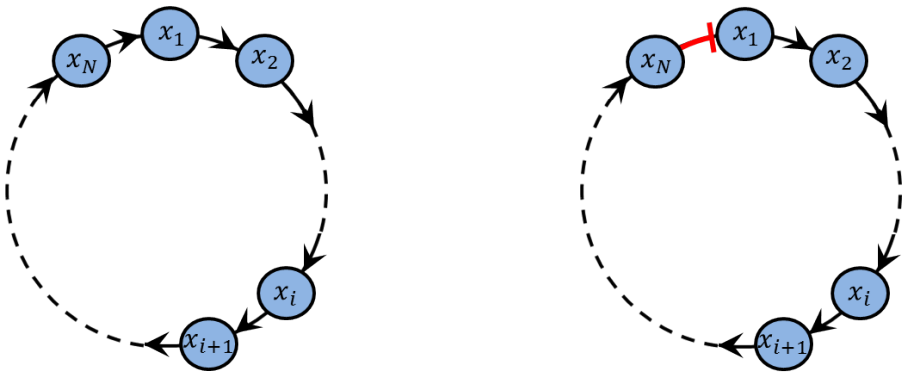

Figure 3.2.2: Graph for the positive (left) and negative (right) canonical genetic feedback loop.

$$\begin{cases} \dot{x}_1(x_1, x_3) = \kappa_{01} + \kappa_1 \mathrm{h}^-(x_3, \theta_3, n_3) - \gamma_1 x_1, \\ \dot{x}_2(x_2, x_1) = \kappa_{02} + \kappa_2 \mathrm{h}^-(x_1, \theta_1, n_1) - \gamma_2 x_2, \\ \dot{x}_3(x_3, x_2) = \kappa_{03} + \kappa_3 \mathrm{h}^-(x_2, \theta_2, n_2) - \gamma_3 x_3, \end{cases}$$

becomes

$$\begin{cases} \dot{x}_1(x_1, x_3) = \kappa_{01} + \kappa_1 \mathrm{h}^-(x_3, \theta_3, n_3) - \gamma_1 x_1, \\ \dot{y}_2(y_2, x_1) = -\kappa_{02} - \kappa_2 \mathrm{h}^-(x_1, \theta_1, n_1) - \gamma_2 y_2, \\ \dot{x}_3(x_3, y_2) = \kappa_{03} + \kappa_3 \mathrm{h}^-(-y_2, \theta_2, n_2) - \gamma_3 x_3, \end{cases}$$

for which x_3 inhibits x_1, x_1 activates y_2 and y_2 activates x_3, as for the canonical negative loop (3.2.1) in dimension 3.

It follows that all the results presented in this manuscript will be given for the two canonical circuits, but perfectly apply to this more general class of systems (see figure 3.2.3).

The vector field of system (3.2.1) can be qualitatively determined with the properties of the null-clines:

Definition 3.2.1.

$$\begin{cases} H_1^*(x) = \dfrac{\kappa_{01} + \kappa_1 h^*(x, \theta_N, n_N)}{\gamma_1}, \\ H_i(x) = \dfrac{\kappa_{0i} + \kappa_i h^+(x, \theta_{i-1}, n_{i-1})}{\gamma_i} \quad \forall\ i \in \{2, ..., N\}. \end{cases}$$

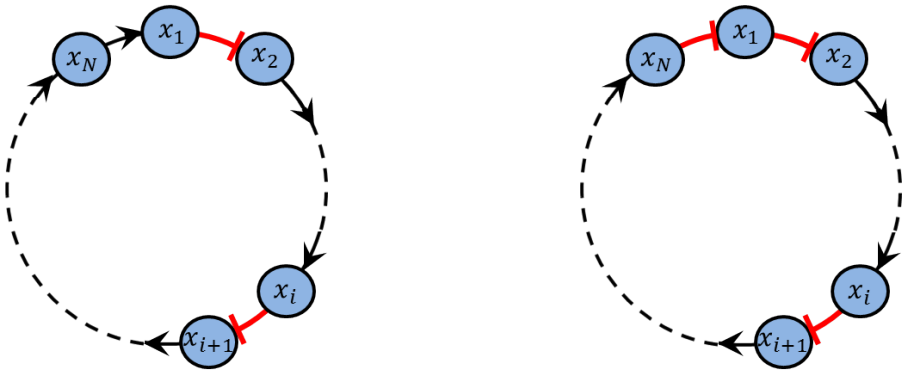

Figure 3.2.3: Graph for general positive (left) and negative (right) feedback loops.

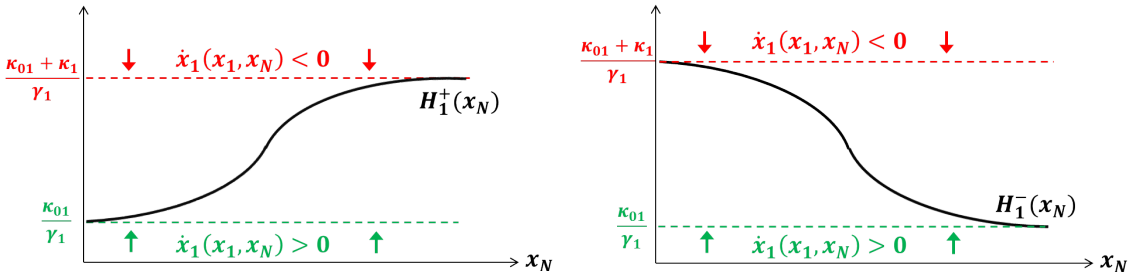

Figure 3.2.4: Illustration of the nullclines H_1^+ and H_1^- and the boundedness proposition 3.2.2. The nullclines H_i $\forall$ $i \in \{1, ..., N\}$ are similar to H_1^+.

Remark 3.2.2. *For the sake of simplicity, when a function or a parameter is introduced for both the negative and the positive loop, it will be labeled with $*$ (for example H_1^*). In this case, in order to refer specifically to one of the two loops, $*$ will be replaced either by $+$ for the positive loop (for example $H_1^+(x)$) or by $-$ for the negative loop (for example $H_1^-(x)$).*

From the structure of the system it is straightforward to see that:

Proposition 3.2.1.

$$\begin{cases} \dot{x}_1(x_1, x_N) = 0 \iff x_1 = H_1^*(x_N), \\ \dot{x}_1(x_i, x_{i-1}) = 0 \iff x_i = H_i(x_{i-1}) \quad \forall\ i \in \{2, ..., N\}\,. \end{cases}$$

From the shape of these nullclines, it is possible to prove that system (3.2.1) is a priori bounded:

Proposition 3.2.2. *For any initial condition in the positive orthant $x_0 \in \mathbb{R}_+^N$, the trajectory of system (3.2.1) will converge towards an invariant region $\mathcal{A}^*$: $\exists\ 0 \leq T < +\infty$ such that $\forall\ t \geq T$, $x(t) \in \mathcal{A}^*$, where:*

$$\begin{cases} \mathcal{A}^+ = \{x | x_i \in [\kappa_{0i}/\gamma_i, (\kappa_{0i}+\kappa_i)/\gamma_i[\ \forall\ i \in \{1, ..., N\}\}\,, \\ \mathcal{A}^- = \{x | x_1 \in\ ]\kappa_{01}/\gamma_1, (\kappa_{01}+\kappa_1)/\gamma_1], x_i \in [\kappa_{0i}/\gamma_i, (\kappa_{0i}+\kappa_i)/\gamma_i[\ \forall\ i \in \{2, ..., N\}\}\,. \end{cases}$$

Proof. From the definition of the vector field :

$$\begin{cases} \dot{x}_1(x_1, x_N) \geq 0 \iff x_1 \leq H_1^*(x_N), \\ \dot{x}_i(x_i, x_{i-1}) \geq 0 \iff x_i \leq H_i(x_{i-1}) \quad \forall\ i \in \{2, ..., N\}\,, \end{cases}$$

and

$$\begin{cases} \dot{x}_1(x_1, x_N) \leq 0 \iff x_1 \geq H_1^*(x_N), \\ \dot{x}_i(x_i, x_{i-1}) \leq 0 \iff x_i \geq H_i(x_{i-1}) \quad \forall\ i \in \{2, ..., N\}\,. \end{cases}$$

From the shape of the nullclines, $\kappa_{01}/\gamma_1 \leq H_1^+(x) < (\kappa_{01}+\kappa_1)/\gamma_1$, $\kappa_{01}/\gamma_1 < H_1^-(x) \leq (\kappa_{01}+\kappa_1)/\gamma_1$ and $\kappa_{0i}/\gamma_i \leq H_i(x) < (\kappa_{0i}+\kappa_i)/\gamma_i$ $\forall\ i \in \{2, ..., N\}$. Then it follows that $\forall\ i \in \{2, ..., N\}$: $\dot{x}_i(x_i, x_{i-1}) < 0$ $\forall\ x_{i-1} \geq 0$ and $\forall\ x_i \geq (\kappa_{0i}+\kappa_i)/\gamma_i$, and $\dot{x}_i(x_i, x_{i-1}) > 0$ $\forall\ x_{i-1} \geq 0$ and $\forall\ x_i < \kappa_{0i}/\gamma_i$. Moreover, for the positive loop, $\dot{x}_1(x_1, x_N) < 0$ $\forall\ x_N \geq 0$ and $\forall\ x_1 \geq (\kappa_{01}+\kappa_1)/\gamma_1$, and $\dot{x}_1(x_1, x_N) > 0$ $\forall\ x_N \geq 0$ and $\forall\ x_1 < \kappa_{01}/\gamma_1$. For the negative loop, $\dot{x}_1(x_1, x_N) < 0$ $\forall\ x_N \geq 0$ and $\forall\ x_1 > (\kappa_{01}+\kappa_1)/\gamma_1$, and $\dot{x}_1(x_1, x_N) > 0$ $\forall\ x_N \geq 0$ and $\forall\ x_1 \leq \kappa_{01}/\gamma_1$. □

This boundedness property, illustrated in figure 3.2.4, guarantees that the differential system stays positive, as expected for a biological system where the variables represent concentrations. All the results that will be presented throughout this manuscript will concern the invariant positive orthant $\mathbb{R}_+^N$.

Due to the non-linearities of system (3.2.1), analytical solutions cannot be determined explicitly. However, qualitative information such as the number of steady states, their local stability, the existence and the number of periodic orbits or even global convergence of trajectories, may be discussed and is presented in next the sections.

3.2.3 Steady states

Determining the exact number of steady states for a dynamical system in general may become a hard task. This is the case for positive feedback loops that are known to display multistability (see for example [10], [115], [14] or [32] among others).

For system (3.2.1) however, the number of steady states for both the negative and positive loops can be determined with the composition of nullclines:

Definition 3.2.2. $\forall\ i \in \{1, ..., N\}$, $S_i^*(x) = H_i \circ H_{i-1} \circ ... \circ H_1^* \circ H_N \circ H_{N-1} \circ ... \circ H_{i+2} \circ H_{i+1}(x)$.

Proposition 3.2.3. *$\tilde{x}^* = (\tilde{x}_1^*, ..., \tilde{x}_N^*)$ is a steady state of system (3.2.1) if and only if $\tilde{x}_1^*$ is a fixed point of $S_1^*(x)$ and $\tilde{x}_i^* = H_i(\tilde{x}_{i-1}^*)\ \forall\ i \in \{2, ..., N\}$.*

Proof. First, let us assume that $\tilde{x}^*$ is a steady state of system (3.2.1). Then $\dot{x}_i(\tilde{x}_i^*, \tilde{x}_{i-1}^*) = 0$ $\forall\ i \in \{1, ..., N\}$ and proposition 3.2.1 holds, leading to $\tilde{x}_i^* = H_i(\tilde{x}_{i-1}^*)\ \forall\ i \in \{2, ..., N\}$. By induction it is easy to see that $\tilde{x}_1^* = S_1^*(\tilde{x}_1^*)$. Conversely, let us assume that $\tilde{x}_1^* = S_1^*(\tilde{x}_1^*)$ and $\tilde{x}_i^* = H_i(\tilde{x}_{i-1}^*)$ $\forall\ i \in \{2, ..., N\}$. Then by induction $\tilde{x}_1^* = H_1^*(\tilde{x}_N^*)$. It follows that proposition 3.2.1 holds and $\dot{x}_i(\tilde{x}_i^*, \tilde{x}_{i-1}^*) = 0\ \forall\ i \in \{1, ..., N\}$. Finally $\tilde{x}^*$ is a steady state of system (3.2.1). □

From this proposition, the number of steady states of system (3.2.1) is directly linked to the number of fixed points of the function $S_1^*(x)$. As the number of fixed points of a function is directly related to its shape, a shape-indicator of $S_1^*(x)$, called "Schwarzian derivative", is calculated [5]. The definition of the Schwarzian derivative of a function can be found in appendix A.1.

Proposition 3.2.4. *The nullcline functions $H_i(x)\ \forall\ i \in \{2, ..., N\}$ and $H_1^*(x)$ have a negative Schwarzian derivative.*

Proof. $\forall\ i \in \{2, ..., N\}$:

$$\begin{aligned}
\mathrm{S}(H_i(x)) &= \mathrm{S}\left(\frac{\kappa_{0i} + \kappa_i \mathrm{h}^+(x, \theta_{i-1}, n_{i-1})}{\gamma_i}\right) \\
&= \mathrm{S}\left(\frac{\kappa_{0i}}{\gamma_i} + \frac{\kappa_i}{\gamma_i} \frac{x^{n_{i-1}}}{x^{n_{i-1}} + {\theta_{i-1}}^{n_{i-1}}}\right)
\end{aligned}$$

Then from property A.1.2 found in appendix A.1:

$$\begin{aligned}
\mathrm{S}(H_i(x)) &= \mathrm{S}\left(\frac{x^{n_{i-1}}}{x^{n_{i-1}} + {\theta_{i-1}}^{n_{i-1}}}\right) \\
&= \mathrm{S}\left(1 - \frac{{\theta_{i-1}}^{n_{i-1}}}{x^{n_{i-1}} + {\theta_{i-1}}^{n_{i-1}}}\right) \\
&= \mathrm{S}\left(\frac{1}{x^{n_{i-1}} + {\theta_{i-1}}^{n_{i-1}}}\right) \\
&= \mathrm{S}(f \circ g(x)),
\end{aligned}$$

where $g(x) = x^{n_{i-1}} + {\theta_{i-1}}^{n_{i-1}}$ and $f(x) = 1/x$. It is easy to calculate: $\mathrm{S}(g(x)) = -(n_{i-1}^2 - 1)/2x^2$ and $\mathrm{S}(f(x)) = 0$. Hence, from property A.1.1 found in appendix A.1, $\mathrm{S}(H_i(x)) = \mathrm{S}(g(x)) = -(n_{i-1}^2 - 1)/2x^2 < 0$ as $n_{i-1} > 1$. Finally, $\forall\ i \in \{2, ..., N\}\ \mathrm{S}(H_i(x)) < 0$.

Similarly, with the same steps:

$$\begin{aligned}
\mathrm{S}(H_1^*(x)) &= \mathrm{S}\left(\frac{\kappa_{01} + \kappa_1 \mathrm{h}^*(x, \theta_N, n_N)}{\gamma_1}\right) \\
&= \mathrm{S}\left(\frac{1}{x^{n_N} + {\theta_N}^{n_N}}\right).
\end{aligned}$$

Hence, $S(H_1^*(x)) = -(n_N^2 - 1)/2x^2 < 0$. □

This proposition induces the following result:

Proposition 3.2.5. *$S_1^*(x)$ has a negative Schwarzian derivative.*

Proof. By definition, $S_1^*(x) = H_1^* \circ H_N \circ H_{N-1} \circ ... \circ H_3 \circ H_2(x)$. From property A.1.1 in appendix A.1, if all the functions in this composition have a negative Schwarzian derivative, then the composed function $S_1^*(x)$ also has a negative Schwarzian derivative. Finally, from proposition 3.2.4, as $S(H_i(x)) < 0 \ \forall \ i \in \{2, ..., N\}$ and $S(H_1^*(x)) < 0$, then $S(S_1^*(x)) < 0$. □

This proposition allows to prove that $S_1^*(x)$ is a sigmoid function:

Proposition 3.2.6. *$S_1^*(x)$ is a sigmoid function.*

Proof. The function $S_1^+(x)$ (resp. $S_1^-(x)$) is strictly monotonically increasing (resp. decreasing) as it is a composition of N strictly monotonically increasing functions (resp. $N-1$ strictly monotonically increasing functions and one srictly monotonically decreasing function). Then ${S_1^+}'(x) > 0$ and ${S_1^-}'(x) < 0 \ \forall \ x \in]0, +\infty[$, ${S_1^*}'(0) = 0$ from the properties of Hill functions, and $S_1^*(x)$ is bounded. As $S_1^*(x)$ has a negative Schwarzian derivative from proposition 3.2.5, it follows that there exists $a > 0$ such that ${S_1^+}'(x)$ (resp. ${S_1^-}'(x)$) is strictly increasing (resp. decreasing) $\forall \ x \in]0, a[$ and ${S_1^+}'(x)$ (resp. ${S_1^-}'(x)$) is strictly decreasing (resp. increasing) $\forall \ x \in]a, +\infty[$ (see [5] for the details). This is exactly the definition of a sigmoid function. □

This sigmoidal shape is essential in order to determine the number of steady states of system (3.2.1):

Proposition 3.2.7. *The negative feedback loop has a unique steady state that will be called $\bar{x}^-$ in the rest of the manuscript. The positive feedback loop cannot have more than three steady states. In this case, they will be called $\bar{x}_{inf}^+$, $\bar{x}_{sup}^+$ and $\bar{x}^+$ in the rest of the manuscript, such that $\bar{x}_{1inf}^+ < \bar{x}_1^+ < \bar{x}_{1sup}^+$.*

Proof. As $S_1^-(x)$ is a monotonically decreasing function, then it can intersect only once the linear function $y = x$. Hence, from proposition 3.2.3, the negative loop version of system (3.2.1) has a unique steady state.

For the positive loop, as $S_1^+(x)$ is a monotonically increasing sigmoid function from proposition 3.2.6, then by definition it cannot have more than three fixed points. It follows from proposition 3.2.3 that the positive loop version of system (3.2.1) has at most three stready states. □

Importantly, due to the boundedness proposition 3.2.2 and the positive conditions on the parameters, the possible steady states of system (3.2.1) do not lie at the borders of the invariant region $\mathcal{A}^*$:

Proposition 3.2.8. *If $\tilde{x}$ is a steady state of system (3.2.1), then $\forall \ i \in \{1, ..., N\}$, $\tilde{x}_i \in]\kappa_{0i}/\gamma_i, (\kappa_{0i} + \kappa_i)/\gamma_i[$.*

The proof of this proposition can be found in appendix A.2. This result will be useful throughout the whole manuscript.

3.2.4 Local Stability

In order to determine the local stability of a steady state $\tilde{x}$ of system (3.2.1), its Jacobian matrix is evaluated at the steady state:

Definition 3.2.3. *The Jacobian matrix of system (3.2.1) evaluated at $\tilde{x}$ is:*

$$J^*(\tilde{x}) = \begin{pmatrix} -\gamma_1 & 0 & \cdots & \cdots & \cdots & 0 & J_1^* \\ J_2^* & -\gamma_2 & 0 & \cdots & \cdots & \cdots & 0 \\ 0 & J_3^* & -\gamma_3 & 0 & \cdots & \cdots & 0 \\ \vdots & \ddots & \ddots & \ddots & \ddots & & \vdots \\ \vdots & & \ddots & \ddots & \ddots & \ddots & \vdots \\ \vdots & & & \ddots & \ddots & \ddots & 0 \\ 0 & \cdots & \cdots & \cdots & 0 & J_N^* & -\gamma_N \end{pmatrix}$$

where $J_1^* = \kappa_1 h^{*\prime}(\tilde{x}_N, \theta_N, n_N)$*, such that* $J_1^+ > 0$ *and* $J_1^- < 0$*, and* $J_i^* = \kappa_i h^{+\prime}(\tilde{x}_{i-1}, \theta_{i-1}, n_{i-1}) > 0$ $\forall\ i \in \{2, ..., N\}$.

In order to investigate the properties of the eigenvalues of $J^*(\tilde{x})$, its associated characteristic polynomial is calculated:

Proposition 3.2.9. *The characteristic polynomial associated to* $J^*(\tilde{x})$ *is:*

$$P^*(X) = \prod_{i=1}^{N}(X + \gamma_i) - \prod_{i=1}^{N} J_i^*.$$

The proof of this proposition can be found in appendix A.3.

From the structure of $P^*(X)$, the stability of the steady states of system (3.2.1) can be investigated:

Proposition 3.2.10. *For the negative feedback loop in dimension* 2*, the unique steady state* $\bar{x}^-$ *is locally stable, no matter the parameters. However, for* $N \geq 3$*,* $\bar{x}^-$ *may either be locally stable or unstable depending on the parameters. In this case, if* $S^{-\prime}(\bar{x}^-) > -1$*, then* $\bar{x}^-$ *is locally stable. For the positive loop, when the three steady states* $\bar{x}^+$*,* $\bar{x}^+_{sup}$ *and* $\bar{x}^+_{inf}$ *exist such that* $\bar{x}^+_{1inf} < \bar{x}^+_1 < \bar{x}^+_{1sup}$*, then* $\bar{x}^+_{sup}$ *and* $\bar{x}^+_{inf}$ *are locally stable and* $\bar{x}^+$ *is locally unstable.*

Proof. With the definition and properties of the steady states, the characteristic polynomial $P^*(X)$ of the Jacobian J^* evaluated at a steady state $\tilde{x}$ of system (3.2.1) can further be expressed as:

$$\begin{aligned} P^*(X) &= \prod_{i=1}^{N}(X + \gamma_i) - \kappa_1 \mathrm{h}^{*\prime}(\tilde{x}_N, \theta_N, n_N) \times \prod_{i=2}^{N} \kappa_i \mathrm{h}^{+\prime}(\tilde{x}_{i-1}, \theta_{i-1}, n_{i-1}), \\ &= \prod_{i=1}^{N}(X + \gamma_i) - \left(\prod_{i=1}^{N} \gamma_i\right) \frac{\kappa_1}{\gamma_1} \mathrm{h}^{*\prime}(\tilde{x}_N, \theta_N, n_N) \times \prod_{i=2}^{N} \frac{\kappa_i}{\gamma_i} \mathrm{h}^{+\prime}(\tilde{x}_{i-1}, \theta_{i-1}, n_{i-1}). \end{aligned}$$

Moreover, from the expression $S_1^*(x) = H_1^* \circ H_N \circ H_{N-1} \circ ... \circ H_3 \circ H_2(x)$, it is easy to calculate its derivative:

$$S_1^{*\prime}(x) = H_1^{*\prime}(H_N \circ ... \circ H_2(x)) \times H_N'(H_{N-1} \circ ... \circ H_2(x)) \times ... \times H_2'(x).$$

From proposition 3.2.3 and definition 3.2.1, the previous expression evaluated on $\tilde{x}_1$ becomes:

$$\begin{aligned} S_1^{*\prime}(\tilde{x}_1) &= H_1^{*\prime}(\tilde{x}_N) \times H_N'(\tilde{x}_{N-1}) \times ... \times H_2'(\tilde{x}_1) \\ &= \frac{\kappa_1}{\gamma_1} \mathrm{h}^{*\prime}(\tilde{x}_N, \theta_N, n_N) \times \prod_{i=2}^{N} \frac{\kappa_i}{\gamma_i} \mathrm{h}^{+\prime}(\tilde{x}_{i-1}, \theta_{i-1}, n_{i-1}). \end{aligned}$$

Hence, the characteristic polynomial $P^*(X)$ of the Jacobian J^* evaluated at the steady state $\tilde{x}$ becomes:

$$P^*(X) = \prod_{i=1}^{N}(X + \gamma_i) - S_1^{*\prime}(\tilde{x}_1) \prod_{i=1}^{N} \gamma_i.$$

For the negative loop in dimension 2, the trace of the Jacobian is negative: $\mathrm{tr}\,(J^-(\tilde{x})) = -\gamma_1 - \gamma_2$. Moreover, the determinant is positive: $\det(J^-(\tilde{x})) = \gamma_1\gamma_2 - J_1^- J_2^- > 0$. It follows that the unique steady state $\bar{x}^-$ is locally stable. For the negative loop in dimension greater than 2, a little information can be deduced from the shape of the characteristic polynomial in the general case [93]. Assume that ${S_1^-}'(\bar{x}_1^-) > -1$ (as a reminder ${S_1^-}'(x) < 0$). Assume further that $\bar{x}^-$ is locally unstable. It is straightforward to see that as $P^-(X)$ is equal to the simple polynomial $\prod_{i=1}^N (X+\gamma_i)$ to which the positive constant $-{S_1^-}'(\bar{x}_1^-)\prod_{i=1}^N \gamma_i$ is added. As $\prod_{i=1}^N (X+\gamma_i)$ has only real negative roots, then $P^-(X)$ cannot have real positive roots. Hence, if $\bar{x}^-$ is locally unstable, then there exists a pair of complex conjugate eigenvalues $a+ib$ and $a-ib$ with positive real part a. By definition, $P^-(a+ib) = 0$:

$$
\begin{aligned}
P^-(a+ib) = \prod_{j=1}^N (a+\gamma_j+ib) - {S_1^-}'(\bar{x}_1^-)\prod_{j=1}^N \gamma_j = 0,& \\
\iff {S_1^-}'(\bar{x}_1^-) = \frac{\prod_{j=1}^N (a+\gamma_j+ib)}{\prod_{j=1}^N \gamma_j},& \\
\implies |{S_1^-}'(\bar{x}_1^-)| = \frac{\prod_{j=1}^N |(a+\gamma_j+ib)|}{\prod_{j=1}^N \gamma_j},& \\
\implies -{S_1^-}'(\bar{x}_1^-) = \frac{\prod_{j=1}^N \sqrt{(a+\gamma_j)^2+b^2}}{\prod_{j=1}^N \gamma_j},& \\
\implies -{S_1^-}'(\bar{x}_1^-) > 1,& \\
\implies {S_1^-}'(\bar{x}_1^-) < -1.&
\end{aligned}
$$

Hence, there is a contradiction. It follows that if ${S_1^-}'(\bar{x}_1^-) > -1$, $\bar{x}^-$ is locally stable.

For the positive loop, assume that the function $S_1^+(x)$ has three fixed points $\bar{x}_{1inf}^+$, $\bar{x}_{1sup}^+$ and $\bar{x}_1^+$ such that $\bar{x}_{1inf}^+ < \bar{x}_1^+ < \bar{x}_{1sup}^+$. Then, from the properties of sigmoid functions, ${S_1^+}'(\bar{x}_{1inf}^+) < 1$, ${S_1^+}'(\bar{x}_{1sup}^+) < 1$ and ${S_1^+}'(\bar{x}_1^+) > 1$ (see figure 3.2.5). If $\bar{x}_{inf}^+$, $\bar{x}_{sup}^+$ and $\bar{x}^+$ are defined as in proposition 3.2.3, they are the three steady states of system (3.2.1).

For the middle steady state $\bar{x}^+$, as $P^+(X=0) = \left[1 - {S_1^+}'(\tilde{x}_1)\right]\prod_{i=1}^N \gamma_i < 0$, and $\lim_{X\to+\infty} P(X) = +\infty$, then $P(X)$ has at least one root with positive real part. Hence, $\bar{x}^+$ is locally unstable. For the two other steady states, assume that they are locally unstable. As $P^+(X)$ is a polynomial with only positive coefficients, it cannot have real positive eigenvalues. Hence, as done for the negative loop, there must exists a pair of complex conjugate eigenvalues $a+ib$ and $a-ib$ with positive real part a. With the same calculations as for the negative loop, this induces:

$$
\begin{aligned}
|{S_1^+}'(\tilde{x}_1)| = \frac{\prod_{j=1}^N |(a+\gamma_j+ib)|}{\prod_{j=1}^N \gamma_j},& \\
\implies {S_1^+}'(\tilde{x}_1) > 1,&
\end{aligned}
$$

where $\tilde{x}$ is either $\bar{x}_{inf}^+$ or $\bar{x}_{sup}^+$. Hence, there is a contradiction. It follows that $\bar{x}_{inf}^+$ and $\bar{x}_{sup}^+$ are locally stable. □

Some global results can also be determined for both loops.

3.2.5 Monotone dynamical systems

A dynamical system defined in an ordered metric space is called monotone if its flow $\Phi_t(x)$ preserves a partial order denoted $\leq$ [67]. In other words, if two initial conditions x and y are such that $x \leq y$, then $\Phi_t(x) \leq \Phi_t(y)$ for any $t \geq 0$.

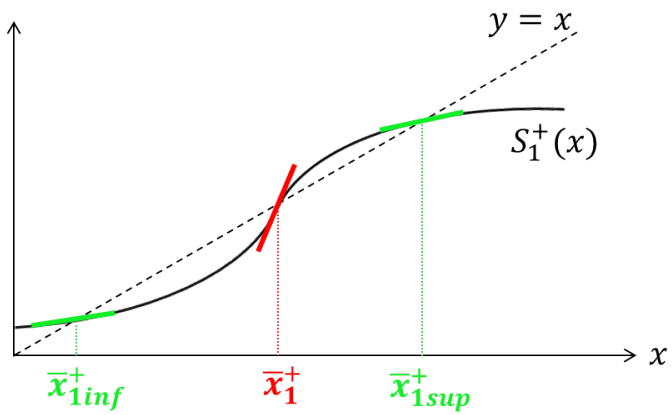

Figure 3.2.5: Illustration of the fixed points of $S_1^+(x)$.

Within the class of ordinary differential equations, cooperative systems are known to generate a monotone flow. More precisely, if the following ordinary differential equation

$$\dot{x} = f(x)$$

is such that $\mathrm{d}f_i/\mathrm{d}x_j(x) \geq 0$ for any $i \neq j$, then the system is cooperative. Due to order preserving, these systems have nice and really convenient global properties regarding convergence and stability, for which chaotic and irregular behaviors are ruled out. In particular, convergence towards the set of steady states becomes generic, meaning that "almost" all trajectories converge towards the set of steady states. More precisely, it has been shown under appropriate conditions that, if a cooperative system has a unique steady state, then this steady state is globally asymptotically stable [71, 34, 72]. Moreover, with good conditions, these systems cannot have attracting periodic orbits (see [109] for exhaustive results about cooperative systems and [108] or [111] for a comprehensive review about monotone systems).

The theory of monotone dynamical systems has been largely applied to biological problems. For example, population dynamics and biological interaction networks are usually well explained with cooperative systems. In particular, it is straightforward to see that the positive feedback loop (3.2.1) is a cooperative dynamical system as well. It follows that, if the dynamical system of the positive loop has a unique steady state, then this steady state is globally asymptotically stable. Moreover, if the dynamical system has three steady states $\bar{x}^+$, $\bar{x}_{inf}^+$ and $\bar{x}_{sup}^+$, almost all the trajectories will converge towards one of the two locally stable steady states $\bar{x}_{inf}^+$ and $\bar{x}_{sup}^+$. This bistable system properly models cell differentiation processes and cell decision making that emerge in biology from genetic positive feedback loops, as introduced in chapter 2. From an undifferentiated state, represented by the unstable steady state $\bar{x}^+$, a cell may differentiate into one type or another type by converging either towards the first stable steady state $\bar{x}_{inf}^+$ or the second stable steady state $\bar{x}_{sup}^+$.

More recently, the theory of monotone, and in particular cooperative systems, has been extended to systems with inputs and outputs, also called monotone control systems (see [111]). With this new framework, a non-monotone system may be decomposed into several interconnected monotone input systems [111, 11]. Under appropriate conditions, these feedback systems are able to recover many of the global convergence properties of classical monotone systems, such as global asymptotic stability of steady states [12], or multi-stability [13].

The dynamical system of negative feedback loops (3.2.1) is not a cooperative dynamical system. However, it is possible to show that if N is odd, it is part of the class of competitive dynamical

systems that satisfy $\mathrm{d}f_i/\mathrm{d}x_j(x) \leq 0$ for any $i \neq j$. It is easy to understand that competitive systems are cooperative systems by time reversal. However, they do not satisfy the strong global results about generic convergence towards steady states. It follows that for negative feedback loops, other arguments and model classes are needed for global dynamical properties.

3.2.6 Monotone cyclic feedback systems

Monotone cyclic feedback systems are defined as:

$$\dot{x}_i = f_i(x_i, x_{i-1}),\ \forall\ i \in \{1, ..., N\}\,,$$

with

$$\delta_i \frac{\partial f_i(x_i, x_{i-1})}{\partial x_{i-1}} \geq 0\ \forall\ i \in \{1, ..., N\}\,,$$

where $\delta_i \in \{+1, -1\}$. Basically, the system is said to be monotone as each variable monotonically influences and interacts with one of the other variable in the system. As for the general type of genetic feedback loops, these systems divide in two groups depending on the value of $\Delta = \prod_{i=1}^{N} \delta_i$. If $\Delta = +1$, the system is a positive feedback loop and is part of the class of cooperative dynamical systems, as introduced in the previous section. If $\Delta = -1$, the system is a negative feedback loop with a unique steady state. The canonical genetic negative feedback loop presented in (3.2.1) is then a monotone cyclic feedback system with $\Delta = -1$. In dimension 2, the examination of the Jacobian matrix and the use of classic theorems such as Poincare-Bendixson and Bendixson-Dulac, prove the global stability of the steady state and appropriate conditions on the parameters can be determined for the emergence of damped oscillations. In dimension greater than 2 the dynamics is much more complex but a couple of results exist thanks to the theory of monotone cyclic feedback systems. In particular, the theorem of Poincare-Bendixson that exists for planar systems has been extended: basically, a trajectory of a monotone cyclic feedback system with $\Delta = -1$ may either converge towards a steady state or a periodic orbit. Any chaotic, homoclinic or heteroclinic orbits are ruled out [83]. Depending on the relation between parameters, more specific global results may be proved: global stability of the steady state under sufficient conditions [8, 105, 121], and emergence of periodic solutions [66, 57, 86]. These two main dynamics properly capture the observed biological behaviors of negative feedback loops, as introduced in chapter 2: homeostasis and sustained oscillations.

3.2.7 Numerical illustrations

Figures 3.2.6 and 3.2.7 respectively simulate the canonical model (3.2.1) for the negative loop in dimension 3 and the positive loop in dimension 2. As expected from analytical results, the negative loop displays two distinct behaviors depending on the parameters: either homeostasis through a global convergence towards its unique steady state $\bar{x}^-$ (see the left plot in figure 3.2.6), or sustained oscillations through the emergence of a globally stable periodic orbit (see the right plot in figure 3.2.6). Similarly, the positive loop displays either a unique globally asymptotically stable steady state (see the left plot of figure 3.2.7), or a decision and differentiation process through the emergence of bistability (see the right plot of figure 3.2.7).

3.3 Piecewise affine differential systems

In order to tackle analytical problems or in case of a lack of detailed information about reaction mechanisms, gene regulatory non-linear ODE models may be simplified and approximated. For this purpose, Leon Glass was the first to introduce in the 1970s the so-called Piecewise Linear (PWL) differential systems, or Glass systems, that approximate non-linear regulations such as Hill functions, by piecewise linear functions [56]. This approximation turns up when the steepness parameter n of a Hill function is considered large enough, leading to a discontinuous step function, also called Heaviside function (see figure 3.3.1):

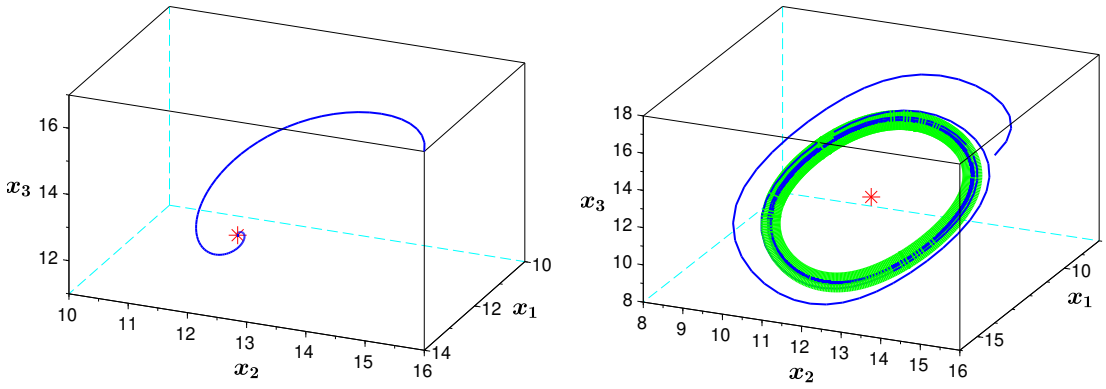

Figure 3.2.6: Simulation of system (3.2.1) for a canonical negative loop in dimension 3. For both plots, the blue line is a trajectory of system (3.2.1) with initial condition $(14, 16, 17)$, and the unique steady state $\bar{x}^- = (12, 12, 12)$ is depicted by a red star. Left: the parameters are $\kappa_{0i} = 2$, $\kappa_i = 8$, $\gamma_i = 0.5$, $\theta_i = 12$ and $n_i = 3$, $\forall\ i \in \{1, 2, 3\}$. The trajectory converges towards $\bar{x}^-$. Right: the parameters are $\kappa_{0i} = 2$, $\kappa_i = 8$, $\gamma_i = 0.5$, $\theta_i = 12$ and $n_i = 7$, $\forall\ i \in \{1, 2, 3\}$. The trajectory converges towards a periodic orbit highlighted by a green line.

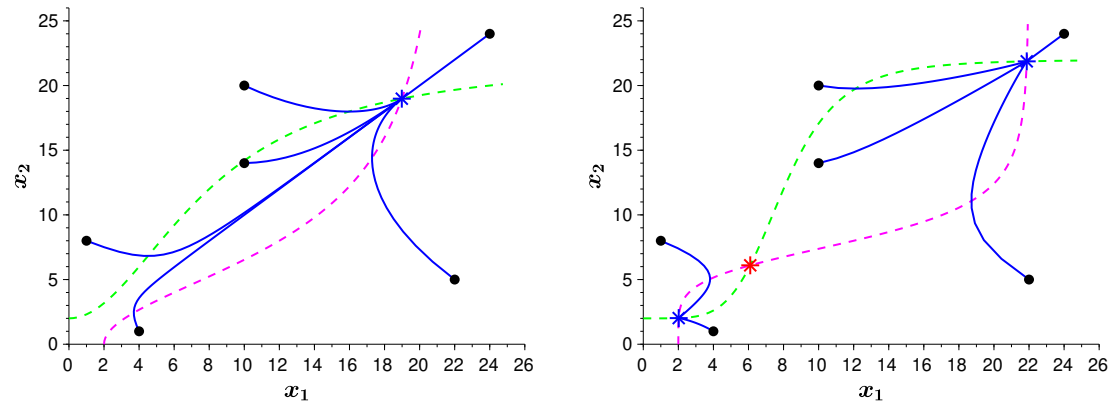

Figure 3.2.7: Simulation of system (3.2.1) for a canonical positive loop in dimension 2. For both plots, the dashed green (resp. magenta) line is the x_2-nullcline (resp. x_1-nullcline). The blue lines are trajectories of system (3.2.1) with different initial conditions depicted by black dots. Left: the parameters are $\kappa_{0i} = 2$, $\kappa_i = 20$, $\gamma_i = 1$, $\theta_i = 8$ and $n_i = 2$, $\forall\ i \in \{1, 2\}$. The unique stable steady state $\bar{x}^+_{sup} = (18.98, 18.98)$ is represented by a blue star and all the trajectories converge towards it. Right: the parameters are $\kappa_{0i} = 2$, $\kappa_i = 20$, $\gamma_i = 1$, $\theta_i = 8$ and $n_i = 5$, $\forall\ i \in \{1, 2\}$. The two stable steady states $\bar{x}^+_{inf} = (2.02, 2.02)$ and $\bar{x}^+_{sup} = (21.87, 21.87)$ are represented by blue stars and $\bar{x}^+ = (6.1, 6.1)$ is represented by the red star. The trajectories converge towards one of the two stable steady states.

$$\lim_{n \to +\infty} \mathrm{h}^*(x, \theta, n) = \mathrm{s}^*(x, \theta),$$

where

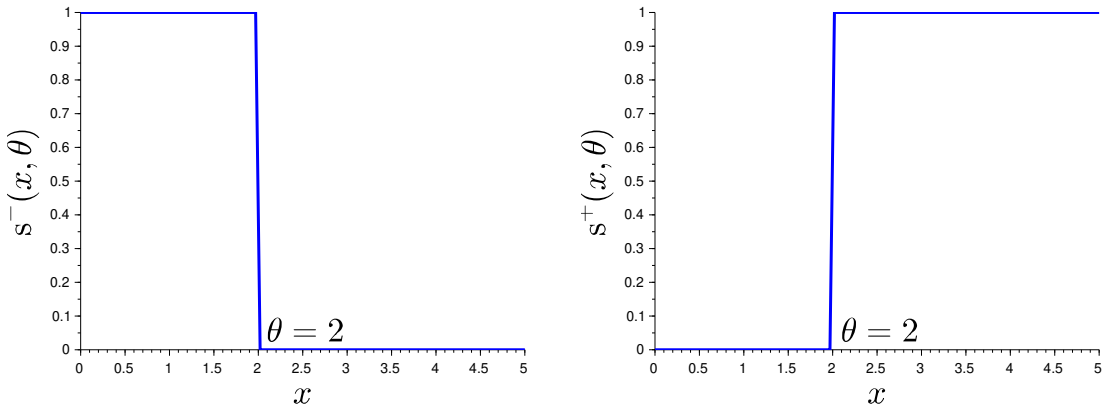

Figure 3.3.1: Decreasing (left) and increasing (right) step functions.

$$\begin{cases} \mathrm{s}^+(x,\theta) = 0 \text{ if } x < \theta, \\ \mathrm{s}^+(x,\theta) = 1 \text{ if } x > \theta, \end{cases}$$

and

$$\begin{cases} \mathrm{s}^-(x,\theta) = 1 \text{ if } x < \theta, \\ \mathrm{s}^-(x,\theta) = 0 \text{ if } x > \theta. \end{cases}$$

In this framework, the interaction between two proteins becomes an on-off process regulated by the constant threshold θ. The biological feedback loop model (3.2.1) becomes:

$$\begin{cases} \dot{x}_1(x_1, x_N) = \kappa_{01} + \kappa_1 \mathrm{s}^*(x_N, \theta_N) - \gamma_1 x_1, \\ \dot{x}_i(x_i, x_{i-1}) = \kappa_{0i} + \kappa_i \mathrm{s}^+(x_{i-1}, \theta_{i-1}) - \gamma_i x_i \quad \forall\, i \in \{2, ..., N\}. \end{cases}$$

These simplifications are reasonable as many gene interactions behave like a switch. Although these types of models have historically emerged for describing physical processes, such as classical mechanics problems for example, they are nowadays widely applied for various biological applications. In neuroscience for example, dynamical systems with autonomous state jumps are extensively used to model neuron dynamics [22].

For the analysis of PWL systems, the state space is traditionally divided into so called "regular" and "switching" domains. Indeed, as step functions are not defined at threshold points, neither is the vector field uniquely defined in the state space. Hence, regular domains consist in regions of the state space where the vector field is uniquely defined: for example $x_i < \theta_i \; \forall\, i \in \{1, ..., N\}$. In regular domains, the differential system is equivalent to a linear system for which analytical solutions can explicitly be calculated. Conversely, switching domains consist in any region where at least one variable is at a threshold point. In this case, the vector field is not defined and classical theory of dynamical systems is not sufficient to determine the qualitative behavior of trajectories. For this purpose, the theory of Filippov has been developed and allows to appropriately define solutions of the PWL differential system [47]. Basically, this theory considers all the possible directions for the trajectories on the switching domain by defining the vector field on the switching domain as the closed convex hull of all possible vector fields. For example, if $x_j = \theta_j$ and all the other variables are such that $x_i \neq \theta_i$ for $i \neq j$, then the extended vector field is defined as:

$$\dot{x} \in H(x)$$

where

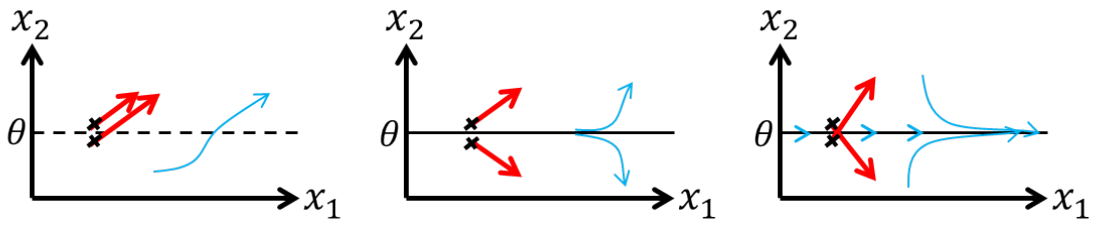

Figure 3.3.2: For all the sketches, the red arrows are vector fields on both sides of a switching domain $x_2 = \theta$ and the blue arrows are trajectories. Left: illustration of a transparent wall that trajectories can cross. Middle: illustration of a white wall that repels all the trajectories. Right: illustration of a black wall that attracts all the trajectories, leading to sliding mode solutions.

$$H(x) = \bar{\text{co}} \left\{ \begin{pmatrix} \dot{x}_1(x_1, x_N) \\ \vdots \\ \kappa_{0j} + \kappa_j - \gamma_j \theta_j \\ \vdots \\ \dot{x}_N(x_N, x_{N-1}) \end{pmatrix}, \begin{pmatrix} \dot{x}_1(x_1, x_N) \\ \vdots \\ \kappa_{0j} - \gamma_j \theta_j \\ \vdots \\ \dot{x}_N(x_N, x_{N-1}) \end{pmatrix} \right\}$$

is the closed convex hull of the set of vector fields. Intuitively, if the vector field on both sides of the switching domain points in the same direction transversely to the switching domain, then the trajectories just cross the switching domain: this type of switching domain is called a transparent wall (see the left sketch in figure 3.3.2). Conversely, if the vector field on both sides of the switching domain points in opposite direction transversely to the switching domain, two cases are distinguished. First, if the vector fields point away from the switching domain, the trajectories cannot reach the switching domain from the adjacent regular domains, and a trajectory starting on the switching domain can reach both adjacent regular domains: this type of switching domain is called a white wall (see the middle sketch in figure 3.3.2). Second, if the vector fields point towards the switching domain, the trajectories can reach the switching domain but a trajectory starting on the switching domain cannot reach any adjacent regular domains: this type of switching domain is called a black wall, and the trajectories emerging from black walls are called "sliding modes" (see the right sketch in figure 3.3.2). These transitions between regular domains are often represented in a transition graph from which qualitative information about dynamics can be deduced.

Most of the time, these systems preserve the main features of the dynamics of their non-linear ordinary version [29], and allow analytical work such as existence of periodic orbits [58, 43, 44], sometimes leading to global results [37]. For example, under good hypotheses on the parameters, such as $\gamma_i = \gamma \ \forall \ i \in \{1, ..., N\}$, uniqueness of periodic orbits for negative loops has been proved [98, 99]. Similarly, under good conditions, the existence of periodic orbits has been shown in [39] for PWL gene regulatory networks with delays. Even if in many cases it has been observed that the qualitative behavior of the non-linear and PWL solutions are similar, some differences may sometimes emerge: for example, when the Hill steepness coefficient n is not large enough in non-linear models, the qualitative trajectories between the two models may differ, sometimes leading to oscillations for the non-linear model and a stable equilibrium for its PWL counterpart [97, 102].

Figure 3.3.3 simulates the PWL version of the canonical model (3.2.1) for the negative loop in dimension 3 and the positive loop in dimension 2. The PWL models are still able to reproduce sustained oscillations for the negative loop and bistability for the positive loop. It is possible to observe that the trajectories are solutions of a linear system in each regular domain, and that the vector field switches in each switching domain.

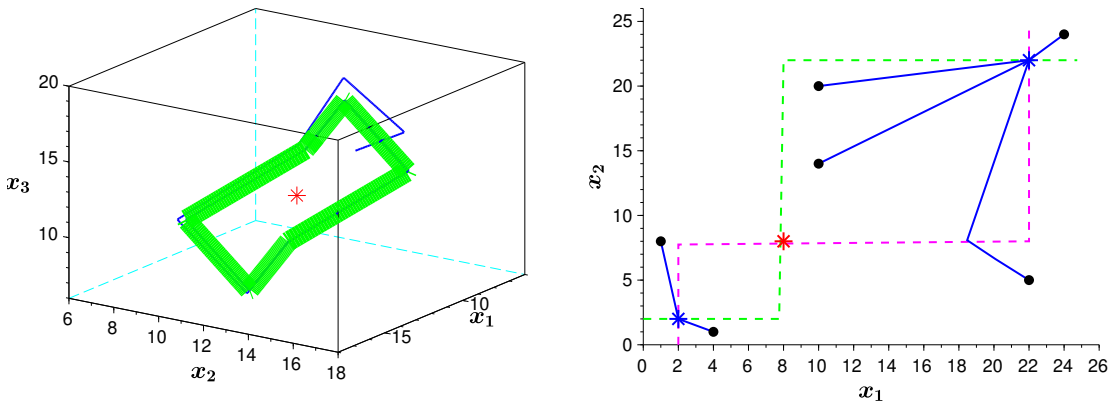

Figure 3.3.3: Left: simulation of the PWL version of system (3.2.1) for a canonical negative loop in dimension 3. The parameters are $\kappa_{0i} = 2$, $\kappa_i = 8$, $\gamma_i = 0.5$ and $\theta_i = 12 \ \forall \ i \in \{1, 2, 3\}$. The trajectory with initial condition $x_0 = (14, 16, 17)$ represented by a blue line converges towards a periodic orbit highlighted by a green line. Right: simulation of the PWL version of system (3.2.1) for a canonical positive loop in dimension 2. The dashed green (resp. magenta) line is the x_2-nullcline (resp. x_1-nullcline). The blue lines are trajectories of system (3.2.1) with different initial conditions depicted by black dots. The parameters are $\kappa_{0i} = 2$, $\kappa_i = 20$, $\gamma_i = 1$ and $\theta_i = 8 \ \forall \ i \in \{1, 2\}$. The two stable steady states $\bar{x}^+_{inf} = (2, 2)$ and $\bar{x}^+_{sup} = (22, 22)$ are represented by blue stars and $\bar{x}^+ = (8, 8)$ is represented by the red star. The trajectories converge towards one of the two stable steady states.

3.4 Boolean systems

It is possible to go even further in the simplification of non-linear ordinary differential equations for gene regulatory networks. As a strong hypothesis, a gene may be considered to have two states: one active (1) and one inactive (0). In this case, the system can be described in purely logical terms where interactions between proteins are modeled by Boolean functions. In this boolean framework, the state of the system $(x_1, ..., x_N)$ is a vector of boolean entries $x_i \in \{0, 1\} \ \forall \ i \in \{1, ..., N\}$. From these states, a successor map can be written as a transition rule with mainly three logical operators: $\vee$ ("or"), $\wedge$ ("and"), and $\neg$ ("not") [114, 74].

With iteration maps, several variables may change state at the same time. For example, with two variables x_1 and x_2 and the successor map $F(x_1, x_2) = (\neg x_2, \neg x_1)$, the successor of the state (00) is (11). This is called "synchronous" dynamics. However, most of the time in biology this evolution is not realistic as there may exist different time-scales or delays in the real biological system, and it is highly unlikely that several variables change at the same time precisely. To deal with this reality, a lot of models consider "asynchronous" dynamics, for which only one variable is allowed to change state at each iteration. In this case, a state can have several successors. With the same example, the successor of (00) is either (01) or (10). By studying the graph of transitions between states, some dynamical properties such as steady states or periodic orbits may emerge.

These types of models have been widely used and give a first simple and qualitative insight into genetic dynamics.

To illustrate that qualitative dynamics of ODE systems may be partially recovered by boolean networks, the boolean model of the canonical negative feedback loop in dimension 3 is investigated. The successor map is simply: $F(x_1, x_2, x_3) = (\neg x_3, x_1, x_2)$. The synchronous and asynchronous truth tables can be constructed:

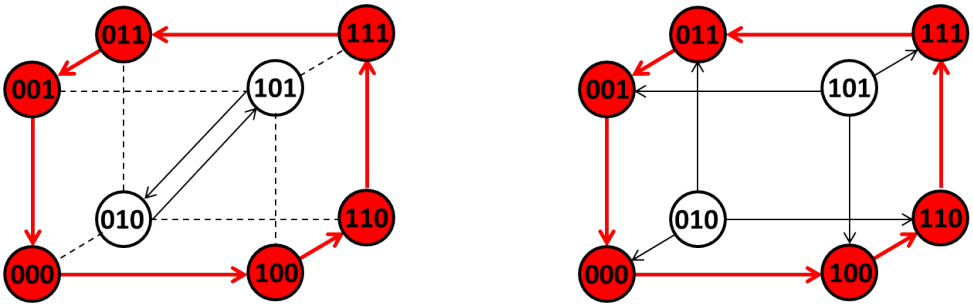

Figure 3.4.1: Transition graph of the synchronous (left) and asynchronous (right) analysis of the boolean model for the canonical negative loop in dimension 3. The periodic orbit is highlighted in red.

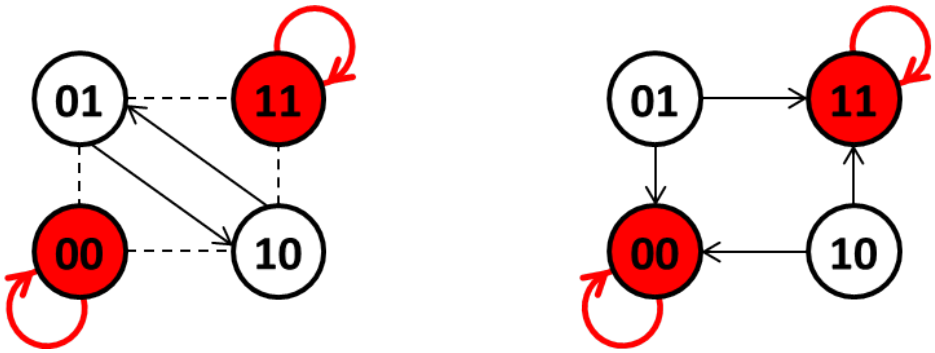

Figure 3.4.2: Transition graph of the synchronous (left) and asynchronous (right) analysis of the boolean model for the canonical positive loop in dimension 2. The bistability is highlighted in red.

000	$\to$	100	000	$\to$	100
001	$\to$	000	001	$\to$	000
010	$\to$	101	010	$\to$	$\{110, 001, 011\}$
011	$\to$	001	011	$\to$	001
100	$\to$	110	100	$\to$	110
101	$\to$	010	101	$\to$	$\{001, 111, 100\}$
110	$\to$	111	110	$\to$	111
111	$\to$	011	111	$\to$	011

The transition graphs obtained for both the synchronous and asynchronous analysis are presented in figure 3.4.1. As expected, the asynchronous dynamics allows to be obtained a globally attractive periodic orbit, giving a good qualitative insight on the negative feedback loop dynamics.
The same analysis can be made for the boolean model of the canonical positive feedback loop in dimension 2. The successor map is: $F(x_1, x_2) = (x_2, x_1)$. Again, the synchronous and asynchronous truth tables can be constructed:

00	$\to$	00	00	$\to$	00
01	$\to$	10	01	$\to$	$\{00, 11\}$
10	$\to$	01	10	$\to$	$\{00, 11\}$
11	$\to$	11	11	$\to$	11

The transition graphs obtained for both the synchronous and asynchronous analysis are presented in figure 3.4.2. As expected, the asynchronous dynamics allows bistability with two locally stable states (00) and (11) that respectively represent a state where both proteins are not expressed, and a state where both proteins are fully expressed.

More generally, many qualitative properties can be deduced from generic Boolean models by looking at the interaction graph between variables [30]. For example, two strong general results were conjectured by René Thomas in the 1990s (see [114] for more details):

- if the system is bistable, then its interaction graph must contain at least a positive loop,
- if the system has a stable periodic orbit, then its interaction graph must contain at least a negative loop.

These results have been rigorously proved for dynamical systems [60]. As usual the interaction graph is the easiest information to obtain, these general results give useful information about dynamical features: for example, if there is no negative loop between genes in an interaction graph, then the system cannot exhibit sustained oscillations.

3.5 Conclusion

As explained in chapter 2, both positive and negative biological feedback loops play an essential role in several biological functions and diseases. In this context, the next chapters present different biologically relevant strategies for the control of these two motifs.

In order to stay as close as possible to the real biological context, the genetic dynamical model is kept as exhaustive and general as possible throughout the whole manuscript, leading to the analysis of the highly non-linear differential system (3.2.1).

The positive feedback system (3.2.1) is supposed to model a cell differentiation process in the rest of the manuscript, as observed in biology. For this reason, it is assumed that the parameters of the positive feedback system (3.2.1) generate three steady states $\bar{x}^+_{sup}$, $\bar{x}^+_{inf}$ and $\bar{x}^+$. The different control strategies have been designed in order to mimic a biological dedifferentiation process, highly promising for pharmacological treatments. From the mathematical point of view, this dedifferentiation process is achieved if the control strategy is able to globally stabilize the undifferentiated state $\bar{x}^+$.

From chapters 4 to 8, the negative feedback system (3.2.1) is supposed to model a disrupted homeostatic circuit that displays a dyshomeostasis, as discussed in chapter 2. For this reason, it is assumed that the parameters of the negative feedback system (3.2.1) generate at least a locally stable periodic orbit leading to undesired sustained oscillations. The different control strategies have been designed in order to suppress undesired periodic behaviors and recover stable biological conditions. From the mathematical point of view, this process is achieved if the control strategy is able to globally stabilize the homeostatic state $\bar{x}^-$. Conversely, in chapter 9, the negative feedback system (3.2.1) is supposed to model a disrupted biological clock, that displays unhealthy and abnormal arrhythmic behavior. For this purpose it will be assumed that the parameters of the negative system (3.2.1) generate a global asymptotic convergence towards the homeostatic state $\bar{x}^-$. Two different control strategies have been designed in order to generate sustained oscillations and recover a functional biological clock.

Chapter 4

Classical control strategy

4.1 Introduction

Control theory is a branch of mathematics that aims at designing appropriate control strategies in order to force a dynamical system to follow a desired output objective.

Historically, classical control theory has been developed for the control of continuous time linear systems or non linear systems linearized around a state of interest. For these types of problems, a lot of theoretical results have been produced and are still widely used nowadays, especially for industrial applications [35]. Usually, linear control systems in the time domain in the form of ODEs can be characterized in the frequency domain through Laplace transforms in order to simplify their manipulations [35]. For industrial control systems, classical control mechanisms such as P (Proportional), PI (Proportional Integral) or PID (Proportional Integral Derivative) controllers are still extensively used. Basically, these controllers calculate in real time the error $e(t)$ between the measured output of the controlled system and the desired tracked objective. From this continuous time error signal, the correction applied by the controller on the system may be proportional to three control terms: the past values of the error signal estimated via an integral calculation (I), the present value of the error signal (P), and the potential future values of the error signal estimated via the computation of its derivative (D). Due to good theoretical properties, such as zero steady state error or moderate overshoots, PID controllers are extensively designed in industrial control problems (for more details about classical control theory, see [35]). However, the three coefficients needed for the derivative, proportional and integral terms, also called gains, may be complex to tune, limiting their use in biology. Instead, many practical applications in synthetic biology have been developing PI controllers capable of producing precise and robust output levels even in case of model uncertainties and external perturbations [80, 87, 116, 50, 49, 88, 48, 63, 64]. Unfortunately, these analytical results are only valid for either linear systems which are not biologically realistic, or tangent linear approximations of non-linear systems leading to only local validity of the control properties. In this chapter, a new methodology will be developed in order to obtain a robust classical control strategy with global results.

Control problems can be divided in two families: open and closed loop systems. In open loop control systems, the control strategy is applied without having any knowledge and feedback about the output and the time dynamics of the controlled system. Conversely, a closed loop controller uses feedback and outputs provided by sensors and measurement tools. If open loop controllers may be well adapted for engineering systems with perfectly known models that always work in normal conditions, they often fail in biological systems due to uncertain models and inherent intracellular fluctuations. Closed loop systems however are able to guarantee performance results even in case of uncertainties and external perturbations. For this purpose, only closed loop control strategies will be designed in this manuscript.

Similarly, MIMO (multi-input multi-output) and SISO (single-input single output) controlled systems can be distinguished. As their names indicate, MIMO systems may have several inputs and outputs whereas SISO systems is only composed of a unique input and a unique output. In the biological context of this manuscript, only SISO systems will be treated in order to minimize the number of measurement and control tools needed. These constraints aim at simplifying a potential biological application.

In this context, a simple affine control law is designed in this chapter in order to stabilize a negative feedback loop that displays a dyshomeostasis, and a positive feedback loop for the design of a dedifferentiation process. The control strategy only depends on the measurement of a unique gene and only acts on a unique genetic interaction. From a biological point of view, this simple control guarantees a minimal biological set-up and helps reducing the complexity of measurement and control devices. A new methodology is presented in order to prove that this simple control law stabilizes the unstable steady state $\bar{x}^*$ of the uncontrolled system. The proof is based on the construction of successive repelling nested hyperrectangles that act as Lyapunov function level-sets.

The control strategy is introduced in section 4.2 and the new methodology about global convergence and stability is presented in section 4.3. In section 4.4, the controlled system is shown to be composed of sigmoid functions, a key property in order to apply the results from section 4.3. Finally, section 4.5 shows that the affine control strategy leads to global stabilization of the steady state, and this result is illustrated with numerical simulations in section 4.6.

The content of this chapter concerning the negative feedback loop can be found in the article published for the conference CDC (see the section "List of publications" in page 5).

4.2 The controlled model

The selected control consists of a classical affine law:

$$\mathrm{u}(x_1) = -\alpha(x_1 - \bar{x}_1^*) + 1, \tag{4.2.1}$$

with $\alpha > 0$, that only depends on the measurement of the first gene x_1 and acts on its production as the following:

$$\begin{cases} \dot{x}_1(x_1, x_N) = \kappa_{01} + \mathrm{u}(x_1)\kappa_1 \mathrm{h}^*(x_N, \theta_N, n_N) - \gamma_1 x_1, \\ \dot{x}_i(x_i, x_{i-1}) = \kappa_{0i} + \kappa_i \mathrm{h}^+(x_{i-1}, \theta_{i-1}, n_{i-1}) - \gamma_i x_i \quad \forall\, i \in \{2, ..., N\}. \end{cases} \tag{4.2.2}$$

This law depends on the estimation error $(x_1 - \bar{x}_1^*)$ and can take both positive and negative values (see figure 4.2.1). The constant $+1$ has been fixed in order to preserve $\bar{x}^*$ as a steady state:

Proposition 4.2.1. *The steady state $\bar{x}^*$ of system (3.2.1) is also a steady state of system (4.2.2) under control (4.2.1). Moreover, for the negative loop, this steady state is unique.*

Proof. As $\mathrm{u}(\bar{x}_1^*) = 1$, it is easy to check that the steady state $\bar{x}^*$ of system (3.2.1) is a steady state of system (4.2.2) under control (4.2.1). For the uniqueness, it is possible to write the equations of the steady states as done previously for the uncontrolled system:

$$\begin{cases} \bar{x}_1^* = \dfrac{\kappa_{01} + \kappa_1 \mathrm{h}^*(\bar{x}_N^*, \theta_N, n_N)(1 + \alpha \bar{x}_1^*)}{\gamma_1 + \alpha \kappa_1 \mathrm{h}^*(\bar{x}_N^*, \theta_N, n_N)} = H_{1\alpha}^*(\bar{x}_N^*), \\ \bar{x}_i^* = \dfrac{\kappa_{0i} + \kappa_i \mathrm{h}^+(\bar{x}_{i-1}^*, \theta_{i-1}, n_{i-1})}{\gamma_i} = H_i(\bar{x}_{i-1}^*) \quad \forall\, i \in \{2, ..., N\}. \end{cases} \tag{4.2.3}$$

Hence, it is possible to show that $\tilde{x} = (\tilde{x}_1, ..., \tilde{x}_N)$ is a steady state of system (4.2.2) under control (4.2.1) if and only if $\tilde{x}_1$ is a fixed point of the function $S_{1\alpha}^*(x) = H_{1\alpha}^* \circ H_N \circ H_{N-1} \circ ... \circ H_3 \circ H_2(x)$ and $\tilde{x}_i = H_i(\tilde{x}_{i-1})\ \forall\, i \in \{2, ..., N\}$. After performing some calculation, it is possible to show that:

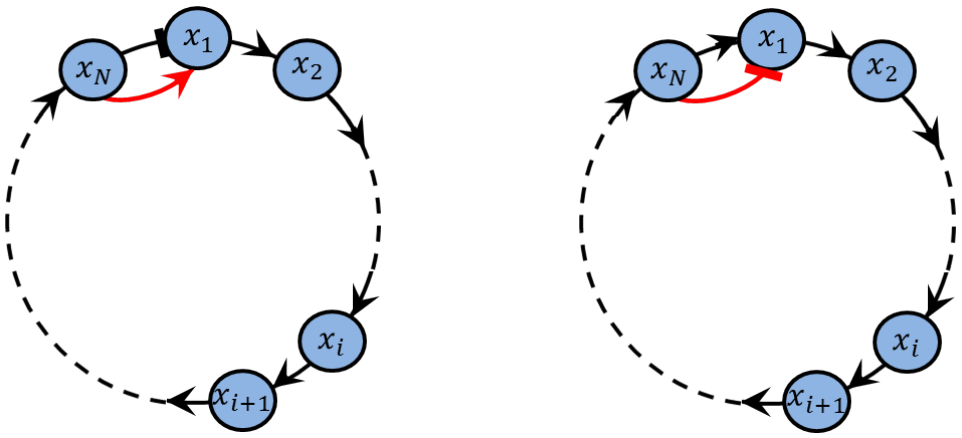

Figure 4.2.1: (Left: negative loop, Right: positive loop). Graph of the uncontrolled system (3.2.1) in black. For system (4.2.2) under control (4.2.1), the graph is the same with the additional red link. In this case, the influence of x_N on x_1 is not fixed: it can either activate or inhibit its production.

$$H_{1\alpha}^{*\prime}(x) = \kappa_1 \frac{\partial \mathrm{h}^*(x, \theta_N, n_N)}{\partial x} \frac{\alpha(\gamma_1 \bar{x}_1^* - \kappa_{01}) + \gamma_1}{(\gamma_1 + \alpha\kappa_1 \mathrm{h}^*(x, \theta_N, n_N))^2}.$$

From proposition 3.2.8, $\bar{x}_1^* > \kappa_{01}/\gamma_1$, inducing $\gamma_1 \bar{x}_1^* - \kappa_{01} > 0$. Moreover, from the properties of Hill functions, $\partial \mathrm{h}^+(x, \theta_N, n_N)/\partial x \geq 0$ and $\partial \mathrm{h}^-(x, \theta_N, n_N)/\partial x \leq 0$. Hence, $H_{1\alpha}^{+\prime}(x) \geq 0$, $H_{1\alpha}^{-\prime}(x) \leq 0$ (it is equal to zero only for $x = 0$), inducing that $H_{1\alpha}^{-}(x)$ is strictly monotonically decreasing and $H_{1\alpha}^{+}(x)$ is strictly monotonically increasing. As a consequence, $S_{1\alpha}^{-}(x)$ is strictly monotonically decreasing as it is the composition of $N-1$ strictly monotonically increasing functions and one strictly monotonically decreasing function. As already explained in section 3.2.3 of chapter 3, the function $S_{1\alpha}^{-}(x)$ can intersect only once the linear function $y = x$ for the negative loop. Finally, $\bar{x}^-$ is the unique steady state of system (4.2.2) for the negative loop. For the positive loop, $S_{1\alpha}^{+}(x)$ is strictly monotonically increasing as it is the composition of N strictly monotonically increasing functions. Hence, the function $S_{1\alpha}^{+}(x)$ can intersect more than once the linear function $y = x$, and $\bar{x}^+$ may not be the unique steady state of system (4.2.2) for the positive loop. □

Under good conditions, it may be possible to show that this affine control law is able to locally stabilize $\bar{x}^*$ with classical control theory [35]. However, the goal here is more challenging, and consists in finding conditions on α such that $\bar{x}^*$ becomes globally asymptotically stable (GAS).

The next section presents a new methodology and gives sufficient conditions on system (4.2.2) such that the steady state $\bar{x}^*$ becomes GAS.

4.3 A new methodology for global results

This methodology is similar to the one developed in [8] or in [12] for SISO monotone dynamical systems. However, system (4.2.2) under control (4.2.1) does not have the appropriate conditions and structure in order to apply the results presented in these two previous studies. Indeed in [8], the first equation must be of the form $\dot{x}_1 = h_N(x_N) - k_1(x_1)$, where the degradation $k_1(x)$ is a positive continuous strictly increasing function that only depends on x_1 and the production $h_N(x)$ is a positive continuous monotonic function that depends on x_N only. However, the first equation in system (4.2.2) under control (4.2.1) is $\dot{x}_1 = \kappa_{01} + (-\alpha(x_1 - \bar{x}_1^*) + 1)\kappa_1 \mathrm{h}^*(x_N, \theta_N, n_N) - \gamma_1 x_1$. After rearrangements, it is possible to observe that the production function has the same features as in [8], but the degradation function depends on both x_1 and x_N. For this reason, similar results as the one presented in [8] are developed for system (4.2.2) under control (4.2.1). The new methodology consists in building consecutive repelling hyperrectangles of the state space.

The condition on system (4.2.2) ensures that these hyperrectangles shrink in all directions around $\bar{x}^*$, so that the dynamics is trapped and cannot do anything else than converging towards $\bar{x}^*$. Basically, this technique is similar to the construction of Lyapunov function level-sets. In the end, the determination of the global stability of $\bar{x}^*$ will be directly related to the number of fixed points of two specific functions: $S^+_{1\alpha}$ for the positive loop, and a function called $F^-_{1\alpha}$ for the negative loop, defined just below:

Definition 4.3.1. *$\forall\ i \in \{1, ..., N\}$, $S^*_{i\alpha}(x) = H_i \circ H_{i-1} \circ ... \circ H^*_{1\alpha} \circ H_N \circ H_{N-1} \circ ... \circ H_{i+2} \circ H_{i+1}(x)$, where $i - 1 = N$ for $i = 1$. Then, $\forall\ i \in \{1, ..., N\}$ the function $F^*_{i\alpha}(x)$ is defined as the composition of $S^*_{i\alpha}(x)$ with itself: $F^*_{i\alpha}(x) = S^*_{i\alpha} \circ S^*_{i\alpha}(x)$. As a reminder, the functions $H_i(x)\ \forall\ i \in \{2, ..., N\}$ are defined in definition 3.2.1 and $H^*_{1\alpha}(x)$ is defined in (4.2.3).*

Some properties about functions $F^*_{i\alpha}(x)$ are given:

Proposition 4.3.1. *$\bar{x}^*_i$ is a fixed point of $S^*_{i\alpha}(x)$ and $F^*_{i\alpha}(x)\ \forall\ i \in \{1, ..., N\}$. Moreover, $S^+_{i\alpha}(x)$ are strictly monotonically increasing functions, $S^-_{i\alpha}(x)$ are strictly monotonically decreasing functions, and $F^*_{i\alpha}(x)$ are strictly monotonically increasing functions.*

Proof. As $\bar{x}^*_1 = H^*_{1\alpha}(\bar{x}^*_N)$ and $\bar{x}^*_i = H_i(\bar{x}^*_{i-1})\ \forall\ i \in \{2, ..., N\}$, it is straightforward to see that $\bar{x}^*_i$ is a fixed point of $S^*_{i\alpha}(x)\ \forall\ i \in \{1, ..., N\}$. As $F^*_{i\alpha}(x)$ is the composition of $S^*_{i\alpha}(x)$ with itself, $\bar{x}^*_i$ is also a fixed point of $F^*_{i\alpha}(x)$. Moreover, $S^+_{i\alpha}(x)$ is strictly monotonically increasing as is the composition of N strictly monotonically increasing functions, and $S^-_{i\alpha}(x)$ is strictly monotonically decreasing as is the composition of $N-1$ strictly monotonically increasing functions and one strictly monotonically decreasing function. For both loops, $F^*_{i\alpha}(x)$ is a strictly monotonically increasing function as it is the composition of $S^*_{i\alpha}(x)$ with itself. □

Proposition 4.3.2. *If there exists $j \in \{1, ..., N\}$ such that $S^*_{j\alpha}(x)$ (resp. $F^*_{j\alpha}(x)$) has a unique fixed point, then $\forall\ i \in \{1, ..., N\}$ $S^*_{i\alpha}(x)$ (resp. $F^*_{i\alpha}(x)$) has a unique fixed point as well, and this fixed point is $\bar{x}^*_i$.*

This proposition is proved by composing carefully nullclines in a special order. The details of this proof can be found in appendix B.1.

Bounds of the state space are now successively defined:

Definition 4.3.2.

- $x^{-1}_{1max} = H^-_{1\alpha}(0)$ *and* $x^{+1}_{1max} = H^+_{1\alpha}(+\infty)$,
- $x^{*1}_{imax} = H_i(x^{*1}_{i-1max})\ \forall\ i \in \{2, ..., N\}$,
- $x^{-1}_{1min} = H^-_{1\alpha}(x^{-1}_{Nmax})$ *and* $x^{+1}_{1min} = H^+_{1\alpha}(0) = \kappa_{01}/\gamma_1$,
- $x^{*1}_{imin} = H_i(x^{*1}_{i-1min})\ \forall\ i \in \{2, ..., N\}$,

where $H^-_{1\alpha}(0) = \big(\kappa_{01} + \kappa_1(1 + \alpha\bar{x}^-_1)\big)/(\gamma_1 + \alpha\kappa_1)$ *and*
$H^+_{1\alpha}(+\infty) = \big(\kappa_{01} + \kappa_1(1 + \alpha\bar{x}^+_1)\big)/(\gamma_1 + \alpha\kappa_1)$. *Then by induction $\forall\ j > 1$, $j \in \mathbb{N}$:*

- $x^{-j}_{1max} = H^-_{1\alpha}(x^{-(j-1)}_{Nmin})$ *and* $x^{+j}_{1max} = H^+_{1\alpha}(x^{+(j-1)}_{Nmax})$,
- $x^{*j}_{imax} = H_i(x^{*j}_{i-1max})\ \forall\ i \in \{2, ..., N\}$,
- $x^{-j}_{1min} = H^-_{1\alpha}(x^{-j}_{Nmax})$ *and* $x^{+j}_{1min} = H^+_{1\alpha}(x^{+(j-1)}_{Nmin})$,
- $x^{*j}_{imin} = H_i(x^{*j}_{i-1min})\ \forall\ i \in \{2, ..., N\}$.

These bounds are illustrated in figure 4.3.1 for the negative loop and figure 4.3.2 for the positive loop.

With the functions introduced in definition 4.3.1, it is easy to prove that the previous bounds can also be defined as:

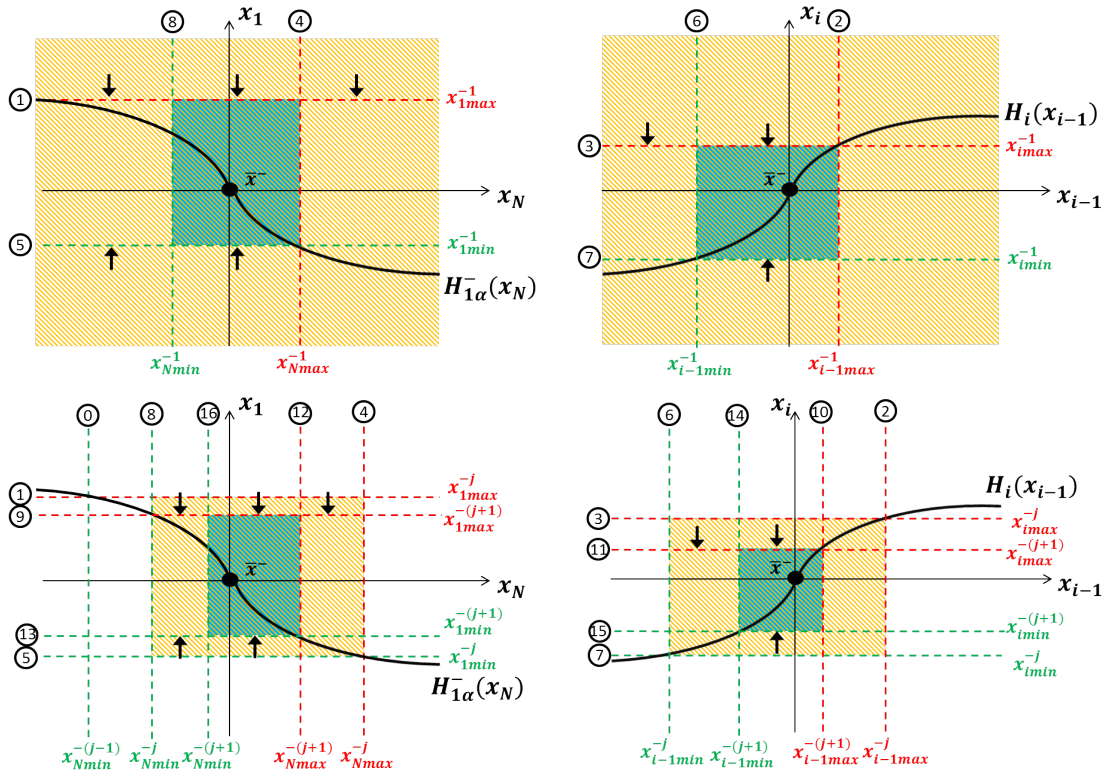

Figure 4.3.1: These four schemes are an illustration of the construction of bounds introduced in definition 4.3.2, the hyperrectangles introduced in definition 4.3.4, and both propositions 4.3.7 and 4.3.8 for the negative loop. Top figures: they initiate the definitions and propositions. The orange rectangles represent $\mathcal{R}_0^-$. The numbers from 1 to 8 on both figures explain the inductions for the construction of the bounds. After step 8, $\mathcal{R}_1^-$ is constructed and is represented by the blue rectangles. It is possible to observe that the vector field at the borders of $\mathcal{R}_1^-$ points inward, illustrating proposition 4.3.7. Moreover, by induction, the black arrows show that any trajectory starting in $\mathcal{R}_0^-$ arrives in finite time in $\mathcal{R}_1^-$, illustrating proposition 4.3.8. Bottom figures: they illustrate the inductive steps of the definitions and propositions. The numbers from 1 to 8 explain the inductions for the construction of the bounds defining $\mathcal{R}_j^-$ (represented by orange rectangles), and the numbers from 9 to 16 explain the inductions for the construction of the bounds defining $\mathcal{R}_{j+1}^-$ (represented by blue rectangles). Again, it is possible to observe that the vector field at the borders of $\mathcal{R}_j^-$ and $\mathcal{R}_{j+1}^-$ points inward, illustrating proposition 4.3.7. Moreover, by induction, the black arrows show that any trajectory starting in $\mathcal{R}_j^-$ arrives in finite time in $\mathcal{R}_{j+1}^-$, illustrating proposition 4.3.8.

Proposition 4.3.3. *$\forall\, j \in \mathbb{N}^*$, and $\forall\, i \in \{1, ..., N\}$: $x_{imax}^{-(j+1)} = F_{i\alpha}^-(x_{imax}^{-j})$, $x_{imin}^{-(j+1)} = F_{i\alpha}^-(x_{imin}^{-j})$, $x_{imax}^{+(j+1)} = S_{i\alpha}^+(x_{imax}^{+j})$, and $x_{imin}^{+(j+1)} = S_{i\alpha}^+(x_{imin}^{+j})$.*

The proof of this proposition is detailed in appendix B.2 and uses the successive construction of the bounds.

For the sake of simplicity, the following notation will be used in the rest of this chapter:

Definition 4.3.3. *$\forall\, i \in \{1, ..., N\}$, $Z_{i\alpha}^*(x)$ is such that $Z_{i\alpha}^+(x) = S_{i\alpha}^+(x)$ and $Z_{i\alpha}^-(x) = F_{i\alpha}^-(x)$.*

The next proposition gives convergence results about sequences defined through function $Z_{i\alpha}^*$:

Proposition 4.3.4. *If $Z_{1\alpha}^*(x)$ has a unique fixed point, then $\forall\, i \in \{1, ..., N\}$, the sequence defined by $x_{imax}^{*(j+1)} = Z_{i\alpha}^*(x_{imax}^{*j})$ with initial term x_{imax}^{*1} (resp. $x_{imin}^{*(j+1)} = Z_{i\alpha}^*(x_{imin}^{*j})$ with initial term x_{imin}^{*1})*

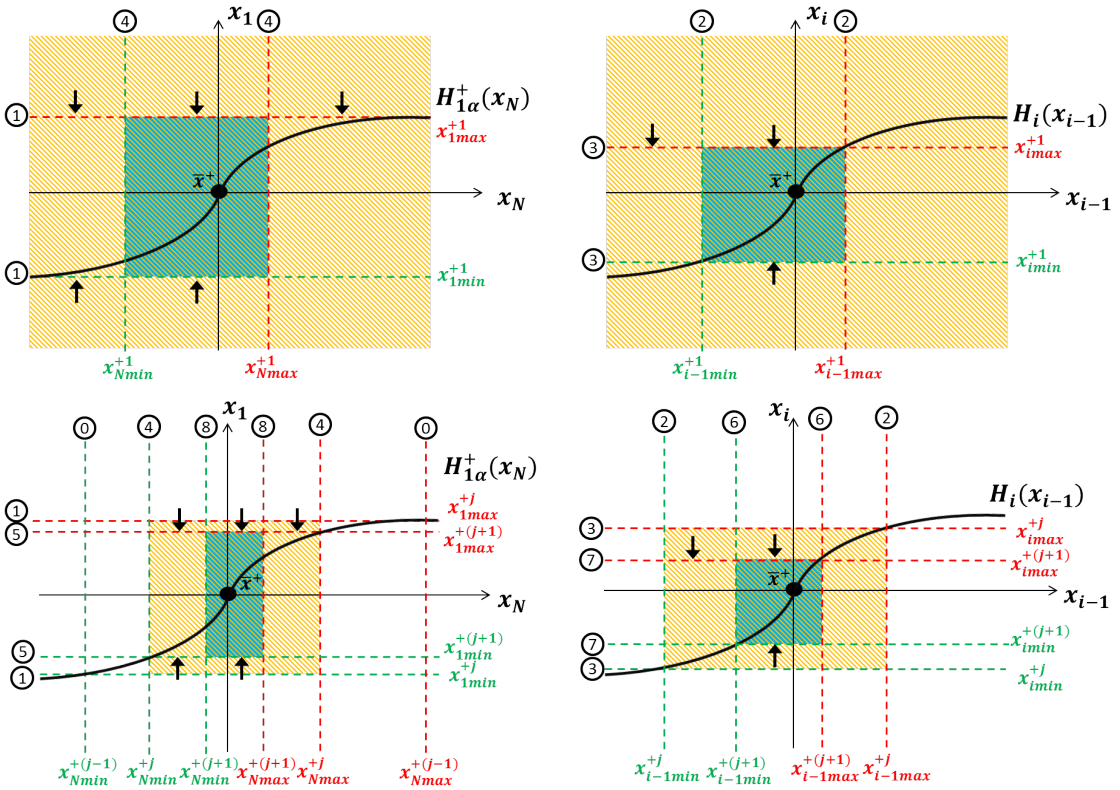

Figure 4.3.2: These four schemes are an illustration of the construction of bounds introduced in definition 4.3.2, the hyperrectangles introduced in definition 4.3.4, and both propositions 4.3.7 and 4.3.8 for the positive loop. Top figures: they initiate the definitions and propositions. The orange rectangles represent $\mathcal{R}_0^+$. The numbers from 1 to 4 on both figures explain the inductions for the construction of the bounds. After step 4, $\mathcal{R}_1^+$ is constructed and is represented by the blue rectangles. It is possible to observe that the vector field at the borders of $\mathcal{R}_1^+$ points inward, illustrating proposition 4.3.8. Moreover, by induction, the black arrows show that any trajectory starting in $\mathcal{R}_0^+$ arrives in finite time in $\mathcal{R}_1^+$, illustrating proposition 4.3.8. Bottom figures: they illustrate the inductive steps of the definitions and propositions. The numbers from 1 to 4 explain the inductions for the construction of the bounds defining $\mathcal{R}_j^+$ (represented by orange rectangles), and the numbers from 5 to 8 explain the inductions for the construction of the bounds defining $\mathcal{R}_{j+1}^+$ (represented by blue rectangles). Again, it is possible to observe that the vector field at the borders of $\mathcal{R}_j^+$ and $\mathcal{R}_{j+1}^+$ points inward, illustrating proposition 4.3.7. Moreover, by induction, the black arrows show that any trajectory starting in $\mathcal{R}_j^+$ arrives in finite time in $\mathcal{R}_{j+1}^+$, illustrating proposition 4.3.8.

is strictly monotonically decreasing (resp. increasing) and converges towards $\bar{x}_i$. *As a consequence,* $\forall\ i \in \{1, ..., N\}$, $x^{*j}_{imin} < \bar{x}_i < x^{*j}_{imax}\ \forall\ j \in \mathbb{N}^*$.

This proposition is easily proved by using the monotonic properties of $Z^*_{i\alpha}(x)\ \forall\ i \in \{1, ..., N\}$ as detailed in appendix B.3 and is illustrated in figure 4.3.3. These sequences of boundaries shape the repelling hyperrectangles mentioned for the methodology:

Definition 4.3.4. *The first hyperrectangle* $\mathcal{R}_0^* = \{x | x_i \geq 0\ \forall\ i \in \{1, ..., N\}\}$ *is the positive orthant. Then* $\forall\ j \in \mathbb{N}^*$, $\mathcal{R}_j^* = \left\{x | x^{*j}_{imin} \leq x_i \leq x^{*j}_{imax}\ \forall\ i \in \{1, ..., N\}\right\}$.

These hyperrectangles are illustrated in figure 4.3.1 for the negative loop and 4.3.2 for the positive loop. They have four principal interesting properties detailed in the four next propositions.

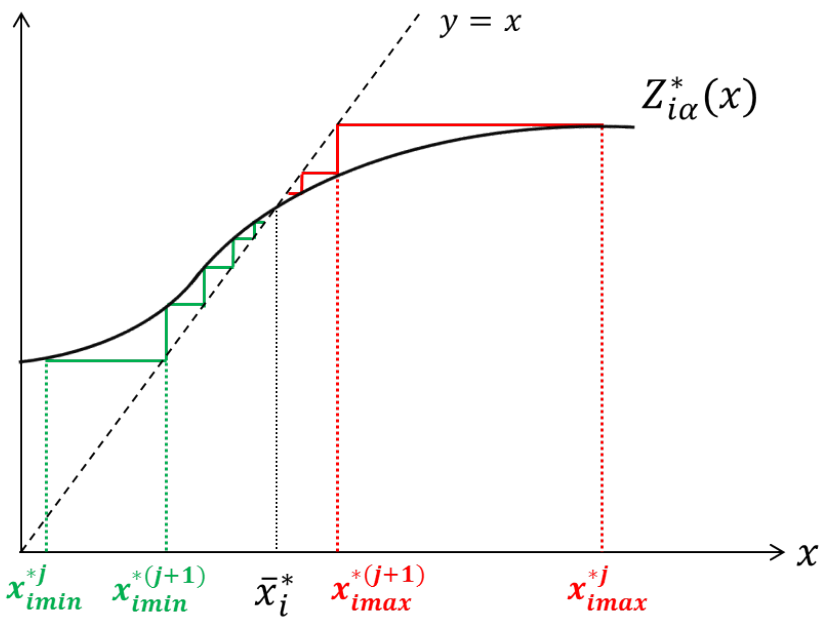

Figure 4.3.3: Illustration of iterations for both sequences: $x^{*(j+1)}_{imax} = Z^*_{i\alpha}(x^{*j}_{imax})$ (in red) with initial term x^{*1}_{imax} and $x^{*(j+1)}_{imin} = Z^*_{i\alpha}(x^{*j}_{imin})$ (in green) with initial term x^{*1}_{imin}, if $Z^*_{1\alpha}(x)$ has a unique fixed point. The two sequences converge towards $\bar{x}^*_i$, with x^{*j}_{imax} decreasing and x^{*j}_{imin} increasing.

Proposition 4.3.5. *If $Z^*_{1\alpha}(x)$ has a unique fixed point, then $\forall\ j \in \mathbb{N}$, $\bar{x}^* \in \mathcal{R}^*_j$.*

Proof. As $\mathcal{R}^*_0$ is the positive orthant, the result for $j = 0$ is straightforward. Moreover, from proposition 4.3.4, $\forall\ j \in \mathbb{N}^*$, $x^{*j}_{imin} < \bar{x}^*_i < x^{*j}_{imax}\ \forall\ i \in \{1, ..., N\}$. Hence, $\forall\ j \in \mathbb{N}^*$, $\bar{x}^* \in \mathcal{R}^*_j$ from definition 4.3.4. □

Proposition 4.3.6. *If $Z^*_{1\alpha}(x)$ has a unique fixed point, then all these hyperrectangles are nested: $\forall\ j \in \mathbb{N}$, $\mathcal{R}^*_{j+1} \subset \mathcal{R}^*_j$ and $\mathcal{R}^*_{j+1} \neq \mathcal{R}^*_j$.*

Proof. First it is straightforward that $\forall\ j \in \mathbb{N}^*$, $\mathcal{R}^*_j \subset \mathcal{R}^*_0$. Now, consider $j \in \mathbb{N}^*$. Let $x \in \mathcal{R}^*_{j+1}$. Then by definition, $x^{*(j+1)}_{imin} \leq x_i \leq x^{*(j+1)}_{imax}\ \forall\ i \in \{1, ..., N\}$. Hence, from proposition 4.3.4, $x^{*j}_{imin} < x^{*(j+1)}_{imin} \leq x_i \leq x^{*(j+1)}_{imax} < x^{*j}_{imax}\ \forall\ i \in \{1, ..., N\}$. Finally, $x \in \mathcal{R}^*_j$. Then $\mathcal{R}^*_{j+1} \subset \mathcal{R}^*_j$. It is straightforward to see that $\mathcal{R}^*_{j+1} \neq \mathcal{R}^*_j$ as the sequences $(x^{*j}_{imin})_j$ and $(x^{*j}_{imax})_j$ are strictly monotonic. □

Proposition 4.3.7. *If $Z^*_{1\alpha}(x)$ has a unique fixed point, then $\forall\ j \in \mathbb{N}$, $\mathcal{R}^*_j$ is invariant.*

This invariant property means that as soon as a trajectory starts in a hyperrectangle, it cannot leave it. In order to prove it, it is shown that the vector field in each border of a hyperrectangle points inwards. The details of the proof can be found in appendix B.4.

This proposition is illustrated in figures 4.3.1 and 4.3.2. The next proposition states that the hyperrectangles are successively repelling:

Proposition 4.3.8. *If $Z^*_{1\alpha}(x)$ has a unique fixed point, then $\forall\ j \in \mathbb{N}$, for all initial conditions $x_0 = x(t = 0) \in \mathcal{R}^*_j$, $\exists\ 0 \leq T^*_j < +\infty$ such that $x(t) \in \mathcal{R}^*_{j+1}\ \forall\ t \geq T^*_j$.*

This proposition simply means that if a trajectory is in hyperrectangle $\mathcal{R}^j$, it will eventually reach the hyperrectangle $\mathcal{R}^{j+1}$ in a finite time. In order to prove it, it is possible to successively show that $\forall\ i \in \{1, ..., N\}$, the x_i-vector field in $\mathcal{R}^j$ points towards $\mathcal{R}^{j+1}$. The details of this proof can be found in appendix B.5.

This proposition is also illustrated in figures 4.3.1 and 4.3.2. From the construction of the hyperrectangles, the next proposition is straightforward:

Proposition 4.3.9. *If $Z^*_{1\alpha}(x)$ has a unique fixed point, then for any $\epsilon > 0$ and its associated ball $\mathcal{B}^*_\epsilon = \{x|\ ||x - \bar{x}^*||_\infty \leq \epsilon\}$, it is possible to find $p^*_\epsilon \in \mathbb{N}^*$ such that $\mathcal{R}^*_j \subset \mathcal{B}^*_\epsilon\ \forall\ j \geq p^*_\epsilon$.*

This proposition simply means that, given a ball around $\bar{x}^*$, it is always possible to find its biggest embedded hyperrectangle. Besides, the infinite norm can be replaced by any other norm.

Proof. From proposition 4.3.4, the sequence $(x^{*j}_{imax})_j$ (resp. $(x^{*j}_{imin})_j$) is strictly monotonically decreasing (resp. increasing) and converges towards $\bar{x}^*_i\ \forall\ i \in \{1, ..., N\}$. Hence, $\forall\ i \in \{1, ..., N\}$ $\exists\ p^{*i}_{\epsilon max} \in \mathbb{N}^*$ (resp. $p^{*i}_{\epsilon min} \in \mathbb{N}^*$) such that $|x^{*j}_{imax} - \bar{x}^*_i| \leq \epsilon\ \forall\ j \geq p^{*i}_{\epsilon max}$ (resp. $|x^{*j}_{imin} - \bar{x}^*_i| \leq \epsilon\ \forall\ j \geq p^{*i}_{\epsilon min}$). Now p^*_ϵ is defined as $p^*_\epsilon = \max_{i\in\{1,...,N\}} \left\{p^{*i}_{\epsilon max}, p^{*i}_{\epsilon min}\right\}$. By definition, $\forall\ j \geq p^*_\epsilon$, $\forall\ i \in \{1, ..., N\}$, $|x^{*j}_{imax} - \bar{x}^*_i| \leq \epsilon$ and $|x^{*j}_{imin} - \bar{x}^*_i| \leq \epsilon$ which implies by proposition 4.3.4 that $x^{*j}_{imax} - \bar{x}^*_i \leq \epsilon$ and $\bar{x}^*_i - x^{*j}_{imin} \leq \epsilon$.

Let us check the result. Let $x \in \mathcal{R}^*_{p^*_\epsilon}$, then by definition of hyperrectangles, $\forall\ i \in \{1, ..., N\}$: $x^{*p^*_\epsilon}_{imin} \leq x_i \leq x^{*p^*_\epsilon}_{imax}$. So from the definition of p^*_ϵ: $\bar{x}^*_i - \epsilon \leq x^{*p^*_\epsilon}_{imin} \leq x_i \leq x^{*p^*_\epsilon}_{imax} \leq \bar{x}^*_i + \epsilon$. Finally, as expected, $-\epsilon \leq x_i - \bar{x}^*_i \leq \epsilon\ \forall\ i \in \{1, ..., N\}$. Hence, $x \in \mathcal{B}^*_\epsilon$. From proposition 4.3.6, $\mathcal{R}^*_j \subset \mathcal{B}^*_\epsilon$ $\forall\ j \geq p^*_\epsilon$. □

Finally, thanks to all the previous definitions and propositions, the main theorem of this section is presented and proved:

Theorem 4.3.1. *If the function $Z^*_{1\alpha}(x)$ has a unique fixed point, then $\bar{x}^*$ is a GAS steady state of system (4.2.2) under control (4.2.1).*

Proof. First, the global convergence is proved:

Let $\epsilon > 0$ and the associated ball $\mathcal{B}^*_\epsilon = \{x|\ ||x - \bar{x}^*||_\infty \leq \epsilon\}$. From proposition 4.3.9, $\exists\ p^*_\epsilon \in \mathbb{N}^*$ such that $\mathcal{R}^*_j \subset \mathcal{B}^*_\epsilon\ \forall\ j \geq p^*_\epsilon$. Let $x_0 = x(t = 0) \in \mathbb{R}^+_N$ an initial condition different from $\bar{x}^*$. From definition 4.3.4, $\exists\ j^*_0 \in \mathbb{N}$ such that $x_0 \in \mathcal{R}^*_j\ \forall\ j \leq j^*_0$, $j \in \mathbb{N}$, and $x_0 \notin \mathcal{R}^*_j\ \forall\ j > j^*_0$. According to proposition 4.3.8, $\exists\ 0 \leq T^*_{j^*_0} < +\infty$ such that $x(t) \in \mathcal{R}^*_{j^*_0+1}\ \forall\ t \geq T^*_{j_0}$. By induction, let $T^*_\epsilon = \sum_{k=j^*_0}^{p^*_\epsilon - 1} T^*_k$ where T^*_k are defined in proposition 4.3.8. Then, $\forall\ t \geq T^*_\epsilon$, $x(t) \in \mathcal{R}^*_{p^*_\epsilon}$. Then from proposition 4.3.9, $\forall\ t \geq T^*_\epsilon$, $x(t) \in \mathcal{B}^*_\epsilon$. In conclusion, it has been shown that $\forall\ x_0 = x(t = 0) \in \mathbb{R}^+_N$ and $\forall\ \epsilon > 0$, $\exists\ 0 \leq T^*_\epsilon < +\infty$ such that $\forall\ t \geq T^*_\epsilon$, $x(t) \in \mathcal{B}^*_\epsilon$. This is the definition of global convergence.

Now, the Lyapunov stability is proved:

Let $\delta > 0$ and the associated ball $\mathcal{B}^*_\delta = \{x|\ ||x - \bar{x}^*||_\infty \leq \delta\}$. From proposition 4.3.9, $\exists\ p^*_\delta \in \mathbb{N}^*$ such that $\mathcal{R}^*_j \subset \mathcal{B}^*_\delta\ \forall\ j \geq p^*_\delta$. From proposition 4.3.7, $\mathcal{R}^*_{p^*_\delta}$ is invariant. Then, $\forall\ x_0 = x(t = 0) \in \mathcal{R}^*_{p^*_\delta}$, $x(t) \in \mathcal{R}^*_{p^*_\delta}\ \forall\ t \geq 0$. Finally, as $\mathcal{R}^*_{p^*_\delta} \subset \mathcal{B}^*_\delta$, $x(t) \in \mathcal{B}^*_\delta\ \forall\ t \geq 0$. This is the definition of Lyapunov stability.

Then, the system converges globally towards the Lyapunov stable steady state $\bar{x}^*$. Finally, $\bar{x}^*$ is globally asymptotically stable. □

In conclusion, it has been shown in this section that if the function $Z^*_{1\alpha}(x)$ has a unique fixed point, then the steady state $\bar{x}^*$ of system (4.2.2) is GAS. In next section, the conditions on α will be given in order to ensure that $Z^*_{1\alpha}(x)$ has a unique fixed point.

4.4 Schwarzian derivatives

As the number of fixed points of a function is directly related to its shape, the shape-indicator of $Z^*_{1\alpha}(x)$, called "Schwarzian derivative" as introduced in chapter 3 [5], is calculated.

Proposition 4.4.1. *$Z^*_{1\alpha}(x)$ has a negative Schwarzian derivative.*

The details of the proof are given in appendix B.6.

The sign of the Schwarzian derivative of a function gives relevant information about the shape of this function:

Proposition 4.4.2. *$Z^*_{1\alpha}(x)$ is a sigmoid function.*

Proof. It is easy to show that ${Z^*_{1\alpha}}'(x) > 0 \ \forall \ x \in]0, +\infty[$, ${Z^*_{1\alpha}}'(0) = 0$ from the properties of Hill functions, and $Z^*_{1\alpha}(x)$ is bounded. From proposition 4.4.1, it follows that there exists $a > 0$ such that ${Z^*_{1\alpha}}'(x)$ is strictly increasing $\forall \ x \in]0, a[$ and ${Z^*_{1\alpha}}'(x)$ is strictly decreasing $\forall \ x \in]a, +\infty[$ (see [5] for the details). This is exactly the definition of a sigmoid function. □

This sigmoidal shape is essential in order to determine the number of fixed points of $Z^*_{1\alpha}(x)$:

Proposition 4.4.3. *$Z^*_{1\alpha}(x)$ cannot have more than three fixed points, and among them is $\bar{x}^*_1$. For the negative loop, if there are three fixed points, $\bar{x}^-_1$ is the middle one. Moreover, $\bar{x}^-_1$ is the unique fixed point of $Z^-_{1\alpha}(x)$ if and only if ${Z^-_{1\alpha}}'(\bar{x}^-_1) < 1$.*

Proof. As $Z^*_{1\alpha}(x)$ is a sigmoid function as explained in proposition 4.4.1, it cannot have more than three fixed points, and $\bar{x}^*_1$ is always one of its fixed point from proposition 4.3.1.

For the negative loop, let us assume that $Z^-_{1\alpha}(x)$ has three fixed points. Let us call one of the two other fixed point $\tilde{x}^-_1 \neq \bar{x}^-_1$. By definition, $\tilde{x}^-_1$ is such that $F^-_{1\alpha}(\tilde{x}^-_1) = \tilde{x}^-_1$. This implies that $S^-_{1\alpha} \circ S^-_{1\alpha}(\tilde{x}^-_1) = \tilde{x}^-_1$. Hence, $F^-_{1\alpha}\left(S^-_{1\alpha}(\tilde{x}^-_1)\right) = S^-_{1\alpha} \circ S^-_{1\alpha}\left(S^-_{1\alpha}(\tilde{x}^-_1)\right) = S^-_{1\alpha}(\tilde{x}^-_1)$. Then $S^-_{1\alpha}(\tilde{x}^-_1)$ is a fixed point of $F^-_{1\alpha}(x)$. Moreover, $S^-_{1\alpha}(\tilde{x}^-_1) \neq \tilde{x}^-_1$ as $\bar{x}^-_1$ is the unique fixed point of $S^-_{1\alpha}(x)$ and $\tilde{x}^-_1 \neq \bar{x}^-_1$ by hypothesis. Finally, $S^-_{1\alpha}(\tilde{x}^-_1)$ is the third fixed point of $F^-_{1\alpha}(x)$. Let us assume that $\tilde{x}^-_1 > \bar{x}^-_1$. Then as $S^-_{1\alpha}(x)$ is a strictly monotonically decreasing function, $S^-_{1\alpha}(\tilde{x}^-_1) < S^-_{1\alpha}(\bar{x}^-_1) = \bar{x}^-_1$ by definition. On the opposite, let us assume that $\tilde{x}^-_1 < \bar{x}^-_1$. Then as $S^-_{1\alpha}(x)$ is a strictly monotonically decreasing function, $S^-_{1\alpha}(\tilde{x}^-_1) > S^-_{1\alpha}(\bar{x}^-_1) = \bar{x}^-_1$ by definition. Finally, if $F^-_{1\alpha}(x)$ has three fixed points, then $\bar{x}^-_1$ is the middle point.

Let us call these two other fixed points $\tilde{x}^-_{1sup} > \bar{x}^-_1$ and $\tilde{x}^-_{1inf} < \bar{x}^-_1$. As a consequence, if $Z^-_{1\alpha}(x)$ is a sigmoid function and has three fixed points, then ${Z^-_{1\alpha}}'(\tilde{x}^-_{1inf}) < 1$, ${Z^-_{1\alpha}}'(\tilde{x}^-_{1sup}) < 1$ and ${Z^-_{1\alpha}}'(\bar{x}^-_1) > 1$. On the contrary, if $Z^-_{1\alpha}(x)$ has a unique fixed point $\bar{x}^-_1$, then ${Z^-_{1\alpha}}'(\bar{x}^-_1) < 1$. □

This proposition is illustrated in figure 4.4.1.

The conclusion of this section is the following: if there exist conditions on α such that $Z^*_{1\alpha}(x)$ has a unique fixed point, then theorem 4.3.1 guarantees $\bar{x}^*$ to be GAS. In particular, for the negative loop, this section brought a convenient condition: if there exist conditions on α such that ${Z^-_{1\alpha}}'(\bar{x}^-_1) < 1$, then proposition 4.4.3 ensures $Z^-_{1\alpha}(x)$ to have a unique fixed point, and theorem 4.3.1 guarantees $\bar{x}^-$ to be GAS. Next section investigates these conditions on α.

4.5 Conditions on α

This section proves that there exist conditions on α such that the steady state $\bar{x}^*$ of system (4.2.2) under control (4.2.1) becomes GAS. However, the condition for the negative loop is explicit, whereas for the positive loop the condition is implicit.

The explicit condition for the negative loop is detailed in the following lemma:

Lemma 4.5.1. *If $\alpha > \left(-\gamma_1 \left({S^-_1}'(\bar{x}^-_1) + 1\right)\right) / \left(\kappa_1 h^-(\bar{x}^-_N, \theta_N, n_N)\right) = \alpha^-_0$, then ${Z^-_{1\alpha}}'(\bar{x}^-_1) < 1$.*

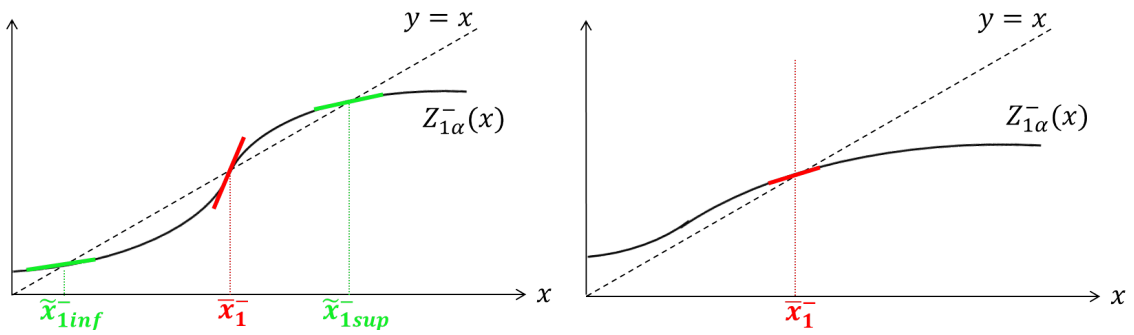

Figure 4.4.1: For both plots, the thick black line is the sigmoid function $Z^-_{1\alpha}(x)$. The intersections with $y = x$ (represented by the dashed black line) are illustrated. Left: $Z^-_{1\alpha}(x)$ has three fixed points, leading to ${Z^-_{1\alpha}}'(\bar{x}^-_1) > 1$. Right: $Z^-_{1\alpha}(x)$ has a unique fixed point $\bar{x}^-_1$, leading to ${Z^-_{1\alpha}}'(\bar{x}^-_1) < 1$.

Proof. The derivative ${Z^-_{1\alpha}}'(\bar{x}^-_1)$ is calculated:

$$\begin{aligned} {Z^-_{1\alpha}}'(\bar{x}^-_1) = {F^-_{1\alpha}}'(\bar{x}^-_1) &= (S^-_{1\alpha} \circ S^-_{1\alpha})'(\bar{x}^-_1), \\ &= {S^-_{1\alpha}}'(S^-_{1\alpha}(\bar{x}^-_1)){S^-_{1\alpha}}'(\bar{x}^-_1). \end{aligned}$$

Moreover, from proposition 4.3.1, $S^-_{1\alpha}(\bar{x}^-_1) = \bar{x}^-_1$. Hence:

$$ {F^-_{1\alpha}}'(\bar{x}^-_1) = \left({S^-_{1\alpha}}'(\bar{x}^-_1)\right)^2. $$

As ${S^-_{1\alpha}}'(x) \leq 0 \ \forall \ x \geq 0$, then ${F^-_{1\alpha}}'(\bar{x}^-_1) = {Z^-_{1\alpha}}'(\bar{x}^-_1) < 1 \iff {S^-_{1\alpha}}'(\bar{x}^-_1) > -1$.
Hence, the derivative ${S^-_{1\alpha}}'(\bar{x}^-_1)$ is investigated:

$$\begin{aligned} {S^-_{1\alpha}}'(\bar{x}^-_1) &= {H^-_{1\alpha}}'(H_N \circ ... \circ H_2(\bar{x}^-_1)){H_N}'(H_{N-1} \circ ... \circ H_2(\bar{x}^-_1))...{H_3}'(H_2(\bar{x}^-_1)){H_2}'(\bar{x}^-_1), \\ &= {H^-_{1\alpha}}'(\bar{x}^-_N){H_N}'(\bar{x}^-_{N-1})...{H_3}'(\bar{x}^-_2){H_2}'(\bar{x}^-_1). \end{aligned}$$

In this last equation, everything is fixed, except the term ${H^-_{1\alpha}}'(\bar{x}^-_N)$ that depends on α.
The function ${S^-_{1\alpha}}'(\bar{x}^-_1)$ can be written:

$$\begin{aligned} {S^-_{1\alpha}}'(\bar{x}^-_1) &= \kappa_1 \frac{\partial \mathrm{h}^-(\bar{x}^-_N, \theta_N, n_N)}{\partial x} \frac{\alpha(\gamma_1 \bar{x}^-_1 - \kappa_{01}) + \gamma_1}{(\gamma_1 + \alpha\kappa_1 \mathrm{h}^-(\bar{x}^-_N, \theta_N, n_N))^2} {H_N}'(\bar{x}^-_{N-1})...{H_3}'(\bar{x}^-_2){H_2}'(\bar{x}^-_1) \\ &= \gamma_1 \frac{\alpha(\gamma_1 \bar{x}^-_1 - \kappa_{01}) + \gamma_1}{(\gamma_1 + \alpha\kappa_1 \mathrm{h}^-(\bar{x}^-_N, \theta_N, n_N))^2} \frac{\kappa_1}{\gamma_1} \frac{\partial \mathrm{h}^-(\bar{x}^-_N, \theta_N, n_N)}{\partial x} {H_N}'(\bar{x}^-_{N-1})...{H_3}'(\bar{x}^-_2){H_2}'(\bar{x}^-_1). \end{aligned}$$

From the definition of $H^-_1(x)$ given in proposition 3.2.1 of chapter 3:

$$ {H^-_1}'(\bar{x}^-_N) = \frac{\kappa_1}{\gamma_1} \frac{\partial \mathrm{h}^-(\bar{x}_N, \theta_N, n_N)}{\partial x}. $$

Hence:

$$\begin{aligned} {S^-_{1\alpha}}'(\bar{x}^-_1) &= \gamma_1 \frac{\alpha(\gamma_1 \bar{x}^-_1 - \kappa_{01}) + \gamma_1}{(\gamma_1 + \alpha\kappa_1 \mathrm{h}^-(\bar{x}^-_N, \theta_N, n_N))^2} {H^-_1}'(\bar{x}^-_N){H_N}'(\bar{x}^-_{N-1})...{H_3}'(\bar{x}^-_2){H_2}'(\bar{x}^-_1) \\ &= \gamma_1 \frac{\alpha(\gamma_1 \bar{x}^-_1 - \kappa_{01}) + \gamma_1}{(\gamma_1 + \alpha\kappa_1 \mathrm{h}^-(\bar{x}^-_N, \theta_N, n_N))^2} {S^-_1}'(\bar{x}^-_1), \end{aligned}$$

where $S_1^-(x)$ is introduced in definition 3.2.2. From the definition of steady states of the uncontrolled system, $\kappa_{01}+\kappa_1 \mathrm{h}^-(\bar{x}_N^-,\theta_N,n_N)-\gamma_1\bar{x}_1^-=0$ which is equivalent to $\gamma_1\bar{x}_1^- - \kappa_{01} = \kappa_1 \mathrm{h}^-(\bar{x}_N^-,\theta_N,n_N)$. This relation is used in the previous equation:

$$\begin{aligned} {S_{1\alpha}^-}'(\bar{x}_1^-) &= \gamma_1 \frac{\alpha\kappa_1 \mathrm{h}^-(\bar{x}_N^-,\theta_N,n_N)+\gamma_1}{(\gamma_1+\alpha\kappa_1 \mathrm{h}^-(\bar{x}_N^-,\theta_N,n_N))^2} {S_1^-}'(\bar{x}_1) \\ &= \frac{\gamma_1}{\gamma_1+\alpha\kappa_1 \mathrm{h}^-(\bar{x}_N^-,\theta_N,n_N)} {S_1^-}'(\bar{x}_1). \end{aligned}$$

Now the derivative of ${S_{1\alpha}^-}'(\bar{x}_1^-)$ with respect to α is calculated:

$$\frac{\partial {S_{1\alpha}^-}'(\bar{x}_1^-)}{\partial\alpha} = -\gamma_1 {S_1^-}'(\bar{x}_1^-) \frac{\kappa_1 \mathrm{h}^-(\bar{x}_N^-,\theta_N,n_N)}{(\gamma_1+\alpha\kappa_1 \mathrm{h}^-(\bar{x}_N^-,\theta_N,n_N))^2}.$$

It is important to notice that for $\alpha=0$, $S_{1\alpha}^-(x)=S_1^-(x)$, where $S_1^-(x)$ is the function defined for the uncontrolled loops in definition 3.2.2 of chapter 3. By hypothesis it is considered that the unique steady state $\bar{x}^-$ of the canonical negative loop 3.2.1 is unstable. Hence, the condition ${Z_{1\alpha}^-}'(\bar{x}_1^-)<1$ cannot hold for $\alpha=0$. Indeed, if ${Z_{1\alpha}^-}'(\bar{x}_1^-)<1$ was true for $\alpha=0$, then by applying proposition 4.4.3 and theorem 4.3.1, the steady state $\bar{x}^-$ of the canonical negative loop (3.2.1) would be GAS. It follows that ${Z_{1\alpha}^-}'(\bar{x}_1^-)>1$ for $\alpha=0$.

Hence, for the negative loop, as ${Z_{1\alpha}^-}'(\bar{x}_1^-) = \left({S_{1\alpha}^-}'(\bar{x}_1^-)\right)^2$ and ${S_{1\alpha}^-}'(\bar{x}_1^-)<0$, if follows that ${S_{1\alpha}^-}'(\bar{x}_1^-)<-1$ for $\alpha=0$. Hence ${S_1^-}'(\bar{x}_1^-)<-1$, as already discussed in proposition 3.2.10 of chapter 3. Finally, for $\alpha\geq 0$, as ${S_1^-}'(\bar{x}_1^-)\leq 0$, then $\partial {S_{1\alpha}^-}'(\bar{x}_1^-)/\partial\alpha \geq 0$. Then, the derivative ${S_{1\alpha}^-}'(\bar{x}_1^-)$ is an increasing function of α. Moreover, it is easy to show that $\lim\limits_{\alpha\to+\infty} {S_{1\alpha}^-}'(\bar{x}_1^-)=0$, and it has been explained previously that when $\alpha=0$, ${S_{1\alpha}^-}'(\bar{x}_1^-) = {S_1^-}'(\bar{x}_1^-)<-1$. Finally, the function ${S_{1\alpha}^-}'(\bar{x}_1^-)$ is an increasing function of α that is strictly smaller than -1 when $\alpha=0$ and that tends to 0 when α tends to infinity. Then, there exists a value of α called α_0^- such that $\forall\ \alpha>\alpha_0^-$, ${S_{1\alpha}^-}'(\bar{x}_1^-)>-1$. This α_0^- is determined by solving ${S_{1\alpha}^-}'(\bar{x}_1^-)=-1$:

$${S_{1\alpha}^-}'(\bar{x}_1^-)=-1 \iff \alpha = \frac{-\gamma_1\left({S_1^-}'(\bar{x}_1^-)+1\right)}{\kappa_1 \mathrm{h}^-(\bar{x}_N^-,\theta_N,n_N)}.$$

Again, by hypothesis ${S_1^-}'(\bar{x}_1^-)<-1$, hence ${S_1^-}'(\bar{x}_1^-)+1<0$.

Finally $\alpha_0^- = -\gamma_1\left({S_1^-}'(\bar{x}_1^-)+1\right)/\left(\kappa_1 \mathrm{h}^-(\bar{x}_N^-,\theta_N,n_N)\right)>0$. The proof is now completed for the negative loop: when $\alpha>\alpha_0^-$, ${F_{1\alpha}^-}'(\bar{x}_1^-) = {Z_{1\alpha}^-}'(\bar{x}_1^-)<1$. □

For the positive loop, the implicit condition on α is given by the following lemma:

Lemma 4.5.2. *$\exists\ \alpha_0^+$ such that $\forall\ \alpha>\alpha_0^+$, $Z_{1\alpha}^+(x)$ has a unique fixed point.*

Proof. The influence of α on the function $Z_{1\alpha}^+(x)=S_{1\alpha}^+(x)$ is investigated:

$$\frac{\partial S_{1\alpha}^+}{\partial\alpha}(x) = \frac{\partial H_{1\alpha}^+}{\partial\alpha}(H_N\circ\ldots\circ H_2(x))$$

where

$$\begin{aligned} \frac{\partial H_{1\alpha}^+}{\partial\alpha}(x) &= \frac{\kappa_1 \mathrm{h}^+(x,\theta_N,n_N)[\bar{x}_1^+\gamma_1-\kappa_{01}-\kappa_1 \mathrm{h}^+(x,\theta_N,n_N)]}{\left(\gamma_1+\alpha\kappa_1 \mathrm{h}^+(x,\theta_N,n_N)\right)^2} \\ &= \frac{\kappa_1^2 \mathrm{h}^+(x,\theta_N,n_N)[\mathrm{h}^+(\bar{x}_N^+,\theta_N,n_N)-\mathrm{h}^+(x,\theta_N,n_N)]}{\left(\gamma_1+\alpha\kappa_1 \mathrm{h}^+(x,\theta_N,n_N)\right)^2} \end{aligned}$$

where the property $-\kappa_{01} + \gamma_1 \bar{x}_1^+ = \kappa_1 \mathrm{h}^+(\bar{x}_N^+, \theta_N, n_N)$ was used.

Hence

$$\begin{aligned}
\frac{\partial S_{1\alpha}^+}{\partial \alpha}(x) \geq 0 &\iff \mathrm{h}^+(\bar{x}_N^+, \theta_N, n_N) - \mathrm{h}^+\left(H_N \circ ... \circ H_2(x), \theta_N, n_N\right) \geq 0 \\
&\iff \bar{x}_N^+ \geq H_N \circ ... \circ H_2(x) \\
&\iff H_N \circ ... \circ H_2(\bar{x}_1^+) \geq H_N \circ ... H_2(x) \\
&\iff \bar{x}_1^+ \geq x.
\end{aligned}$$

Hence, $\forall\ x < \bar{x}_1^+$, $S_{1\alpha}^+(x)$ increases with α and $\forall\ x > \bar{x}_1^+$, $S_{1\alpha}^+(x)$ decreases with α. Moreover, $S_{1\alpha}^+(x)$ is a monotonically increasing function and it is easy to check that:

$$\lim_{\alpha \to +\infty} S_{1\alpha}^+(x) = \bar{x}_1^+.$$

Hence, $\exists\ \alpha_{0inf}^+$ such that $\forall\ \alpha > \alpha_{0inf}^+$, $S_{1\alpha}^+(x) > x\ \forall\ x < \bar{x}_1^+$. Moreover, $\exists\ \alpha_{0sup}^+$ such that $\forall\ \alpha > \alpha_{0sup}^+$, $S_{1\alpha}^+(x) < x\ \forall\ x > \bar{x}_1^+$. Then $\forall\ \alpha > \alpha_0^+ = \max\left\{\alpha_{0inf}^+, \alpha_{0sup}^+\right\}$, $Z_{1\alpha}^+(x)$ has a unique fixed point. □

The condition for the positive loop cannot be explicit as for the negative loop because the condition ${Z_{1\alpha}^+}'(\bar{x}_1^+) < 1$ is not sufficient to prove the uniqueness of the fixed point. Indeed, when $Z_{1\alpha}^+(x)$ has three fixed points, $\bar{x}_1^+$ may not be the central point. However, in order to find numerically the value α_0^+ for a given model, it is important to notice that only three cases can happen: first, for $\alpha = \alpha_0^+$, $Z_{1\alpha}^+(x)$ is tangent to $y = x$ at $x = x_0^+ < \bar{x}_1^+$; second, for $\alpha = \alpha_0^+$, $Z_{1\alpha}^+(x)$ is tangent to $y = x$ at $x = x_0^+ > \bar{x}_1^+$; third, for $\alpha = \alpha_0^+$, $Z_{1\alpha}^+(x)$ is tangent to $y = x$ at $\bar{x}_1^+$. More precisely, α_0^+ satisfies one of the three following conditions:

- For $\alpha = \alpha_0^+$, $\exists\ x_0^+ < \bar{x}_1^+$ such that $Z_{1\alpha}^+(x_0^+) = x_0^+$ and ${Z_{1\alpha}^+}'(x_0^+) = 1$,
- For $\alpha = \alpha_0^+$, $\exists\ x_0^+ > \bar{x}_1^+$ such that $Z_{1\alpha}^+(x_0^+) = x_0^+$ and ${Z_{1\alpha}^+}'(x_0^+) = 1$,
- For $\alpha = \alpha_0^+$, ${Z_{1\alpha}^+}'(\bar{x}_1^+) = 1$.

Lemmas 4.5.1 and 4.5.2 allow the statement of the main result:

Theorem 4.5.1. *If $\alpha > \alpha_0^*$, then $\bar{x}^*$ is a GAS steady state of system (4.2.2) under control (4.2.1).*

Proof. For the negative loop, if $\alpha > \alpha_0^-$, then with lemma 4.5.1, ${Z_{1\alpha}^-}'(\bar{x}_1^-) < 1$. It follows from proposition 4.4.3 that $Z_{1\alpha}^-(x)$ has a unique fixed point. Theorem 4.3.1 ends the proof.
For the positive loop, if $\alpha > \alpha_0^+$, then with lemma 4.5.2, $Z_{1\alpha}^+(x)$ has a unique fixed point and theorem 4.3.1 applies. □

4.6 Numerical illustrations

Figures 4.6.1 and 4.6.2 present a simulation for respectively a negative feedback loop of dimension 3 and a positive feedback loop of dimension 2. As explained in section 3.5 of chapter 3, without control, the feedback loops were constructed in order to show undesired sustained oscillations for the negative loop and bistability for the positive loop. With the affine control meeting the condition $\alpha^* > \alpha_0^*$, the simulations show global convergence towards $\bar{x}^*$, as analytically proved.

Moreover, figure 4.6.3 illustrates the influence of α on the function $F_{1\alpha}^-(x)$ for the negative loop. First, it is possible to observe that the shape of the function $F_{1\alpha}^-(x)$ is indeed sigmoidal. As explained in the previous section, it is possible to observe in figure 4.6.3 that the function $F_{1\alpha}^-(x)$ is such that ${F_{1\alpha}^-}'(\bar{x}_1^-) > 1$ when $\alpha = 0$ (without control in other words) and presents three fixed points. As

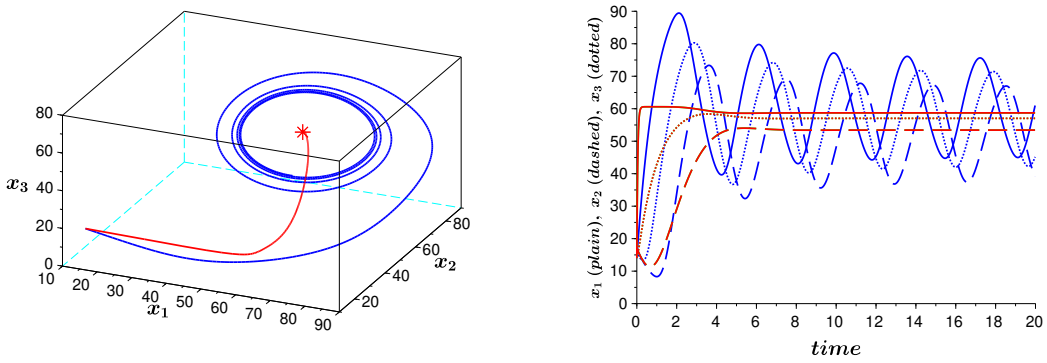

Figure 4.6.1: Simulation for a negative feedback loop in dimension 3: for both plots, the parameters are: $\kappa_{0i} = 2$, $\kappa_i = 100$, $\gamma_i = 1$, $\theta_i = 56.39$ and $n_i = 5$, $\forall\, i \in \{1, 2, 3\}$, leading to $\bar{x}^- = (58.7, 57, 53.4)$. The initial condition for the simulation is $x_0 = (14, 16, 17)$. With these parameters, $\alpha_0^- = 0.17$, and α is fixed to $\alpha = 0.22$. Left: trajectories in the state space. The steady state is represented by the red star. The blue line is a simulation of the uncontrolled system (3.2.1) with initial condition x_0 and converges towards a periodic orbit. The red line is a simulation of system (4.2.2) under control (4.2.1) with same initial condition x_0 and converges towards $\bar{x}^-$. Right: same trajectory against time. The blue (resp. red) lines are without (resp. with) control.

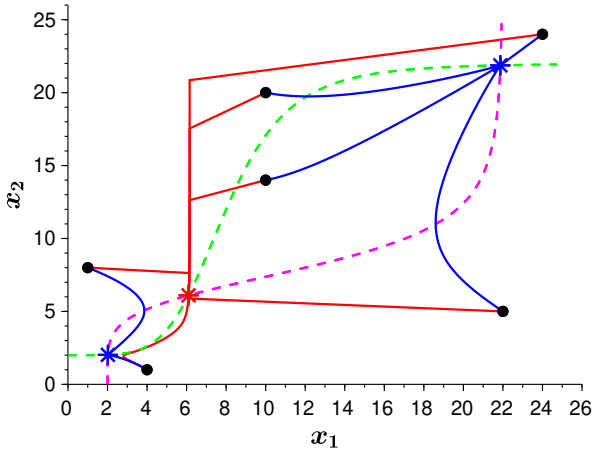

Figure 4.6.2: Simulation for a positive feedback loop: for both plots, the parameters are: $\kappa_{0i} = 2$, $\kappa_i = 20$, $\gamma_i = 1$, $\theta_i = 8$ and $n_i = 5$, $\forall\, i \in \{1, 2\}$. With these parameters, $\alpha_0^+ = 13.66$, and α is fixed to $\alpha = 14.66$. The two stable steady states $\bar{x}^+_{inf} = (2.02, 2.02)$ and $\bar{x}^+_{sup} = (21.87, 21.87)$ of the uncontrolled system are represented by blue stars and $\bar{x}^+ = (6.1, 6.1)$ is represented by the red star. The dashed green (resp. magenta) line is the x_2-nullcline (resp. x_1-nullcline). The blue lines are trajectories of the uncontrolled system (3.2.1) with different initial conditions depicted by black dots and converge towards one of the two stable steady states. The red lines are trajectories of system (4.2.2) under control (4.2.1) with same initial conditions and converge towards $\bar{x}^+$.

proved, when $\alpha = \alpha_0^-$, the function $F^-_{1\alpha}(x)$ becomes tangent to $y = x$ with ${F^-_{1\alpha}}'(\bar{x}^-_1) = 1$, and for any $\alpha > \alpha_0^-$, $F^-_{1\alpha}(x)$ has a unique fixed point, which guarantees global convergence.

Figure 4.7.1 illustrates the influence of α on the function $S^+_{1\alpha}(x)$ for the positive loop. Again, it is possible to observe that the shape of the function $S^+_{1\alpha}(x)$ is sigmoidal. Moreover, as analytically

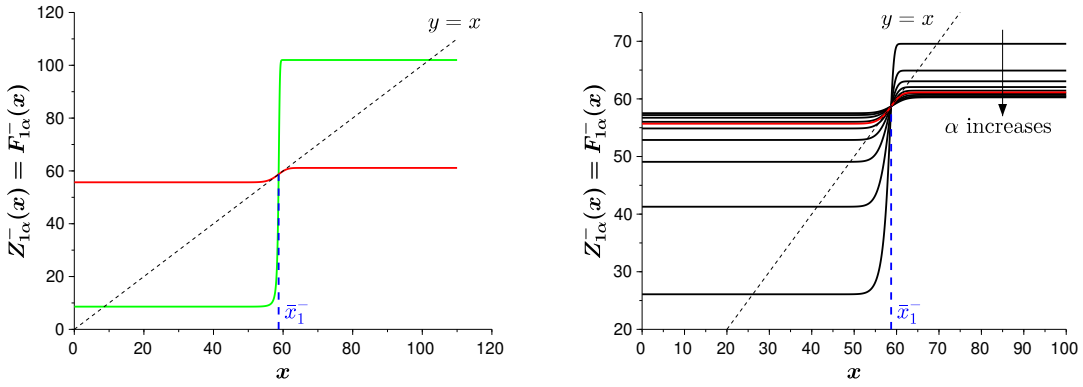

Figure 4.6.3: Both plots present the function $Z^-_{1\alpha}(x)$ for the negative loop in dimension 3 for different values of α. The parameters of the three dimensional system are the same as in figure 4.6.1. Left: the green line is $F_1^-(x)$ of the uncontrolled loop (3.2.1), hence $F^-_{1\alpha}(x)$ with $\alpha = 0$. It is possible to observe that as $\bar{x}^-$ is unstable, the function has three fixed points and ${F_1^-}'(\bar{x}_1^-) > 1$. The red line is $F^-_{1\alpha}(x)$ of system (4.2.2) under control (4.2.1) with $\alpha = \alpha_0^-$. As proved, $F^-_{1\alpha_0^-}(x)$ is tangent to $y = x$ and then ${F^-_{1\alpha_0^-}}'(\bar{x}_1^-) = 1$. Right: the red line is still $F^-_{1\alpha_0^-}(x)$. The thin black lines are $F^-_{1\alpha}(x)$ for different increasing values of $\alpha > 0$. It is possible to observe that for $\alpha > \alpha_0^-$, the functions loose their three fixed points, and ${F^-_{1\alpha}}'(\bar{x}_1^-) < 1$, leading to global convergence towards $\bar{x}^-$.

proved, the function $S^+_{1\alpha}(x)$ has three fixed points for $\alpha < \alpha_0^+$, in particular for $\alpha = 0$, meaning that the controlled system shows bistability for values of α not large enough. For $\alpha > \alpha_0^+$, $S^+_{1\alpha}(x)$ has a unique fixed point, which guarantees global convergence. This figure also confirms that the condition ${S^+_{1\alpha}}'(\bar{x}_1^+) = 1$ is not sufficient in order to have a unique fixed point for the positive loop.

4.7 Conclusion

In this chapter it has been shown that an affine control is able to globally stabilize both a negative feedback loop that presents undesired oscillations and a positive feedback loop that presents bistability. Indeed, for a control parameter α chosen large enough, the unstable steady state of both loops becomes GAS. Due to the non-linearities of this controlled system, a new methodology has been developed in order to obtain global results. A nested sequence of repelling hyperrectangles has been constructed and has been shown to act as Lyapunov function level-sets. The affine control law presented in this chapter is only dependent on the first variable x_1 and only acts on its expression. It is interesting to note that this simple control law is able to stabilize a whole system in any dimension N. Moreover, from a biological point of view, this control law minimizes the experimental set-up complexity. On the one hand, only the first gene must be measured: this is convenient as measurements in biology are usually tedious. On the other hand, the control only impacts the interaction between the last gene and the first gene. Again, this suggests that only one control device is enough, simplifying the experiment.

A couple of remarks can be given regarding a possible biological implementation. Firstly, as mentioned, the control may take arbitrarily large positive and negative values. This is illustrated in figure 4.7.2 with the two numerical examples presented in section 4.6. From a biological point of view, this means that the control device must be able to either influence the production of the first molecule x_1 (when $\mathrm{u}(x_1) > 0$) or degrade it (when $\mathrm{u}(x_1) < 0$). In the first case, the biological tools mentioned in the introduction may allow the application of this control. However, for a negative control, the biological implementation does not seem straightforward. This situation may be

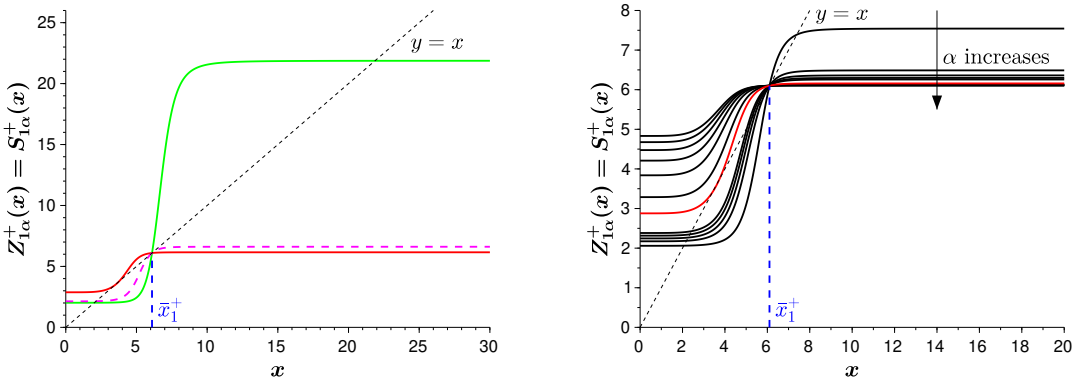

Figure 4.7.1: Both plots present the function $Z^+_{1\alpha}(x)$ for the positive loop in dimension 2 for different values of α. The parameters of the two dimensional system are the same as in figure 4.6.2. Left: the green line is $S^+_1(x)$ of the uncontrolled loop (3.2.1), hence $S^+_{1\alpha}(x)$ with $\alpha = 0$. It is possible to observe that as the uncontrolled system is bistable, the function has three fixed points. The dashed magenta line is $S^+_{1\alpha}(x)$ of system (4.2.2) under control (4.2.1) with $\alpha = \alpha_0$ such that $S^{+\prime}_{1\alpha_0}(\bar{x}^+_1) = 1$. Contrary to the negative loop, it is possible to observe that this condition is not sufficient in order to have uniqueness of the fixed point. Indeed, for any α such that $\alpha_0 < \alpha < \alpha^+_0$, $S^+_{1\alpha}(x)$ has still three fixed points and $\bar{x}^+_1$ is not the middle one. The red line is $S^+_{1\alpha^+_0}(x)$. As proved, $S^+_{1\alpha^+_0}(x)$ has a unique fixed point. Right: the red line is still $S^+_{1\alpha^+_0}(x)$. The thin black lines are $S^+_{1\alpha}(x)$ for different increasing values of $\alpha > 0$. It is possible to observe that for $\alpha > \alpha^+_0$, the functions loose their three fixed points leading to global convergence towards $\bar{x}^+$.

avoided if the control parameter α can be chosen small enough. In this case, the control law stays positive in the invariant bounded region of the state space. If this is not possible, the control law may be saturated: the tools developed in this chapter for the global convergence can be adapted in this new context. This is the subject of next chapter.

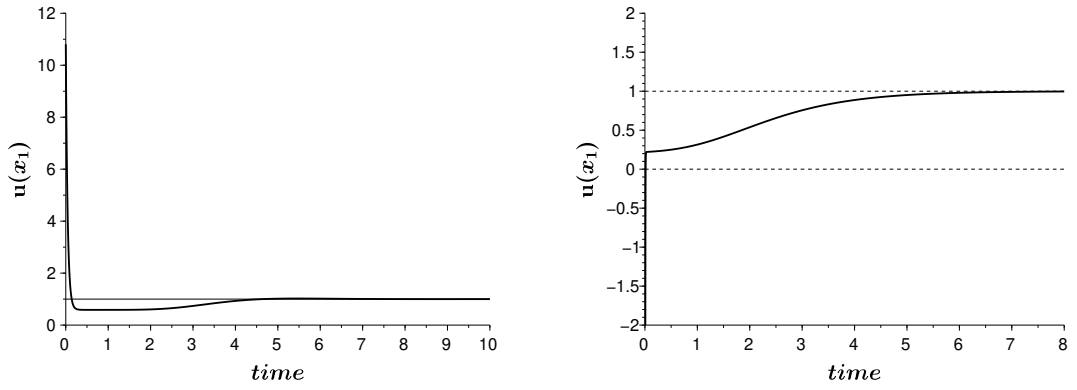

Figure 4.7.2: Both plots illustrate the evolution with time of the control law $\mathrm{u}(x_1)$. Left: control dynamics for the negative loop where the parameters and the initial condition are the same as in figure 4.6.1. For this initial condition, the control law stays positive for all time, but can be large for early times. Left: control dynamics for the positive loop where the parameters are the same as in figure 4.6.2 and the initial condition is $x_0 = (10, 14)$. For this initial condition, the control law starts below zero, and increases to reach $\mathrm{u}(x_1) = 1$.

Chapter 5

Saturated control strategy

5.1 Introduction

As introduced at the end of the previous chapter, the classical control strategy $\mathrm{u}(x_1) = -\alpha(x_1 - \bar{x}_1^*) + 1$ may not be adapted for biological circuits and biological control means. First, the control can reach high values for x_1 small. Indeed, $\mathrm{u}(0) = \alpha\bar{x}_1^* + 1$, and due to the results explained in the previous chapter, the classical control strategy leads to a global stabilization of $\bar{x}^*$ if the control parameter α can be chosen large enough. In this case, $\alpha\bar{x}_1^* + 1$ may become large as well. In the case of inducer molecule inputs, these high values may be harmful for the controlled circuit and may damage its components. Second, for arbitrarily large values of x_1 the classical control strategy becomes negative. Indeed, for any $x_1 \geq \bar{x}_1^* + 1/\alpha$, $\mathrm{u}(x_1) \leq 0$. However, as previously explained, in order to globally stabilize $\bar{x}^*$, α must be chosen large enough. It follows that $1/\alpha$ may become small. In this case, the control strategy becomes negative for values of x_1 arbitrarily close to $\bar{x}_1^*$. From a biological point of view, these negative values may be complicated to interpret, especially if the control inputs correspond to concentrations of molecules. To answer these two problems, this chapter will focus on the saturation of a classical control law that prevents the input from reaching too high or too small values.

The saturated control system is presented in section 5.2 and is shown to globally converge towards the unstable steady state $\bar{x}^*$ under appropriate conditions on the bounds of saturation in section 5.3. This result is obtained by defining two repellent regions in direction x_1 and by applying the methodology and the theorems proved in the previous chapter.

5.2 The controlled model

The control law $\mathrm{u}(x_1) = -\alpha(x_1 - \bar{x}_1^*) + 1$ is saturated by two positive constants: u_{max} greater than 1, and u_{min} smaller than 1, leading to the following new controlled system:

$$\begin{cases} \dot{x}_1(x_1, x_N) = \kappa_{01} + \mathrm{u}(x_1)\kappa_1 \mathrm{h}^*(x_N, \theta_N, n_N) - \gamma_1 x_1 \\ \dot{x}_i(x_i, x_{i-1}) = \kappa_{0i} + \kappa_i \mathrm{h}^+(x_{i-1}, \theta_{i-1}, n_{i-1}) - \gamma_i x_i \quad \forall\ i \in \{2, ..., N\}\,, \end{cases} \tag{5.2.1}$$

where

$$\begin{cases} \mathrm{u}(x_1) = u_{max} \ \forall\ 0 \leq x_1 \leq x_{1min}^* \text{ where } 1 \leq u_{max} \leq 1 + \alpha\bar{x}_1^*, \\ \mathrm{u}(x_1) = -\alpha(x_1 - \bar{x}_1^*) + 1 \ \forall\ x_{1min}^* \leq x_1 \leq x_{1max}^*, \\ \mathrm{u}(x_1) = u_{min} \ \forall\ x_1 \geq\ x_{1max}^* \text{ where } 0 \leq u_{min} \leq 1\ , \end{cases} \tag{5.2.2}$$

with $x_{1min}^* = \bar{x}_1^* - (u_{max} - 1)/\alpha < \bar{x}_1^*$ and $x_{1max}^* = \bar{x}_1^* + (1 - u_{min})/\alpha > \bar{x}_1^*$. These conditions on x_{1min}^* and x_{1max}^* guarantee the continuity of the control law (see figure 5.3.1 for an illustration).

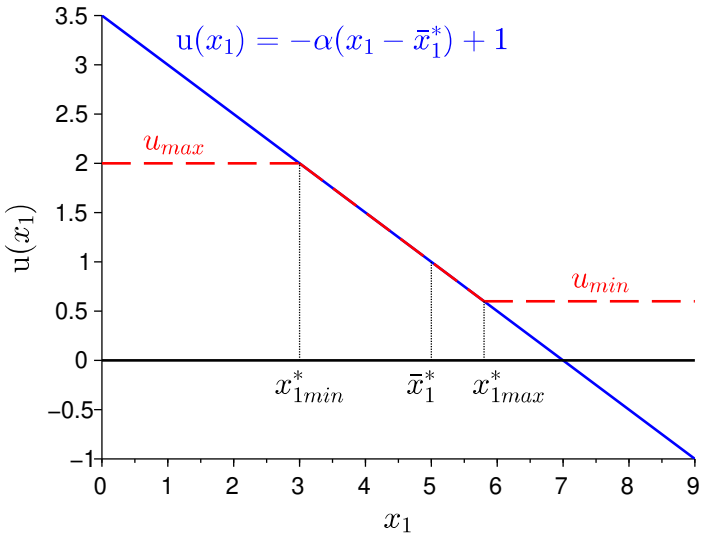

Figure 5.3.1: The blue line is the classical affine control strategy (4.2.1) presented in chapter 4. The saturated control strategy (5.2.2) in red prevents too high and negative inputs.

The condition on u_{max} guarantees that the control law is up-saturated while the one on u_{min} guarantees that it is down-saturated.

Proposition 5.2.1. *$\bar{x}^*$ is still a steady state of system (5.2.1) under control (5.2.2).*

This is easily proved as discussed in the proof of proposition 4.2.1 in the previous chapter.

5.3 Global asymptotic stability

In order to obtain global convergence results, the following assumption will be assumed in the rest of the section:

Assumption 5.3.1.

$$\begin{cases} \alpha\left(\bar{x}_1^* - \dfrac{\kappa_{01}}{\gamma_1}\right) + 1 \leq u_{max} \leq 1 + \alpha\bar{x}_1^*, \\ 0 \leq u_{min} \leq \dfrac{\alpha(\gamma_1\bar{x}_1^* - \kappa_{01}) + \gamma_1}{\alpha\kappa_1 + \gamma_1}. \end{cases}$$

From this assumption, it is possible to check that the control inputs satisfy the constraints given in (5.2.2):

Proposition 5.3.1. *Under assumption 5.3.1,* $1 \leq \alpha(\bar{x}_1^* - \kappa_{01}/\gamma_1) + 1 \leq u_{max} \leq 1 + \alpha\bar{x}_1^*$ *and* $0 \leq u_{min} \leq \left(\alpha(\gamma_1\bar{x}_1^* - \kappa_{01}) + \gamma_1\right) / \left(\alpha\kappa_1 + \gamma_1\right) \leq 1$.

In other words, this proposition confirms that u_{max} and u_{min} given in assumption 5.3.1 are well defined.

Proof. First, it is straightforward to see that $1 + \alpha(\bar{x}_1^* - \kappa_{01}/\gamma_1) > 1$ as from proposition 3.2.8, $\bar{x}_1^* > \kappa_{01}/\gamma_1$. Moreover, $1 + \alpha(\bar{x}_1^* - \kappa_{01}/\gamma_1) = 1 + \alpha\bar{x}_1^* - \alpha\kappa_{01}/\gamma_1 \leq 1 + \alpha\bar{x}_1^*$. For u_{min}, the properties of the uncontrolled system (3.2.1) lead to $\gamma_1\bar{x}_1^* - \kappa_{01} = \kappa_1 \mathrm{h}^*(\bar{x}_N^*, \theta_N, n_N)$. It follows that:

$$\frac{\alpha(\gamma_1\bar{x}_1^* - \kappa_{01}) + \gamma_1}{\alpha\kappa_1 + \gamma_1} = \frac{\alpha\kappa_1 \mathrm{h}^*(\bar{x}_N^*\theta_N, n_N) + \gamma_1}{\alpha\kappa_1 + \gamma_1}.$$

As $0 \leq \mathrm{h}^*(\bar{x}_N^*, \theta_N, n_N) \leq 1$, then $\alpha\kappa_1 \mathrm{h}^*(\bar{x}_N^*, \theta_N, n_N) + \gamma_1 \leq \alpha\kappa_1 + \gamma_1$.
Finally, $0 \leq (\alpha(\gamma_1 \bar{x}_1^* - \kappa_{01}) + \gamma_1) / (\alpha\kappa_1 + \gamma_1) \leq 1$. □

With these conditions on u_{min} and u_{max}, two regions of the state space become repellent.

Lemma 5.3.1. *Under assumption 5.3.1, the region of the state space defined by $x_1 > x_{1max}^*$ is repellent.*

Proof. In order to prove this lemma, it will be shown that $\dot{x}_1(x_1, x_N) < 0$ for any $x_1 > x_{1max}^*$. First, in the region $x_1 > x_{1max}^*$, the x_1-vector field is defined as:
$\dot{x}_1(x_1, x_N) = \kappa_{01} + u_{min}\kappa_1 \mathrm{h}^*(x_N, \theta_N, n_N) - \gamma_1 x_1$.
With the condition $u_{min} \leq (\alpha(\gamma_1 \bar{x}_1^* - \kappa_{01}) + \gamma_1) / (\alpha\kappa_1 + \gamma_1)$ the x_1-vector field becomes:

$$\dot{x}_1(x_1, x_N) \leq \kappa_{01} + \frac{\alpha(\gamma_1 \bar{x}_1^* - \kappa_{01}) + \gamma_1}{\alpha\kappa_1 + \gamma_1} \kappa_1 \mathrm{h}^*(x_N, \theta_N, n_N) - \gamma_1 x_1.$$

By evaluating this expression at the border $x_1 = x_{1max}^* = \bar{x}_1^* + ((1 - u_{min})/\alpha)$, the vector field becomes:

$$\begin{aligned}\dot{x}_1(x_{1max}^*, x_N) &\leq \kappa_{01} + \frac{\alpha(\gamma_1 \bar{x}_1^* - \kappa_{01}) + \gamma_1}{\alpha\kappa_1 + \gamma_1} \kappa_1 \mathrm{h}^*(x_N, \theta_N, n_N) - \gamma_1 \left(\bar{x}_1^* + \frac{1 - u_{min}}{\alpha} \right) \\ &= \frac{\alpha(\gamma_1 \bar{x}_1^* - \kappa_{01}) + \gamma_1}{\alpha\kappa_1 + \gamma_1} \kappa_1 \mathrm{h}^*(x_N, \theta_N, n_N) + \kappa_{01} - \gamma_1 \bar{x}_1^* - \frac{\gamma_1}{\alpha} + \gamma_1 \frac{u_{min}}{\alpha}.\end{aligned}$$

With the condition on u_{min}, this expression becomes:

$$\begin{aligned}\dot{x}_1(x_{1max}^*, x_N) &\leq \frac{\alpha(\gamma_1 \bar{x}_1^* - \kappa_{01}) + \gamma_1}{\alpha\kappa_1 + \gamma_1} \kappa_1 \mathrm{h}^*(x_N, \theta_N, n_N) + \kappa_{01} - \gamma_1 \bar{x}_1^* - \frac{\gamma_1}{\alpha} + \frac{\gamma_1}{\alpha} \frac{\alpha(\gamma_1 \bar{x}_1^* - \kappa_{01}) + \gamma_1}{\alpha\kappa_1 + \gamma_1} \\ &= \frac{\alpha(\gamma_1 \bar{x}_1^* - \kappa_{01}) + \gamma_1}{\alpha\kappa_1 + \gamma_1} \kappa_1 \mathrm{h}^*(x_N, \theta_N, n_N) - \kappa_1 \frac{\alpha(\gamma_1 \bar{x}_1^* - \kappa_{01}) + \gamma_1}{\alpha\kappa_1 + \gamma_1} \\ &= \kappa_1 \frac{\alpha(\gamma_1 \bar{x}_1^* - \kappa_{01}) + \gamma_1}{\alpha\kappa_1 + \gamma_1} \left[\mathrm{h}^*(x_N, \theta_N, n_N) - 1 \right].\end{aligned}$$

From the properties of the uncontrolled system (3.2.1), as $\gamma_1 \bar{x}_1^* - \kappa_{01} = \kappa_1 \mathrm{h}^*(\bar{x}_N^*, \theta_N, n_N)$ and $\mathrm{h}^*(x_N, \theta_N, n_N) \leq 1$, $\gamma_1 \bar{x}_1^* - \kappa_{01} \geq 0$. Hence, $\dot{x}_1(x_{1max}^*, x_N) \leq 0$ for any $x_N \geq 0$. Then, because of the linear degradation term $-\gamma_1 x_1$ in the vector field, $\dot{x}_1(x_1, x_N) < \dot{x}_1(x_{1max}^*, x_N) \leq 0$ for any $x_1 > x_{1max}^*$. Finally, $\dot{x}_1(x_1, x_N) < 0$ for any $x_1 > x_{1max}^*$ and $x_N \geq 0$. This induces that the region of the state space defined by $x_1 > x_{1max}^*$ is repellent. □

Lemma 5.3.2. *Under assumption 5.3.1, the region of the state space defined by $x_1 < x_{1min}^*$ is repellent.*

Proof. In order to prove this lemma, it will be shown that $\dot{x}_1(x_1, x_N) > 0$ for any $x_1 < x_{1min}^*$. First, in the region $x_1 < x_{1min}^*$, the x_1-vector field is defined as:
$\dot{x}_1(x_1, x_N) = \kappa_{01} + u_{max}\kappa_1 \mathrm{h}^*(x_N, \theta_N, n_N) - \gamma_1 x_1$. With the condition $u_{max} \geq \alpha\,(\bar{x}_1^* - \kappa_{01}/\gamma_1) + 1$ the x_1-vector field becomes:

$$\dot{x}_1(x_1, x_N) \geq \kappa_{01} + \left(\alpha \left(\bar{x}_1^* - \frac{\kappa_{01}}{\gamma_1} \right) + 1 \right) \kappa_1 \mathrm{h}^*(x_N, \theta_N, n_N) - \gamma_1 x_1.$$

By evaluating this expression at the border $x_1 = x_{1min}^* = \bar{x}_1^* - ((u_{max} - 1)/\alpha)$, the vector field becomes:

$$\begin{aligned}\dot{x}_1(x_{1min}^*, x_N) &\geq \kappa_{01} + \left(\alpha \left(\bar{x}_1^* - \frac{\kappa_{01}}{\gamma_1} \right) + 1 \right) \kappa_1 \mathrm{h}^*(x_N, \theta_N, n_N) - \gamma_1 \left(\bar{x}_1^* - \frac{u_{max} - 1}{\alpha} \right) \\ &= \kappa_{01} + \left(\alpha \left(\bar{x}_1^* - \frac{\kappa_{01}}{\gamma_1} \right) + 1 \right) \kappa_1 \mathrm{h}^*(x_N, \theta_N, n_N) - \gamma_1 \bar{x}_1^* - \frac{\gamma_1}{\alpha} + u_{max} \frac{\gamma_1}{\alpha}.\end{aligned}$$

With the condition on u_{max}, this expression becomes:

$$\begin{aligned}
&\dot{x}_1(x^*_{1min}, x_N) \\
&\geq \kappa_{01} + \left(\alpha\left(\bar{x}^*_1 - \frac{\kappa_{01}}{\gamma_1}\right) + 1\right)\kappa_1 \mathrm{h}^*(x_N, \theta_N, n_N) - \gamma_1 \bar{x}^*_1 - \frac{\gamma_1}{\alpha} + \frac{\gamma_1}{\alpha}\left[\alpha\left(\bar{x}^*_1 - \frac{\kappa_{01}}{\gamma_1}\right) + 1\right] \\
&= \left(\alpha\left(\bar{x}^*_1 - \frac{\kappa_{01}}{\gamma_1}\right) + 1\right)\kappa_1 \mathrm{h}^*(x_N, \theta_N, n_N).
\end{aligned}$$

As $\gamma_1 \bar{x}^*_1 - \kappa_{01} \geq 0$ then $\dot{x}_1(x^*_{1min}, x_N) \geq 0$ for any $x_N \geq 0$. Then, because of the linear degradation term $-\gamma_1 x_1$ in the vector field, $\dot{x}_1(x_1, x_N) > \dot{x}_1(x^*_{1min}, x_N) \geq 0$ for any $x_1 < x^*_{1min}$. Finally, $\dot{x}_1(x_1, x_N) > 0$ for any $x_1 < x^*_{1min}$ and $x_N \geq 0$. This induces that the region of the state space defined by $x_1 < x^*_{1min}$ is repellent. □

These two lemmas allow to state a global convergence and stability theorem for the saturated control strategy:

Theorem 5.3.1. *Under assumption 5.3.1 and if $\alpha > \alpha^*_0$ as stated in theorem 4.5.1, then the steady state $\bar{x}^*$ of system (5.2.1) under control (5.2.2) is globally asymptotically stable.*

Thanks to the methodology developed in the previous chapter, the proof of this theorem is straightforward:

Proof. Under assumption 5.3.1, lemmas 5.3.1 and 5.3.2 allow to deduce that system (5.2.1) under control (5.2.2) globally converges towards the region of the state space defined by $x^*_{1min} \leq x_1 \leq x^*_{1max}$. In this region and with the definition of the saturated control law (5.2.2), the dynamical system is now equivalent to system (5.2.1) under control $\mathrm{u}(x_1) = -\alpha(x_1 - \bar{x}^*_1) + 1$. Then, as α satisfies the constraints given in theorem 4.5.1, $\bar{x}^*$ is globally asymptotically stable. □

This saturated control problem does not seem straightforward at a first glance. However, with the methodology developed in the previous chapter, it is sufficient to find conditions on u_{min} and u_{max} in order to force the system to converge and stay in a region of the state space within which the control law is a classical linear control strategy. In this case, the results proved in the previous chapter apply.

This result is convenient because it guarantees that the control strategy stays positive. This is important for the biological interpretation of the control law. Moreover, in some cases, the saturating constant u_{max} allows to reduce the maximal strength of the input. This may be important when the control input is external to the controlled system and may be harmful at high dosage.

The results presented in this chapter are illustrated in figure 5.3.2 for the negative loop, and 5.3.3 for the positive loop. For both examples, it is possible to observe that the control law saturates when the classical control strategy reaches high or negative values, but the global convergence is still guaranteed.

5.4 Conclusion

In this small chapter, it has been shown that the saturation of an affine control strategy that globally stabilizes the unstable steady state $\bar{x}^*$ of both a positive and a negative feedback loop, is also able to globally stabilize the systems. This result is not straightforward: indeed, the saturation of the affine control strategy is expected to locally stabilize $\bar{x}^*$, but not necessarily induce global results. Interestingly, this global result has been shown really easily by using the methodology and the theorems that have been developed in the previous chapter for the classical affine control strategy. This confirms that this qualitative methodology is general enough so that it can be extended for non trivial and non classical control strategies. Moreover, from a biological point of view, this saturated control strategy allows the input to stay bounded, preventing extreme values. This property is really important for a biological application.

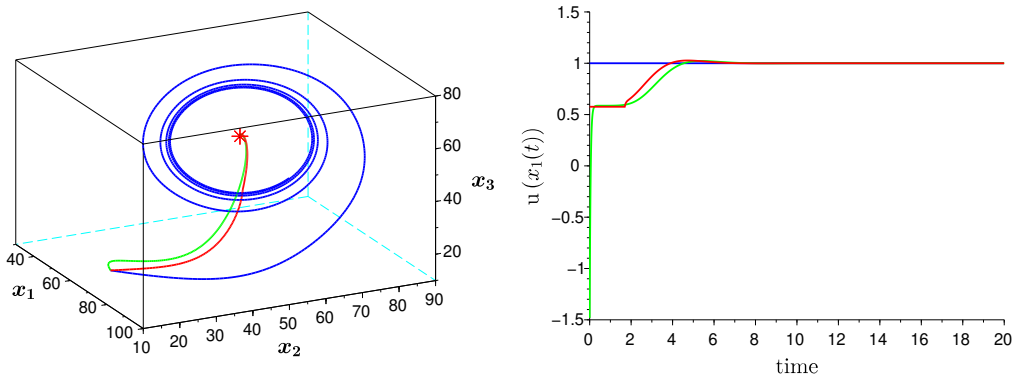

Figure 5.3.2: Simulation for a negative loop: the parameters are $\kappa_{0i} = 2$, $\kappa_i = 100$, $\gamma_i = 1$, $\theta_i = 56.39$ and $n_i = 5$, $\forall\ i \in \{1, 2, 3\}$, leading to $\bar{x}^- = (58.7, 57, 53.4)$. The initial condition for the simulation is $x_0 = (70, 16, 17)$. With these parameters, $\alpha_0^- = 0.17$, and α is fixed to $\alpha = 0.22$. Left: trajectories in the state space. The steady state is represented by the red star. The blue line is a simulation of the uncontrolled negative loop (3.2.1) with initial condition x_0 and converges towards a periodic orbit. The green line is a simulation of system (5.2.1) under affine control (4.2.1), and the red line under control (5.2.2) with $u_{min} = 0.58$ and $u_{max} = 13.49$ and same initial condition x_0: there is converge towards $\bar{x}^-$. Right: control laws against time for the trajectories depicted on the left figure, with the corresponding colors. It is possible to observe that for the classical control law, the control is negative for initial times, and for the saturated control strategy, the input saturates at u_{min} for initial times.

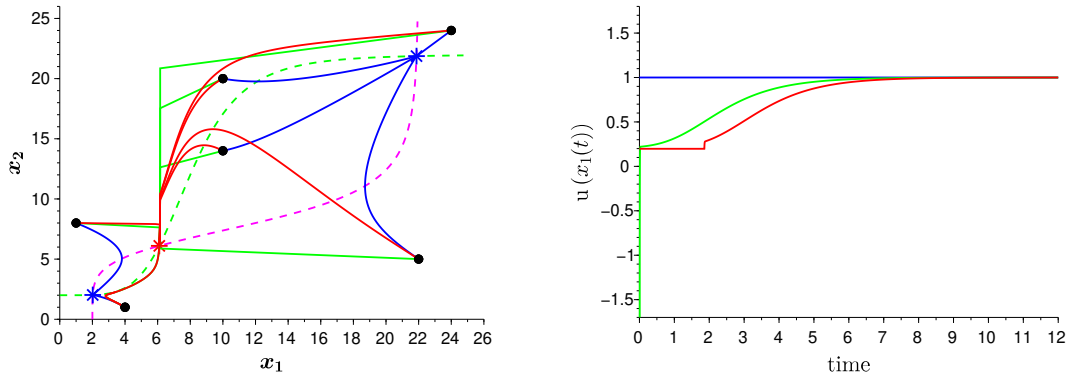

Figure 5.3.3: Simulation for a positive loop: the parameters are $\kappa_{0i} = 2$, $\kappa_i = 20$, $\gamma_i = 1$, $\theta_i = 8$ and $n_i = 5$, $\forall\ i \in \{1, 2\}$. With these parameters, $\alpha_0^+ = 13.66$, and α is fixed to $\alpha = 14.66$. Left: The two stable steady states $\bar{x}^+_{inf} = (2.02, 2.02)$ and $\bar{x}^+_{sup} = (21.87, 21.87)$ of the uncontrolled system are represented by blue stars and $\bar{x}^+ = (6.1, 6.1)$ is represented by the red star. The dashed green (resp. magenta) line is the x_2-nullcline (resp. x_1-nullcline). The blue lines are simulations of the uncontrolled positive loop (3.2.1) and converge towards one of the two stable steady states. The green lines are simulations of system (5.2.1) under affine control (4.2.1), and the red lines under control (5.2.2) with $u_{min} = 0.19$ and $u_{max} = 61.12$. The different initial conditions are depicted by black dots. Right: control laws against time for the trajectory with initial condition $x_0 = (10, 14)$ depicted on the left figure, with the corresponding colors. It is possible to observe that for the classical control law, the control is negative for initial times, and for the saturated control strategy, the input saturates at u_{min} for initial times.

One drawback to this result is its sharp dependence on precise measurements. Indeed, this saturated control technique depends on the precise knowledge of the variable x_1 in the central region $x_{1min}^* \leq x_1 \leq x_{1max}^*$. However, most of the time the measurements available in biology are of qualitative nature leading to partially known systems. To deal with this constraint, it will be considered in next chapter that the state of the system is partially known, leading to piecewise linear control laws.

Chapter 6

Piecewise constant control strategy

6.1 Introduction

For classical control methods such as the affine control law designed in chapter 4, or the saturated control designed in chapter 5, the variable of interest is continuously measured, and the control law depends dynamically and precisely on this measurement. In biotechnology however, quantitative measurements are mostly inaccessible: indeed, genes expressions are often evaluated by quantifying the levels of the genes products as explained in chapter 2. The intensity of fluorescence leads to a discrete estimation of the temporal and spatial gene expression level within the cell. Moreover, biological control techniques, such as the one reviewed in chapter 2, often lead to constant inputs [62]. These biological realities prevent the implementation of classical control strategies that depend on precise knowledge of the state, and naturally encourage qualitative control depending on regions of the state space only and producing constant control inputs. This class of control strategy has been already applied for different biological systems such as piecewise affine (PWA) gene regulatory networks. In [28] for example, the authors designed a qualitative control in order to globally stabilize the different steady states of a two-dimensional PWA genetic positive feedback loop. This system was also controlled in [80] in order to stabilize its unstable steady state, and real biological implementations were performed by a bang-bang controller in order to support the analytical results. A similar idea is presented in [38], where the production rate of a two-dimensional PWA genetic feedback loop is controlled in order to create a periodic orbit. More theoretically, a general framework has been developed in [45] and [42] in order to control PWA gene regulatory networks. In practice, the outputs of classical controllers such as PI are converted into constant inputs with Pulse Width Modulation (PWM) techniques that transform a continuous-time signal into pulses of duration proportional to the amplitude of the signal [87, 49, 48, 63, 64].

These biological realities lead to the analysis of hybrid systems for which classical results about dynamics and control do not apply. For this purpose, new theory and new methods have been developed [81]. As explained in chapter 3, for hybrid systems with discontinuous right-hand sides in particular, the solutions can be defined with the theory of Filippov and differential inclusions [47], leading to specific dynamics such as sliding modes. The same limits occur when treating stability problems [101]. For example, the construction of smooth Lyapunov functions is a hard task for these types of systems [16]. Yet, few methods have been developed to answer stability questions for particular cases [25].

Aside from these previous studies, little is found in the literature for the biological control of complete gene regulatory networks. In this context, this chapter presents a piecewise constant control strategy which considers the new synthetic control approaches as well as the main biological constraints just presented, in order to recover the stable biological conditions of a disrupted negative feedback loop that exhibits undesired sustained oscillations, and design a dedifferentiation process for a positive feedback loop.

The piecewise constant control strategy leads to the analysis of a hybrid system with autonomous switch of its dynamics (section 6.2). As already presented in chapters 4 and 5, the control law is designed as simply as possible: it only depends on the position of the system relative to its steady state of interest and acts on the expression of a unique gene. In section 6.3, the construction of successive repelling regions allows one to determine the qualitative dynamics of both the positive and negative controlled loops. In section 6.4, the asymptotic stability is demonstrated by constructing specific nested balls and provides robust properties to the resulting system. A slight modification of this PWL control strategy is introduced in section 6.5 and illustrated with a calibration of the Toggle Switch presented in chapter 2. Finally, section 6.6 introduces a trade-off between the possible strength of inputs and the speed of convergence of solutions.

The content of section 6.5 can be found in the article published for the conference DYCOPS (see the section "List of publications" on page 5).

6.2 The controlled model

As explained in the introduction, the piecewise constant structure of the designed control law $\mathrm{u}(x_1)$ is motivated by the quantized nature of the available biological measurements. To recover homeostatic conditions for the negative loop and dedifferentiation for the positive loop, the control strategy must lead to a global convergence towards the unstable steady state $\bar{x}^*$ of the system.

The controlled feedback loop is defined by:

$$\begin{cases} \dot{x}_1(x_1, x_N) = \kappa_{01} + \mathrm{u}(x_1)\kappa_1 \mathrm{h}^*(x_N, \theta_N, n_N) - \gamma_1 x_1, \\ \dot{x}_i(x_i, x_{i-1}) = \kappa_{0i} + \kappa_i \mathrm{h}^+(x_{i-1}, \theta_{i-1}, n_{i-1}) - \gamma_i x_i \quad \forall\, i \in \{2, ..., N\}, \end{cases} \tag{6.2.1}$$

where

$$\begin{cases} \mathrm{u}(x_1) = u_{min} \leq 1 \quad \text{when} \quad x_1 \geq \bar{x}_1^*, \\ \mathrm{u}(x_1) = u_{max} \geq 1 \quad \text{when} \quad x_1 \leq \bar{x}_1^*. \end{cases} \tag{6.2.2}$$

In a more compact form, this dynamical system can be denoted $\dot{x} = F(\mathrm{u}(x_1), x)$.

In order to keep the biological experiments as simple as possible, the control law $\mathrm{u}(x_1)$ is arbitrarily dependent on the measurement of the first gene x_1 and acts on its own expression only. A control dependent on the measurements of any of the other $N-1$ genes, as well as the control of their expression, are possible extensions of this work. Here, the control $\mathrm{u}(x_1)$ appears outside the Hill function: in biology, this strategy may be applied by introducing inside the network a new molecule able to directly interact with the promoter of the first gene, either an inducer or a repressor. In section 6.5, another strategy will be presented, in which the control $\mathrm{u}(x_1)$ appears inside the Hill function. In this case, the control must be interpreted differently in biology.

The two constants u_{min} and u_{max} describe respectively a reduction and an amplification of the natural influence of component N on component 1 of the loop, and are adapted to the input types generated by biological control means. Moreover, the measurements of x_1 are considered qualitative, leading to partial knowledge of the system. The gene can either be detected highly expressed ($x_1 \geq \bar{x}_1^*$) or weakly expressed ($x_1 \leq \bar{x}_1^*$). As soon as x_1 is inside the uncertain domain $\bar{x}_1^*$ (also called a switching domain), the control law is undetermined and may either take the value u_{min} or u_{max}. Therefore, system (6.2.1) under the qualitative control law (6.2.2) is a differential system with discontinuous right-hand side and its solutions are appropriately defined in the sense of Filippov as the solutions of the following differential inclusion [47]:

$$\dot{x} \in H(x)$$

such that $H(x) = F(u_{min}, x)$ when $x_1 \geq \bar{x}_1^*$, $H(x) = F(u_{max}, x)$ when $x_1 \leq \bar{x}_1^*$ and

$$H(x) = \bar{co}\{F(u_{min}, x), F(u_{max}, x)\}$$

on the switching domain, where $\bar{co}$ is the closed convex hull of the set of values of the vector field. These types of solutions often lead to the emergence of sliding modes along the switching domains, as discussed in chapter 3.

Remark 6.2.1. *This new controlled system is also a priori bounded: for the negative loop,* $x_1 \in]\kappa_{01}/\gamma_1, \max\left((\kappa_{01} + u_{min}\kappa_1)/\gamma_1, \bar{x}_1^-\right)]$ *and* $x_1 \in [\kappa_{01}/\gamma_1, \max\left((\kappa_{01} + u_{min}\kappa_1)/\gamma_1, \bar{x}_1^+\right)[$ *for the positive loop. For* $i \in \{2, ..., N\}$, $x_i \in [\kappa_{0i}/\gamma_i, (\kappa_{0i} + \kappa_i)/\gamma_i[$.

6.3 Global convergence

In this section it will be shown that, under appropriate conditions on the two constant inputs u_{min} and u_{max}, the global stability of $\bar{x}^*$ is achieved. This will be proved by identifying specific dynamical transitions between zones of the state space.

6.3.1 Global convergence for the negative loop

For the negative loop, the space is partitioned as follows:

Definition 6.3.1. *The N-dimensional space is partitioned in* 3^N *zones. Each zone is called* $(a_1 a_2 ... a_{N-1} a_N)$ *such that* $\forall\ i \in \{1, ..., N\}$*:*

- $a_i = 0$ *if* $x_i < \bar{x}_i^-$,
- $a_i = 1$ *if* $x_i = \bar{x}_i^-$,
- $a_i = 2$ *if* $x_i > \bar{x}_i^-$.

An illustration of the partitioning in dimension 3 is presented in figure 6.3.1.

Remark 6.3.1. *The term region will further refer to a union of zones. For example the region* $a_1 = 2$ *is the union of* 3^{N-1} *zones:* $(2a_2 ... a_{N-1} a_N)$ *where* $a_i \in \{0, 1, 2\}\ \forall\ i \in \{2, ..., N\}$.

Definition 6.3.2. *A region of the state space is repellent if:*

- *for each trajectory starting in this region, there is a time* $T > 0$ *after which the trajectory leaves the region,*
- *no trajectory enters this region.*

Practically, if the vector field $\dot{x}_i$ in a region $(a_1 ... a_N)$ keeps a non-zero constant sign in the whole region, including at the borders, the region is repellent in direction i. When the region is upper (resp. lower) bounded in direction i, if $\dot{x}_i > 0$ (resp. $\dot{x}_i < 0$), the trajectories will leave the region through the upper (resp. lower) bound defining a_i.

The following conditions on u_{min} and u_{max} allow the statement of four lemmas that successively define repelling regions of the state space:

Assumption 6.3.1.

$$\begin{cases} u_{min} \leq (\gamma_1 \bar{x}_1^- - \kappa_{01})/\kappa_1, \\ u_{max} = 1. \end{cases}$$

Lemma 6.3.1. *Under assumption 6.3.1, the region defined by* $a_1 = 2$ *is repellent.*

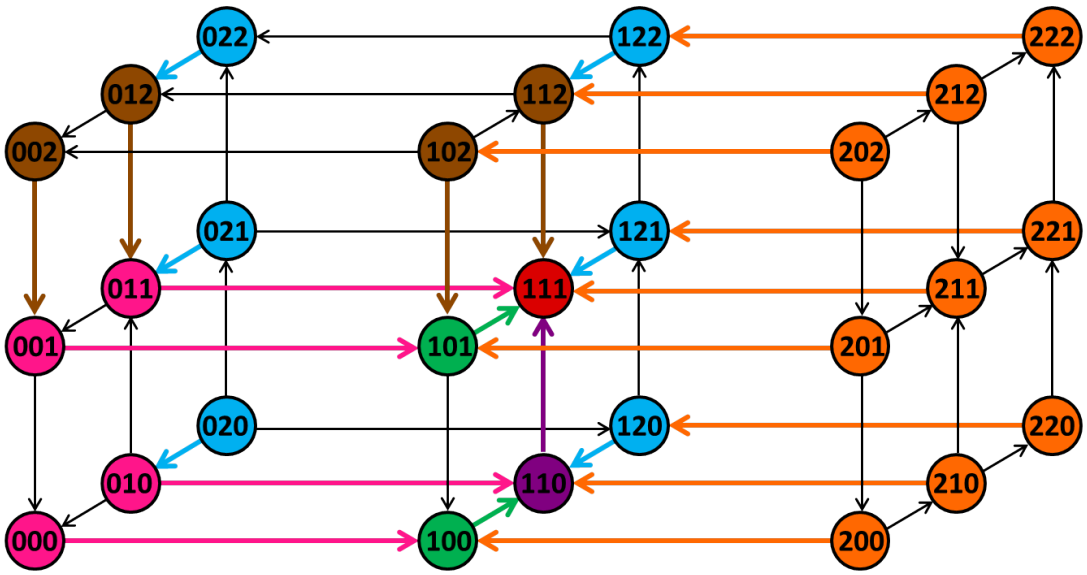

Figure 6.3.1: Partitioning of the state space in dimension 3 according to definition 6.3.1, and graph of transitions. The space is split in different zones of different dimensions, all represented as nodes in this figure: any zone with $a_i \in \{0,2\}\ \forall\ i \in \{1,2,3\}$ is 3-dimensional; any zone with $a_i = 1$ for a unique $i \in \{1,2,3\}$ is 2-dimensional; any zone with $a_i = 1$ for exactly two indexes $i \in \{1,2,3\}$ is 1-dimensional; and (111) is 0-dimensional. The arrows represent transitions between zones. As explained, some transitions represented here by the black arrows do not play any role in the construction of the proof of theorem 6.3.1. The repellent regions are represented with different colors: lemma 6.3.1 is illustrated with orange arrows leaving orange region. Lemma 6.3.2 is successively illustrated with blue arrows leaving blue region and brown arrows leaving brown region. Afterwards, lemma 6.3.3 is illustrated with pink arrows leaving pink region, followed by lemma 6.3.4 successively illustrated with green arrows leaving green region and purple arrows leaving purple region. In the end, the trajectories converge towards the steady state represented by the red zone (111).

Proof. In the region $x_1 > \bar{x}_1^-$ the x_1-vector field is defined as:
$\dot{x}_1(x_1, x_N) = \kappa_{01} + u_{min}\kappa_1 \mathrm{h}^-(x_N, \theta_N, n_N) - \gamma_1 x_1$. By evaluating this expression on the wall $x_1 = \bar{x}_1^-$ and using the condition on u_{min}, the following inequality comes up: $\dot{x}_1(\bar{x}_1^-, x_N) \leq (\kappa_{01} - \gamma_1 \bar{x}_1^-)\left(1 - \mathrm{h}^-(x_N, \theta_N, n_N)\right)$. The properties of the uncontrolled system explained in proposition 3.2.8 give $\bar{x}_1^- \in\ ]\kappa_{01}/\gamma_1, (\kappa_{01} + \kappa_1)/\gamma_1]$ and the decreasing Hill function meets the condition $\mathrm{h}^-(x_N, \theta_N, n_N) \in\ ]0, 1]$. This implies $\dot{x}_1(\bar{x}_1^-, x_N) \leq 0$. Moreover, for x_N fixed and $x_1 > \bar{x}_1^-$, the linear degradation term $-\gamma_1 x_1$ in the x_1-vector field expression gives: $\dot{x}_1(x_1, x_N) < \dot{x}_1(\bar{x}_1^-, x_N) \leq 0$. Hence, $\dot{x}_1(x_1, x_N) < 0\ \forall\ x_N \geq 0$ and $\forall\ x_1 > \bar{x}_1^-$. Finally, as $a_1 = 2$ is lower-bounded by $x_1 = \bar{x}_1^-$, the region is repellent. □

This first lemma is illustrated in the left plot of figure 6.3.2 by the three blue arrows.

Lemma 6.3.2. *For any $i \in \{1, ..., N-1\}$, if the region defined by $a_i = 2$ is repellent, then the region $a_{i+1} = 2$ is repellent as well.*

Proof. In the whole space, the x_{i+1}-vector field is defined as:
$\dot{x}_{i+1}(x_{i+1}, x_i) = \kappa_{0i+1} + \kappa_{i+1}\mathrm{h}^+(x_i, \theta_i, n_i) - \gamma_{i+1} x_{i+1}$. By evaluating this expression on the wall $x_{i+1} = \bar{x}_{i+1}^-$ and using the definition of the steady state $\bar{x}_{i+1}^- = \left(\kappa_{0i+1} + \kappa_{i+1}\mathrm{h}^+(\bar{x}_i^-, \theta_i, n_i)\right)/\gamma_{i+1}$, the equality becomes: $\dot{x}_{i+1}(\bar{x}_{i+1}^-, x_i) = \kappa_{i+1}\left(\mathrm{h}^+(x_i, \theta_i, n_i) - \mathrm{h}^+(\bar{x}_i^-, \theta_i, n_i)\right)$. From the hypothesis, $a_i = 2$ is repellent, which is equivalent to $x_i \leq \bar{x}_i^-$. The strictly monotonic property of the increasing Hill function implies $\mathrm{h}^+(x_i, \theta_i, n_i) \leq \mathrm{h}^+(\bar{x}_i^-, \theta_i, n_i)$. Then $\dot{x}_{i+1}(\bar{x}_{i+1}^-, x_i) \leq 0\ \forall\ x_i \leq \bar{x}_i^-$.

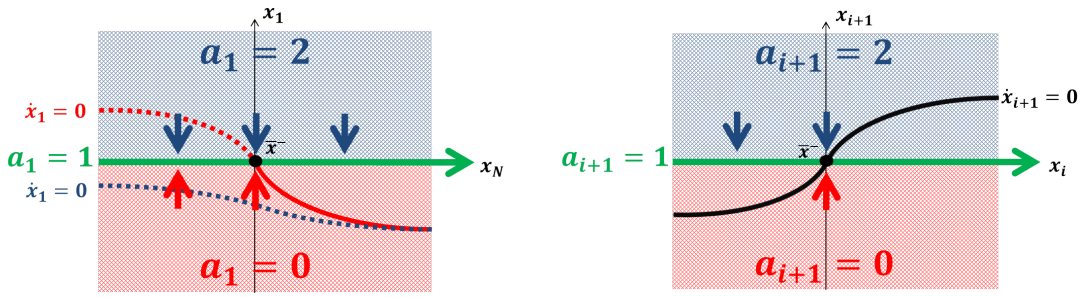

Figure 6.3.2: Left: Transitions properties in the (x_1, x_N) plane. The dashed blue line is the x_1-nullcline for the region $a_1 = 2$. The half-plain half-dashed red line is the x_1-nullcline for the region $a_1 = 0$. The dashed style corresponds to nullclines situated in another region, and the plain style for nullclines situated in their proper region. The arrows represent the vector field in the x_1-direction. Lemma 6.3.1 is illustrated by blue arrows, and lemma 6.3.3 by red arrows. Right: Transition properties in the (x_i, x_{i+1}) plane. The black line is the x_{i+1}-nullcline. The arrows represent the vector field in the x_{i+1}-direction. Lemma 6.3.2 is illustrated by blue arrows, and lemma 6.3.4 by red arrows.

Moreover, for x_i fixed and $x_{i+1} > \bar{x}_{i+1}^-$, the linear degradation term $-\gamma_{i+1}x_{i+1}$ in the x_{i+1}-vector field expression gives: $\dot{x}_{i+1}(x_{i+1}, x_i) < \dot{x}_{i+1}(\bar{x}_{i+1}^-, x_i) \leq 0$. Hence, $\dot{x}_{i+1}(x_{i+1}, x_i) < 0 \ \forall \ x_i \leq \bar{x}_i^-$ and $\forall \ x_{i+1} > \bar{x}_{i+1}^-$. Finally, as $a_{i+1} = 2$ is lower-bounded by $x_{i+1} = \bar{x}_{i+1}^-$, if $a_i = 2$ is repellent, then the region $a_{i+1} = 2$ is repellent as well. □

The two blue arrows in the right plot of figure 6.3.2 illustrate this second lemma.

Lemma 6.3.3. *Under assumption 6.3.1, within the region $a_i \in \{0, 1\} \ \forall \ i \in \{1, ..., N\}$, the region defined by $a_1 = 0$ is repellent.*

Proof. In the region $x_1 < \bar{x}_1^-$ the x_1-vector field is defined as:
$\dot{x}_1(x_1, x_N) = \kappa_{01} + \kappa_1 \mathrm{h}^-(x_N, \theta_N, n_N) - \gamma_1 x_1$. By evaluating this expression on the wall $x_1 = \bar{x}_1^-$ and using the definition of the steady state $\bar{x}_1^- = \left(\kappa_{01} + \kappa_1 \mathrm{h}^-(\bar{x}_N^-, \theta_N, n_N)\right)/\gamma_1$, the equality becomes: $\dot{x}_1(\bar{x}_1^-, x_N) = \kappa_1 \left(\mathrm{h}^-(x_N, \theta_N, n_N) - \mathrm{h}^-(\bar{x}_N^-, \theta_N, n_N)\right)$. From the hypothesis, $a_N \in \{0, 1\}$, which is equivalent to $x_N \leq \bar{x}_N^-$. The strictly monotonic property of the decreasing Hill function implies $\mathrm{h}^-(x_N, \theta_N, n_N) \geq \mathrm{h}^-(\bar{x}_N^-, \theta_N, n_N)$. Then $\dot{x}_1(\bar{x}_1^-, x_N) \geq 0 \ \forall \ x_N \leq \bar{x}_N^-$. Moreover, for x_N fixed and $x_1 < \bar{x}_1^-$, the linear degradation term $-\gamma_1 x_1$ in the x_1-vector field expression gives: $\dot{x}_1(x_1, x_N) > \dot{x}_1(\bar{x}_1^-, x_N) \geq 0$. Hence, $\dot{x}_1(x_1, x_N) > 0 \ \forall \ x_N \leq \bar{x}_N^-$ and $\forall \ x_1 < \bar{x}_1^-$. Finally, as $a_1 = 0$ is upper-bounded by $x_1 = \bar{x}_1^-$, $a_1 = 0$ is repellent within the region $a_N \in \{0, 1\}$. □

The two red arrows in the left plot of figure 6.3.2 illustrate this third lemma.

Lemma 6.3.4. *For any $i \in \{1, ..., N-1\}$, if the regions defined by $a_i = 0$ and $a_i = 2$ are repellent, then the region $a_{i+1} = 0$ is repellent as well.*

Proof. In the whole space, the x_{i+1}-vector field is defined as:
$\dot{x}_{i+1}(x_{i+1}, x_i) = \kappa_{0i+1} + \kappa_{i+1} \mathrm{h}^+(x_i, \theta_i, n_i) - \gamma_{i+1} x_{i+1}$. By evaluating this expression on the wall $x_{i+1} = \bar{x}_{i+1}^-$ and using the definition of the steady state $\bar{x}_{i+1}^-$, the equality becomes: $\dot{x}_{i+1}(\bar{x}_{i+1}^-, x_i) = \kappa_{i+1} \left(\mathrm{h}^+(x_i, \theta_i, n_i) - \mathrm{h}^+(\bar{x}_i^-, \theta_i, n_i)\right)$. From the hypothesis, $a_i = 2$ and $a_i = 0$ are repellent, which is equivalent to $x_i = \bar{x}_i^-$. Then $\dot{x}_{i+1}(\bar{x}_{i+1}^-, \bar{x}_i^-) = 0$. Moreover, for $x_{i+1} < \bar{x}_{i+1}^-$, the linear degradation term $-\gamma_{i+1} x_{i+1}$ in the x_{i+1}-vector field expression gives: $\dot{x}_{i+1}(x_{i+1}, \bar{x}_i^-) > \dot{x}_{i+1}(\bar{x}_{i+1}^-, \bar{x}_i^-) = 0$. Hence, $\dot{x}_{i+1}(x_{i+1}, \bar{x}_i^-) > 0 \ \forall \ x_{i+1} < \bar{x}_{i+1}^-$. Finally, as $a_{i+1} = 0$ is upper-bounded by $x_{i+1} = \bar{x}_{i+1}^-$, $a_{i+1} = 0$ is repellent within the region $a_i = 1$. □

This final lemma is illustrated by the red arrow in the right plot of figure 6.3.2. These four lemmas finally allow the statement of the main result of this section for the negative loop:

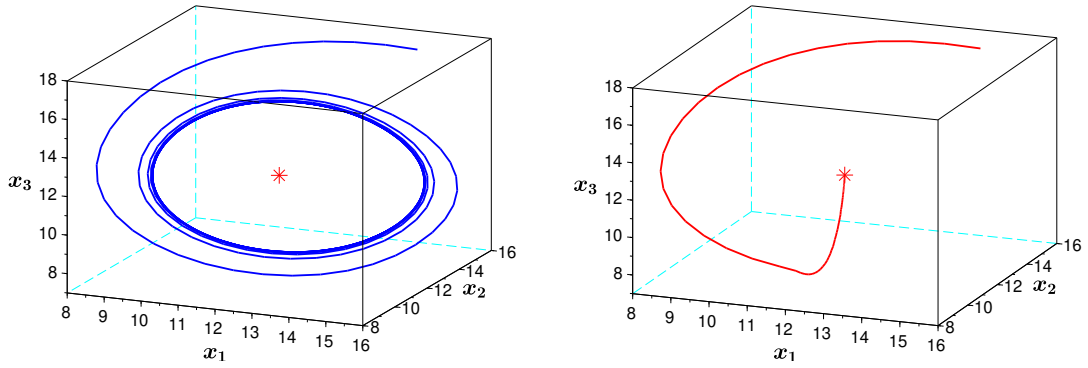

Figure 6.3.3: Left: Simulation of system (3.2.1) without control in dimension 3. The locally unstable steady state $\bar{x}^- = (12, 12, 12)$, represented by a red star, leads to the emergence of a periodic orbit. Right: Simulation of system (6.2.1) in dimension 3 with control $u_{min} = 0.4$ and $u_{max} = 1$. There is convergence towards the globally attractive steady state $\bar{x}^-$ through a sliding mode on the plane $x_1 = \bar{x}_1^-$. For both figures, $\kappa_{0i} = 2$, $\kappa_i = 8$, $\gamma_i = 0.5$, $\theta_i = 12$, $n_i = 7$ for $i \in \{1, 2, 3\}$, and the initial condition is $x_0 = (14, 16, 17)$.

Theorem 6.3.1. *If assumption 6.3.1 holds, system (6.2.1) under control law (6.2.2) converges globally towards the zone* $(a_1...a_N) = (1...1)$ *where* $a_i = 1 \ \forall \ i \in \{1, ..., N\}$.

Proof. As a base case, lemma 6.3.1 states that any trajectory is contained in the region $a_1 \neq 2$. By a mathematical induction, lemma 6.3.2 states that any trajectory is contained in the region $a_i \neq 2$ $\forall \ i \in \{1, ..., N\}$. As a new base case lemma 6.3.3 states that any trajectory stands in the region $a_1 = 1$ and $a_i \neq 2 \ \forall \ i \in \{2, ..., N\}$. Finally, by a second mathematical induction, lemma 6.3.4 states that the trajectories are further constrained in the zone $a_i = 1 \ \forall \ i \in \{1, ..., N\}$. In other words, all the trajectories converge towards the steady state $\bar{x}^-$ through a sliding mode in the subspace $x_1 = \bar{x}_1^-$, ending the proof of global convergence. □

This type of demonstration has been already exploited for similar systems [119, 96, 19, 20, 43]. In this paper however, the analysis intentionally considers a restricted number of transitions (colored arrows in figure 6.3.1) in comparison with classical proofs that analyze all potential transitions (supplementary black arrows in figure 6.3.1). While the traditional method gives more material about trajectories, this reduced approach greatly facilitates the understanding of the global dynamics in any dimension N.

Remark 6.3.2. *The condition* $u_{max} = 1$ *in assumption 6.3.1 is equivalent to the uncontrolled system (3.2.1) in the half-space* $x_1 \leq \bar{x}_1$. *Theorem 6.3.1 means that the system is only controlled in the half-space* $x_1 \geq \bar{x}_1$. *The condition* $u_{max} = 1$ *can be reduced to* $u_{max} \geq 1$. *By introducing new zones, a proof based on the same ideas lead to the same global convergence result. However, as controlling biological systems is a complicated task, the result with* $u_{max} = 1$ *limits the control complexity and is more convenient for real implementation.*

A simulation of global convergence in dimension 3 is illustrated in figure 6.3.3.

6.3.2 Global convergence for the positive loop

For the positive loop, the space is partitioned as follows:

Definition 6.3.3. *The N-dimensional space is partitioned in* 4^N *zones. Again, each zone is called* $(a_1 a_2 ... a_{N-1} a_N)$ *such that* $\forall \ i \in \{1, ..., N\}$*:*

- $a_i = 0$ *if* $x_i < \bar{x}_i^+ - \nu_i$,
- $a_i = 1$ *if* $\bar{x}_i^+ - \nu_i \leq x_i < \bar{x}_i^+$,

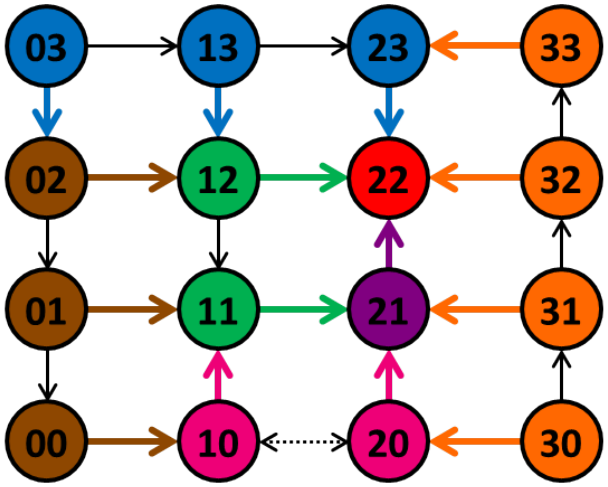

Figure 6.3.4: Partitioning of the state space in dimension 2 according to definition 6.3.3, and graph of transitions. The space is split in different zones of different dimensions, all represented as nodes in this figure: any zone with $a_i \in \{0, 1, 3\}\ \forall\ i \in \{1, 2\}$ is 2-dimensional; any zone with $a_i = 2$ for a unique $i \in \{1, 2\}$ is 1-dimensional and (22) is 0-dimensional. The arrows represent transitions between zones. As explained, some transitions represented here by the plain black arrows do not play any role in the construction of the proof of theorem 6.3.2. Moreover, some transitions, represented by dashed black arrows, are undetermined. The repellent regions are represented with different colors: lemma 6.3.5 is illustrated with orange arrows leaving orange region. Lemma 6.3.6 is illustrated with blue arrows leaving blue region. Afterwards, lemma 6.3.7 is illustrated with brown arrows leaving brown region, followed by lemma 6.3.8 illustrated with pink arrows leaving pink region. Next, lemma 6.3.9 is illustrated with green arrows leaving green region, followed by lemma 6.3.10 illustrated with purple arrows leaving purple region. In the end, the trajectories converge towards the steady state represented by the red zone (22).

- $a_i = 2$ *if* $x_i = \bar{x}_i^+$,
- $a_i = 3$ *if* $x_i > \bar{x}_i^+$,

where:

- $\nu_1 = \bar{x}_1^+ - \kappa_{01}/\gamma_1$,
- $\nu_i = \bar{x}_i^+ - \left(\kappa_{0i} + \kappa_i h^+(\bar{x}_{i-1}^+ - \nu_{i-1}, \theta_{i-1}, n_{i-1})\right)/\gamma_i\ \forall\ i \in \{2, ..., N\}$.

An illustration of the partitioning in dimension 2 is presented in figure 6.3.4.

The following conditions on u_{min} and u_{max} allow the statement of six lemmas that successively define repelling regions of the state space:

Assumption 6.3.2.

$$\begin{cases} u_{min} \leq \dfrac{\gamma_1 \bar{x}_1^+ - \kappa_{01}}{\kappa_1}, \\ u_{max} \geq \dfrac{\gamma_1 \bar{x}_1^+ - \kappa_{01}}{\kappa_1 h^+(\bar{x}_N^+ - \nu_N, \theta_N, n_N)} \end{cases}$$

The condition on u_{min} given in assumption 6.3.2 gives the first observation:

Lemma 6.3.5. *Under assumption 6.3.2, the region defined by* $a_1 = 3$ *is repellent.*

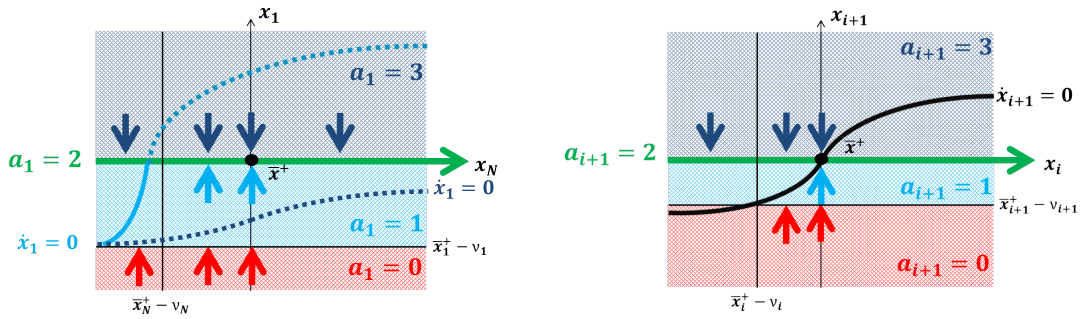

Figure 6.3.5: Left: Transitions properties in the (x_1, x_N) plane. The dashed dark blue line is the x_1-nullcline for the region $a_1 = 3$. The half-plain half-dashed light blue line is the x_1-nullcline for the regions $a_1 = 0$ and $a_1 = 1$. The dashed style corresponds to nullclines situated in another region, and the plain style for nullclines situated in their proper region. The arrows represent vector field in x_1-direction. Lemma 6.3.5 is illustrated by dark blue arrows, lemma 6.3.7 by red arrows and lemma 6.3.9 by light blue arrows. Right: Transitions properties in the (x_i, x_{i+1}) plane. The black line is the x_{i+1}-nullcline. The arrows represent vector field in x_{i+1}-direction. Lemma 6.3.6 is illustrated by dark blue arrows, lemma 6.3.8 by red arrows, and lemma 6.3.10 by light blue arrows.

Proof. In the region $x_1 > \bar{x}_1^+$ the x_1-vector field is defined as:
$\dot{x}_1(x_1, x_N) = \kappa_{01} + u_{min}\kappa_1 \mathrm{h}^+(x_N, \theta_N, n_N) - \gamma_1 x_1$. By evaluating this expression on the wall $x_1 = \bar{x}_1^+$ and using the condition on u_{min}, the following inequality comes up: $\dot{x}_1(\bar{x}_1^+, x_N) \leq (\kappa_{01} - \gamma_1 \bar{x}_1^+)\left(1 - \mathrm{h}^+(x_N, \theta_N, n_N)\right)$. The properties of the uncontrolled system explained proposition 3.2.8 gives $\bar{x}_1^+ \in [\kappa_{01}/\gamma_1, (\kappa_{01} + \kappa_1)/\gamma_1[$ and the increasing Hill function meets the condition $\mathrm{h}^+(x_N, \theta_N, n_N) \in [0, 1[$. This induces $\dot{x}_1(\bar{x}_1^+, x_N) \leq 0$. Moreover, for x_N fixed and $x_1 > \bar{x}_1^+$, the linear degradation term $-\gamma_1 x_1$ in the x_1-vector field expression gives: $\dot{x}_1(x_1, x_N) < \dot{x}_1(\bar{x}_1^+, x_N) \leq 0$. Hence, $\dot{x}_1(x_1, x_N) < 0 \ \forall \ x_N \geq 0$ and $\forall \ x_1 > \bar{x}_1^+$. Finally, as $a_1 = 3$ is lower-bounded by $x_1 = \bar{x}_1^+$, the region is repellent. □

This first lemma is illustrated in the left plot of figure 6.3.5 by the four dark blue arrows.

Lemma 6.3.6. *For any $i \in \{1, ..., N-1\}$, if the region defined by $a_i = 3$ is repellent, then the region $a_{i+1} = 3$ is repellent as well.*

Proof. In the whole space, the x_{i+1}-vector field is defined as:
$\dot{x}_{i+1}(x_{i+1}, x_i) = \kappa_{0i+1} + \kappa_{i+1}\mathrm{h}^+(x_i, \theta_i, n_i) - \gamma_{i+1} x_{i+1}$. By evaluating this expression on the wall $x_{i+1} = \bar{x}_{i+1}^+$ and using the definition of the steady state $\bar{x}_{i+1}^+ = \left(\kappa_{0i+1} + \kappa_{i+1}\mathrm{h}^+(\bar{x}_i^+, \theta_i, n_i)\right)/\gamma_{i+1}$, the equality becomes: $\dot{x}_{i+1}(\bar{x}_{i+1}^+, x_i) = \kappa_{i+1}\left(\mathrm{h}^+(x_i, \theta_i, n_i) - \mathrm{h}^+(\bar{x}_i^+, \theta_i, n_i)\right)$. From the hypothesis $a_i = 3$ is repellent, which is equivalent to $x_i \leq \bar{x}_i^+$. The strictly monotonous property of the increasing Hill function induces $\mathrm{h}^+(x_i, \theta_i, n_i) \leq \mathrm{h}^+(\bar{x}_i^+, \theta_i, n_i)$. Then $\dot{x}_{i+1}(\bar{x}_{i+1}^+, x_i) \leq 0 \ \forall \ x_i \leq \bar{x}_i^+$. Moreover, for x_i fixed and $x_{i+1} > \bar{x}_{i+1}^+$, the linear degradation term $-\gamma_{i+1} x_{i+1}$ in the x_{i+1}-vector field expression gives: $\dot{x}_{i+1}(x_{i+1}, x_i) < \dot{x}_{i+1}(\bar{x}_{i+1}^+, x_i) \leq 0$. Hence, $\dot{x}_{i+1}(x_{i+1}, x_i) < 0 \ \forall \ x_i \leq \bar{x}_i^+$ and $\forall \ x_{i+1} > \bar{x}_{i+1}^+$. Finally, as $a_{i+1} = 3$ is lower-bounded by $x_{i+1} = \bar{x}_{i+1}^+$, if $a_i = 3$ is repellent, the region $a_{i+1} = 3$ is repellent as well. □

The three dark blue arrows in the right plot of figure 6.3.5 illustrate this second lemma.

Lemma 6.3.7. *Under assumption 6.3.2, within the region $a_i \in \{0, 1, 2\} \ \forall \ i \in \{1, ..., N\}$, the region defined by $a_1 = 0$ is repellent.*

Proof. In the region $x_1 < \bar{x}_1^+ - \nu_1$ the x_1-vector field is defined as:
$\dot{x}_1(x_1, x_N) = \kappa_{01} + u_{max}\kappa_1 \mathrm{h}^-(x_N, \theta_N, n_N) - \gamma_1 x_1$. By evaluating this expression on the wall $x_1 = \bar{x}_1^+ - \nu_1 = \kappa_{01}/\gamma_1$, the equality becomes: $\dot{x}_1(\bar{x}_1^+ - \nu_1, x_N) = u_{max}\kappa_1 \mathrm{h}^+(x_N, \theta_N, n_N)$. The increasing Hill function meets the condition $\mathrm{h}^+(x_N, \theta_N, n_N) \in [0, 1[$. Then $\dot{x}_1(\bar{x}_1^+ - \nu_1, x_N) \geq 0$

$\forall\ x_N \leq \bar{x}_N^+$. Moreover, for x_N fixed and $x_1 < \bar{x}_1^+ - \nu_1$, the linear degradation term $-\gamma_1 x_1$ in the x_1-vector field expression gives: $\dot{x}_1(x_1, x_N) > \dot{x}_1(\bar{x}_1^+ - \nu_1, x_N) \geq 0$. Hence, $\dot{x}_1(x_1, x_N) > 0\ \forall$ $x_N \leq \bar{x}_N^+$ and $\forall\ x_1 < \bar{x}_1^+ - \nu_1$. Finally, as $a_1 = 0$ is upper-bounded by $x_1 = \bar{x}_1^+ - \nu_1$, $a_1 = 0$ is repellent within the region $a_N \in \{0, 1, 2\}$. □

The three red arrows in the left plot of figure 6.3.5 illustrate this third lemma.

Lemma 6.3.8. *For any $i \in \{1, ..., N-1\}$, if the regions defined by $a_i = 0$ and $a_i = 3$ are repellent, then the region $a_{i+1} = 0$ is repellent as well.*

Proof. In the whole space, the x_{i+1}-vector field is defined as:
$\dot{x}_{i+1}(x_{i+1}, x_i) = \kappa_{0i+1} + \kappa_{i+1}\mathrm{h}^+(x_i, \theta_i, n_i) - \gamma_{i+1}x_{i+1}$. By evaluating this expression on the wall $x_{i+1} = \bar{x}_{i+1}^+ - \nu_{i+1}$ and using the definition ν_{i+1}, the equality becomes: $\dot{x}_{i+1}(\bar{x}_{i+1}^+ - \nu_{i+1}, x_i) = \kappa_{0i+1} + \kappa_{i+1}\mathrm{h}^+(x_i, \theta_i, n_i) - \gamma_{i+1}\bar{x}_{i+1}^+ - \gamma_{i+1}\nu_{i+1} = \kappa_{i+1}\left(\mathrm{h}^+(x_i, \theta_i, n_i) - \mathrm{h}^+(\bar{x}_i^+ - \nu_i, \theta_i, n_i)\right)$. From the hypothesis, $a_i = 0$ and $a_i = 3$ are repellent, which is equivalent to $\bar{x}_i^+ - \nu_i \leq x_i \leq \bar{x}_i^+$. Then $\dot{x}_{i+1}(\bar{x}_{i+1}^+ - \nu_{i+1}, x_i) \geq 0\ \forall\ \bar{x}_i^+ - \nu_i \leq x_i \leq \bar{x}_i^+$. Moreover, for $x_{i+1} < \bar{x}_{i+1}^+ - \nu_{i+1}$, the linear degradation term $-\gamma_{i+1}x_{i+1}$ in the x_{i+1}-vector field expression gives: $\dot{x}_{i+1}(x_{i+1}, x_i) > \dot{x}_{i+1}(\bar{x}_{i+1}^+ - \nu_{i+1}, x_i) \geq 0$. Hence, $\dot{x}_{i+1}(x_{i+1}, x_i) > 0\ \forall\ x_{i+1} < \bar{x}_{i+1}^+ - \nu_{i+1}$ and $\forall\ \bar{x}_i^+ - \nu_i \leq x_i \leq \bar{x}_i^+$. Finally, as $a_{i+1} = 0$ is upper-bounded by $x_{i+1} = \bar{x}_{i+1}^+ - \nu_{i+1}$, $a_{i+1} = 0$ is repellent within the region $a_i \in \{1, 2\}$. □

This lemma is illustrated by the two red arrows in the right plot of figure 6.3.5.

Lemma 6.3.9. *Under assumption 6.3.2, within the region $a_i \in \{1, 2\}\ \forall\ i \in \{1, ..., N\}$, the region defined by $a_1 = 1$ is repellent.*

Proof. In the region $\bar{x}_1^+ - \nu_1 \leq x_1 < \bar{x}_1^+$ the x_1-vector field is defined as:
$\dot{x}_1(x_1, x_N) = \kappa_{01} + u_{max}\kappa_1\mathrm{h}^+(x_N, \theta_N, n_N) - \gamma_1 x_1$. With the conditions given on u_{max}, the equality becomes:

$$\begin{aligned}\dot{x}_1(x_1, x_N) &\geq \kappa_{01} + \frac{\gamma_1\bar{x}_1^+ - \kappa_{01}}{\kappa_1\mathrm{h}^+(\bar{x}_N^+ - \nu_N, \theta_N, n_N)}\kappa_1\mathrm{h}^+(x_N, \theta_N, n_N) - \gamma_1 x_1 \\ &= \frac{\mathrm{h}^+(x_N, \theta_N, n_N)}{\mathrm{h}^+(\bar{x}_N^+ - \nu_N, \theta_N, n_N)}\left[\gamma_1\bar{x}_1^+ - \kappa_{01}\right] + \left[\kappa_{01} - \gamma_1 x_1\right].\end{aligned}$$

As $\kappa_{01}/\gamma_1 \leq x_1 < \bar{x}_1^+$, hence $\kappa_{01} - \gamma_1 x_1 \leq 0$ and $|\kappa_{01} - \gamma_1 x_1| = \gamma_1 x_1 - \kappa_{01}$. Moreover the properties of the uncontrolled system, explained in proposition 3.2.8, give $\bar{x}_1^+ \in [\kappa_{01}/\gamma_1, (\kappa_{01} + \kappa_1)/\gamma_1[$, hence $\gamma_1\bar{x}_1^+ - \kappa_{01} \geq 0$. As $\bar{x}_1^+ - \nu_1 \leq x_1 < \bar{x}_1^+$, $|\gamma_1\bar{x}_1^+ - \kappa_{01}| > |\kappa_{01} - \gamma_1 x_1|$. On the other hand, $a_N \in \{1, 2\}$, equivalent to $\bar{x}_N^+ - \nu_N \leq x_N \leq \bar{x}_N^+$. Then with the strictly monotonic property of the increasing Hill function, $\mathrm{h}^+(x_N, \theta_N, n_N) \geq \mathrm{h}^+(\bar{x}_N^+ - \nu_N, \theta_N, n_N)$ leading to:
$\mathrm{h}^+(x_N, \theta_N, n_N)/\mathrm{h}^+(\bar{x}_N^+ - \nu_N, \theta_N, n_N) \geq 1$. Then:

$$\begin{aligned}&\frac{\mathrm{h}^+(x_N, \theta_N, n_N)}{\mathrm{h}^+(\bar{x}_N^+ - \nu_N, \theta_N, n_N)}|\gamma_1\bar{x}_1^+ - \kappa_{01}| > |\kappa_{01} - \gamma_1 x_1| \\ &\frac{\mathrm{h}^+(x_N, \theta_N, n_N)}{\mathrm{h}^+(\bar{x}_N^+ - \nu_N, \theta_N, n_N)}\left[\gamma_1\bar{x}_1^+ - \kappa_{01}\right] > \left[\gamma_1 x_1 - \kappa_{01}\right] \\ &\frac{\mathrm{h}^+(x_N, \theta_N, n_N)}{\mathrm{h}^+(\bar{x}_N^+ - \nu_N, \theta_N, n_N)}\left[\gamma_1\bar{x}_1^+ - \kappa_{01}\right] + \left[\kappa_{01} - \gamma_1 x_1\right] > 0.\end{aligned}$$

Therefore, $\dot{x}_1(x_1, x_N) > 0\ \forall\ \bar{x}_N^+ - \nu_N \leq x_N \leq \bar{x}_N^+$ and $\forall\ \bar{x}_1^+ - \nu_1 \leq x_1 < \bar{x}_1^+$. Finally, as $a_1 = 1$ is upper-bounded by $x_1 = \bar{x}_1^+$, $a_1 = 1$ is repellent within the region $a_N \in \{1, 2\}$. □

This lemma is illustrated by the two light blue arrows in the left plot of figure 6.3.5.

Lemma 6.3.10. *For any $i \in \{1, ..., N-1\}$, if the regions defined by $a_i = 0$, $a_i = 1$ and $a_i = 3$ are repellent, then the region $a_{i+1} = 1$ is repellent as well.*

Proof. In the whole space, the x_{i+1}-vector field is defined as:
$\dot{x}_{i+1}(x_{i+1}, x_i) = \kappa_{0i+1} + \kappa_{i+1} \mathrm{h}^+(x_i, \theta_i, n_i) - \gamma_{i+1} x_{i+1}$. An evaluation of the vector field on the wall $x_{i+1} = \bar{x}^+_{i+1}$ and using the definition of the steady state $\bar{x}^+_{i+1}$, the equality becomes: $\dot{x}_{i+1}(\bar{x}^+_{i+1}, x_i) = \kappa_{i+1} \left(\mathrm{h}^+(x_i, \theta_i, n_i) - \mathrm{h}^+(\bar{x}^+_i, \theta_i, n_i) \right)$. From the hypothesis $a_i = 3$, $a_i = 1$ and $a_i = 0$ are repellent, which is equivalent to $x_i = \bar{x}^+_i$. Then $\dot{x}_{i+1}(\bar{x}^+_{i+1}, \bar{x}^+_i) = 0$. Moreover, for $x_{i+1} < \bar{x}^+_{i+1}$, the linear degradation term $-\gamma_{i+1} x_{i+1}$ in the x_{i+1}-vector field expression gives: $\dot{x}_{i+1}(x_{i+1}, \bar{x}^+_i) > \dot{x}_{i+1}(\bar{x}^+_{i+1}, \bar{x}^+_i) = 0$. Hence, $\dot{x}_{i+1}(x_{i+1}, \bar{x}^+_i) > 0 \; \forall \; \bar{x}^+_{i+1} - \nu_{i+1} \leq x_{i+1} < \bar{x}^+_{i+1}$. Finally, as $a_{i+1} = 1$ is upper-bounded by $x_{i+1} = \bar{x}^+_{i+1}$, $a_{i+1} = 1$ is repellent within the region $a_i = 2$. □

These six lemmas finally allow the statement of the main result of this section for the positive loop:

Theorem 6.3.2. *If assumption 6.3.2 holds, system (6.2.1) under control law (6.2.2) converges globally towards the zone* $(a_1 ... a_N) = (2...2)$ *where* $a_i = 2 \; \forall \; i \in \{1, ..., N\}$.

Proof. As a base case, lemma 6.3.5 states that any trajectory is contained in the region $a_1 \neq 3$. By a mathematical induction, lemma 6.3.6 states that any trajectory is contained in the region $a_i \neq 3$ $\forall \; i \in \{1, ..., N\}$. As a new base case lemma 6.3.7 states that any trajectory stands in the region $a_1 \in \{1, 2\}$ and $a_i \neq 3 \; \forall \; i \in \{2, ..., N\}$. By a second mathematical induction, lemma 6.3.8 states that the trajectories are further constrained in the zone $a_i \in \{1, 2\} \; \forall \; i \in \{1, ..., N\}$. As a last base case, lemma 6.3.9 states that any trajectory stands in the region $a_1 = 2$ and $a_i \in \{1, 2\} \; \forall \; i \in \{2, ..., N\}$. Finally, by a last mathematical induction, lemma 6.3.10 states that the trajectories are further constrained in the zone $a_i = 2 \; \forall \; i \in \{1, ..., N\}$. In other words, all the trajectories converge towards the steady state $\bar{x}^+$ through a sliding mode in the subspace $x_1 = \bar{x}^+_1$, ending the proof of global convergence. □

Figure 6.3.4 gives an illustration of the successive repelling regions in dimension 2 determined by the six previous lemmas.

A simulation of global convergence in dimension 2 is illustrated in figure 6.3.6. It is possible to observe that the red trajectories do not slide perfectly on the switching domain $x_1 = \bar{x}^+_1$. This is a numerical artefact called chattering. However, this artefact illustrates what may happen in reality if the timescale of evolution of the control is slow compared to the time scale of evolution of the dynamical system.

Remark 6.3.3. *For the positive loop, the state space has to be partitioned in more zones than for the negative loop, and the condition* $u_{max} = 1$ *is not enough for the global convergence. This is explained by the fact that the succession of the repelling regions for the positive loop must be initialized twice: indeed the upper and lower repelling regions are defined separately, whereas for the negative loop, the upper and lower repelling regions are defined together in the same induction steps thanks to the decreasing nullcline for* $\dot{x}_1$ *that switches the boundaries.*

6.4 Global stability

In this section, the global stability of the attracting point $\bar{x}^*$ is investigated for both loops by constructing balls of specific radius that satisfy the classical definition of Lyapunov stability [75]: a large ball called $\mathcal{B}^*_\delta$ in which trajectories that start inside a smaller ball must stay, an intermediary region called $\mathcal{B}^*$ such that $\mathcal{B}^* \subset \mathcal{B}^*_\delta$ and $\mathcal{B}^*$ invariant, and a small ball $\mathcal{B}^*_\epsilon$ of initial conditions such that $\mathcal{B}^*_\epsilon \subset \mathcal{B}^* \subset \mathcal{B}^*_\delta$. The next definition introduces the largest ball $\mathcal{B}^*_\delta$ of radius δ:

Definition 6.4.1. *For any* $\delta > 0$ *fixed, the ball* $\mathcal{B}^*_\delta$ *is defined by:* $\mathcal{B}^*_\delta = \{x | \; ||x(t) - \bar{x}^*||_\infty \leq \delta\}$, *where* $||x(t)||_\infty = \max_i |x_i(t)|$.

The following definition is essential for the construction of the intermediary invariant region $\mathcal{B}^*$:

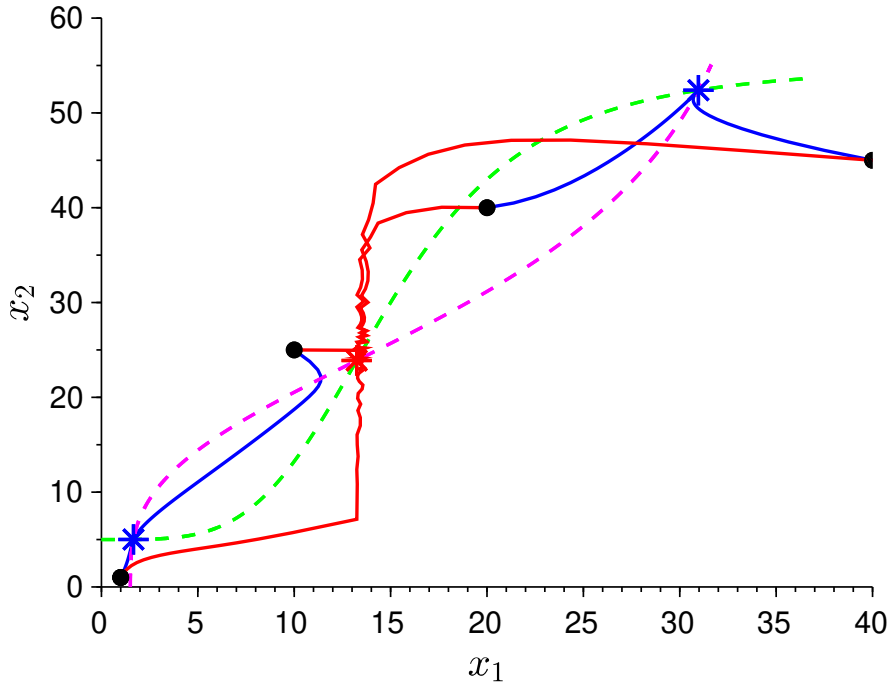

Figure 6.3.6: Comparison of trajectories of system (3.2.1) in dimension 2 with and without control. The green dashed line is the x_2-nullcline and the magenta dashed line the x_1-nullcline. The four blue lines are trajectories without control with initial conditions $x_0 \in \{(1,1),(10,25),(20,40),(40,45)\}$: the two locally stable steady states $\bar{x}^+_{inf} = (1.66, 5)$ and $\bar{x}^+_{sup} = (31, 52.4)$ are represented by blue stars and are attractive without control; the locally unstable steady state $\bar{x}^+ = (13.2, 23.9)$ represented by a red star is repellent without control. The four red lines are trajectories of system (6.2.1) with control $u_{min} = 0.32$, and $u_{max} = 72.58$, and same initial conditions. The two locally stable steady states become repellent, and all the trajectories converge towards $\bar{x}^+$ through a sliding mode on the line $x_1 = \bar{x}^+_1$. For both situations, $\kappa_{01} = 0.3$, $\kappa_1 = 7$, $\gamma_1 = 0.2$, $\theta_1 = 15$, $n_1 = 4$ and $\kappa_{02} = 0.5$, $\kappa_2 = 5$, $\gamma_2 = 0.1$, $\theta_2 = 30$, $n_2 = 3$.

Definition 6.4.2. *For any $y \in [0,1[$ and for any $i \in \{2,...,N\}$, the function $\phi_i(y)$ is defined as the inverse function of $h^+(x, \theta_{i-1}, n_{i-1})$. In the same way, for any $y \in]0,1]$, the function $\phi_1^-(y)$ is defined as the inverse function of $h^-(x, \theta_N, n_N)$ and for any $y \in [0,1[$, the function $\phi_1^+(y)$ is defined as the inverse function of $h^+(x, \theta_N, n_N)$.*

These inverse functions satisfy the following property:

Property 6.4.1. *By definition 6.4.2, for any $i \in \{2,...,N\}$, $h^+(x, \theta_{i-1}, n_{i-1}) = y$ implies that $x = \phi_i(y)$ where ϕ_i are monotonically increasing functions that satisfy $\bar{x}^*_{i-1} = \phi_i\left((\gamma_i \bar{x}^*_i - \kappa_{0i})/\kappa_i\right)$. Likewise, $h^+(x, \theta_N, n_N) = y$ implies that $x = \phi_1^+(y)$ where ϕ_1^+ is a monotonically increasing function that satisfies $\bar{x}^+_N = \phi_1^+\left((\gamma_1 \bar{x}^+_1 - \kappa_{01})/\kappa_1\right)$. Finally, $h^-(x, \theta_N, n_N) = y$ implies that $x = \phi_1^-(y)$ where ϕ_1^- is a monotonically decreasing function that satisfies $\bar{x}^-_N = \phi_1^-\left((\gamma_1 \bar{x}^-_1 - \kappa_{01})/\kappa_1\right)$.*

6.4.1 Global stability for the negative loop

For the negative loop, the global stability of $\bar{x}^-$ is first proved with the following assumption:

Assumption 6.4.1. $0 < \delta < \bar{x}^-_1 - \kappa_{01}/\gamma_1$, *and* $0 < \delta < \min\left(\bar{x}^-_i - \kappa_{0i}/\gamma_i, (\kappa_{0i} + \kappa_i)/\gamma_i - \bar{x}^-_i\right)$ $\forall\ i \in \{2,...,N\}$.

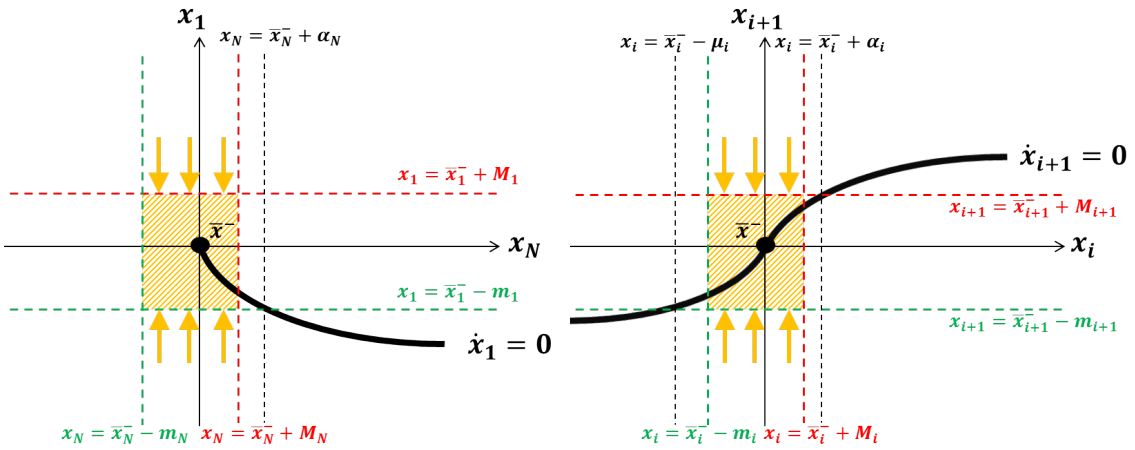

Figure 6.4.1: Left: x_1-vector field in the (x_1, x_N) plane. The plain black line is the x_1-nullcline in the region $x_1 < \bar{x}_1^-$. In the region $x_1 > \bar{x}_1^-$ the x_1-vector field is strictly negative because of the control u_{min}. The horizontal red and green dashed lines are respectively the upper and lower boundaries in direction x_1 of the region $\mathcal{B}^-$. The black vertical dashed line is defined in order to keep a constant sign of the vector field in the x_1-direction at the lower boundary. No vertical line is necessary in order to keep a constant sign of the vector field in the x_1-direction at the upper boundary as the x_1-vector field is already strictly negative there. The vertical red and green dashed lines are respectively the upper and lower boundaries in direction x_N. The region $\mathcal{B}^-$ is highlighted in yellow. The yellow arrows represent vector field in x_1-direction at the boundaries of $\mathcal{B}^-$ and illustrate the invariance of the region in direction x_1. Right: x_{i+1}-vector field in the (x_i, x_{i+1}) plane. The plain black line is the x_{i+1}-nullcline. The horizontal red and green dashed lines are respectively the upper and lower boundaries in direction x_{i+1} of the region $\mathcal{B}^-$. The two black vertical dashed lines are defined in order to keep a constant sign of the vector field in the x_{i+1}-direction at the upper and lower boundaries. The vertical red and green dashed lines are respectively the upper and lower boundaries in direction x_i. The region $\mathcal{B}^-$ is highlighted in yellow. The yellow arrows represent vector field in direction x_{i+1} at the boundaries of $\mathcal{B}^-$ and illustrate the invariance of the region in direction x_{i+1}.

From proposition 3.2.8, it is possible to choose such a $\delta > 0$, and the ball $\mathcal{B}^-$ can be defined:

Definition 6.4.3. *Under assumption 6.4.1, the region $\mathcal{B}^-$ is defined with:*

- $\mu_N = \delta$ *and* $m_N = \mu_N$,
- $\mu_i = \bar{x}_i^- - \phi_{i+1}\left(\left(\gamma_{i+1}(\bar{x}_{i+1}^- - m_{i+1}) - \kappa_{0i+1}\right)/\kappa_{i+1}\right)$
  and $m_i = \min(\delta, \mu_i)$, $\forall\ i \in \{N-1, ..., 1\}$,
- $\alpha_N = \phi_1^-\left(\left(\gamma_1(\bar{x}_1^- - m_1) - \kappa_{01}\right)/\kappa_1\right) - \bar{x}_N^-$ *and* $M_N = \min(\delta, \alpha_N)$,
- $\alpha_i = \phi_{i+1}\left(\left(\gamma_{i+1}(\bar{x}_{i+1}^- + M_{i+1}) - \kappa_{0i+1}\right)/\kappa_{i+1}\right) - \bar{x}_i^-$
  and $M_i = \min(\delta, \alpha_i)$, $\forall\ i \in \{N-1, ..., 1\}$.

Then $\mathcal{B}^- = \left\{x | \bar{x}_i^- - m_i \leq x_i \leq \bar{x}_i^- + M_i \quad \forall\ i \in \{1, ..., N\}\right\}$.

An illustration of these bounds is given in figure 6.4.1.

The following property certifies that μ_i, α_i, m_i and M_i are well defined for all $i \in \{1, ..., N\}$:

Proposition 6.4.1. *Under assumption 6.4.1, $\mu_i > 0$ and $\alpha_i > 0$ $\forall\ i \in \{1, ..., N\}$, and as a consequence:*

- $\kappa_{0i}/\gamma_i < \bar{x}_i^- - m_i < \bar{x}_i^-$ *and* $\bar{x}_i^- < \bar{x}_i^- + M_i < (\kappa_{0i} + \kappa_i)/\gamma_i \ \forall \ i \in \{2, ..., N\}$,
- $\kappa_{01}/\gamma_1 < \bar{x}_1^- - m_1 < \bar{x}_1^-$ *and* $\bar{x}_1^- < \bar{x}_1^- + M_1$.

The proof of this proposition is detailed in appendix C.1.

The next proposition is a consequence of the construction of the region $\mathcal{B}^-$:

Proposition 6.4.2. *The region $\mathcal{B}^-$ is included in the ball $\mathcal{B}_\delta^-$.*

Proof. For all $i \in \{1, ..., N\}$, $\bar{x}_i^- - m_i = \bar{x}_i^- - \min(\delta, \mu_i)$, then $\bar{x}_i^- - m_i \geq \bar{x}_i^- - \delta$. In the same way, for all $i \in \{1, ..., N\}$, $\bar{x}_i^- + M_i = \bar{x}_i^- + \min(\delta, \alpha_i)$, then $\bar{x}_i^- + M_i \leq \bar{x}_i^- + \delta$. □

The main lemma of this section can now be introduced:

Lemma 6.4.1. *Under assumptions 6.4.1 and 6.3.1, for any $x(0) \in \mathcal{B}^-$, $x(t) \in \mathcal{B}^- \ \forall \ t \geq 0$.*

In other words, this lemma states that the region $\mathcal{B}^-$ is invariant. The details of the proof can be found in appendix C.2 and an illustration is presented in figure 6.4.1. Now, in order to prove the Lyapunov stability of the attracting point $\bar{x}^-$, the initial conditions ball $\mathcal{B}_\epsilon^-$ is constructed:

Definition 6.4.4. *Under the assumption 6.4.1, the constant ϵ is defined as:*

$$\epsilon = \min(\min_i m_i, \min_i M_i).$$

The ball $\mathcal{B}_\epsilon^-$ is defined as: $\mathcal{B}_\epsilon^- = \left\{x | \bar{x}_i^- - \epsilon \leq x_i \leq \bar{x}_i^- + \epsilon \quad \forall \ i \in \{1, ..., N\}\right\}$.

The following lemma states dynamical properties of trajectories starting in the ball $\mathcal{B}_\epsilon^-$:

Lemma 6.4.2. *Under assumptions 6.4.1 and 6.3.1, for all $x(0) \in \mathcal{B}_\epsilon^-$, $x(t) \in \mathcal{B}_\delta^- \ \forall \ t \geq 0$.*

Proof. As $\mathcal{B}_\epsilon^- \subset \mathcal{B}^-$ by construction, then for all $x(0) \in \mathcal{B}_\epsilon^-$, $x(0) \in \mathcal{B}^-$ which implies from lemma 6.4.1 that $x(t) \in \mathcal{B}^- \ \forall \ t \geq 0$. Now, as $\mathcal{B}^- \subset \mathcal{B}_\delta^-$, then for all $x(0) \in \mathcal{B}_\epsilon^-$, $x(t) \in \mathcal{B}^- \ \forall \ t \geq 0$, which implies that $x(t) \in \mathcal{B}_\delta^- \ \forall \ t \geq 0$. □

In order to conclude, the following last remark is essential to relax assumption 6.4.1

Remark 6.4.1. *If assumption 6.4.1 is not fulfilled for a $\delta > 0$, then it is sufficient to consider any ball of radius $\delta' > 0$ such that $\mathcal{B}_{\delta'}^- \subset \mathcal{B}_\delta^-$ and such that δ' fulfills assumption 6.4.1. The region $\mathcal{B}^-$ is constructed for $\mathcal{B}_{\delta'}^-$, as well as the initial condition ball $\mathcal{B}_\epsilon^-$. In these conditions, for all $x(0) \in \mathcal{B}_\epsilon^-$, $x(t) \in \mathcal{B}_{\delta'}^- \ \forall \ t \geq 0$ with lemma 6.4.2, which implies that $x(t) \in \mathcal{B}_\delta^- \ \forall \ t \geq 0$.*

The main theorem for the negative loop is now introduced:

Theorem 6.4.1. *Under assumption 6.3.1, the equilibrium point $\bar{x}^-$ is globally asymptotically stable.*

Proof. For any $\delta > 0$, there exists an $\epsilon = \min(\min_i m_i, \min_i M_i) > 0$, as stated in definition 6.4.4 and remark 6.4.1, such that every solution $x(t)$ having initial conditions in the ball $\mathcal{B}_\epsilon^-$ (i.e. within a distance ϵ of the equilibrium: $||x(0) - \bar{x}^-||_\infty \leq \epsilon$), remains in the ball $\mathcal{B}_\delta^-$ (i.e. within a distance δ of the equilibrium: $||x(t) - \bar{x}^-||_\infty \leq \delta$) for all $t \geq 0$, as stated by lemma 6.4.2 and remark 6.4.1. Moreover the equilibrium $\bar{x}^-$ is globally attractive with theorem 6.3.1. Then it follows that $\bar{x}^-$ is globally asymptotically stable. □

An illustration of the different balls and regions in dimension 3 as well as a dynamical simulation of the system are illustrated in figure 6.4.2. This stability result provides robustness properties to the resulting controlled system.

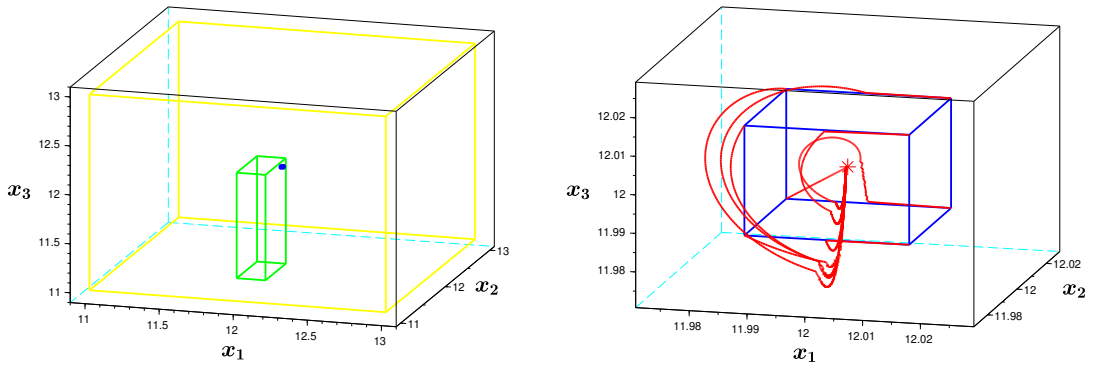

Figure 6.4.2: Left: Simulation of the balls and regions in dimension 3 for $\delta = 1$: the largest ball $\mathcal{B}_\delta^-$ is in yellow, the invariant region $\mathcal{B}^-$ is in green and the smallest initial conditions ball $\mathcal{B}_\epsilon^-$ is in dark blue with $\epsilon \approx 0.014$. Right: Zoom in the ball $\mathcal{B}_\epsilon^-$, with a simulation of 8 trajectories of system (6.2.1) starting at the 8 corners of the cube $\mathcal{B}_\epsilon^-$, with control $u_{min} = 0.4$ and $u_{max} = 1$. As previously determined, there is convergence towards the globally asymptotically stable steady state $\bar{x}^-$ illustrated by a red star, through a sliding mode on the plane $x_1 = \bar{x}_1^-$. Some of the trajectories leave the ball $\mathcal{B}_\epsilon^-$ but they all stay in the largest ball $\mathcal{B}_\delta^-$ (not represented in the figure for more clarity as it is a lot larger). For both plots, the parameters are the same as in figure 6.3.3.

6.4.2 Global stability for the positive loop

For the positive loop, the global stability of $\bar{x}^+$ is proved with relaxed conditions on u_{min} and u_{max} compared to the conditions given in assumption 6.3.2:

Assumption 6.4.2.

$$\begin{cases} u_{min} < 1, \\ u_{max} > 1. \end{cases}$$

As for the negative loop, the stability of $\bar{x}^+$ will be first proved with the following assumption:

Assumption 6.4.3. $\forall\ i \in \{2, ..., N\}\ 0 < \delta < \min\left(\bar{x}_i^+ - \kappa_{0i}/\gamma_i, (\kappa_{0i} + \kappa_i)/\gamma_i - \bar{x}_i^+\right)$. *Moreover,* $0 < \delta < \min\left(\bar{x}_1^+ - \kappa_{01}/\gamma_1, (\kappa_{01} + u_{min}\kappa_1)/\gamma_1 - \bar{x}_1^+\right)$ *if* $1 > u_{min} > (\gamma_1 \bar{x}_1^+ - \kappa_{01})/\kappa_1$ *and* $0 < \delta < \bar{x}_1^+ - \kappa_{01}/\gamma_1$ *otherwise.*

From proposition 3.2.8, it is possible to choose such a $\delta > 0$. The following definition is essential for the construction of the ball $\mathcal{B}^+$:

Definition 6.4.5. *If* $1 > u_{min} > (\gamma_1 \bar{x}_1^+ - \kappa_{01})/\kappa_1$, *then* x_{Nmax} *is defined as the intersection between the* x_1*-nullcline in the space* $x_1 > \bar{x}_1$ *and the line* $x_1 = \bar{x}_1$. *In this case,* $x_{Nmax} = \phi_1^+\left((\gamma_1 \bar{x}_1^+ - \kappa_{01})/(u_{min}\kappa_1)\right)$. *Otherwise,* $x_{Nmax} = +\infty$. *Similarly,* x_{Nmin} *is defined as the intersection between the* x_1*-nullcline in the space* $x_1 < \bar{x}_1$ *and the line* $x_1 = \bar{x}_1$. *In this case,* $x_{Nmin} = \phi_1^+\left((\gamma_1 \bar{x}_1^+ - \kappa_{01})/(u_{max}\kappa_1)\right)$.

Definition 6.4.6. *Under assumption 6.4.3, the region* $\mathcal{B}^+$ *is defined with:*

- $\alpha_N = \min\left(\delta, x_{Nmax} - \bar{x}_N^+\right)$ *and* $M_N = \alpha_N$,
- $\alpha_i = \phi_{i+1}\left(\left(\gamma_{i+1}(\bar{x}_{i+1}^+ + M_{i+1}) - \kappa_{0i+1}\right)/\kappa_{i+1}\right) - \bar{x}_i^+$
  and $M_i = \min\left(\delta, \alpha_i\right)$, *for all* $i \in \{N-1, ..., 1\}$,
- $\mu_N = \min\left(\delta, \bar{x}_N^+ - x_{Nmin}\right)$ *and* $m_N = \mu_N$,
- $\mu_i = \bar{x}_i^+ - \phi_{i+1}\left(\left(\gamma_{i+1}(\bar{x}_{i+1}^+ - m_{i+1}) - \kappa_{0i+1}\right)/\kappa_{i+1}\right)$
  and $m_i = \min\left(\delta, \mu_i\right)$, *for all* $i \in \{N-1, ..., 1\}$,

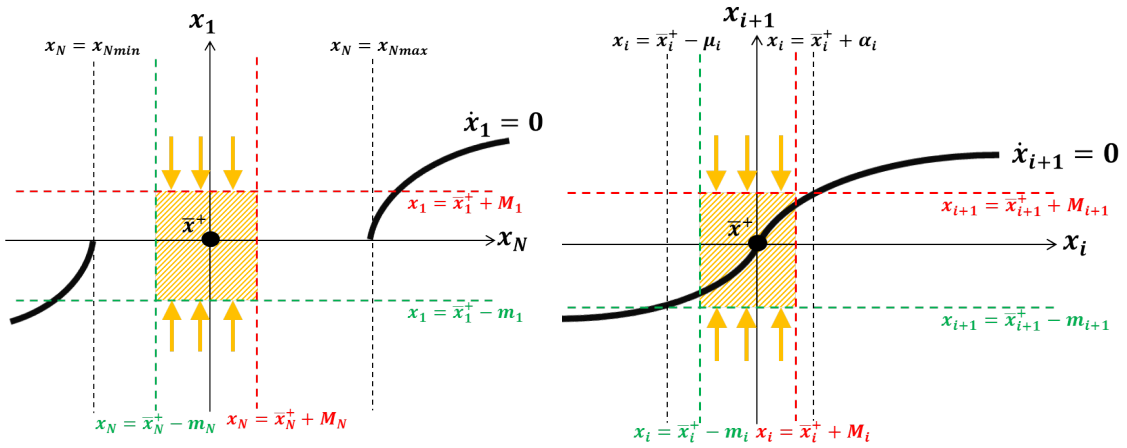

Figure 6.4.3: Left: x_1-vector field properties in the (x_1, x_N) plane. The plain black lines are the x_1-nullclines. The horizontal red and green dashed lines are respectively the upper and lower boundaries in direction x_1 of the region $\mathcal{B}^+$. The black vertical dashed lines are x_{Nmax} and x_{Nmin} as defined in 6.4.5 (in the case $1 > u_{min} > (\gamma_1 \bar{x}_1^+ - \kappa_{01})/\kappa_1$). They are defined in order to keep a constant sign of the vector field in the x_1-direction at the upper and lower boundary. The vertical red and green dashed lines are respectively the upper and lower boundaries in direction x_N. The region $\mathcal{B}^+$ is highlighted in yellow. The yellow arrows represent vector field in x_1-direction at the boundaries of $\mathcal{B}^+$ and illustrate the invariance of the region in direction x_1. Right: x_{i+1}-vector field properties in the (x_i, x_{i+1}) plane. The plain black line is the x_{i+1}-nullcline. The horizontal red and green dashed lines are respectively the upper and lower boundaries in direction x_{i+1} of the region $\mathcal{B}^+$. The two black vertical dashed lines are defined in order to keep a constant sign of the vector field in the x_{i+1}-direction at the upper and lower boundaries. The vertical red and green dashed lines are respectively the upper and lower boundaries in direction x_i. The region $\mathcal{B}^+$ is highlighted in yellow. The yellow arrows represent vector field in x_{i+1}-direction at the boundaries of $\mathcal{B}^+$ and illustrate the invariance of the region in direction x_{i+1}.

Then $\mathcal{B}^+ = \{x | \bar{x}_i^+ - m_i \leq x_i \leq \bar{x}_i^+ + M_i \quad \forall\, i \in \{1, ..., N\}\}$.

These boundaries are illustrated in figure 6.4.3.

The following property certifies that μ_i, α_i, m_i and M_i are well defined for all $i \in \{1, ..., N\}$:

Proposition 6.4.3. *Under assumption 6.4.3,* $\mu_i > 0$ *and* $\alpha_i > 0$ *for all* $i \in \{1, ..., N\}$, *and as a consequence:*

- $\kappa_{0i}/\gamma_i < \bar{x}_i^+ - m_i < \bar{x}_i^+$ *and* $\bar{x}_i^+ < \bar{x}_i^+ + M_i < (\kappa_{0i} + \kappa_i)/\gamma_i \;\forall\, i \in \{2, ..., N\}$,
- $\kappa_{01}/\gamma_1 < \bar{x}_1^+ - m_1 < \bar{x}_1^+$ *and* $\bar{x}_1^+ < \bar{x}_1^+ + M_1$. *Moreover, if* $1 > u_{min} > (\gamma_1 \bar{x}_1^+ - \kappa_{01})/\kappa_1$, $\bar{x}_1^+ + M_1 < (\kappa_{01} + u_{min}\kappa_1)/\gamma_1$.

The proof of this proposition can be found in appendix C.3.

Exactly as for the negative loop, next proposition is a consequence of the construction of the region $\mathcal{B}^+$:

Proposition 6.4.4. *The region* $\mathcal{B}^+$ *is included in the ball* $\mathcal{B}_\delta^+$.

Proof. For all $i \in \{1, ..., N-1\}$, $\bar{x}_i^+ - m_i = \bar{x}_i^+ - \min(\delta, \mu_i)$, then $\bar{x}_i^+ - m_i \geq \bar{x}_i^+ - \delta$. For $i = N$, $\bar{x}_N^+ - m_N = \bar{x}_N^+ - \mu_N = \bar{x}_N^+ - \min(\delta, \bar{x}_N^+ - x_{Nmin})$, then $\bar{x}_N^+ - m_N \geq \bar{x}_N^+ - \delta$. In the same way, for all $i \in \{1, ..., N-1\}$, $\bar{x}_i^+ + M_i = \bar{x}_i^+ + \min(\delta, \alpha_i)$, then $\bar{x}_i^+ + M_i \leq \bar{x}_i^+ + \delta$. For $i = N$, $\bar{x}_N^+ + M_N = \bar{x}_N^+ + \alpha_N = \bar{x}_N^+ + \min(\delta, x_{Nmax} - \bar{x}_N^+)$, then $\bar{x}_N^+ + M_N \geq \bar{x}_N^+ + \delta$. □

The main lemma for the positive loop can now be introduced:

Lemma 6.4.3. *Under assumptions 6.4.2 and 6.4.3, for any* $x(0) \in \mathcal{B}^+$, $x(t) \in \mathcal{B}^+ \ \forall \ t \geq 0$.

In other words, the previous lemma states that the region $\mathcal{B}^+$ is invariant. The proof is detailed in appendix C.4 and an illustration is presented in figure 6.4.3. Now, in order to prove the stability of the attracting point $\bar{x}^+$, the initial conditions ball $\mathcal{B}_\epsilon^+$ is constructed:

Definition 6.4.7. *Under the assumption 6.4.3, the constant* ϵ *is defined as in definition 6.4.4, and the ball* $\mathcal{B}_\epsilon^+$ *is defined as:* $\mathcal{B}_\epsilon^+ = \left\{x | \bar{x}_i^+ - \epsilon \leq x_i \leq \bar{x}_i^+ + \epsilon \quad \forall \ i \in \{1, ..., N\}\right\}$.

The following lemma states dynamical properties of trajectories starting in the ball $\mathcal{B}_\epsilon^+$:

Lemma 6.4.4. *Under assumptions 6.4.2 and 6.4.3, for any* $x(0) \in \mathcal{B}_\epsilon^+$, $x(t) \in \mathcal{B}_\delta^+ \ \forall \ t \geq 0$.

Proof. As $\mathcal{B}_\epsilon^+ \subset \mathcal{B}^+$ by construction, then for all $x(0) \in \mathcal{B}_\epsilon^+$, $x(0) \in \mathcal{B}^+$ which implies from lemma 6.4.3 that $x(t) \in \mathcal{B}^+ \ \forall \ t \geq 0$. Now, as $\mathcal{B}^+ \subset \mathcal{B}_\delta^-$, then for all $x(0) \in \mathcal{B}_\epsilon^+$, $x(t) \in \mathcal{B}^+ \ \forall \ t \geq 0$, which implies that $x(t) \in \mathcal{B}_\delta^+ \ \forall \ t \geq 0$. □

In order to conclude, the following last remark is essential to relax assumption 6.4.3

Remark 6.4.2. *If assumption 6.4.3 is not fulfilled for a* $\delta > 0$*, then it is sufficient to consider any ball of radius* $\delta' > 0$ *such that* $\mathcal{B}_{\delta'}^+ \subset \mathcal{B}_\delta^+$ *and such that* δ' *fulfills assumption 6.4.3. The region* $\mathcal{B}^+$ *is constructed for* $\mathcal{B}_{\delta'}^+$*, as well as the initial condition ball* $\mathcal{B}_\epsilon^+$*. In these conditions, for all* $x(0) \in \mathcal{B}_\epsilon^+$, $x(t) \in \mathcal{B}_{\delta'}^+ \ \forall \ t \geq 0$ *with lemma 6.4.4, which implies that* $x(t) \in \mathcal{B}_\delta^+ \ \forall \ t \geq 0$.

The main theorem for the positive loop is now introduced:

Theorem 6.4.2. *Under assumption 6.4.2, the equilibrium point* $\bar{x}^+$ *is locally stable.*

Proof. For any $\delta > 0$, there exists an $\epsilon = \min\left(\min_i m_i, \min_i M_i\right) > 0$, as stated in definition 6.4.7 and remark 6.4.2, such that every solution $x(t)$ having initial conditions in the ball $\mathcal{B}_\epsilon^+$ (i.e. within a distance ϵ of the equilibrium: $||x(0) - \bar{x}^+||_\infty \leq \epsilon$), remains in the ball $\mathcal{B}_\delta^+$ (i.e. within a distance δ of the equilibrium: $||x(t) - \bar{x}^+||_\infty \leq \delta$) for all $t \geq 0$, as stated by lemma 6.4.4 and remark 6.4.2. □

The conditions on u_{min} and u_{max} given in theorem 6.4.2 are relaxed compared to the one given in theorem 6.3.2. Indeed, if u_{min} and u_{max} are not small and large enough, $\bar{x}^+$ becomes locally stable through a sliding mode. However, one or two other stable steady states are still present and stable as well, preventing global convergence towards $\bar{x}^+$. This situation is illustrated in dimension 2 in figure 6.4.4.

Finally, the global asymptotic stability can be stated:

Theorem 6.4.3. *Under assumption 6.3.2, the equilibrium point* $\bar{x}^+$ *is globally asymptotically stable.*

Proof. Under assumption 6.3.2, theorem 6.4.2 proves the local stability of $\bar{x}^+$, and theorem 6.3.2 proves its global attractivity. Then it follows that $\bar{x}^+$ is globally asymptotically stable. □

This result for both loops does not seem straightforward as $\bar{x}^*$ is neither a steady state of the system controlled by u_{max} nor of the system controlled by u_{min}. One must keep in mind that these types of switching systems are not classic continuous dynamical systems and that more complex dynamical behaviors may happen. The theory of Filippov enables us to show that the convergence arises through an "artificial" sliding mode along the hyperplane $x_1 = \bar{x}_1^*$, due to the opposite sign of the x_1 vector-field on both sides of the switching domain [47, 25].

This theoretical control strategy has a few convenient biological properties. First, the switch between the two positive constants u_{min} and u_{max} may be biologically applicable with optogenetics or with the introduction of doses of inducer molecules for example, as long as the following method is applied: when the first gene x_1 is detected highly (resp. weakly) expressed compared to its normal homeostatic conditions, its inhibition by the last gene x_N must be reduced (resp. amplified).

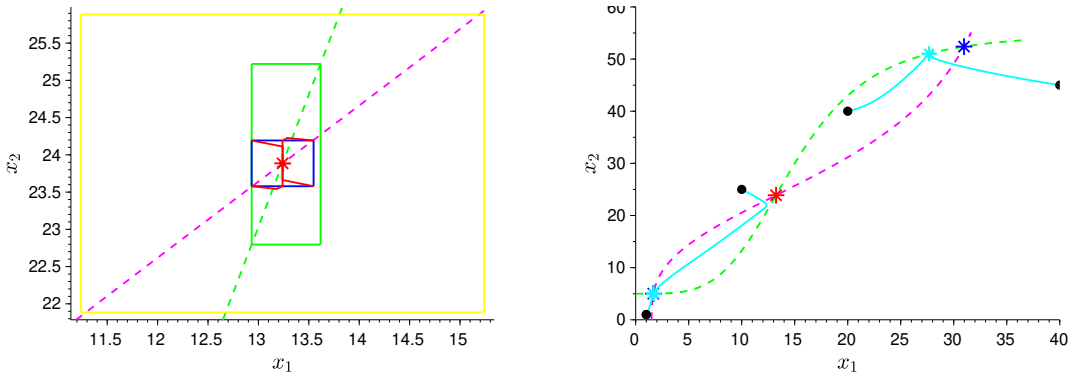

Figure 6.4.4: Left: Simulation of the balls and regions in dimension 2 for $\delta = 2$: the largest ball $\mathcal{B}_\delta^+$ is in yellow, the invariant region $\mathcal{B}^+$ is in green and the smallest initial conditions ball $\mathcal{B}_\epsilon^+$ is in dark blue with $\epsilon \approx 0.3$. The red lines are simulations of 4 trajectories of system (6.2.1) starting at the 4 corners of the cube $\mathcal{B}_\epsilon^+$, with control $u_{min} = 0.9$ and $u_{max} = 1.1$. Some of the trajectories leave the ball $\mathcal{B}_\epsilon^+$ but they all stay in the largest ball $\mathcal{B}_\delta^+$. Right: with $u_{min} = 0.9$ and $u_{max} = 1.1$, the conditions for the global convergence given in theorem 6.3.2 are not verified. In this case, $\bar{x}^+$ is locally stable, but two other locally stable steady states, depicted by light blue stars, still exist. The trajectories illustrated by light blue lines converge towards one of the three steady states depending on the initial condition. For both plots, the parameters are the same as in figure 6.3.6.

Second, as long as u_{min} and u_{max} meet assumptions 6.3.1 for the negative loop and 6.3.2 for the positive loop, the global convergence towards the attractive zone is still guaranteed, even if they fluctuate over time. In other words, in the region $x_1 \leq \bar{x}_1^*$ (resp. $x_1 \geq \bar{x}_1^*$), u_{max} (resp. u_{min}) can take any value and even fluctuate with time as long as the inequality is met, without changing the global dynamics of the system, namely the global convergence towards $\bar{x}^*$. Moreover, the successive repellent regions and the attractive zone remain unchanged. If the control input is a dose of inducer molecule for example, it means that this dose must only be bigger (resp. smaller) than the critical value determined by the inequality in assumptions 6.3.1 and 6.3.2. This allows uncertainties and fluctuations in the biological control input.

6.5 The PWC control inside Hill functions: an illustration

This section illustrates the idea that the previous results obtained for a qualitative control strategy that multiply the Hill function in the uncontrolled model can be generalized for a qualitative control strategy inside the Hill function. Indeed, the tools presented in the previous sections can also be applied in this new context. For this reason, this section does not prove all the results in any dimension N for both the positive and negative loop, but illustrates this new strategy with the Toggle Switch in dimension 2 presented in chapter 2.

As presented in chapter 2, Gardner, Cantor, and Collins synthetically constructed the first Toggle Switch in the organism *Escherichia Coli* [54]. This motif was composed of two genes *lacI* and *tetR* that mutually repressed each other through the proteins LacI and TetR for which they code. This circuit presented two stable states and an unstable state: from an undifferentiated state, cells eventually converged towards one of the two stable states. The use of both inducer molecules IPTG and aTc allowed switching from one to the other. Very recently, [80] achieved reversal of the decision process: the cells were forced to converge towards the unstable steady state. This objective was achieved by measuring and controlling both genes. The level of expression of *lacI* and *tetR* was estimated with fluorescent microscopy techniques, by measuring levels of two fluorescent proteins: RFP and GFP. These measurements affected microfluidics devices behaviors: the inhibition of *lacI* was dynamically controlled by aTc and *tetR* by IPTG.

The control of the unstable steady state of the Toggle Switch has also been analytically investigated in [48] with an open-loop control strategy based on a PI controller and PWM technique. By a periodic averaging method, it has been analytically proved that if the introduction period of the inducer molecules is small compared to the time-scale of the uncontrolled Toggle Switch, then the controlled system has a stable periodic solution contained in a neighborhood of the unstable steady state of interest. The same authors designed later in [63] and [64] a closed-loop version of this controlled problem in which the average model is used to tune the input features such as the amplitude and the period.

This section will focus on the comparison between this biological control approach developed by [80] and the qualitative control strategy inside the Hill function. As explained, in the experiment conducted by [80], both genes *lacI* and *tetR* that compose the Toggle Switch were measured and controlled. From a mathematical point of view, this system is always controllable and it is a lot more challenging to control and measure only one gene. From a biological point of view, the present work aims to reduce measurement devices by using a unique fluorescent protein (GFP) and facilitate control implementation by introducing a unique inducer molecule (aTc).

6.5.1 The controlled Toggle Switch model

Due to the two inhibitions between *lacI* and *tetR*, the controlled Toggle Switch model is composed of two decreasing Hill functions:

$$\begin{cases} \dot{x}_1(x_1, x_N) = \kappa_{01} + \kappa_1 \mathrm{h}^-(\mathrm{u}(x_1)x_2, \theta_2, n_2) - \gamma_1 x_1, \\ \dot{x}_2(x_i, x_{i-1}) = \kappa_{02} + \kappa_2 \mathrm{h}^-(x_1, \theta_1, n_1) - \gamma_2 x_2, \end{cases} \tag{6.5.1}$$

with

$$\begin{cases} \mathrm{u}(x_1) = u_{min} < 1 \text{ if } x_1 \leq \bar{x}_1^+, \\ \mathrm{u}(x_1) = u_{max} > 1 \text{ if } x_1 \geq \bar{x}_1^+. \end{cases} \tag{6.5.2}$$

This control strategy is adapted to qualitative measurements available for the first gene: if x_1 is weakly expressed ($x_1 \leq \bar{x}_1^+$) the control decreases the influence of x_2 on x_1, and if x_1 is highly expressed ($x_1 \geq \bar{x}_1^+$), the control increases the influence of x_2 on x_1. The control $\mathrm{u}(x_1)$ appears in the Hill function because it is considered that the control element is able to facilitate or prevent the second protein from binding to the promoter of the first gene. This hypothesis was also made in [80], and models appropriately the influence of aTc on the interaction between TetR and *lacI*.

Although the results presented in this section are valid for any parameters of (6.5.1), they will be illustrated with a calibration of the Toggle Switch introduced in [80] in order to allow constructive comparisons between the two control processes. With the classic hypothesis that mRNA degrades faster than proteins, their 4-dimensional model can be reduced to (6.5.1) where $x_1 = \mathrm{LacI}$ and $x_2 = \mathrm{TetR}$. The uncontrolled Toggle Switch in [80] was obtained under reference conditions $\mathrm{aTc}_{ref} = 20\mathrm{ng} \cdot \mathrm{ml}^{-1}$ and $\mathrm{IPTG}_{ref} = 0.25\mathrm{mM}$. Thus, the calibration is obtained for a re-scaled system: $\dot{x}_1 = \kappa_{01} + \kappa_1 \mathrm{h}^-(u_1 x_2, \theta_2, n_2) - \gamma_1 x_1$ and $\dot{x}_2 = \kappa_{02} + \kappa_2 \mathrm{h}^-(u_2 x_1, \theta_1, n_1) - \gamma_2 x_2$ where $u_1 = \theta_{\mathrm{aTc}}^{\eta_{\mathrm{aTc}}} / (\theta_{\mathrm{aTc}}^{\eta_{\mathrm{aTc}}} + \mathrm{aTc}_{ref}^{\eta_{\mathrm{aTc}}}) \approx 0.25$ and $u_2 = \theta_{\mathrm{IPTG}}^{\eta_{\mathrm{IPTG}}} / (\theta_{\mathrm{IPTG}}^{\eta_{\mathrm{IPTG}}} + \mathrm{IPTG}_{ref}^{\eta_{\mathrm{IPTG}}}) \approx 0.12$. The parameters γ_1, γ_2, n_1, n_2, θ_{aTc}, η_{aTc}, θ_{IPTG}, and η_{IPTG} were directly taken from their supplementary information, and the remaining six parameters were computed in order to get the same three steady states. These values are merged in table 6.5.1.

For the Toggle Switch, the control strategy (6.5.2) can be performed with the inducer molecule aTc: the control condition $u_{max} > 1$ (resp. $u_{min} < 1$) results in increasing above (resp. reducing below) $20\mathrm{ng} \cdot \mathrm{ml}^{-1}$ the dose of aTc. As explained previously, the network was maintained near the unstable steady state by measuring and controlling both genes with IPTG and aTc. With the control technique (6.5.2) only one gene must be measured and controlled (see figure 6.5.1).

The next section states and proves global results about convergence and stability.

κ_{01}	κ_1	θ_2	n_2	γ_1	θ_{aTc}	η_{aTc}
1.56	61.7	34.2	2	0.0165	11.65	2
κ_{02}	κ_2	θ_1	n_1	γ_2	θ_{IPTG}	η_{IPTG}
1.47	17.6	42.1	2	0.0165	0.0906	2

Table 6.5.1: Calibration parameters of the Toggle Switch based on [80] data.

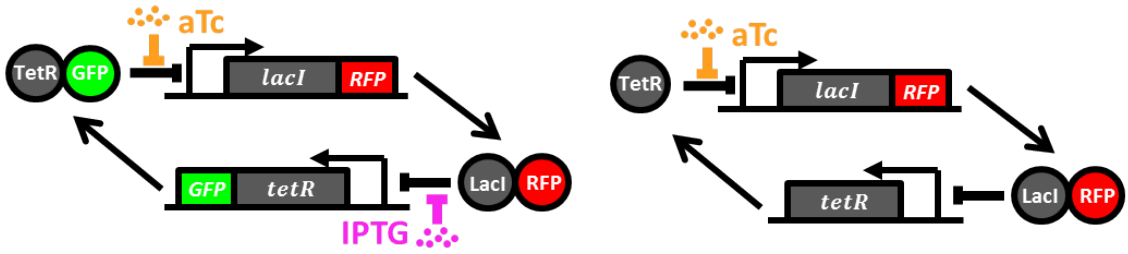

Figure 6.5.1: Left: illustration of the control strategy performed by [80]. Right: illustration of the aTc control strategy.

6.5.2 Global results

In this section, appropriate conditions on u_{min} and u_{max} are determined in order to make $\bar{x}^+$ globally asymptotically stable. The state space is partitioned in 5^2 zones called $(a_1 a_2)$:

Definition 6.5.1. *For $i \in \{1,2\}$:*

- $a_i = 0$ *if* $x_i < \bar{x}_i^+ - \nu_i$,
- $a_i = 1$ *if* $\bar{x}_i^+ - \nu_i \leq x_i < \bar{x}_i^+$,
- $a_i = 2$ *if* $x_i = \bar{x}_i^+$,
- $a_i = 3$ *if* $\bar{x}_i^+ < x_i \leq \bar{x}_i + \delta_i$,
- $a_i = 4$ *if* $\bar{x}_i^+ + \delta_i < x_i$,

where:

- $\delta_1 = (\kappa_{01} + \kappa_1)/\gamma_1 - \bar{x}_1^+$,
- $\nu_2 = \bar{x}_2^+ - \left(\kappa_{02} + \kappa_2 h^-(\bar{x}_1^+ + \delta_1, \theta_1, n_1)\right)/\gamma_2$,
- $\nu_1 = \bar{x}_1^+ - \kappa_{01}/\gamma_1$,
- $\delta_2 = \left(\kappa_{02} + \kappa_2 h^-(\bar{x}_1^+ - \nu_1, \theta_1, n_1)\right)/\gamma_2 - \bar{x}_2^+$.

It is easy to show that $\forall\, i \in \{1,2\}$, $\nu_i > 0$, $\delta_i > 0$, and $\nu_i < \bar{x}_i^+$. Moreover, the central zone $(2,2)$ is the steady state $\bar{x}^+$. An illustration of this partitioning is presented as a graph in figure 6.5.2.

This partitioning allows the statement of a first convergence theorem:

Theorem 6.5.1. *With $u_{min} \leq \bar{x}_2^+/(\bar{x}_2^+ + \delta_2)$ and $u_{max} \geq \bar{x}_2^+/(\bar{x}_2^+ - \nu_2)$, system (6.5.1) under control (6.5.2) converges globally towards $\bar{x}^+$.*

With the properties of Hill functions, it is easy to check that $u_{min} < 1$ and $u_{max} > 1$. As done in the previous sections of this chapter, the proof of this theorem is built by studying successively repelling regions of the state space.

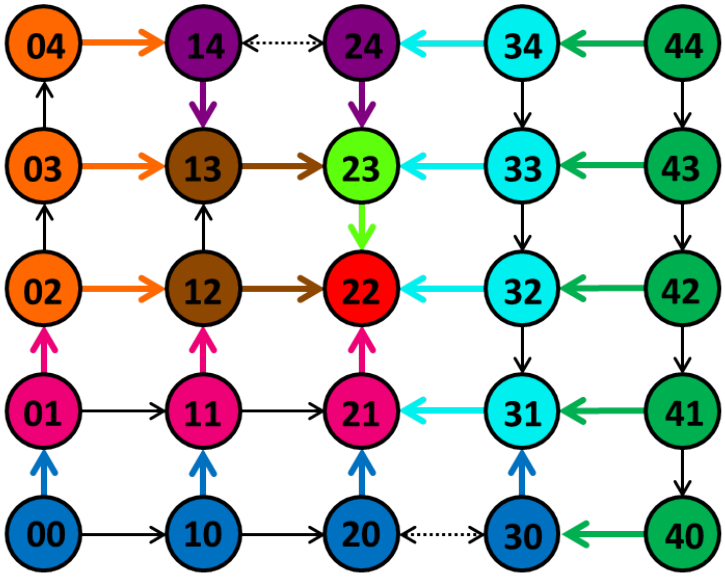

Figure 6.5.2: Partitioning of the state space according to definition 6.5.1. The arrows represent transitions between zones. Some transitions represented by the black arrows do not play any role in lemma 6.5.1, and dashed black arrows illustrate unknown transitions. The successive repelling regions are represented with different colors and illustrate the repelling order given in lemma 6.5.1.

Lemma 6.5.1. *These specific regions are successively repelling:*

1. *The region $a_1 = 4$ is repelling.*
2. *If the region $a_1 = 4$ is repelling, then the region $a_2 = 0$ is repelling as well.*
3. *If the region $a_2 = 0$ is repelling, then the region $a_1 = 3$ is repelling as well.*
4. *If the regions $a_1 = 4$ and $a_1 = 3$ are repelling, then the region $a_2 = 1$ is repelling as well.*
5. *The region $a_1 = 0$ is repelling.*
6. *If the region $a_1 = 0$ is repelling, then the region $a_2 = 4$ is repelling as well.*
7. *If the region $a_2 = 4$ is repelling, then the region $a_1 = 1$ is repelling as well.*
8. *If the regions $a_1 = 0$ and $a_1 = 1$ are repelling, then the region $a_2 = 3$ is repelling as well.*

Proof. The proof is only detailed for the first item for the sake of clarity, as the proof for all other items follows the same idea. These eight items are illustrated in figure 6.5.3. The vector field keeps a constant sign in each case:

1. In the region $a_1 = 4$ the x_1-vector field is $\dot{x}_1(x_1, x_2) = \kappa_{01} + \kappa_1 \mathrm{h}^-(u_{max} x_2, \theta_2, n_2) - \gamma_1 x_1$. With the definition of δ_1, this vector field calculated at the boundary $\bar{x}_1^+ + \delta_1$ becomes: $\dot{x}_1(\bar{x}_1^+ + \delta_1, x_2) = \kappa_1[\mathrm{h}^-(u_{max} x_2, \theta_2, n_2) - 1]$, leading to $\dot{x}_1(\bar{x}_1^+ + \delta_1, x_2) \leq 0$ with the properties of Hill functions. For x_2 fixed, the linear degradation term $-\gamma_1 x_1$ induces that $\dot{x}_1(x_1, x_2) < \dot{x}_1(\bar{x}_1^+ + \delta_1, x_2) \leq 0 \ \forall \ x_1 > \bar{x}_1^+ + \delta_1$. Then the x_1-vector field is strictly negative in $a_1 = 4$. As $a_1 = 4$ is lower-bounded by $x_1 = \bar{x}_1^+ + \delta_1$, the region is repellent.
2. Show that $\dot{x}_2(x_2, x_1) > 0 \ \forall \ x_1 \leq \bar{x}_1^+ + \delta_1$ and $x_2 < \bar{x}_2^+ - \nu_2$.
3. Show that $\dot{x}_1(x_1, x_2) < 0 \ \forall \ x_2 \geq \bar{x}_2^+ - \nu_2$ and $x_1 > \bar{x}_1^+$.

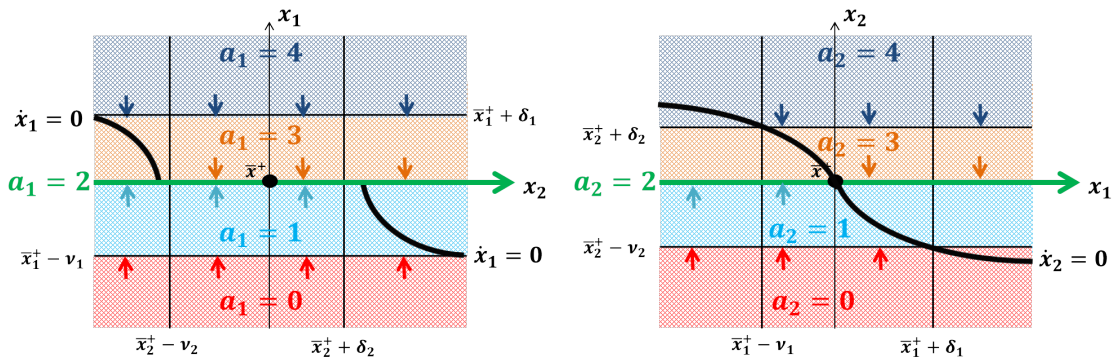

Figure 6.5.3: Left: Transitions properties in the (x_2, x_1) plane. The dark lines are the x_1-nullclines. The arrows represent vector field in the x_1-direction. Right: Transitions properties in the (x_1, x_2) plane. The dark line is the x_2-nullclines. The arrows represent vector field in the x_2-direction.

4. Show that $\dot{x}_2(x_2, x_1) > 0 \; \forall \; x_1 \leq \bar{x}_1^+$ and $x_2 < \bar{x}_2^+$.
5. Show that $\dot{x}_1(x_1, x_2) > 0 \; \forall \; x_2 \geq 0$ and $x_1 < \bar{x}_1^+ - \nu_1$.
6. Show that $\dot{x}_2(x_2, x_1) < 0 \; \forall \; x_1 \geq \bar{x}_1^+ - \nu_1$ and $x_2 > \bar{x}_2^+ + \delta_2$.
7. Show that $\dot{x}_1(x_1, x_2) > 0 \; \forall \; x_2 \leq \bar{x}_2^+ + \delta_2$ and $x_1 < \bar{x}_1^+$.
8. Show that $\dot{x}_2(x_2, x_1) < 0 \; \forall \; x_1 \geq \bar{x}_1^+$ and $x_2 > \bar{x}_2^+$.

□

This lemma allows the construction of theorem 6.5.1.

Proof. With item 1, the trajectories are restricted to region $a_1 \neq 4$. From this result, item 2 restricts trajectories in region $a_1 \neq 4$ and $a_2 \neq 0$, followed by item 3 that restricts trajectories in region $a_1 \neq (3, 4)$ and $a_2 \neq 0$ and finally from item 4, the region shrinks to $a_1 \neq (3, 4)$ and $a_2 \neq (0, 1)$. In parallel, without any conditions, with item 5 trajectories are restricted to region $a_1 \neq (0, 3, 4)$ and $a_2 \neq (0, 1)$. From this result, item 6 restricts trajectories in region $a_1 \neq (0, 3, 4)$ and $a_2 \neq (0, 1, 4)$, followed by item 7 that restricts trajectories in region $a_1 \neq (0, 1, 3, 4)$ and $a_2 \neq (0, 1, 4)$ and finally from item 8, the region shrinks to $a_1 \neq (0, 1, 3, 4)$ and $a_2 \neq (0, 1, 3, 4)$. This last region is nothing else than $(a_1, a_2) = (2, 2)$, the steady state $\bar{x}^+$. □

Finally, the trajectories globally converge towards $\bar{x}^+$ through a sliding mode on the line $x_1 = \bar{x}_1^+$. A summary of this result is illustrated by a transition graph in figure 6.5.2.

The second main result states the stability of $\bar{x}^+$:

Theorem 6.5.2. *With $u_{min} < 1$ and $u_{max} > 1$, $\bar{x}^+$ is Lyapunov stable.*

The conditions on u_{min} and u_{max} given in theorem 6.5.2 are relaxed compared to the one given in theorem 6.5.1. Indeed, as discussed in section 6.4.2, if u_{min} is not small enough, and u_{max} large enough, $\bar{x}^+$ becomes locally stable through a sliding mode. However, $\bar{x}_{inf}^+$ and $\bar{x}_{sup}^+$ are still present and stable as well, preventing global convergence towards $\bar{x}^+$.

As done in the previous sections, in order to verify the classic definition of Lyapunov stability, the proof uses the construction of specific squares and rectangles: for any square of length $\delta > 0$ centered on $\bar{x}^+$ defined by $\mathcal{B}_\delta = \{x | \; ||x(t) - \bar{x}^+||_\infty \leq \delta\}$, an invariant rectangle $\mathcal{B}$ centered on $\bar{x}^+$ can be constructed such that $\mathcal{B} \subset \mathcal{B}_\delta$. Finally this rectangle $\mathcal{B}$ is restricted to a square of initial conditions of length $\epsilon > 0$ called $\mathcal{B}_\epsilon = \{x | \; ||x(t) - \bar{x}^+||_\infty \leq \epsilon\}$ centered on $\bar{x}^+$.

Initially, the length δ is restricted:

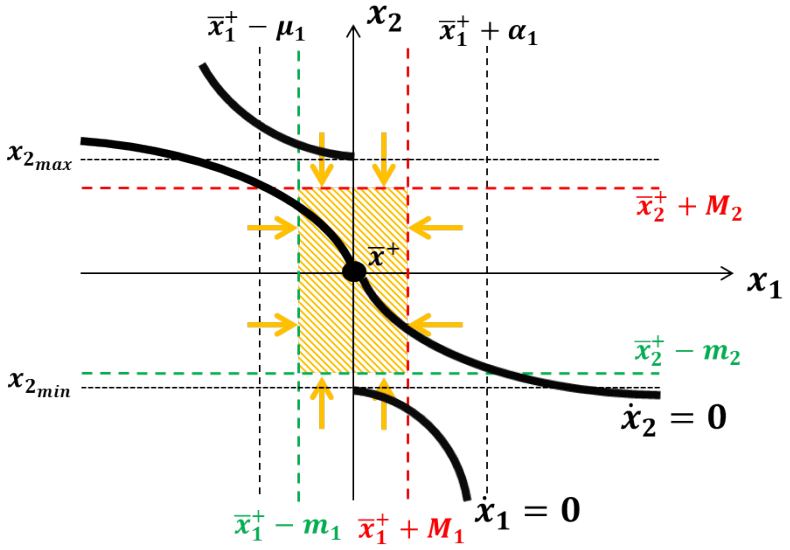

Figure 6.5.4: Illustration of rectangle constructions for Lyapunov stability: the plain black lines are the nullclines, the red (resp. green) dashed lines are the upper (resp. lower) boundaries of rectangle $\mathcal{B}$, that is highlighted in yellow. The yellow arrows represent vector field in the perpendicular direction of $\mathcal{B}$ boundaries.

Assumption 6.5.1. $\forall\ i \in \{1,2\}$ *the length* δ *satisfies:* $\delta < \min\left(\bar{x}_i^+ - \kappa_{0i}/\gamma_i, (\kappa_{0i}+\kappa_i)/\gamma_i - \bar{x}_i^+\right)$.

With boundedness properties of the uncontrolled system (3.2.1) given in proposition 3.2.8, it is possible to find such a $\delta > 0$. From the corresponding square $\mathcal{B}_\delta$, the invariant rectangle $\mathcal{B}$ can be constructed:

Definition 6.5.2. *For a fixed* $\delta > 0$ *under assumption 6.5.1, the region* $\mathcal{B}$ *is defined with:*

- $\alpha_2 = \min(\delta, x_{2max})$ *and* $M_2 = \alpha_2$,
- $\mu_1 = \bar{x}_1^+ - \phi_2^-\left(\left(\gamma_2(\bar{x}_2^+ + M_2) - \kappa_{02}\right)/\kappa_2\right)$ *and* $m_1 = \min(\delta, \mu_1)$,
- $\mu_2 = \min(\delta, x_{2min})$ *and* $m_2 = \mu_2$,
- $\alpha_1 = \phi_2^-\left(\left(\gamma_2(\bar{x}_2^+ - m_2) - \kappa_{02}\right)/\kappa_2\right) - \bar{x}_1^+$ *and* $M_1 = \min(\delta, \alpha_1)$,

where $x_{2max} = \bar{x}_2^+/u_{min}$ *is the intersection between the* x_1*-nullcline in the space* $x_1 < \bar{x}_1^+$ *and the line* $x_1 = \bar{x}_1^+$, $x_{2min} = \bar{x}_2^+/u_{max}$ *is the intersection between the* x_1*-nullcline in the space* $x_1 > \bar{x}_1^+$ *and the line* $x_1 = \bar{x}_1^+$, *and* ϕ_2^- *is the inverse function of* $h^-(x_1, \theta_1, n_1)$.
Then $\mathcal{B} = \left\{x | \bar{x}_i^+ - m_i \le x_i \le \bar{x}_i^+ + M_i \quad \forall\ i \in \{1,2\}\right\}$.

This definition is illustrated in figure 6.5.4.

It is easy to check that $\forall\ i \in \{1,2\}$ $\bar{x}_i^+ < \bar{x}_i^+ + M_i < (\kappa_{0i}+\kappa_i)/\gamma_i$, $\kappa_{0i}/\gamma_i < \bar{x}_i^+ - m_i < \bar{x}_i^+$, and $\mathcal{B} \subset \mathcal{B}_\delta$. It is possible to prove that the rectangle $\mathcal{B}$ is invariant:

Lemma 6.5.2. *For any initial condition* $x(0) \in \mathcal{B}$, $x(t) \in \mathcal{B}$ *for any* $t \ge 0$.

To prove this lemma, it is shown that the vector field in the perpendicular direction of each of the four boundaries of rectangle $\mathcal{B}$ points inward.

Proof. For the sake of clarity, the proof is detailed in only one boundary of the rectangle, and is illustrated in figure 6.5.4. The proof for the three remaining boundaries follow the same ideas:

- At the boundary $x_2 = \bar{x}_2^+ + M_2$ and $\bar{x}_1^+ - m_1 \leq x_1 \leq \bar{x}_1^+ + M_1$: the x_2-vector field at the point $(\bar{x}_2^+ + M_2, \bar{x}_1^+ - \mu_1)$ is: $\dot{x}_2(\bar{x}_2^+ + M_2, \bar{x}_1^+ - \mu_1) = \kappa_{02} + \kappa_2 \mathrm{h}^-(\bar{x}_1^+ - \mu_1, \theta_1, n_1) - \gamma_2(\bar{x}_2^+ + M_2)$. With the definition of μ_1, and ϕ_2^-, the vector field becomes $\dot{x}_2(\bar{x}_2^+ + M_2, \bar{x}_1^+ - \mu_1) = 0$. For $x_2 = \bar{x}_2^+ + M_2$ fixed and $\forall\ x_1 \geq \bar{x}_1^+ - \mu_1$, the decreasing property of the Hill function gives $\dot{x}_2(\bar{x}_2^+ + M_2, x_1) \leq \dot{x}_2(\bar{x}_2^+ + M_2, \bar{x}_1^+ - \mu_1) = 0$. In particular, as $m_1 = \min(\delta, \mu_1)$ then $\bar{x}_1^+ + M_1 \geq \bar{x}_1^+ - m_1 \geq \bar{x}_1^+ - \mu_1$. Finally $\dot{x}_2(\bar{x}_2^+ + M_2, x_1) \leq 0\ \forall\ x_1 \in [\bar{x}_1^+ - m_1, \bar{x}_1^+ + M_1]$. This inequality means that any trajectory starting in $\mathcal{B}$ cannot leave the rectangle through the boundary $x_2 = \bar{x}_2^+ + M_2$.
- Show that $\dot{x}_2(\bar{x}_2^+ - m_2, x_1) \geq 0\ \forall\ x_1 \in [\bar{x}_1^+ - m_1, \bar{x}_1^+ + M_1]$. Any trajectory starting in $\mathcal{B}$ cannot leave the rectangle through the boundary $x_2 = \bar{x}_2^+ - m_2$.
- Show that $\dot{x}_1(\bar{x}_1^+ + M_1, x_2) \leq 0\ \forall\ x_2 \in [\bar{x}_2^+ - m_2, \bar{x}_2^+ + M_2]$. Any trajectory starting in $\mathcal{B}$ cannot leave the rectangle through the boundary $x_1 = \bar{x}_1^+ + M_1$.
- Show that $\dot{x}_1(\bar{x}_1^+ - m_1, x_2) \geq 0\ \forall\ x_2 \in [\bar{x}_2^+ - m_2, \bar{x}_2^+ + M_2]$. Any trajectory starting in $\mathcal{B}$ cannot leave the rectangle through the boundary $x_1 = \bar{x}_1^+ - m_1$.

□

The length ϵ of the last square $\mathcal{B}_\epsilon$ is now introduced:

Definition 6.5.3. *For a fixed $\delta > 0$ under assumption 6.5.1, $\epsilon = \min(\min_i m_i, \min_i M_i)$.*

Basically, the square $\mathcal{B}_\epsilon$ is the restriction of rectangle $\mathcal{B}$ to its biggest embedded square.

Remark 6.5.1. *If assumption 6.5.1 is not fulfilled for a $\delta > 0$, then as explained in the previous section, it is sufficient to consider any square of length $\delta' > 0$ such that $\mathcal{B}_{\delta'} \subset \mathcal{B}_\delta$ and such that δ' fulfills assumption 6.5.1.*

All these lemmas, definitions and remarks allow the construction of the final proof for theorem 6.5.2

Proof. For any $\delta > 0$, there exists an $\epsilon > 0$, as stated in definition 6.5.3 and remark 6.5.1, such that every solution $x(t)$ having initial conditions in the square $\mathcal{B}_\epsilon$ remains in the rectangle $\mathcal{B}$ as stated by lemma 6.5.2. As $\mathcal{B} \subset \mathcal{B}_\delta$, the trajectories stay in $\mathcal{B}_\delta$ for all $t \geq 0$. Finally $\bar{x}^+$ is Lyapunov stable. □

As a conclusion, under appropriate conditions on u_{min} and u_{max}, the last main result of this section can be presented:

Theorem 6.5.3. *With $u_{min} \leq \bar{x}_2^+/(\bar{x}_2^+ + \delta_2)$ and $u_{max} \geq \bar{x}_2^+/(\bar{x}_2^+ - \nu_2)$, the steady state $\bar{x}^+$ of system (6.5.1) under control (6.5.2) is globally asymptotically stable.*

This last theorem is a simple corollary of theorem 6.5.1 and theorem 6.5.2.

A simulation of this control strategy applied to the calibration of the system used in [80] is presented in figure 6.5.5. The multiplication by $u_{max} = 3$ of the reference control $u_1 = 0.25$ is equivalent to reducing the aTc dose to $6.5\mathrm{ng} \cdot \mathrm{ml}^{-1}$. Similarly, the multiplication by $u_{min} = 0.27$ of the reference control $u_1 = 0.25$ is equivalent to increasing the aTc dose to $42.9\mathrm{ng} \cdot \mathrm{ml}^{-1}$. It can be observed that the switch between $\mathrm{aTc} = 6.5\mathrm{ng} \cdot \mathrm{ml}^{-1}$ and $\mathrm{aTc} = 42.9\mathrm{ng} \cdot \mathrm{ml}^{-1}$ leads to a stabilization of $\bar{x}^+$, as analytically predicted. This control strategy may lead to a simplification of the experimental set-ups as it only needs one measurement system for *lacI* and one inducer molecule aTc. Moreover, the global results are still valid if u_{min} and u_{max} vary, as long as they satisfy the conditions stated in theorem 6.5.3. In other words, if the low dose of aTc is smaller than $6.5\mathrm{ng} \cdot \mathrm{ml}^{-1}$ (it can even be 0) and the upper dose greater than $42.9\mathrm{ng} \cdot \mathrm{ml}^{-1}$, the convergence is guaranteed. This property allows fluctuations in the doses of aTc.

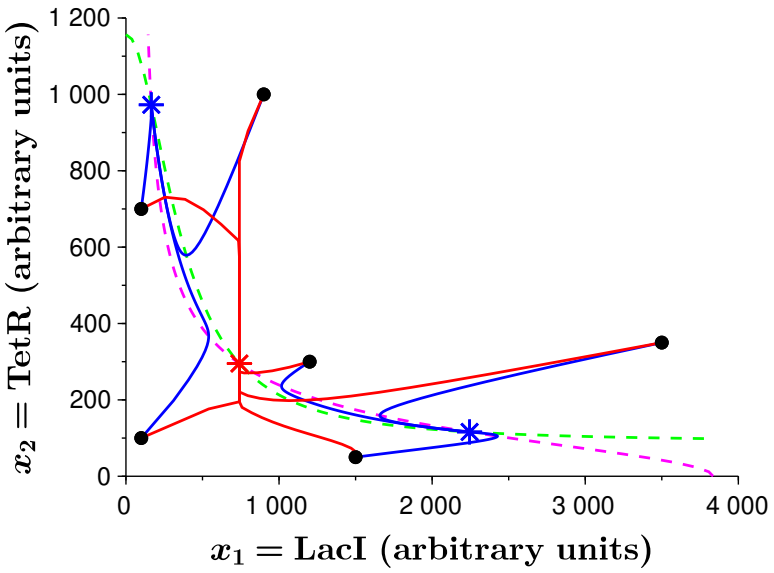

Figure 6.5.5: The parameters are the ones in table 6.5.1, the pink (resp. green) dashed line is the x_1 (resp. x_2) nullcline of the uncontrolled system (3.2.1) with two inhibitions, the blue stars are the stable steady states, the red star the unstable steady state, the blue lines are simulations of the uncontrolled system with six initial conditions depicted with black dots. The red lines are simulations of system (6.5.1) under control (6.5.2) with a switch between $\mathrm{aTc} = 6.5\mathrm{ng} \cdot \mathrm{ml}^{-1}$ and $\mathrm{aTc} = 42.9\mathrm{ng} \cdot \mathrm{ml}^{-1}$.

6.6 A trade-off between speed of convergence and strength of inputs

The conditions given in assumptions 6.3.1 and 6.3.2 on the control parameters u_{min} and u_{max} can easily be relaxed. Indeed, these conditions were defined in order to reduce the number of successive repulsive regions and simplify the proof of global convergence and stability theorems. However, it is possible to observe that these simplified proofs follow the same ideas as the methodology presented in chapter 4. Indeed, the construction of repellent regions can also be seen as the construction of repellent hyperrectangles. The only difference is that only a few successive hyperrectangles have been constructed due to the high constraints given on u_{max} and u_{min}. It follows from these constraints and the number of hyperrectangles constructed that the convergence towards $\bar{x}^*$ is really fast, at least for the variable x_1. In this section, the methodology presented in chapter 4 is generalized to the positive feedback loop with a PWC control strategy inside a Hill function. It will be explained that it is possible to find a maximal value of u_{min} and a minimal value of u_{max} such that successive hyperrectangles can be constructed leading to a global asymptotic stability of $\bar{x}^+$. However, as the number of hyperrectangles increases, the time of convergence may increase as well. It follows that a trade-off exists between the strength of the inputs u_{max} and u_{min} and the time of convergence towards $\bar{x}^+$. Obviously the same results can be extended to a PWC control strategy multiplying a Hill function, and to the negative feedback loop.

The definitions and results will apply to the following controlled system:

$$\begin{cases} \dot{x}_1(x_1, x_N) = \kappa_{01} + \kappa_1 \mathrm{h}^+(\mathrm{u}(x_1)x_N, \theta_N, n_N) - \gamma_1 x_1, \\ \dot{x}_i(x_i, x_{i-1}) = \kappa_{0i} + \kappa_i \mathrm{h}^+(x_{i-1}, \theta_{i-1}, n_{i-1}) - \gamma_i x_i \quad \forall\, i \in \{2, ..., N\}, \end{cases} \tag{6.6.1}$$

where $\mathrm{u}(x_1)$ is defined as in (6.2.2):

$$\begin{cases} \mathrm{u}(x_1) = u_{min} \leq 1 & \text{when} \quad x_1 \geq \bar{x}_1^+, \\ \mathrm{u}(x_1) = u_{max} \geq 1 & \text{when} \quad x_1 \leq \bar{x}_1^+. \end{cases} \tag{6.6.2}$$

The nullclines and the functions $S_i^+(x)$ presented in definition 3.2.2 of chapter 3 can be generalized:

Definition 6.6.1. *The nullclines of system (6.6.1) under control (6.6.2) becomes:*

$$\begin{cases} \dot{x}_1 = 0 \iff x_1 = H_{1u}^+(x_1, x_N), \\ \dot{x}_i = 0 \iff x_i = H_i(x_{i-1}) \quad \forall\ i \in \{2, ..., N\}, \end{cases}$$

where $H_i(x)$ are introduced in definition 3.2.1 of chapter 3, and:

$$\begin{cases} H_{1u}^+(x_1, x_N) = \dfrac{\kappa_{01} + \kappa_1 h^+(u_{max} x_N, \theta_N, n_N)}{\gamma_1} = H_{1max}^+(x_N) \quad \forall\ x_1 \leq \bar{x}_1^+, \\ H_{1u}^+(x_1, x_N) = \dfrac{\kappa_{01} + \kappa_1 h^+(u_{min} x_N, \theta_N, n_N)}{\gamma_1} = H_{1min}^+(x_N) \quad \forall\ x_1 \geq \bar{x}_1^+. \end{cases}$$

From these nullclines, their composition can be defined as done in chapter 4: $\forall\ i \in \{1, ..., N\}$, if $x < \bar{x}_i^+$, $S_{imax}^+(x) = H_i \circ H_{i-1} \circ ... \circ H_{1max}^+ \circ H_N \circ H_{N-1} \circ ... \circ H_{i+2} \circ H_{i+1}(x)$, and if $x > \bar{x}_i^+$, $S_{imin}^+(x) = H_i \circ H_{i-1} \circ ... \circ H_{1min}^+ \circ H_N \circ H_{N-1} \circ ... \circ H_{i+2} \circ H_{i+1}(x)$.

From these definitions it is possible to deduce the following property:

Proposition 6.6.1. *If $x < \bar{x}_i^+$, $\partial S_{imax}^+(x)/\partial u_{max} \geq 0$ and $\lim\limits_{u_{max} \to +\infty} S_{imax}^+(x) > \lim\limits_{x \to +\infty} S_i^+(x) > \bar{x}_i^+\ \forall\ i \in \{1, ..., N\}$. Similarly, if $x > \bar{x}_i^+$, $-\partial S_{imin}^+(x)/\partial u_{min} \leq 0$ and $\lim\limits_{u_{min} \to 0} S_{imin}^+(x) < \lim\limits_{x \to 0} S_i^+(x) < \bar{x}_i^+\ \forall\ i \in \{1, ..., N\}$.*

This property simply means that it is possible to find u_{min} small enough and u_{max} big enough such that the functions $S_{imin}^+(x)$ and $S_{imax}^+(x)$ are respectively below and above the linear function $y = x$, leading to the following lemma:

Lemma 6.6.1. *$\exists\ u_{min}^+ < 1$ and $u_{max}^+ > 1$ such that $\forall\ u_{min} < u_{min}^+$, $S_{imin}^+(x) < x\ \forall\ x > \bar{x}_i^+$ and $\forall\ u_{max} > u_{max}^+$, $S_{imax}^+(x) > x\ \forall\ x < \bar{x}_i^+$.*

This lemma is illustrated in figure 6.6.1. From this lemma, the following assumption will be assumed in the rest of the section:

Assumption 6.6.1. *The control parameters u_{max} and u_{min} of (6.6.2) are chosen such that $u_{min} < u_{min}^+$ and $u_{max} > u_{max}^+$.*

As done in chapter 4, bounds of the state space can be defined for the construction of hyperrectangles:

Definition 6.6.2. *Under assumption 6.6.1:*

- $x_{1max}^{+1} = (\kappa_{01} + \kappa_1)/\gamma_1$,
- $x_{imax}^{+1} = H_i(x_{i-1max}^{+1})\ \forall\ i \in \{2, ..., N\}$,
- $x_{1min}^{+1} = \kappa_{01}/\gamma_1$,
- $x_{imin}^{+1} = H_i(x_{i-1min}^{+1})\ \forall\ i \in \{2, ..., N\}$,

Then by induction $\forall\ j > 1$, $j \in \mathbb{N}$:

- $x_{1max}^{+j} = \max\left\{H_{1min}^+(x_{Nmax}^{+(j-1)}), \bar{x}_1^+\right\}$,

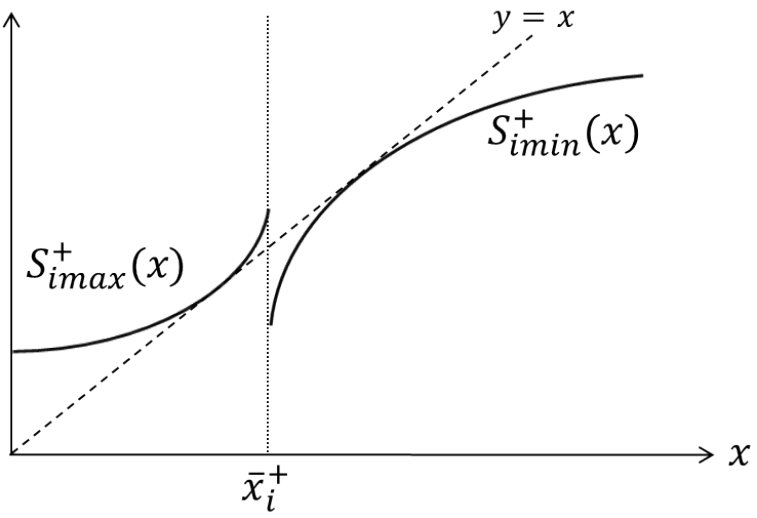

Figure 6.6.1: Illustration of lemma 6.6.1: for $u_{min} = u^+_{min}$ and $u_{max} = u^+_{max}$, the functions $S^+_{imin}(x)$ and $S^+_{imax}(x)$ become tangent to $y = x$ in their domain of definition. When $u_{min} < u^+_{min}$ and $u_{max} > u^+_{max}$, $S^+_{imin}(x)$ becomes smaller than $y = x$ and $S^+_{imax}(x)$ bigger than $y = x$.

- $x^{+j}_{imax} = H_i(x^{+j}_{i-1max}) \ \forall \ i \in \{2, ..., N\}$,
- $x^{+j}_{1min} = \min\left\{H^+_{1max}(x^{+(j-1)}_{Nmin}), \bar{x}^+_1\right\}$,
- $x^{+j}_{imin} = H_i(x^{+j}_{i-1min}) \ \forall \ i \in \{2, ..., N\}$.

The construction of these bounds is illustrated in figure 6.6.2. From definition 6.6.1, they can also be defined by the following sequences:

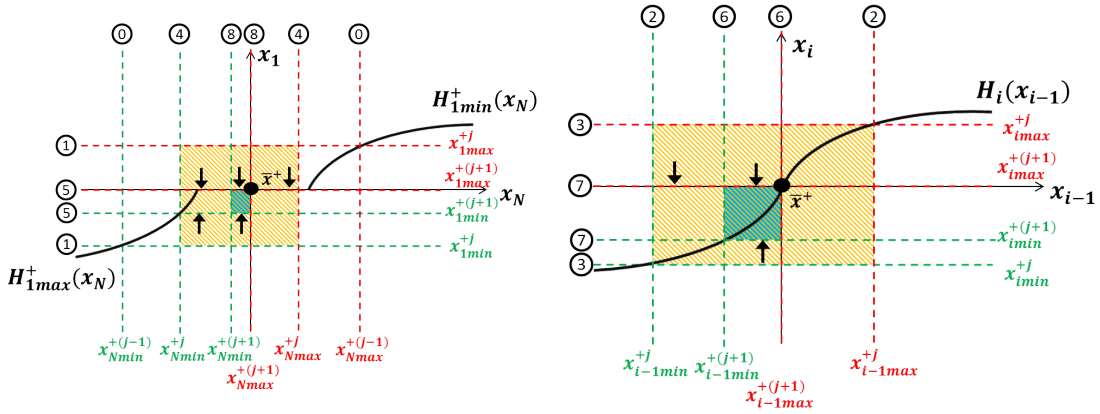

Figure 6.6.2: These two sketches are an illustration of the construction of bounds introduced in definition 6.6.2, the hyperrectangles introduced in definition 6.6.4, and proposition 6.6.3 under assumption 6.6.1. The numbers from 1 to 4 explain the inductions for the construction of the bounds defining $\mathcal{R}^+_j$ (represented by orange rectangles), and the numbers from 5 to 8 explain the inductions for the construction of the bounds defining $\mathcal{R}^+_{j+1}$ (represented by blue rectangles). Again, it is possible to observe that the vector field at the borders of $\mathcal{R}^+_j$ and $\mathcal{R}^+_{j+1}$ points inward. Moreover, by induction, the black arrows show that any trajectory starting in $\mathcal{R}^+_j$ arrives in $\mathcal{R}^+_{j+1}$.

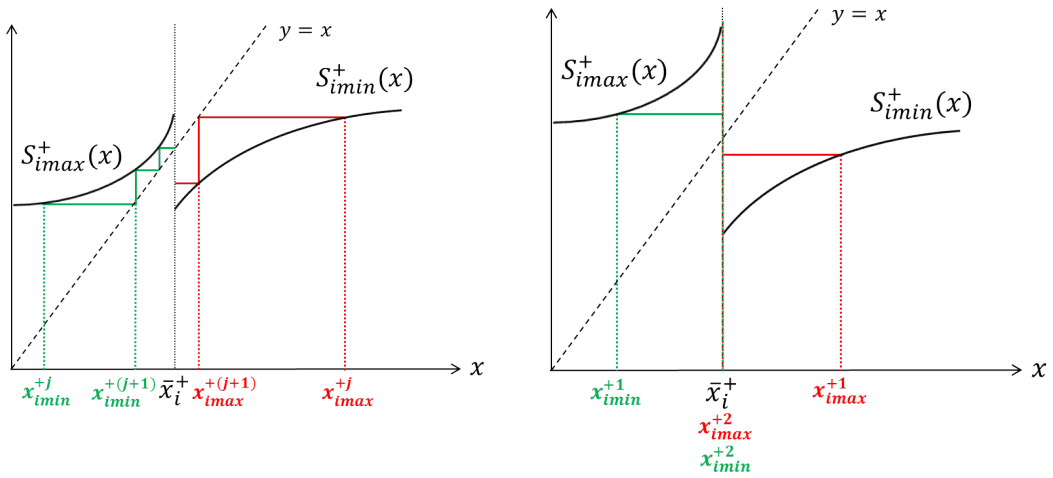

Figure 6.6.3: Left: illustration of iterations for both sequences $(x^{+j}_{imax})_j$ (in red) and $(x^{+j}_{imin})_j$ (in green). Under assumption 6.6.1, the two sequences converge towards $\bar{x}^+_i$, with $(x^{+j}_{imax})_j$ decreasing and $(x^{+j}_{imin})_j$ increasing. Right: illustration of iterations for both sequences $(x^{+j}_{imax})_j$ (in red) and $(x^{+j}_{imin})_j$ (in green) for system (6.5.1) under control (6.5.2) where u_{max} and u_{min} satisfy the conditions given in theorem 6.5.1. The two sequences converge towards $\bar{x}^+_i$ in only one iteration. It follows that the number of hyperrectangles (including the positive orthant and the steady state $\bar{x}^+$) is 3.

Proposition 6.6.2. *Under assumption 6.6.1 and for any $i \in \{1, ..., N\}$, the sequence $(x^{+j}_{imax})_j$ is defined as $x^{+j}_{imax} = \max\left\{S^+_{imin}(x^{+(j-1)}_{imax}), \bar{x}^+_i\right\}$ with initial term x^{+1}_{imax}, and the sequence $(x^{+j}_{imin})_j$ is defined as $x^{+j}_{imin} = \min\left\{S^+_{imax}(x^{+(j-1)}_{imin}), \bar{x}^+_i\right\}$ with initial term x^{+1}_{imin}.*

From this new proposition and lemma 6.6.1, the convergence of bounds can be stated:

Lemma 6.6.2. *If assumption 6.6.1 holds, then for any $i \in \{1, ..., N\}$:*

- *$\exists\ j_{imax}$ such that $\forall\ j < j_{imax}$, the sequence $(x^{+j}_{imax})_j$ is monotonically decreasing, and $\forall\ j \geq j_{imax}$, $x^{+j}_{imax} = \bar{x}^+_i$.*
- *$\exists\ j_{imin}$ such that $\forall\ j < j_{imin}$, the sequence $(x^{+j}_{imin})_j$ is monotonically increasing, and $\forall\ j \geq j_{imin}$, $x^{+j}_{imin} = \bar{x}^+_i$.*

The convergence of these sequences is illustrated in the left sketch of figure 6.6.3.

From this lemma it is possible to define the minimum index j such that all the sequences become constant:

Definition 6.6.3. *Under assumption 6.6.1, $j_0 = \max_{i \in \{1,...,N\}} \{j_{imax}, j_{imin}\}$.*

This integer j_0 represents the number of different successive hyperrectangles that can be constructed, including the steady state $\bar{x}^+$ itself:

Definition 6.6.4. *Under assumption 6.6.1, the first hyperrectangle is the positive orthant: $\mathcal{R}^+_0 = \{x | x_i \geq 0\ \forall\ i \in \{1, ..., N\}\}$. Then $\forall\ 1 \leq j \leq j_0$, $\mathcal{R}^+_j = \left\{x | x^{+j}_{imin} \leq x_i \leq x^{+j}_{imax}\ \forall\ i \in \{1, ..., N\}\right\}$.*

From the definition of j_0, it is straightforward to see that the last hyperrectangle $\mathcal{R}^+_{j_0}$ is the steady state $\bar{x}^+$. As already explained in chapter 4, these hyperrectangles have several good properties:

Proposition 6.6.3. *Under assumption 6.6.1, the hyperrectangles constructed in definition 6.6.4 verify the following properties:*

1. $\forall\ 0 \leq j \leq j_0$, $\bar{x}^+ \in \mathcal{R}_j^+$,
2. *all these hyperrectangles are nested:* $\forall\ 0 \leq j \leq j_0 - 1$, $\mathcal{R}_{j+1}^+ \subset \mathcal{R}_j^+$ *and* $\mathcal{R}_{j+1}^+ \neq \mathcal{R}_j^+$,
3. $\forall\ 0 \leq j \leq j_0$, $\mathcal{R}_j^+$ *is invariant,*
4. *the hyperrectangles are successively repellent:* $\forall\ 0 \leq j \leq j_0 - 2$ *and for all initial condition* $x_0 = x(t=0) \in \mathcal{R}_j^+$, $\exists\ 0 \leq T_j^+ < +\infty$ *such that* $x(t) \in \mathcal{R}_{j+1}^+\ \forall\ t \geq T_j^+$. *Moreover, for any* $x_0 = x(t=0) \in \mathcal{R}_{j_0-1}^+$, $\lim\limits_{t \to +\infty} x(t) \in \mathcal{R}_{j_0}^+$.

This last proposition allows to state the final theorem:

Theorem 6.6.1. *Under assumption 6.6.1, system (6.6.1) under control (6.6.2) globally converges towards* $\bar{x}^+$.

This theorem allows to relax the constraints of u_{min} and u_{max} given in the previous sections. This reduction of constraints on the inputs leads to the construction of a larger number of hyperrectangles for the convergence of the proof. This may induce a larger time of convergence.

For the example given in section 6.5 with the Toggle Switch, the constraints imposed on u_{min} and u_{max} in theorem 6.5.1 for the global convergence lead to the construction of only 3 hyperrectangles with the technique presented above. This is illustrated in the right sketch of figure 6.6.3.

For small values of u_{min} and large values of u_{max}, the speed of convergence towards $\bar{x}^+$ may be increased (see figure 6.7.1 for an illustration). However, from a biological point of view, the two constant inputs u_{max} and u_{min} may represent the concentration of inducer molecules or the strength of light intensity for example, and extreme inputs may induce damages to cells or biological circuits as already explained in chapter 5. It follows that reducing the strength of these inputs may also be an objective. Hence, in some cases, there may exist a trade-off between a desired speed of convergence and a safe amount of inputs for the biological system.

6.7 Conclusion

In this chapter, the control strategy has been designed in order to take into account two main biotechnological constraints. First, the qualitative nature of the measurements: in contrast with classical control theory, measures in biology are incomplete. Second, the qualitative nature of the inputs: either optogenetics or classical introduction of chemicals often lead to discrete inputs. From these two constraints, a qualitative control strategy has been shown to lead to a global convergence towards the unstable steady state of the system. The asymptotic stability of the steady state has also been proved, providing robustness properties to the control strategy. Despite the hybrid nature of the system and the sliding modes generated by the control law, qualitative methodologies have been developed to deal with this challenging problem.

Importantly this new control strategy suggests that the biological implementations presented in [80], for which two inducer molecules and two fluorescent proteins are needed for the control of the Toggle Switch, may be reduced to a unique measurement and a unique control for an equivalent result.

However, due to the nature of the control suggested, as soon as $\bar{x}_1^*$ is not perfectly determined, the global convergence towards $\bar{x}^*$ cannot be guaranteed any more. It is more realistic to assume that estimations in biotechnology are not perfectly accurate. The aim of next chapter is to introduce a qualitative control strategy effective in the case of noisy measurements.

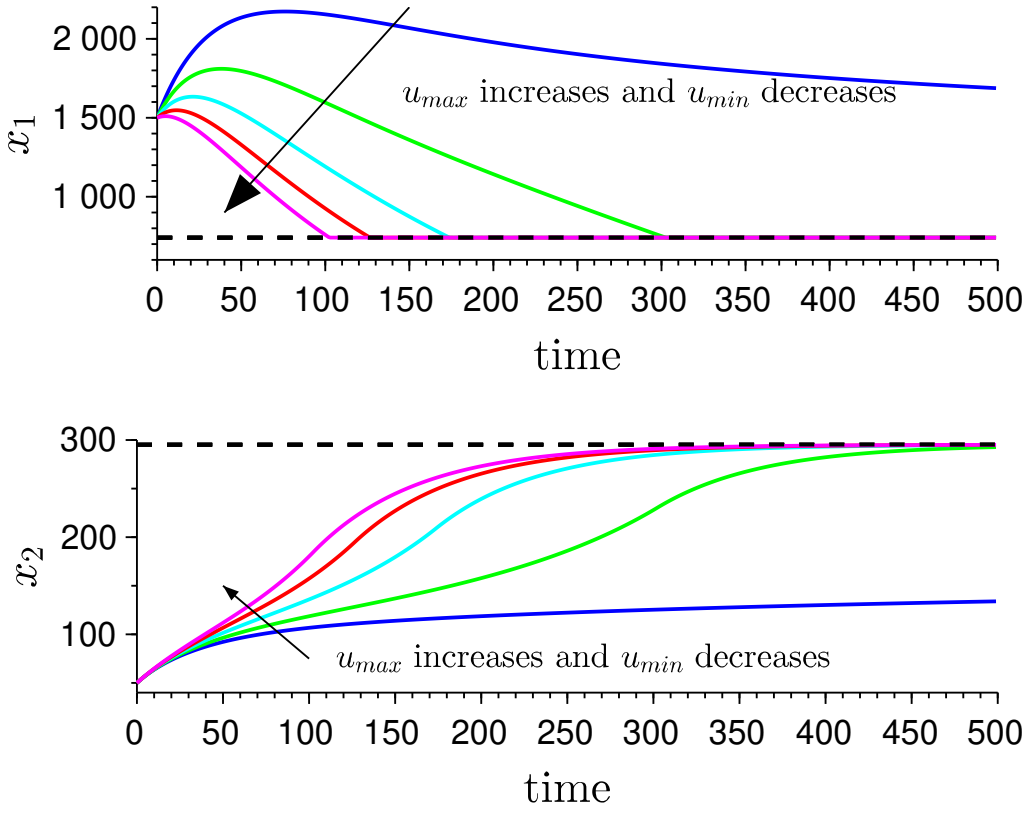

Figure 6.7.1: Influence of u_{min} and u_{max} on the time of convergence of system (6.5.1) under control (6.5.2) towards $\bar{x}^+$. The parameters are calibrated to the experiments presented in [80] and are the same as in figure 6.5.5. For these parameters, u^+_{min} and u^+_{max} can be determined: $u^+_{min} \approx 0.77$ and $u^+_{max} \approx 1.18$. The straight lines are the trajectories of system (6.5.1) under control (6.5.2) with initial condition $x_0 = (1500, 50)$ and with five different pairs of inputs (u_{min}, u_{max}): $(0.76, 1.19)$ (dark blue), $(0.57, 1.64)$ (green), $(0.38, 2.09)$ (light blue), $(0.19, 2.55)$ (red), $(0, 3)$ (magenta).

Chapter 7

Piecewise constant control strategy with uncertain measurements

7.1 Introduction

The control approach presented in the previous chapter requires a precise measurement of the boundary $x_1 = \bar{x}_1^*$, which is not biologically realistic due to uncertainties in the measurements. In addition to the qualitative nature of the measurements presented in the previous chapter, inherent cells specificities and heterogeneities as well as limited sensitivity of measurement devices often induce noisy information. Uncertain control laws have been already applied for control strategies of biochemical processes. In [82] for example, this type of control law has been designed in order to stabilize a working set point of a bioreactor and prevent washout. In this context, the aim of this chapter is to present a qualitative control strategy effective in the case of noisy measurements, and that considers the new synthetic control approaches and the main biological constraints presented in the previous chapter.

The unpredictable piecewise constant control strategy leads to the analysis of a hybrid system with autonomous switching of its dynamics (section 7.2). As for the previous chapter, the construction of successive repelling regions allows one to determine the qualitative dynamics of this system. It is shown that, under appropriate conditions on the control inputs, the trajectories globally converge towards a small zone around $\bar{x}^*$ (section 7.3). Finally, this control strategy is illustrated with the synthetic Repressilator (section 7.4), the p53-Mdm2 negative feedback loop (section 7.5) and the Toggle Switch (section 7.6).

The parts of this chapter about the negative feedback loop have been published in the journal Automatica and the content in section 7.6 has been published for the conference DYCOPS (see the section "List of publications" in page 5).

7.2 The controlled model

The new controlled biological feedback loop is described with the following system:

$$\begin{cases} \dot{x}_1(x_1, x_N) = \kappa_{01} + \mathrm{u}(x_1)\kappa_1 \mathrm{h}^*(x_N, \theta_N, n_N) - \gamma_1 x_1 \\ \dot{x}_i(x_i, x_{i-1}) = \kappa_{0i} + \kappa_i \mathrm{h}^+(x_{i-1}, \theta_{i-1}, n_{i-1}) - \gamma_i x_i \quad \forall\, i \in \{2, ..., N\}\,, \end{cases} \tag{7.2.1}$$

where

$$\begin{cases} \mathrm{u}(x_1) = u_{min} \leq 1 \;\forall\; x_1 \geq \bar{x}_1^* + \delta_1, \\ \mathrm{u}(x_1) = u_{max} \geq 1 \;\forall\; x_1 \leq \bar{x}_1^* - \delta_1, \\ \mathrm{u}(x_1) \in \{u_{min}, u_{max}\} \;\forall\; x_1 \in]\bar{x}_1^* - \delta_1, \bar{x}_1^* + \delta_1[. \end{cases} \tag{7.2.2}$$

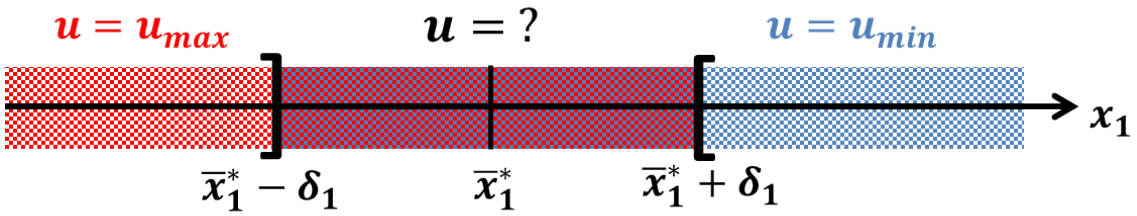

Figure 7.2.1: The control takes the value u_{min} when $x_1 \geq \bar{x}_1^* + \delta_1$, u_{max} when $x_1 \leq \bar{x}_1^* - \delta_1$, and is undetermined when $\bar{x}_1^* - \delta_1 < x_1 < \bar{x}_1^* + \delta_1$.

In a more compact form, this dynamical system can be denoted $\dot{x} = F(\mathrm{u}(x_1), x)$.

The measurements of x_1 are considered qualitative and uncertain, leading to partial knowledge of the system. The gene can either be detected highly expressed ($x_1 \geq \bar{x}_1^*$) or weakly expressed ($x_1 \leq \bar{x}_1^*$) and for a given measured x_1, the real system may be anywhere in the range $[x_1 - \delta_1, x_1 + \delta_1]$ where $2\delta_1 \geq 0$ models fluctuations, precision and sensitivity of the measurement device [82]. As soon as x_1 is inside the uncertain domain $]\bar{x}_1^* - \delta_1, \bar{x}_1^* + \delta_1[$ (also called switching domain), the control law is undetermined and may either take the value u_{min} or u_{max} (see figure 7.2.1 for an illustration). Therefore, system (7.2.1) under the unpredictable control law (7.2.2) is a differential system with discontinuous right-hand side and its solutions are defined in the sense of Filippov as the solutions of the following differential inclusion [47]:

$$\dot{x} \in H(x)$$

such that $H(x) = F(u_{min}, x)$ when $x_1 \geq \bar{x}_1^* + \delta_1$, $H(x) = F(u_{max}, x)$ when $x_1 \leq \bar{x}_1^* - \delta_1$ and

$$H(x) = \bar{co}\{F(u_{min}, x), F(u_{max}, x)\}$$

on the switching domain, where $\bar{co}$ is the closed convex hull of the set of values of the vector field.

7.3 Global convergence

In this section it will be shown that, under appropriate conditions on the two constant inputs u_{min} and u_{max}, the biological feedback loop will converge inside a small region around $\bar{x}^*$. As done in the previous chapter, this will be proved by identifying specific dynamical transitions between zones of the state space. However, the uncertain control must be carefully treated.

7.3.1 Global convergence for the negative loop

For the negative loop, the space is partitioned as follows:

Definition 7.3.1. *The N-dimensional space is partitioned in* 3^N *zones called* $(a_1 a_2 ... a_{N-1} a_N)$ *such that* $\forall\ i \in \{1, ..., N\}$*:*

- $a_i = 0$ *if* $x_i < \bar{x}_i^- - \nu_i$,
- $a_i = 1$ *if* $\bar{x}_i^- - \nu_i \leq x_i \leq \bar{x}_i^- + \delta_i$,
- $a_i = 2$ *if* $x_i > \bar{x}_i^- + \delta_i$,

where $\forall\ i \in \{2, ..., N\}$*:*

- $\nu_1 = \delta_1$,

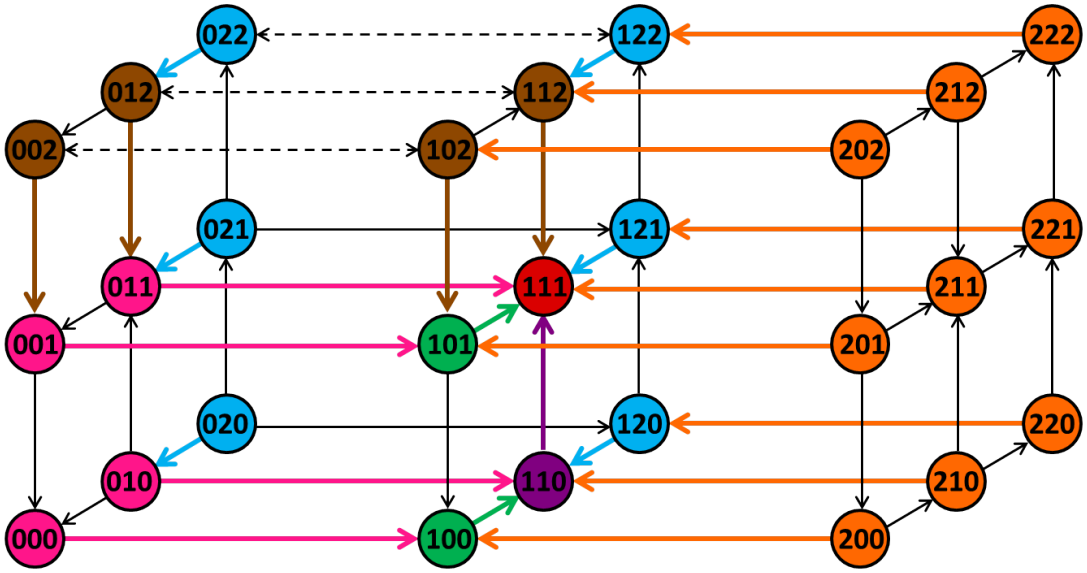

Figure 7.3.1: Partitioning of the state space in dimension 3 according to definition 7.3.1, and graph of transitions. The space is split in different zones of dimension 3 all represented as nodes in this figure. The arrows represent transitions between zones. Some transitions represented here by the plain black arrows do not play any role in the construction of the proof of theorem 7.3.1. Moreover, because of the condition on u_{max}, some transitions (represented by dashed black lines) are undetermined. The successive repelling regions stated in theorem 7.3.1 are represented with different colors. In the end, the trajectories converge towards the red zone (111).

- $\delta_i = \left(\kappa_{0i} + \kappa_i h^+(\bar{x}_{i-1}^- + \delta_{i-1}, \theta_{i-1}, n_{i-1})\right)/\gamma_i - \bar{x}_i^-$,
- $\nu_i = \bar{x}_i^- - \left(\kappa_{0i} + \kappa_i h^+(\bar{x}_{i-1}^- - \nu_{i-1}, \theta_{i-1}, n_{i-1})\right)/\gamma_i$.

An illustration of the partitioning in dimension 3 is presented in figure 7.3.1.

The following conditions on u_{min} and u_{max} allow the statement of four lemmas that successively define repelling regions of the state space:

Assumption 7.3.1. *With $\delta_1 \leq \bar{x}_1^- - \kappa_{01}/\gamma_1$:*

$$\begin{cases} u_{min} \leq \dfrac{\gamma_1(\bar{x}_1^- + \delta_1) - \kappa_{01}}{\kappa_1}, \\ u_{max} \geq \dfrac{\gamma_1(\bar{x}_1^- - \delta_1) - \kappa_{01}}{\kappa_1 h^-(\bar{x}_N^- + \delta_N, \theta_N, n_N)}. \end{cases}$$

Lemma 7.3.1. *Under assumption 7.3.1, the region defined by $a_1 = 2$ is repellent.*

Proof. It is shown that the region $a_1 = 2$ is repellent in direction 1, namely $\dot{x}_1 < 0$ in the whole region.

For $x_1 > \bar{x}_1^- + \delta_1$ the x_1-vector field is defined as:
$\dot{x}_1(x_1, x_N) = \kappa_{01} + u_{min}\kappa_1 \mathrm{h}^-(x_N, \theta_N, n_N) - \gamma_1 x_1$. By evaluating this expression at the boundary $x_1 = \bar{x}_1^- + \delta_1$ and using assumption 7.3.1 on u_{min}, the following inequality comes up: $\dot{x}_1(\bar{x}_1^- + \delta_1, x_N) \leq \left[\kappa_{01} - \gamma_1(\bar{x}_1^- + \delta_1)\right]\left(1 - \mathrm{h}^-(x_N, \theta_N, n_N)\right)$. The bounded properties of system (7.2.1) with $\mathrm{u}(x_1) = 1$ explained in proposition 3.2.8 give $\bar{x}_1^- \in]\kappa_{01}/\gamma_1, \kappa_{01} + \kappa_1/\gamma_1]$ and by definition $\mathrm{h}^-(x_N, \theta_N, n_N) \in]0, 1]$. This implies $\dot{x}_1(\bar{x}_1^- + \delta_1, x_N) \leq 0$. Moreover, for x_N fixed and $x_1 >$

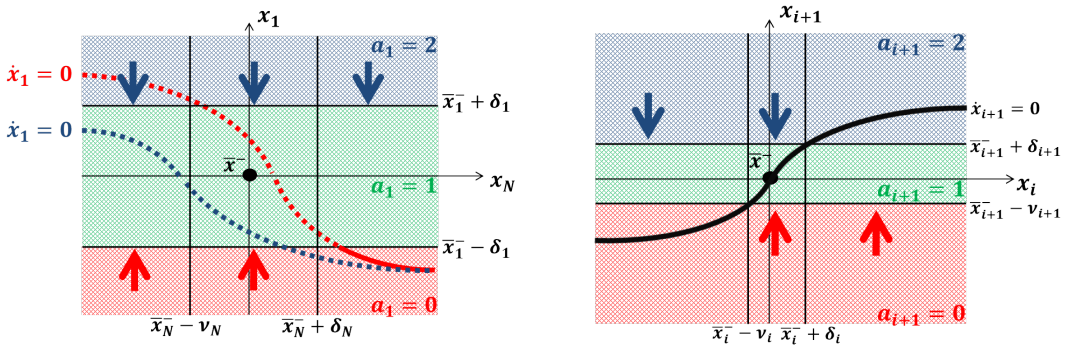

Figure 7.3.2: Left: Transitions properties in the (x_1, x_N) plane. The dashed blue line is the x_1-nullcline for the region $a_1 = 2$. The half-plain half-dashed red line is the x_1-nullcline for the region $a_1 = 0$. The dashed style corresponds to nullclines situated in another region, and the plain style for nullclines situated in their proper region. There are no nullclines in the region $a_1 = 1$ as the control is undetermined. The arrows represent vector field in x_1-direction. Lemma 7.3.1 is illustrated by blue arrows, and lemma 7.3.3 by red arrows. Right: Transitions properties in the (x_i, x_{i+1}) plane. The black line is the x_{i+1}-nullcline. The arrows represent vector field in x_{i+1}-direction. Lemma 7.3.2 is illustrated by blue arrows, and lemma 7.3.4 by red arrows.

$\bar{x}_1^- + \delta_1$, the linear degradation term $-\gamma_1 x_1$ in the x_1-vector field expression gives: $\dot{x}_1(x_1, x_N) < \dot{x}_1(\bar{x}_1^- + \delta_1, x_N) \leq 0$. Hence, $\dot{x}_1(x_1, x_N) < 0 \ \forall \ x_N \geq 0$ and $\forall \ x_1 > \bar{x}_1^- + \delta_1$. Finally, as $a_1 = 2$ is lower-bounded by $x_1 = \bar{x}_1^- + \delta_1$, the region is repellent in direction 1. □

This first lemma is illustrated in the left plot of figure 7.3.2 by the three blue arrows.

Lemma 7.3.2. *For any $i \in \{1, ..., N-1\}$, the region defined by $a_i \in \{0, 1\} \cup a_{i+1} = 2$ is repellent.*

Proof. It is shown that for any $i \in \{1, ..., N-1\}$, the region $a_i \in \{0, 1\} \cup a_{i+1} = 2$ is repellent in direction $i + 1$, namely $\dot{x}_{i+1} < 0$ in the whole region.

By evaluating the x_{i+1}-vector field at the boundary $x_{i+1} = \bar{x}_{i+1}^- + \delta_{i+1}$ and using the definition of δ_{i+1}, the following inequality comes up:
$\dot{x}_{i+1}(\bar{x}_{i+1}^- + \delta_{i+1}, x_i) = \kappa_{i+1}\left(\mathrm{h}^+(x_i, \theta_i, n_i) - \mathrm{h}^+(\bar{x}_i^- + \delta_i, \theta_i, n_i)\right)$. Moreover, in the relevant region, $x_i \leq \bar{x}_i^- + \delta_i$ leading to $\dot{x}_{i+1}(\bar{x}_{i+1}^- + \delta_{i+1}, x_i) \leq 0 \ \forall \ x_i \leq \bar{x}_i^- + \delta_i$. For any $x_{i+1} > \bar{x}_{i+1}^- + \delta_{i+1}$ and x_i fixed, the linear degradation term $-\gamma_{i+1} x_{i+1}$ in the x_{i+1}-vector field expression gives: $\dot{x}_{i+1}(x_{i+1}, x_i) < \dot{x}_{i+1}(\bar{x}_{i+1}^- + \delta_{i+1}, x_i) \leq 0$. Hence, $\dot{x}_{i+1}(x_{i+1}, x_i) < 0 \ \forall \ x_i \leq \bar{x}_i^- + \delta_i$ and $\forall \ x_{i+1} > \bar{x}_{i+1}^- + \delta_{i+1}$. Finally, as $a_i \in \{0, 1\} \cup a_{i+1} = 2$ is lower-bounded by $x_{i+1} = \bar{x}_{i+1}^- + \delta_{i+1}$, the region is repellent in direction $i + 1$. □

The two blue arrows in the right plot of figure 7.3.2 illustrate this second lemma.

Lemma 7.3.3. *Under assumption 7.3.1, the region defined by $a_N \in \{0, 1\} \cup a_1 = 0$ is repellent.*

Proof. It is shown that the region $a_N \in \{0, 1\} \cup a_1 = 0$ is repellent in direction 1, namely $\dot{x}_1 > 0$ in the whole region.

For $x_1 < \bar{x}_1^- - \delta_1$ the x_1-vector field is defined as: $\dot{x}_1(x_1, x_N) = \kappa_{01} + u_{max}\kappa_1 \mathrm{h}^-(x_N, \theta_N, n_N) - \gamma_1 x_1$. By evaluating this expression at the boundary $x_1 = \bar{x}_1^- - \delta_1$ and using assumption 7.3.1 on u_{max}, the following inequality comes up: $\dot{x}_1(\bar{x}_1^- - \delta_1, x_N) \geq$

$$\left(\gamma_1(\bar{x}_1^- - \delta_1) - \kappa_{01}\right)\left[\frac{\mathrm{h}^-(x_N, \theta_N, n_N)}{\mathrm{h}^-(\bar{x}_N^- + \delta_N, \theta_N, n_N)} - 1\right].$$

Moreover, in the relevant region, $x_N \leq \bar{x}_N^- + \delta_N$, and assumption 7.3.1 gives $\gamma_1(\bar{x}_1^- - \delta_1) \geq \kappa_{01}$, leading to $\dot{x}_1(\bar{x}_1^- - \delta_1, x_N) \geq 0 \ \forall \ x_N \leq \bar{x}_N^- + \delta_N$. For any $x_1 < \bar{x}_1^- - \delta_1$ and x_N fixed, the linear

degradation term $-\gamma_1 x_1$ in the x_1-vector field expression gives: $\dot{x}_1(x_1, x_N) > \dot{x}_1(\bar{x}_1^- - \delta_1, x_N) \geq 0$. Hence, $\dot{x}_1(x_1, x_N) > 0 \ \forall \ x_N \leq \bar{x}_N^- + \delta_N$ and $\forall \ x_1 < \bar{x}_1^- - \delta_1$. Finally, as $a_1 = 0$ is upper-bounded by $x_1 = \bar{x}_1^- - \delta_1$, the region is repellent in direction 1. □

The two red arrows in the left plot of figure 7.3.2 illustrate this third lemma.

Lemma 7.3.4. *For any $i \in \{1, ..., N-1\}$, the region defined by $a_i \in \{1, 2\} \cup a_{i+1} = 0$ is repellent.*

Proof. It is shown that for any $i \in \{1, ..., N-1\}$, the region $a_i \in \{1, 2\} \cup a_{i+1} = 0$ is repellent in direction $i+1$, namely $\dot{x}_{i+1} > 0$ in the whole region.

The argumentation follows the same structure as the proof of lemma 7.3.2 by reversing all the inequalities and replacing all $+\delta$ by $-\nu$, giving: $\dot{x}_{i+1}(x_{i+1}, x_i) > 0 \ \forall \ x_i \geq \bar{x}_i^- - \nu_i$ and $\forall \ x_{i+1} < \bar{x}_{i+1}^- - \nu_{i+1}$. Finally, as $a_{i+1} = 0$ is upper-bounded by $x_{i+1} = \bar{x}_{i+1}^- - \nu_{i+1}$, the region is repellent in direction $i+1$. □

This final lemma is illustrated by the two red arrows in the right plot of figure 7.3.2. These four lemmas finally allow the statement of the main result of this section for the negative loop:

Theorem 7.3.1. *If assumption 7.3.1 holds, system (7.2.1) under unpredictable control law (7.2.2) converges globally towards the zone $(a_1...a_N) = (1...1)$ where $a_i = 1 \ \forall \ i \in \{1, ..., N\}$.*

Proof. As a base case, lemma 7.3.1 states that any trajectory ends up in the region $a_1 \in \{0, 1\}$ (illustrated by the orange arrows in figure 7.3.1). Through an immediate mathematical induction, lemma 7.3.2 states that any trajectory is further contained in the region $a_i \in \{0, 1\} \ \forall \ i \in \{1, ..., N\}$ (illustrated by the blue arrows, followed by the brown arrows in figure 7.3.1). As a new base case lemma 7.3.3 states that any trajectory stands in the region $a_i \in \{0, 1\} \cup a_1 = 1 \ \forall \ i \in \{2, ..., N\}$ (illustrated by the pink arrows in figure 7.3.1). Finally, by a second immediate mathematical induction, lemma 7.3.4 states that any trajectory ends up in the zone $a_i = 1 \ \forall \ i \in \{1, ..., N\}$ (illustrated by the green arrows, followed by the purple arrow in figure 7.3.1). In other words, the system is trapped in the zone $a_i = 1 \ \forall \ i \in \{1, ..., N\}$, ending the proof of global convergence for the negative loop. □

Due to the unpredictable control law in the switching domain and the borders of the defined zones, some transitions are not unidirectional: in this case, the border of the two adjacent zones may be crossed in both directions (dashed black arrows in figure 7.3.1). This means that some cycles may emerge *between zones* (see for example the cycle $102 \rightarrow 112 \rightarrow 012 \rightarrow 002 \rightarrow 102$ in figure 7.3.1). However, these cycles are not *periodic trajectories* (for the latter example, the variable x_3 decreases until the trajectory leaves the brown region).

A simulation of global convergence towards the uncertain region around $\bar{x}^-$ in dimension 3 is illustrated in figure 7.3.3.

Remark 7.3.1. *With the condition $\delta_1 > \bar{x}_1^- - \kappa_{01}/\gamma_1$, the result is the same and the proof is straightforward. In this case, the value given to u_{max} has no influence on the invariant zone. Indeed, the region $a_1 = 0$ is naturally repellent as explained in proposition 3.2.2. In other words, $u_{max} = 1$ is enough to guarantee convergence towards (1...1). This control strategy simplifies the biological set-up as $u_{max} = 1$ is equivalent to no control, inducing that the system must only be controlled in the half space $x_1 \geq \bar{x}_1^-$.*

7.3.2 Global convergence for the positive loop

The results presented here for the positive feedback loop are really similar to the one presented in the previous chapter with perfect measurements. Basically all the results are the same, with adapted notations and regions.

The partitioning of the state space is equivalent to the one presented in the previous chapter:

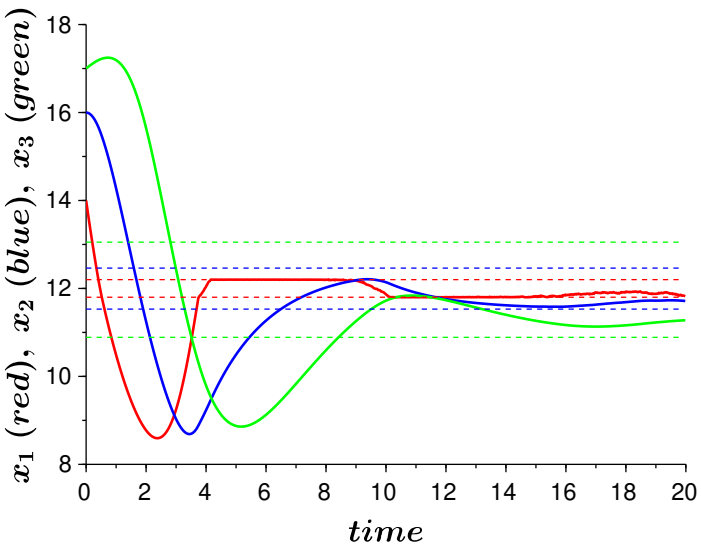

Figure 7.3.3: Simulation of system (7.2.1) in dimension 3 with control $u_{min} = 0.21$, $u_{max} = 1.38$ and $\delta_1 = 0.2$. The trajectory for each variable is depicted with different colors (x_1: red, x_2: blue, x_3: green) and the initial condition is $x_0 = (14, 16, 17)$. The parameters are fixed to $\kappa_{0i} = 2$, $\kappa_i = 8$, $\gamma_i = 0.5$, $\theta_i = 12$, $n_i = 7$ for $i \in \{1, 2, 3\}$. As predicted, the trajectories converge towards the globally attractive zone defined with $\delta_2 = 0.46$, $\nu_2 = 0.47$, $\delta_3 = 1.05$ and $\nu_3 = 1.1$ represented by colored bands.

Definition 7.3.2. *The N-dimensional space is partitioned in 4^N zones. Each zone is called $a = a_1 a_2 ... a_{N-1} a_N$ such that $\forall\ i \in \{1, ..., N\}$:*

- $a_i = 0$ *if* $x_i < \bar{x}_i^+ - \eta_i$,
- $a_i = 1$ *if* $\bar{x}_i^+ - \eta_i \leq x_i < \bar{x}_i^+ - \nu_i$,
- $a_i = 2$ *if* $\bar{x}_i^+ - \nu_i \leq x_i \leq \bar{x}_i^+ + \delta_i$,
- $a_i = 3$ *if* $x_i > \bar{x}_i^+ + \delta_i$,

where:

- $\eta_1 = \bar{x}_1^+ - \kappa_{01}/\gamma_1$,
- $\eta_i = \bar{x}_i^+ - \left(\kappa_{0i} + \kappa_i h^+(\bar{x}_{i-1}^+ - \eta_{i-1}, \theta_{i-1}, n_{i-1})\right)/\gamma_i\ \forall\ i \in \{2, ..., N\}$,
- $\nu_1 = \delta_1$,
- $\nu_i = \bar{x}_i^+ - \left(\kappa_{0i} + \kappa_i h^+(\bar{x}_{i-1}^+ - \nu_{i-1}, \theta_{i-1}, n_{i-1})\right)/\gamma_i\ \forall\ i \in \{2, ..., N\}$,
- $\delta_i = \left(\kappa_{0i} + \kappa_i h^+(\bar{x}_{i-1}^+ + \delta_{i-1}, \theta_{i-1}, n_{i-1})\right)/\gamma_i - \bar{x}_i^+\ \forall\ i \in \{2, ..., N\}$,

An illustration of the partitioning in dimension 2 is presented in figure 7.3.4.

The following conditions on u_{min} and u_{max} allow the statement of six lemmas that successively define repelling regions of the state space:

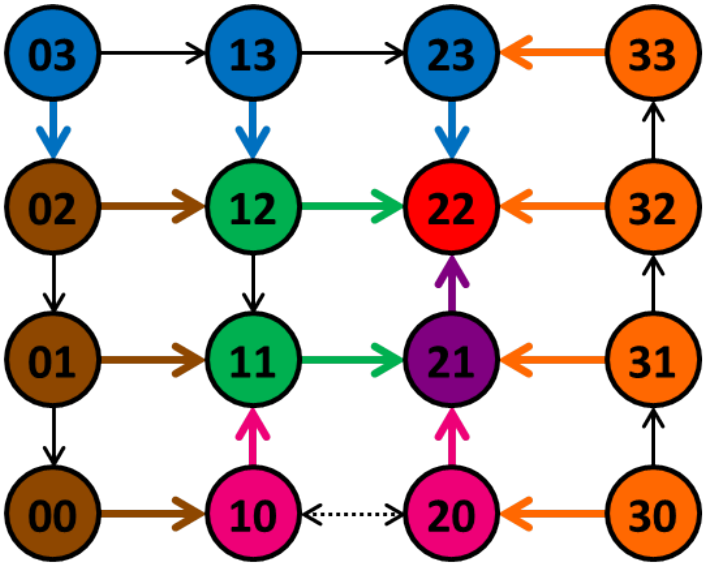

Figure 7.3.4: Partitioning of the state space in dimension 2 according to definition 7.3.2, and graph of transitions. The space is split in different zones of dimension 2 all represented as nodes in this figure. The arrows represent transitions between zones. Some transitions represented here by the plain black arrows do not play any role in the construction of the proof of theorem 7.3.2. Moreover, because of the condition on u_{max}, some transitions (represented by dashed black lines) are undetermined. The successive repelling regions stated in theorem 7.3.2 are represented with different colors. In the end, the trajectories converge towards the red zone (22).

Assumption 7.3.2. *With* $\delta_1 \leq \bar{x}_1^+ - \kappa_{01}/\gamma_1$*:*

$$\begin{cases} u_{min} \leq \dfrac{\gamma_1(\bar{x}_1^+ + \delta_1) - \kappa_{01}}{\kappa_1}, \\ u_{max} \geq \dfrac{\gamma_1(\bar{x}_1^+ - \delta_1) - \kappa_{01}}{\kappa_1 h^+(\bar{x}_N^+ - \eta_N, \theta_N, n_N)}. \end{cases}$$

Lemma 7.3.5. *Under assumption 7.3.2, the region defined by* $a_1 = 3$ *is repellent.*

Proof. In the region $x_1 > \bar{x}_1^+ + \delta_1$ the x_1-vector field is defined as:
$\dot{x}_1(x_1, x_N) = \kappa_{01} + u_{min}\kappa_1 \mathrm{h}^+(x_N, \theta_N, n_N) - \gamma_1 x_1$. By evaluating this expression on the wall $x_1 = \bar{x}_1^+ + \delta_1$ and using the condition on u_{min}, the following inequality comes up: $\dot{x}_1(\bar{x}_1^+ + \delta_1, x_N) \leq \left(\gamma_1(\bar{x}_1^+ + \delta_1) - \kappa_{01}\right)\left(\mathrm{h}^+(x_N, \theta_N, n_N) - 1\right)$. The properties of the system explained in proposition 3.2.8 give $\bar{x}_1^+ \in [\kappa_{01}/\gamma_1, (\kappa_{01} + \kappa_1)/\gamma_1[$ leading to $\left(\gamma_1(\bar{x}_1^+ + \delta_1) - \kappa_{01}\right) \geq 0$ and the increasing Hill function meets the condition $\mathrm{h}^+(x_N, \theta_N, n_N) \in [0, 1[$. This induces $\dot{x}_1(\bar{x}_1^+, x_N) \leq 0$. Moreover, for x_N fixed and $x_1 > \bar{x}_1^+ + \delta_1$, the linear degradation term $-\gamma_1 x_1$ in the x_1-vector field expression gives: $\dot{x}_1(x_1, x_N) < \dot{x}_1(\bar{x}_1^+ + \delta_1, x_N) \leq 0$. Hence, $\dot{x}_1(x_1, x_N) < 0 \ \forall \ x_N \geq 0$ and $\forall \ x_1 \geq \bar{x}_1^+ + \delta_1$. Finally, as $a_1 = 3$ is lower-bounded by $x_1 = \bar{x}_1^+ + \delta_1$, the region is repellent. □

This first lemma is illustrated by the four dark blue arrows in the left plot of figure 7.3.5.

Lemma 7.3.6. *For any* $i \in \{1, ..., N-1\}$*, if the region defined by* $a_i = 3$ *is repellent, then the region* $a_{i+1} = 3$ *is repellent as well.*

Proof. In the whole space, the x_{i+1}-vector field is defined as:
$\dot{x}_{i+1}(x_{i+1}, x_i) = \kappa_{0i+1} + \kappa_{i+1}\mathrm{h}^+(x_i, \theta_i, n_i) - \gamma_{i+1}x_{i+1}$. By evaluating this expression on the wall $x_{i+1} = \bar{x}_{i+1}^+ + \delta_i$ and using the definition of $\bar{x}_{i+1}^+ + \delta_{i+1} = \left(\kappa_{0i+1} + \kappa_{i+1}\mathrm{h}^+(\bar{x}_i^+ + \delta_i, \theta_i, n_i)\right)/\gamma_{i+1}$,

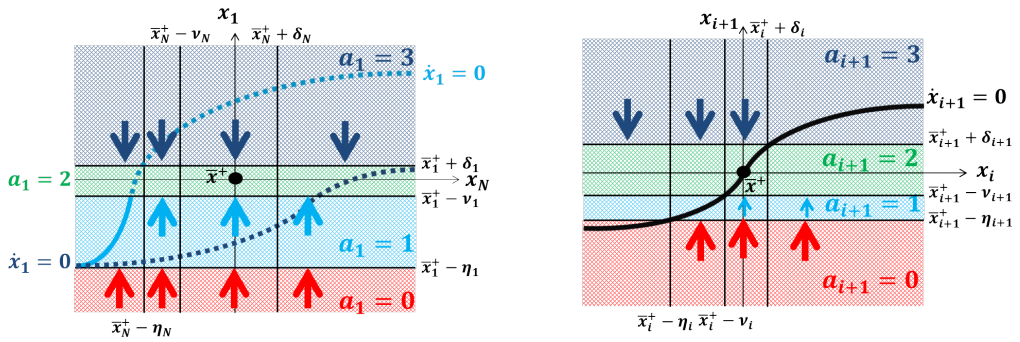

Figure 7.3.5: Left: Transitions properties in the (x_1, x_N) plane. The dashed dark blue line is the x_1-nullcline for the region $a_1 = 3$. The half-plain half-dashed light blue line is the x_1-nullcline for the regions $a_1 = 0$ and $a_1 = 1$. The dashed style corresponds to nullclines situated in another region, and the plain style for nullclines situated in their proper region. The arrows represent vector field in x_1-direction. Lemma 7.3.7 is illustrated by red arrows, lemma 7.3.9 by light blue arrows and lemma 7.3.5 by dark blue arrows. Right: Transitions properties in the (x_i, x_{i+1}) plane. The black line is the x_{i+1}-nullcline. The arrows represent vector field in x_{i+1}-direction. Lemma 7.3.8 is illustrated by red arrows, lemma 7.3.10 by light blue arrows and lemma 7.3.6 by dark blue arrows.

the equality becomes: $\dot{x}_{i+1}(\bar{x}_{i+1}^+ + \delta_{i+1}, x_i) = \kappa_{i+1}\left(\mathrm{h}^+(x_i, \theta_i, n_i) - \mathrm{h}^+(\bar{x}_i^+ + \delta_i, \theta_i, n_i)\right)$. From the hypothesis $a_i = 3$ is repellent, which is equivalent to $x_i \leq \bar{x}_i^+ + \delta_i$. The strictly monotonous property of the increasing Hill function induces $\mathrm{h}^+(x_i, \theta_i, n_i) \leq \mathrm{h}^+(\bar{x}_i^+, \theta_i, n_i)$. Then $\dot{x}_{i+1}(\bar{x}_{i+1}^+ + \delta_{i+1}, x_i) \leq 0$ $\forall\ x_i \leq \bar{x}_i^+ + \delta_i$. Moreover, for x_i fixed and $x_{i+1} > \bar{x}_{i+1}^+ + \delta_{i+1}$, the linear degradation term $-\gamma_{i+1}x_{i+1}$ in the x_{i+1}-vector field expression gives: $\dot{x}_{i+1}(x_{i+1}, x_i) < \dot{x}_{i+1}(\bar{x}_{i+1}^+ + \delta_{i+1}, x_i) \leq 0$. Hence, $\dot{x}_{i+1}(x_{i+1}, x_i) < 0$ $\forall\ x_i \leq \bar{x}_i^+ + \delta_{i+1}$ and $\forall\ x_{i+1} > \bar{x}_{i+1}^+ + \delta_{i+1}$. Finally, as $a_{i+1} = 3$ is lower-bounded by $x_{i+1} = \bar{x}_{i+1}^+ + \delta_{i+1}$, if $a_i = 3$ is repellent the region $a_{i+1} = 3$ is repellent as well. □

The three dark blue arrows in the right plot of figure 7.3.5 illustrate this second lemma.

Lemma 7.3.7. *The region defined by $a_1 = 0$ is repellent.*

Proof. In the region $x_1 < \bar{x}_1^+ - \eta_1$ the x_1-vector field is defined as:
$\dot{x}_1(x_1, x_N) = \kappa_{01} + u_{max}\kappa_1 \mathrm{h}^+(x_N, \theta_N, n_N) - \gamma_1 x_1$. By evaluating this expression on the wall $x_1 = \bar{x}_1^+ - \eta_1 = \kappa_{01}/\gamma_1$ the equality becomes: $\dot{x}_1(\bar{x}_1^+ - \eta_1, x_N) = u_{max}\kappa_1 \mathrm{h}^+(x_N, \theta_N, n_N)$. As the increasing Hill function meets the condition $\mathrm{h}^+(x_N, \theta_N, n_N) \in [0, 1[$, then $\dot{x}_1(\bar{x}_1^+ - \eta_1, x_N) \geq 0$. Moreover, for x_N fixed and $x_1 < \bar{x}_1^+ - \eta_1$, the linear degradation term $-\gamma_1 x_1$ in the x_1-vector field expression gives: $\dot{x}_1(x_1, x_N) > \dot{x}_1(\bar{x}_1^+ - \eta_1, x_N) \geq 0$. Hence, $\dot{x}_1(x_1, x_N) > 0$ $\forall\ x_N \geq 0$ and $\forall$ $x_1 < \bar{x}_1^+ - \eta_1$. Finally, as $a_1 = 0$ is upper-bounded by $x_1 = \bar{x}_1^+ - \eta_1$, the region is repellent. □

An illustration of this lemma is presented in the left plot of figure 7.3.5 by the four red arrows.

Lemma 7.3.8. *For any $i \in \{1, ..., N-1\}$, if the region defined by $a_i = 0$ is repellent, then the region $a_{i+1} = 0$ is repellent as well.*

Proof. In the whole space, the x_{i+1}-vector field is defined as:
$\dot{x}_{i+1}(x_{i+1}, x_i) = \kappa_{0i+1} + \kappa_{i+1}\mathrm{h}^+(x_i, \theta_i, n_i) - \gamma_{i+1}x_{i+1}$. By evaluating this expression on the wall $x_{i+1} = \bar{x}_{i+1}^+ - \eta_{i+1}$ and using the definition η_{i+1}, the equality becomes: $\dot{x}_{i+1}(\bar{x}_{i+1}^+ - \eta_{i+1}, x_i) = \kappa_{0i+1} + \kappa_{i+1}\mathrm{h}^+(x_i, \theta_i, n_i) - \gamma_{i+1}\bar{x}_{i+1}^+ + \gamma_{i+1}\eta_{i+1} = \kappa_{i+1}\left(\mathrm{h}^+(x_i, \theta_i, n_i) - \mathrm{h}^+(\bar{x}_i^+ - \eta_i, \theta_i, n_i)\right)$. From the hypothesis, $a_i = 0$ is repellent, which is equivalent to $x_i \geq \bar{x}_i^+ - \eta_i$. The strictly monotonous property of the increasing Hill function induces $\mathrm{h}^+(x_i, \theta_i, n_i) \geq \mathrm{h}^+(\bar{x}_i^+ - \eta_i, \theta_i, n_i)$. Then $\dot{x}_{i+1}(\bar{x}_{i+1}^+ - \eta_{i+1}, x_i) \geq 0$ $\forall\ x_i \geq \bar{x}_i^+ - \eta_i$. Moreover, for $x_{i+1} < \bar{x}_{i+1}^+ - \eta_{i+1}$, the linear degradation term $-\gamma_{i+1}x_{i+1}$ in the x_{i+1}-vector field expression gives: $\dot{x}_{i+1}(x_{i+1}, x_i) > \dot{x}_{i+1}(\bar{x}_{i+1}^+ - \eta_{i+1}, x_i) \geq 0$.

Hence, $\dot{x}_{i+1}(x_{i+1}, x_i) > 0 \ \forall \ x_{i+1} < \bar{x}^+_{i+1} - \eta_{i+1}$ and $\forall \ x_i \geq \bar{x}^+_i - \eta_i$. Finally, as $a_{i+1} = 0$ is upper-bounded by $x_{i+1} = \bar{x}^+_{i+1} - \eta_{i+1}$, $a_{i+1} = 0$ is repellent within the region $a_i \in \{1, 2, 3\}$. □

This lemma is illustrated in the right plot of figure 7.3.5 by the three red arrows.

Lemma 7.3.9. *Within the region $a_i \in \{1, 2, 3\} \ \forall \ i \in \{1, ..., N\}$, the region defined by $a_1 = 1$ is repellent.*

Proof. In the region $\bar{x}^+_1 - \eta_1 \leq x_1 < \bar{x}^+_1 - \delta_1$ the x_1-vector field is defined as: $\dot{x}_1(x_1, x_N) = \kappa_{01} + u_{max}\kappa_1 \mathrm{h}^+(x_N, \theta_N, n_N) - \gamma_1 x_1$. With the conditions given on u_{max}, and evaluating the expression on the wall $x_1 = \bar{x}^+_1 - \delta_1$ the equality becomes:

$$\begin{aligned}\dot{x}_1(\bar{x}^+_1 - \delta_1, x_N) &\geq \kappa_{01} + \frac{\gamma_1(\bar{x}^+_1 - \delta_1) - \kappa_{01}}{\kappa_1 \mathrm{h}^+(\bar{x}^+_N - \eta_N, \theta_N, n_N)} \kappa_1 \mathrm{h}^+(x_N, \theta_N, n_N) - \gamma_1(\bar{x}^+_1 - \delta_1) \\ &= \left(\frac{\mathrm{h}^+(x_N, \theta_N, n_N)}{\mathrm{h}^+(\bar{x}^+_N - \eta_N, \theta_N, n_N)} - 1 \right) \left[\gamma_1(\bar{x}^+_1 - \delta_1) - \kappa_{01} \right].\end{aligned}$$

The definition of these bounds give $\kappa_{01}/\gamma_1 = \bar{x}^+_1 - \eta_1 \geq \bar{x}^+_1 - \delta_1$, hence $\left[\gamma_1(\bar{x}^+_1 - \delta_1) - \kappa_{01}\right] \geq 0$. On the other hand, $a_N \in \{1, 2, 3\}$ is equivalent to $x_N \geq \bar{x}^+_N - \eta_N$. Then with the strictly monotonous property of the increasing Hill function: $\mathrm{h}^+(x_N, \theta_N, n_N) \geq \mathrm{h}^+(\bar{x}^+_N - \eta_N, \theta_N, n_N)$ leading to $\mathrm{h}^+(x_N, \theta_N, n_N)/\mathrm{h}^+(\bar{x}^+_N - \eta_N, \theta_N, n_N) \geq 1$. Therefore, $\dot{x}_1(\bar{x}^+_1 - \delta_1, x_N) \geq 0 \ \forall \ x_N \geq \bar{x}^+_N - \eta_N$. Moreover, for $\bar{x}^+_1 - \eta_1 \leq x_1 < \bar{x}^+_1 - \delta_1$, the linear degradation term $-\gamma_1 x_1$ in the x_1-vector field expression gives: $\dot{x}_1(x_1, x_N) > \dot{x}_1(\bar{x}^+_1 - \delta_1, x_N) \geq 0$. Hence, $\dot{x}_1(x_1, x_N) > 0 \ \forall \ \bar{x}^+_1 - \eta_1 \leq x_1 < \bar{x}^+_1 - \delta_1$ and $\forall \ x_N \geq \bar{x}^+_N - \eta_N$. Finally, as $a_1 = 1$ is upper-bounded by $x_1 = \bar{x}^+_1 - \delta_1$, $a_1 = 1$ is repellent within the region $a_N \in \{1, 2, 3\}$. □

This lemma is illustrated by three light blue arrows in the left plot of figure 7.3.5.

Lemma 7.3.10. *For any $i \in \{1, ..., N-1\}$, if the regions defined by $a_i = 0$ and $a_i = 1$ are repellent, then the region $a_{i+1} = 1$ is repellent as well.*

Proof. In the whole space, the x_{i+1}-vector field is defined as:
$\dot{x}_{i+1}(x_{i+1}, x_i) = \kappa_{0i+1} + \kappa_{i+1}\mathrm{h}^+(x_i, \theta_i, n_i) - \gamma_{i+1}x_{i+1}$. By evaluating this expression on the wall $x_{i+1} = \bar{x}^+_{i+1} - \nu_{i+1}$, and using the definition of $\bar{x}^+_{i+1} - \nu_{i+1} = \left(\kappa_{0i+1} + \kappa_{i+1}\mathrm{h}^+(\bar{x}^+_i - \nu_i, \theta_i, n_i)\right)/\gamma_{i+1}$, the equality becomes: $\dot{x}_{i+1}(\bar{x}^+_{i+1} - \nu_{i+1}, x_i) = \kappa_{0i+1} + \kappa_{i+1}\mathrm{h}^+(x_i, \theta_i, n_i) - \gamma_{i+1}(\bar{x}^+_{i+1} - \nu_{i+1}) = \kappa_{i+1}(\mathrm{h}^+(x_i, \theta_i, n_i) - \mathrm{h}^+(\bar{x}^+_i - \nu_i, \theta_i, n_i))$. As $a_i \in \{2, 3\}$, $x_i \geq \bar{x}^+_i - \nu_i$. Then with the strictly monotonous property of the increasing Hill function: $\mathrm{h}^+(x_i, \theta_i, n_i) \geq \mathrm{h}^+(\bar{x}^+_i - \nu_i, \theta_i, n_i)$ leading to $\dot{x}_{i+1}(\bar{x}^+_{i+1} - \nu_{i+1}, x_i) \geq 0 \ \forall \ x_i \geq \bar{x}^+_i - \nu_i$. Moreover, for $x_{i+1} < \bar{x}^+_{i+1} - \nu_{i+1}$, the linear degradation term $-\gamma_{i+1}x_{i+1}$ in the x_{i+1}-vector field expression gives: $\dot{x}_{i+1}(x_{i+1}, x_i) > \dot{x}_{i+1}(\bar{x}^+_{i+1} - \nu_{i+1}, x_i) \geq 0$. Hence, $\dot{x}_{i+1}(x_{i+1}, x_i) > 0 \ \forall \ x_{i+1} < \bar{x}^+_{i+1} - \nu_{i+1}$ and $\forall \ x_i \geq \bar{x}^+_i - \nu_i$. Finally, as $a_{i+1} = 1$ is upper-bounded by $x_{i+1} = \bar{x}^+_{i+1} - \nu_{i+1}$, $a_{i+1} = 1$ is repellent within the region $a_i \in \{2, 3\}$. □

This final lemma is illustrated by the two light blue arrows in the right plot of figure 7.3.5. These six lemmas finally allow the statement of the theorem for the positive loop:

Theorem 7.3.2. *If assumption 7.3.2 holds, system (7.2.1) under unpredictable control law (7.2.2) converges globally towards the zone $(a_1...a_N) = (2...2)$ where $a_i = 2 \ \forall \ i \in \{1, ..., N\}$.*

Proof. As a base case, lemma 7.3.5 states that any trajectory is contained in the region $a_1 \neq 3$ (illustrated by the orange arrows in figure 7.3.4). By mathematical induction, lemma 7.3.6 states that any trajectory is contained in the region $a_i \neq 3 \ \forall \ i \in \{1, ..., N\}$ (illustrated by the blue arrows in figure 7.3.4). As a new base case lemma 7.3.7 states that any trajectory stands in the region $a_1 \in \{1, 2\}$ and $a_i \neq 3 \ \forall \ i \in \{2, ..., N\}$ (illustrated by the brown arrows in figure 7.3.4). By a second mathematical induction, lemma 7.3.8 states that the trajectories are further constrained in the zone $a_i \in \{1, 2\} \ \forall \ i \in \{1, ..., N\}$ (illustrated by the pink arrows in figure 7.3.4). As a last base case, lemma 7.3.9 states that any trajectory stands in the region $a_1 = 2$ and $a_i \in \{1, 2\}$ $\forall \ i \in \{2, ..., N\}$ (illustrated by the green arrows in figure 7.3.4). Finally, by a last mathematical

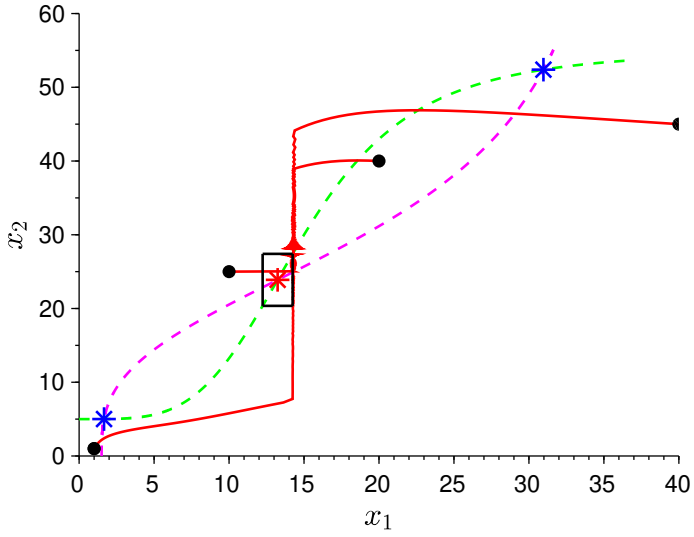

Figure 7.3.6: Trajectories of system (7.2.1) under control (7.2.2) in dimension 2 with an uncertainty range of $\delta_1 = 1$ and with parameters $\kappa_{01} = 0.3$, $\kappa_1 = 7$, $\gamma_1 = 0.2$, $\theta_1 = 15$, $n_1 = 4$ and $\kappa_{02} = 0.5$, $\kappa_2 = 5$, $\gamma_2 = 0.1$, $\theta_2 = 30$, $n_2 = 3$. The two locally stable steady states $\bar{x}^+_{inf} = (1.66, 5)$ and $\bar{x}^+_{sup} = (31, 52.4)$ are represented by blue stars and the locally unstable steady state $\bar{x}^+ = (13.2, 23.9)$ is represented by a red star. The green dashed line is the x_2-nullcline and the magenta dashed line the x_1-nullcline of the uncontrolled system. The four red lines are trajectories with control $u_{min} = 0.16$, and $u_{max} = 71.4$ with initial conditions $x_0 \in \{(1, 1), (10, 25), (20, 40), (40, 45)\}$. All the trajectories converge towards the uncertain region around $\bar{x}^+$ depicted by the black square and defined by $\nu_2 \approx \delta_2 \approx 3.52$.

induction, lemma 7.3.10 states that the trajectories are further constrained in the zone $a_i = 2$ $\forall\, i \in \{1, ..., N\}$ (illustrated by the purple arrow in figure 7.3.4). In other words, all the trajectories converge towards the attractive region $(2, ..., 2)$ surrounding the steady state $\bar{x}^+$, ending the proof of global convergence for the positive loop. □

As for the negative loop, some transitions are not unidirectional (dashed black arrows in figure 7.3.4), and some transitions are not used for the proof of theorem 7.3.2 (black arrows in figure 7.3.4). A simulation of global convergence towards the uncertain region around $\bar{x}^+$ in dimension 2 is illustrated in figure 7.3.6. In this plot, it is possible to observe that the trajectories converge towards the up-right corner of the uncertain region. This is due to the fact that in this simulation, u_{max} is really large compared to 1. It follows that the stochastic control law inside the uncertain region is more or less equal to u_{max}.

Remark 7.3.2. *As for the negative loop, if assumption 7.3.2 does not hold, namely* $\delta_1 > \bar{x}^+_1 - \kappa_{01}/\gamma_1$*, the result is the same and the proof is straightforward. In this case, the value given to* u_{max} *has no influence on the invariant zone. Indeed, the regions* $a_1 = 0$ *and* $a_1 = 1$ *are merged, and this region is naturally repellent as explained in proposition 3.2.2. In other words,* $u_{max} = 1$ *is enough to guarantee convergence towards* $(2...2)$.

For both loops, this adapted piecewise constant control strategy can be biologically interpreted and implemented as the one presented in chapter 6. In case of uncertain measurements, this control approach guarantees convergence towards a region around $\bar{x}^*$. This small domain is satisfactory as strict convergence is not likely to occur in biology due to inherent and devices uncertainties. Theoretically, the boundaries of this convergence area may be tuned as close as desired from $\bar{x}^*$

by restricting the zone of fluctuation $2\delta_1$: indeed as δ_1 converges towards zero, the region shrinks around $\bar{x}^*$. In the case of perfect measurements, namely $\delta_1 = 0$, the results of chapter 6 are recovered and $\bar{x}^*$ becomes a globally asymptotically stable steady state of this ideal system. However, the convergence result is no longer accurate if the measure is not continuous in time or if there is a delay between the controller and the measure. In this case, the boundaries of the convergence region would be fuzzier and a detailed study of this situation might be an interesting extension of the work.

7.4 A synthetic example: the Repressilator

As introduced in chapter 2, the Repressilator was synthetically designed by Michael Elowitz and Stanislas Leibler in 2000 [40]. The aim of this work was to generate a synthetic gene regulatory network mimicking a biological oscillator. Three genes were assembled in a negative feedback loop as illustrated in the left sketch of figure 7.4.1.

The first protein LacI expressed by the first gene *lacI* represses the expression of the second gene *tetR*. Its protein product TetR is in turn responsible for the inhibition of a third gene *cI*. Lastly, the third resulting protein CI represses the first gene *lacI*. This circuit was finally implemented in *Escherichia Coli*. Thanks to a Green Fluorescence Protein, sustained oscillations were measured. As already explained in chapter 3, this loop is equivalent to the canonical negative loop (3.2.1) provided a change of variable. In order to illustrate the control strategies presented in chapter 6 and 7, the data provided by [40] is fitted using a least squares method performed with Scilab with the classical cost function: $J(p) = \sum_{i=1}^{m} (x_1(t_i, p) - y_i)^2$, where m is the number of time points, y_i is the fluorescence measurement at time t_i provided by the data, and $x_1(t_i, p)$ is the evaluation of the first variable of model (3.2.1) with the vector of parameters p. For the sake of simplicity, the model is supposed to be symmetric: the parameters κ_{0i}, κ_i, θ_i, n_i and γ_i are supposed to be equal for

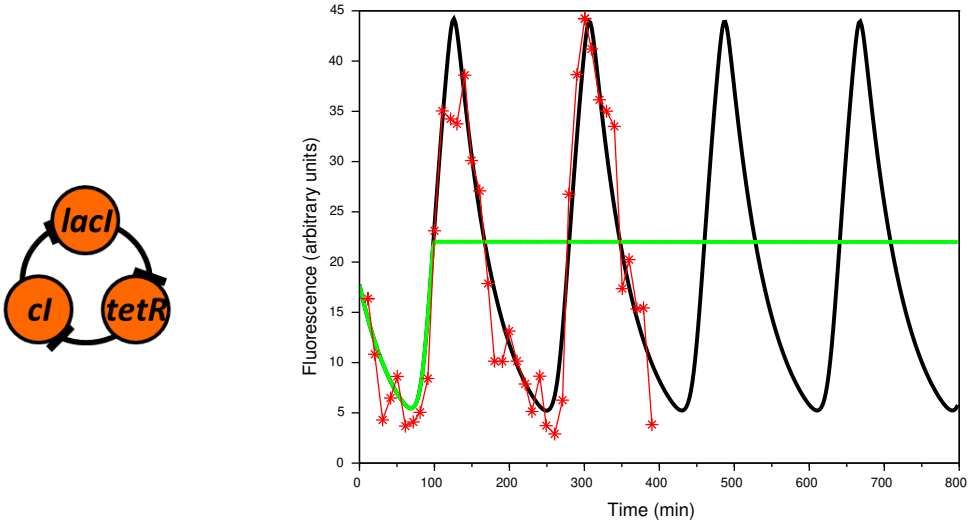

Figure 7.4.1: Left: The three components of the Repressilator negative feedback loop. Right: The red star-plain line represents Repressilator data from [40]. The black plain line is a simulation of the uncontrolled system (3.2.1) with three inhibitions, with parameters determined using a least squares routine in Scilab with a symmetrical hypothesis: $\kappa_{0i} = 0.003$, $\kappa_i = 1.6$, $\gamma_i = 0.02$, $\theta_i = 24.6$, $n_i = 9$ for $i \in \{1, 2, 3\}$, leading to $\bar{x}^- = (22, 22.7, 27.6)$. The green plain line is the system controlled with $u_{min} = 0.2$ and $u_{max} = 1$ without uncertainties. The trajectory converges towards the globally attractive steady state $\bar{x}^-$.

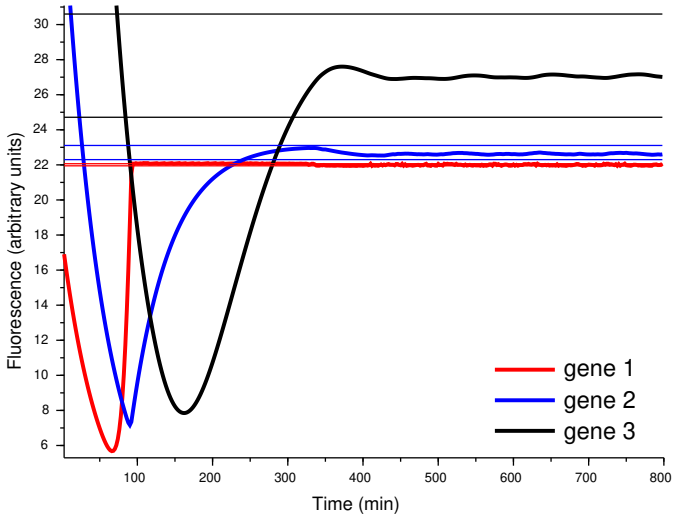

Figure 7.4.2: A trajectory of the Repressilator with control $u_{min} = 0.2$, $u_{max} = 1.5$ and uncertainties $\delta_1 = 0.06$. The other parameters are the same as in figure 7.4.1, with initial conditions $x_0 = (17.7, 37.6, 73.5)$. The trajectory converges towards the attractive zone defined with $\delta_2 = \nu_2 = 0.2$ and $\delta_3 = \nu_3 = 1.5$ and represented by colored bands.

any $i \in \{1, 2, 3\}$. In the end, the vector of parameters p contains 5 unknowns: $p = (\kappa_0, \kappa, \theta, n, \gamma)$. The calibration is effectuated on the first two oscillations presented in [40] for which the undesired increasing trend of fluorescence (possibly due to an increase of the cell population during time) is removed by considering $y_i = y_i - 0.07t_i$. The result of this calibration is shown in the right plot of figure 7.4.1.

The two control strategies are checked with this fitted model. As expected, the first strategy without uncertainties in the measurement induces a global convergence towards the unstable steady state $\bar{x}^-$. This result is illustrated in the right plot of figure 7.4.1. The PWC strategy with uncertain measurements satisfactorily results in the convergence of the three variables towards the expected attractive region. This result is illustrated in figure 7.4.2. These control strategies may allow control of the natural behavior of the synthetic Repressilator and stop its oscillations when needed.

7.5 A biological example: the p53-Mdm2 negative loop

As explained in chapter 2, the protein p53 is involved in tumor suppression, apoptosis, and DNA repair. In healthy organisms and unstressed conditions, this protein is kept at low levels thanks to tight homeostatic control mechanisms [21]. In various stress conditions however, such as the presence of malignant cells or in case of DNA damages, it has been observed that the concentration of p53 starts to oscillate [85]. These sustained oscillations have been interpreted as essential for DNA repair or tumor suppression.

These two main dynamical behaviors have been partly explained through a negative regulation of p53 by another protein called Mdm2. Several models have been built in order to recover these different observations (see for example [55] for a review), and some of them, such as in [4] and [92], also incorporate DNA damage. Among these possible models, one is similar to the uncontrolled model (3.2.1) presented in section 3.2.2 of chapter 3 with x_1 representing the concentration of p53, x_2 representing the concentration of a precursor of Mdm2, such as Mdm2 mRNA (messenger RNA),

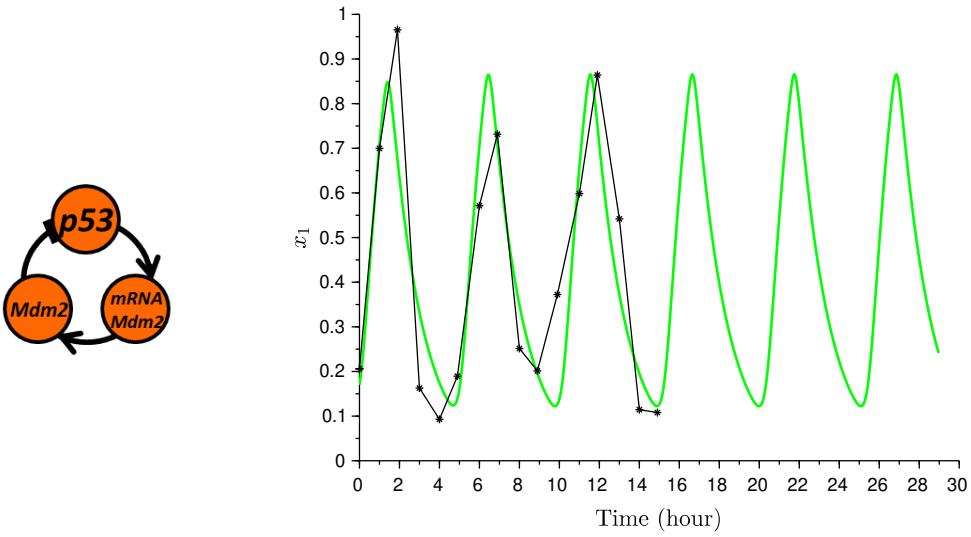

Figure 7.5.1: Left: The three components of the p53-Mdm2 negative feedback loop. Right: The black star-plain line represents the p53-Mdm2 data from [55]. The green plain line is a simulation of the uncontrolled system (3.2.1) with parameters determined using a least squares routine in Scilab with a symmetrical hypothesis: $\kappa_{0i} = 0.001$, $\kappa_i = 0.95$, $\gamma_i = 0.65$, $\theta_i = 0.49$ and $n_i = 10$ for $i \in \{1, 2, 3\}$.

and x_3 representing the concentration of the protein Mdm2. The protein p53 is known to enhance the production of Mdm2 mRNA, itself enhancing the production of the protein Mdm2, and this latter inhibits the production of p53 as explained previously (see the left sketch in figure 7.5.1).

Importantly, it has also been recently observed that, due to its important role in apoptosis, inappropriate activity of p53 with too high or too low concentrations can lead to various diseases, such as neurodegenerative disorders characterized by a neuronal loss like Alzheimer [113], or early embryonic lethality [21]. In this context, the control strategy explained in the previous section may be a useful tool in order to force a disrupted p53-Mdm2 loop that exhibits extreme undesirable values of p53 to recover healthy homeostatic conditions.

In order to illustrate the control strategy presented in section 7.3, the oscillating p53 data points provided by [55] are fitted using a least squares method performed with Scilab with the classical cost function: $J(p) = \sum_{i=1}^{m} \left(x_1(t_i, p) - y_i\right)^2$, where m is the number of time points, y_i is the fluorescence measurement at time t_i provided by the data, and $x_1(t_i, p)$ is the evaluation of the first variable of model (7.2.1) with the vector of parameters p. For the sake of simplicity, the model is supposed to be symmetric: the parameters κ_{0i}, κ_i, θ_i, n_i and γ_i are supposed to be equal for any $i \in \{1, 2, 3\}$. In the end, the vector of parameters p contains 5 unknowns: $p = (\kappa_0, \kappa, \theta, n, \gamma)$. A last constraint consists in imposing n as an integer. The result of this calibration is shown in figure 7.5.1.

The four left plots of figure 7.5.2 present a simulation of this uncontrolled fitted model with sustained oscillations. With a measurement error arbitrarily fixed to $\delta_1 = 0.001$, it is possible to observe in the four right plots of figure 7.5.2 that the control strategy presented in this chapter induces a global convergence towards the analytic attractive region (111) around the unstable steady state, preventing unsafe extreme concentrations of p53. The convergence of the attractive zone towards $\bar{x}^-$ when $\delta_1 \to 0$, as discussed in the previous section, is illustrated in figure 7.5.3. This graph can be used in order to estimate the measurement precision needed for a desired convergence result.

However, it is possible to observe that an over-sized time step for the numerical resolution of the ODE produces a thicker convergence band than the one predicted for the first variable (see the top

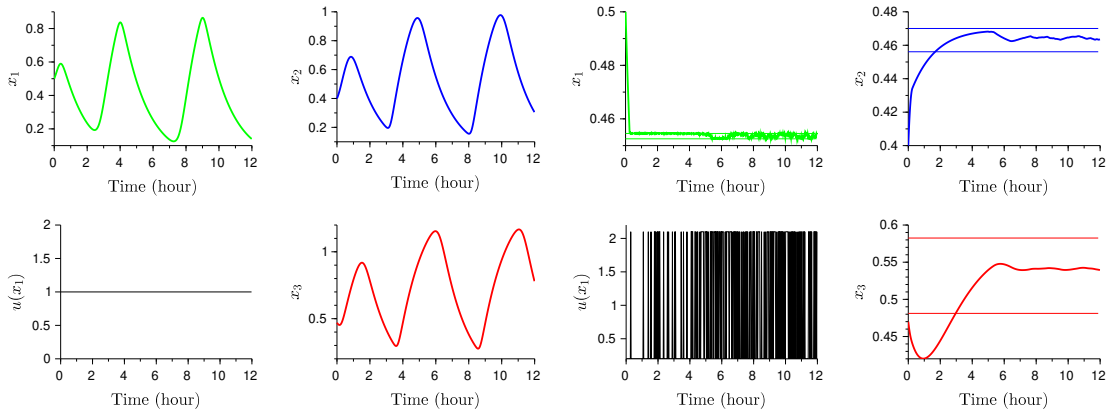

Figure 7.5.2: For all plots, the parameters are the same as in figure 7.5.1. The trajectory for each variable is depicted with different colors (x_1: green, x_2: blue, x_3: red) and the black color is dedicated to the control law u(x_1). The four left plots represent a simulation of the uncontrolled system (3.2.1) with initial conditions $x_0 = (0.5, 0.4, 0.47)$: the three variables oscillate around the steady state $\bar{x}^- = (0.45, 0.46, 0.53)$ and the control is fixed to 1. The four right plots represent a simulation of system (7.2.1) with same initial conditions x_0, under control law (7.2.2) with $\delta_1 = 0.001$, $u_{min} = 0.2$ and $u_{max} = 2.1$. As predicted, the trajectories converge towards the globally attractive zone defined with $\delta_2 \approx \nu_2 \approx 0.007$ and $\delta_3 \approx \nu_3 \approx 0.05$ represented by colored bands. As $x_1 \geq \bar{x}_1^- + \delta_1$ initially, the control stays constant to u_{min} for a very short period of time. As soon as x_1 arrives in the unpredictable zone, the control starts switching stochastically between u_{min} and u_{max} with the same probability.

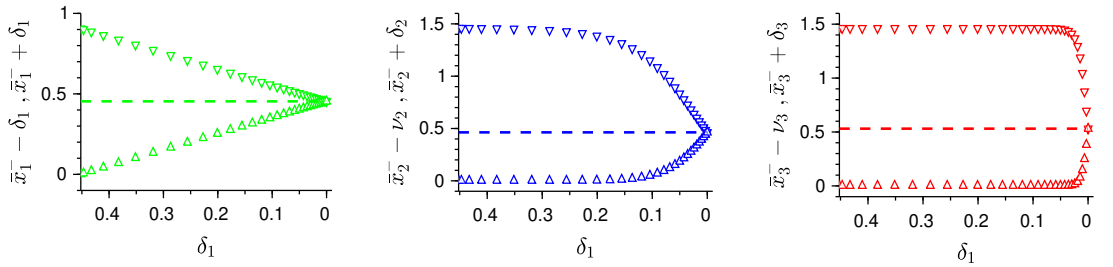

Figure 7.5.3: Convergence of the attractive zone when δ_1 decreases from $\bar{x}_1^- - \kappa_{01}/\gamma_1$ to 0. The parameters are the same as in figure 7.5.1. For each variable (x_1: green, x_2: blue, x_3: red), the upper bound $\bar{x}_i^- + \delta_i$ (resp. lower bound $\bar{x}_i^- - \nu_i$) is depicted with inverted (resp. upright) triangles. As explained, the convergence region shrinks around $\bar{x}^-$ (represented by dashed lines) as δ_1 tends to zero.

third plot of figure 7.5.2). This illustrates the fact that if the controller is limited in speed or if the measurements are slow compared to the time evolution of the system, the convergence result is no longer accurate. In this case, the boundaries of the convergence region would be fuzzier and a detailed study of this situation might be an interesting extension of the work.

As a remark, simulations need a probability distribution for the control in the region $a_1 = 1$ as it may take any of the two values u_{min} and u_{max}. As no a priori probability is evident about fluctuations in the measures, the numerical results are presented here with a classical discrete uniform distribution: the probability $p(.)$ that the control takes the value u_{min} is the same as the probability that the control takes the value u_{max}: $p(u_{min}) = p(u_{max}) = 0.5$. Another choice would have been to consider a spatially dependent control law where the probability depends on the distances to the boundaries

$\bar{x}_1^- - \delta_1$ and $\bar{x}_1^- + \delta_1$. For a fixed x_1 in the uncertain zone, the probability $p(.|x_1)$ that the control takes the value u_{min} becomes $p(u_{min}|x_1) = (1/(2\delta_1))\,(x_1 - \bar{x}_1^-) + 1/2$, and the probability that the control takes the value u_{max} is defined as $p(u_{max}|x_1) = 1 - p(u_{min}|x_1)$. Another really easy choice would have been to fix the control either to u_{min} or u_{max} in the whole switching domain. This hypothesis would have led to the convergence of each variable towards one of the two boundaries of the convergence region. However, this error measurement model is not really likely to happen. Obviously, this probability distribution choice is only needed for a simulation purpose and does not affect the zone of convergence determined analytically.

Finally, this strategy allows recovery of healthy homeostatic conditions, preventing unsafe extreme concentrations of p53.

7.6 The PWC control with uncertainties inside Hill functions: an illustration

Similarly to what was done in section 6.5 of chapter 6, the same results can be easily obtained when the uncertain and qualitative control law acts inside the Hill function. In this section, this new result is only illustrated in dimension two with the Toggle Switch.

7.6.1 The controlled Toggle Switch model

From what was presented in section 6.5 of chapter 6, the introduction of imperfect measurements lead to the following controlled problem:

$$\begin{cases} \dot{x}_1(x_1, x_N) = \kappa_{01} + \kappa_1 \mathrm{h}^-(\mathrm{u}(x_1)x_2, \theta_2, n_2) - \gamma_1 x_1, \\ \dot{x}_2(x_i, x_{i-1}) = \kappa_{02} + \kappa_2 \mathrm{h}^-(x_1, \theta_1, n_1) - \gamma_2 x_2, \end{cases} \tag{7.6.1}$$

with

$$\begin{cases} \mathrm{u}(x_1) = u_{min} < 1 \text{ if } x_1 \leq \bar{x}_1^+ - \delta_1, \\ \mathrm{u}(x_1) = u_{max} > 1 \text{ if } x_1 \geq \bar{x}_1^+ + \delta_1, \\ \mathrm{u}(x_1) \in \{u_{min}, u_{max}\} \text{ if } x_1 \in]\bar{x}_1^+ - \delta_1, \bar{x}_1^+ + \delta_1[. \end{cases} \tag{7.6.2}$$

In the uncertain region, the control is undetermined and may take either u_{min} or u_{max} without any specific transition law or probability distribution.

7.6.2 Global results

Initially it is assumed that δ_1 is small enough for simplicity:

Assumption 7.6.1. *δ_1 satisfies:* $0 < \delta_1 < \min\left(\bar{x}_1^+ - \kappa_{01}/\gamma_1, (\kappa_{01} + \kappa_1)/\gamma_1 - \bar{x}_1^+\right)$.

Similarly to what was done in section 6.5 of chapter 6, under assumption 7.6.1 the space is partitioned in 5^2 zones ($a_1 a_2$):

Definition 7.6.1. *For $i \in \{1, 2\}$:*

- $a_i = 0$ *if* $x_i < \bar{x}_i^+ - \eta_i$,
- $a_i = 1$ *if* $\bar{x}_i - \eta_i \leq x_i < \bar{x}_i - \nu_i$,
- $a_i = 2$ *if* $\bar{x}_i - \nu_i \leq x_i \leq \bar{x}_i + \delta_i$,
- $a_i = 3$ *if* $\bar{x}_i + \delta_i < x_i \leq \bar{x}_i + \beta_i$,
- $a_i = 4$ *if* $\bar{x}_i + \beta_i < x_i$,

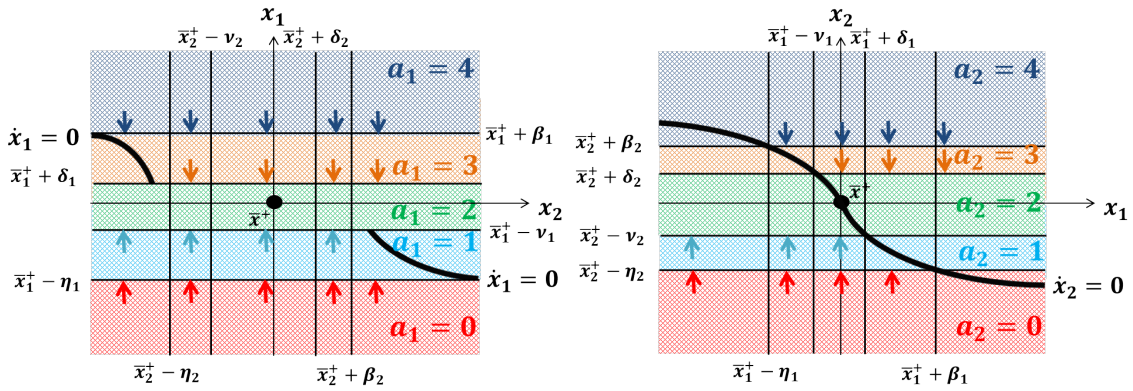

Figure 7.6.1: Transition properties with uncertain measurements. Left: Transitions properties in the (x_2, x_1) plane. The dark lines are the x_1-nullclines. The arrows represent vector field in the x_1-direction. Right: Transitions properties in the (x_1, x_2) plane. The dark line is the x_2-nullclines. The arrows represent vector field in the x_2-direction.

where

- $\beta_1 = (\kappa_{01} + \kappa_1)/\gamma_1 - \bar{x}_1^+$,
- $\eta_2 = \bar{x}_2^+ - \left(\kappa_{02} + \kappa_2 h^-(\bar{x}_1^+ + \beta_1, \theta_1, n_1)\right)/\gamma_2$,
- $\eta_1 = \bar{x}_1^+ - \kappa_{01}/\gamma_1$,
- $\beta_2 = \left(\kappa_{02} + \kappa_2 h^-(\bar{x}_1^+ - \eta_1, \theta_1, n_1)\right)/\gamma_2 - \bar{x}_2^+$.
- $\nu_1 = \delta_1$,
- $\nu_2 = \bar{x}_2^+ - \left(\kappa_{02} + \kappa_2 h^-(\bar{x}_1^+ + \delta_1, \theta_1, n_1)\right)\gamma_2$,
- $\delta_2 = \left(\kappa_{02} + \kappa_2 h^-(\bar{x}_1^+ - \nu_1, \theta_1, n_1)\right)/\gamma_2 - \bar{x}_2^+$.

It is easy to check that $\kappa_{01}/\gamma_1 = \bar{x}_1^+ - \eta_1 < \bar{x}_1^+ - \nu_1 < \bar{x}_1^+ < \bar{x}_1 + \delta_1 < \bar{x}_1^+ + \beta_1 = (\kappa_{01} + \kappa_1)/\gamma_1$ and $\kappa_{02}/\gamma_2 < \bar{x}_2^+ - \eta_2 < \bar{x}_2^+ - \nu_2 < \bar{x}_2^+ < \bar{x}_2 + \delta_2 < \bar{x}_2^+ + \beta_2 < (\kappa_{02} + \kappa_2)/\gamma_2$.

This new partitioning allows the statement of a global convergence theorem:

Theorem 7.6.1. *With $u_{min} \leq \bar{x}_2^+/(\bar{x}_2^+ + \beta_2)$ and $u_{max} \geq \bar{x}_2^+/(\bar{x}_2^+ - \eta_2)$, system (7.6.1) under control law (7.6.2) converges globally towards the zone* (22).

The proof of this theorem follows exactly the same ideas as the one constructed for theorem 6.5.1 in section 6.5 of chapter 6. Lemma 6.5.1 is fully valid for this new system and is illustrated in figure 7.6.1. Its proof is slightly modified by adapting the evaluation of the vector fields in the new regions. If δ_1 does not fulfill assumption 7.6.1, results of theorem 7.6.1 are still valid: if $\delta_1 \geq (\kappa_{01} + \kappa_1)/\gamma_1 - \bar{x}_1^+$ (resp. $\delta_1 \geq \bar{x}_1^+ - \kappa_{01}/\gamma_1$), from the natural bounds of the uncontrolled system (3.2.1) presented in proposition 3.2.2, it is sufficient to define $\delta_1 = \beta_1$ (resp. $\nu_1 = \eta_1$). In this case, the regions $a_1 = 3$ and $a_2 = 1$ (resp. $a_1 = 1$ and $a_2 = 3$) do not exist, and the proof follows the same steps by skipping those about missing regions. The transition graph summarizing the construction of the proof is exactly the same as the one illustrated in figure 6.5.2 in the previous chapter.

A simulation of this control strategy under uncertain measurements applied to the calibration of the system used in [80] is presented in figure 7.6.2. It can be observed that with an uncertainty range of arbitrary length $2\delta_1 = 2 \times 100$, the switch between aTc $= 6.5\text{ng}\cdot\text{ml}^{-1}$ and aTc $= 42.9\text{ng}\cdot\text{ml}^{-1}$ leads

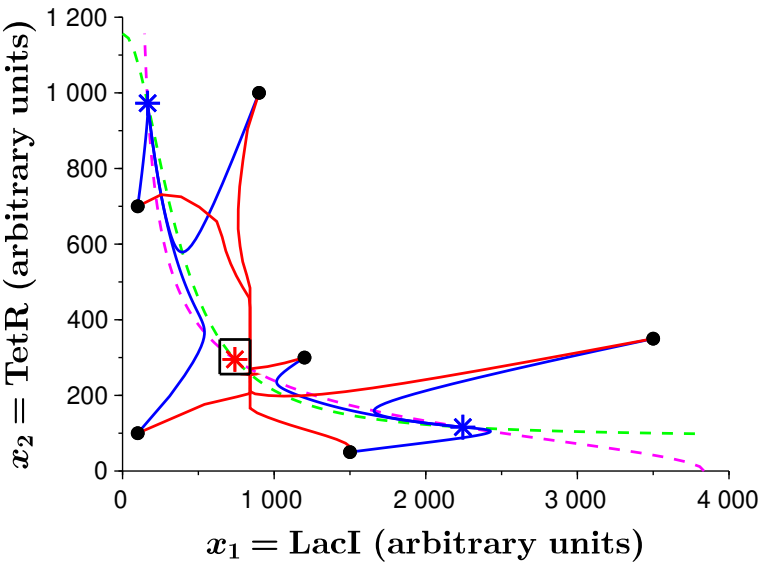

Figure 7.6.2: The parameters are the one in table 6.5.1, the pink (resp. green) dashed line is the x_1 (resp. x_2) nullcline of the uncontrolled system (3.2.1), the blue stars are the stable steady states, the red star the unstable steady state, the blue lines are simulations of the uncontrolled system with six initial conditions depicted with black dots. The red lines are simulations of system (7.6.1) under control (7.6.2) with a switch between $\text{aTc} = 6.5\text{ng} \cdot \text{ml}^{-1}$ and $\text{aTc} = 42.9\text{ng} \cdot \text{ml}^{-1}$, and an uncertain range of $\delta_1 = 100$. The black square is the convergence region.

to a stabilization of the zone $\left\{x_1 \in [\bar{x}_1^+ - 100, \bar{x}_1^+ + 100], x_2 \in [\bar{x}_2^+ - 39, \bar{x}_2^+ + 52.6]\right\}$, as analytically predicted. Simulations need a probability distribution for the control in the region $a_1 = 2$ as it may take any of the two values u_{min} and u_{max}. Again, as no a priori probability is evident about fluctuations in the measurements, the numerical results are presented here with a classic discrete uniform distribution where the probability for u_{min} and u_{max} is the same.

This control strategy is able to guarantee a zone of convergence around $\bar{x}^+$ when measurements are not perfect. This result is satisfactory as a strict convergence towards $\bar{x}^+$ would not have any importance if the measurement device was not able to detect it. Moreover, when the uncertainty range decreases, the convergence zone (22) shrinks around $\bar{x}^+$.

Unfortunately, this control strategy has the disadvantage of switching relatively quickly between u_{min} and u_{max}, meaning that in the biological context, the introduction and the removal of aTc must be fast as well. However, removing an inducer molecule from a biological system is not an easy task. To address this issue, optogenetic techniques might be a good alternative to implement this control strategy in the context of the Toggle Switch presented in [80]. Indeed, *lacI* is repressed by an homodimer of TetR and biologists have tools to create photosensitive homodimers that are able to dissociate after being exposed to light [31]. Moreover, optogenetics is able to mimic this on-off type approach and is known to be fast, non-invasive, and well targeted.

7.7 Conclusion

In this chapter, the control strategy was designed in order to take into account three main biotechnological constraints. Besides the qualitative nature of the measurements and the discrete nature of the inputs introduced in the previous chapter, uncertainties often arise from measurements due

to inherent stochastic properties of biological systems. From these three constraints, an uncertain qualitative control strategy was shown to lead to a global convergence of the dynamical system towards a small zone around the unstable steady state, by determining a sequence of successive repelling regions.

With these types of control strategies however, as soon as the inputs are removed, the system recovers its original behavior. A more viable strategy may be to modify intrinsically the genetic motif by either changing, removing or adding promoters within specific genes. These strategies are almost achievable nowadays thanks to the tools provided by synthetic biology as discussed in chapter 2. This idea motivates the next chapter.

Chapter 8

Design of synthetic modifications

8.1 Introduction

This chapter tries to address the following problem: *is it possible to globally stabilize the unstable state of a biological loop by only modifying intrinsically the genetic circuit ?* It will be shown that the addition of a simple synthetic self-inhibition of one gene in the loop is indeed able to solve the problem. Compared to the strategies presented in the previous chapters, this strategy avoids the use of any input and measurements devices. Only the synthetic redesign of the cells is needed, which may lead to a simplification of the biological set-up.

The synthetic addition of the self-inhibition is presented in section 8.2 and is shown to globally stabilize the unstable steady state $\bar{x}^*$ of the system under tight conditions in section 8.3. For the positive loop, these conditions are relaxed in section 8.4 when biological uncertainties are taken into account. In this case, the undifferentiated state is defined as a small region around $\bar{x}^+$. Thanks to monotone properties of the network, it is shown that the undifferentiated region is globally attractive as soon as all the possible steady states of the synthetic circuit are confined into it.

The content of this chapter about cooperative properties of positive feedback loops has been published for the conference FOSBE (see the section "List of publications" in page 5).

8.2 The controlled model

In the previous chapters, it has been shown that a piecewise constant control law is able to make the unstable steady state $\bar{x}^*$ of the uncontrolled system (3.2.1) globally asymptotically stable. For biological purpose, this control law was only dependent on qualitative measurements of the first gene x_1 and acted on its own expression: when the first gene was weakly expressed ($x_1 < \bar{x}_1^*$), the input enhanced its production, and in the opposite sense when the first gene was highly expressed ($x_1 > \bar{x}_1^*$), the input inhibited its production. Inspired by these results, it seems possible to modify intrinsically the genetic motif by adding a self-inhibition of the first gene x_1 in order to stabilize the unstable steady state. This hypothesis leads to the following new differential system:

$$\begin{cases} \dot{x}_1(x_1, x_N) = \kappa_{01} + \mathrm{u}(x_1)\kappa_1 \mathrm{h}^*(x_N, \theta_N, n_N) - \gamma_1 x_1, \\ \dot{x}_i(x_i, x_{i-1}) = \kappa_{0i} + \kappa_i \mathrm{h}^+(x_{i-1}, \theta_{i-1}, n_{i-1}) - \gamma_i x_i \quad \forall\, i \in \{2, ..., N\}, \end{cases} \tag{8.2.1}$$

where

$$\mathrm{u}(x_1) = \alpha \mathrm{h}^-(x_1, \theta, n) \tag{8.2.2}$$

models the synthetic modification of the loop. Besides the natural influence of the gene x_N on x_1 (an activation for the positive loop and an inhibition for the negative loop), the expression of the

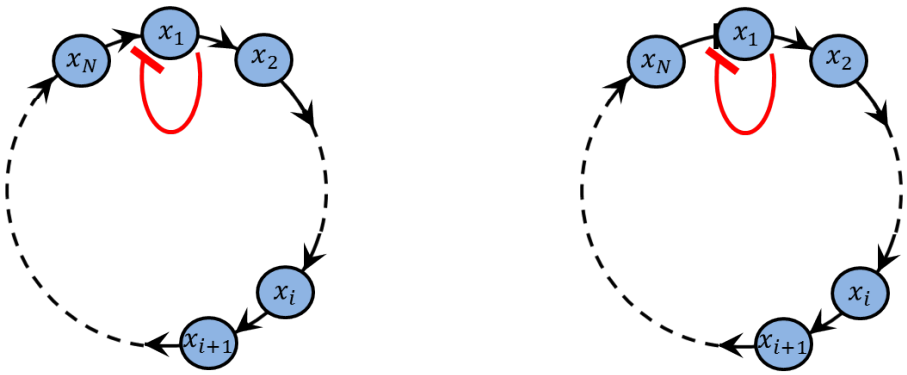

Figure 8.2.1: The black arrows illustrate the classical positive feedback loop on the left and the classical negative loop on the right. The supplementary red repression illustrates the synthetic modified circuit.

first gene is also inhibited by its own production through the decreasing sigmoid function $\mathrm{h}^-(x,\theta,n)$ where $n \geq 2$ and $\theta > 0$. The two sigmoid functions $\mathrm{h}^*(x_N,\theta_N,n_N)$ and $\mathrm{h}^-(x_1,\theta,n)$ are multiplied as it is considered that the transcription of the first gene is restricted as soon as the repressor x_1 is present. Practically, this is often the case in biology when the repressor binds to the DNA and prevents the binding of RNA Polymerase as discussed in chapter 2. The parameter $\alpha > 0$ is playing the same role as κ_1: it allows tuning of the sensitivity of the interaction between x_N and x_1. The graph of this new circuit is presented for both loops in figure 8.2.1.

The nullclines of this modified system are detailed in the next proposition:

Proposition 8.2.1.

$$\begin{cases} \dot{x}_1(x_1,x_N) = 0 \iff x_1 = H_{1n}^*(x_N), \\ \dot{x}_1(x_i,x_{i-1}) = 0 \iff x_i = H_i(x_{i-1}) \quad \forall\ i \in \{2,...,N\}, \end{cases}$$

where $H_i(x)$ are given in definition 3.2.1 $\forall\ i \in \{2,...,N\}$ and are strictly monotonically increasing functions. $H_{1n}^-(x)$ is a strictly monotonically decreasing function, and $H_{1n}^+(x)$ is strictly monotonically increasing.

As explained previously in other chapters, it follows that $\tilde{x} = (\tilde{x}_1,\tilde{x}_2,...,\tilde{x}_N)$ is a steady state of system (8.2.1) $\iff$ $\tilde{x} = (\tilde{x}_1, H_2(\tilde{x}_1), H_3(\tilde{x}_2),..., H_N(\tilde{x}_{N-1}))$ where $\tilde{x}_1$ is a fixed point of $S_{1n}^*(x) = H_{1n}^* \circ H_N \circ H_{N-1} \circ ... \circ H_2(x)$.

Proof. For $i \in \{2,...,N\}$ the result is straightforward as the x_i-nullclines are the same as for the uncontrolled system (3.2.1). For $i = 1$, the x_1-nullcline gives the condition $\mathrm{h}^*(x_N,\theta_N,n_N) = H_n(x_1)$ where:

$$H_n(x_1) = \frac{(\gamma_1 x_1 - \kappa_{01})(\theta^n + x_1^n)}{\kappa_1 \alpha \theta^n}.$$

The conditions on x_1 such that $H_n(x_1) \in [0,1]$ are investigated. First, $H_n(x_1) \geq 0 \Leftrightarrow x_1 \geq \kappa_{01}/\gamma_1$, and $H_n(\kappa_{01}/\gamma_1) = 0$. Furthermore:

$$\frac{\partial H_n}{\partial x_1} = \frac{\gamma_1(\theta^n + x_1^n) + n x_1^{n-1}(\gamma_1 x_1 - \kappa_{01})}{\kappa_1 \alpha \theta^n}.$$

As $\lim\limits_{x_1 \to +\infty} H_n(x_1) = +\infty$, for $x_1 \geq \kappa_{01}/\gamma_1$, $\partial H_n/\partial x_1 > 0$. Then, $H_n(x_1)$ is strictly increasing and positive for $x_1 \geq \kappa_{01}/\gamma_1$. Finally, there exists $x_{1sup} > \kappa_{01}/\gamma_1$ such that $H_n(x_{1sup}) = 1$. The x_1-nullcline is then defined as $x_1 = H_{1n}^*(x_N) = H_n^{-1}(\mathrm{h}^*(x_N,\theta_N,n_N))$ for $x_N \geq 0$. As H_n is a strictly increasing function on $\kappa_{01}/\gamma_1 \leq x_1 \leq x_{1sup}$, then H_{1n}^+ is a strictly increasing function such that $H_{1n}^+(0) = \kappa_{01}/\gamma_1$ and $\lim\limits_{x_N \to +\infty} H_{1n}^+(x_N) = x_{1sup}$ for the positive loop, and a strictly decreasing

function such that $H_{1n}^-(0) = x_{1sup}$ and $\lim_{x_N \to +\infty} H_{1n}^-(x_N) = \kappa_{01}/\gamma_1$ for the negative loop. Finally, $\dot{x}_1(x_1, x_N) = 0 \iff x_1 = H_{1n}^*(x_N)$.

□

Importantly, this modified system is still a priori bounded:

Proposition 8.2.2. *System (8.2.1) under synthetic modification (8.2.2) satisfies:* $x_i \in [\kappa_{0i}/\gamma_i, (\kappa_{0i} + \kappa_i)/\gamma_i[\ \forall \ i \in \{2, ..., N\}$, *and* $x_1 \in [\kappa_{01}/\gamma_1, x_{1sup}[$ *for the positive loop and* $x_1 \in]\kappa_{01}/\gamma_1, x_{1sup}]$ *for the negative loop.*

Proof. For $i \in \{2, ..., N\}$ the result is straightforward as the x_i-nullclines are the same as in system (3.2.1).
From proposition 8.2.1, it is possible to check that the sign of the x_1-vector field is separated by the curve $x_1 = H_{1n}^*(x_N)$. For $x_N \geq 0$ fixed, the x_1-vector field can be calculated at a precise point:

$$\begin{aligned}
\dot{x}_1(H_{1n}^*(x_N), x_N) &= \kappa_{01} + \mathrm{u}(H_{1n}^*(x_N))\kappa_1 \mathrm{h}^*(x_N, \theta_N, n_N) - \gamma_1 H_{1n}^*(x_N) \\
&= \frac{\kappa_1 \alpha \theta^n}{\theta^n + H_{1n}^*(x_N)^n} \left[\mathrm{h}^*(x_N, \theta_N, n_N) - \frac{(\gamma_1 H_{1n}^*(x_N) - \kappa_{01})\,(\theta^n + H_{1n}^*(x_N)^n)}{\kappa_1 \alpha \theta^n} \right] \\
&= \frac{\kappa_1 \alpha \theta^n}{\theta^n + H_{1n}^*(x_N)^n} \left[\mathrm{h}^*(x_N, \theta_N, n_N) - H_n\left(H_n^{-1}(\mathrm{h}^*(x_N, \theta_N, n_N)) \right) \right] \\
&= 0.
\end{aligned}$$

Hence, for x_N fixed and $x_1 > H_{1n}^*(x_N)$ (resp. $<$), as $\mathrm{h}^-(x_1, \theta, n) < \mathrm{h}^-(H_{1n}^*(x_N), \theta, n)$ (resp. $>$) and $-\gamma_1 x_1 < -\gamma_1 H_{1n}^*(x_N)$ (resp. $>$), it follows that $\dot{x}_1(x_1, x_N) < \dot{x}_1(H_{1n}^*(x_N), x_N) = 0$ (resp. $\dot{x}_1(x_1, x_N) > \dot{x}_1(H_{1n}^*(x_N), x_N) = 0$). Finally, $\dot{x}_1(x_1, x_N) > 0$ (resp. < 0) $\iff$ $x_1 < H_{1n}^*(x_N)$ (resp. $>$). In conclusion, the trajectories are bounded between the lower bound and the upper bound of H_{1n}^*, namely $x_1 \in [\kappa_{01}/\gamma_1, x_{1sup}[$ for the positive loop and $x_1 \in]\kappa_{01}/\gamma_1, x_{1sup}]$ for the negative loop. □

As done in chapter 4, the composition of the nullclines define functions with interesting properties:

Definition 8.2.1. $S_{1n}^*(x) = H_{1n}^* \circ H_N \circ H_{N-1} \circ ... \circ H_2(x)$ *and* $F_{1n}^*(x) = S_{1n}^* \circ S_{1n}^*(x)$. *Moreover, for the sake of simplicity, the function* Z_{1n}^* *is defined such that* $Z_{1n}^+ = S_{1n}^+$ *and* $Z_{1n}^- = F_{1n}^-$.

In the next section, the conditions on n, θ, and α are given such that $\bar{x}^*$ becomes globally asymptotically stable.

8.3 Global asymptotic stability

Obviously, in order to stabilize the unstable steady state $\bar{x}^*$ of system (3.2.1), $\bar{x}^*$ must at least be a steady state of system (8.2.1) under synthetic modification (8.2.2). This is verified with the following constraint:

Assumption 8.3.1.

$$\alpha = \frac{1}{h^-(\bar{x}_1^*, \theta, n)}.$$

This assumption leads to the following lemma:

Lemma 8.3.1. *Under assumption 8.3.1 and if* $\theta < \bar{x}_1^*$, *it is possible to find* $\tilde{n}^* \geq 2$ *such that* $\forall \ n \geq \tilde{n}^*$, Z_{1n}^* *has a unique fixed point.*

The proof of this lemma is detailed in appendix D.1.

From this lemma, the methodology that has been presented in chapter 4 can be applied, and leads to the global stabilization of $\bar{x}^*$:

Theorem 8.3.1. *Under assumption 8.3.1 and if $\theta < \bar{x}_1^*$, it is possible to find $\tilde{n}^* \geq 2$ such that $\forall\ n \geq \tilde{n}^*$, $\bar{x}^*$ is globally asymptotically stable.*

Proof. From lemma 8.3.1, if $\theta < \bar{x}_1^*$, it is possible to find $\tilde{n}^* \geq 2$ such that $\forall\ n \geq \tilde{n}^*$, Z_{1n}^* has a unique fixed point. By applying theorem 4.3.1 from chapter 4, it is possible to conclude that $\bar{x}^*$ is globally asymptotically stable. □

This result highlights the importance of the methodology presented in chapter 4. Indeed, for three different types of control, namely a classical control, a saturated control, and a control with a Hill function, the same method can be applied in order to prove the global attractivity of a steady state.

For the positive loop, theorem 8.3.1 can also be proved with the theory of monotone dynamical systems.

Proposition 8.3.1. *System (8.2.1) with synthetic modification (8.2.2) is cooperative and irreducible on $\mathbb{R}_+^N$.*

Proof. For cooperativity, it is easy to check that $\forall\ i \in \{1, ..., N\}$, $\partial \dot{x}_i(x_i, x_{i-1})/\partial x_j \geq 0\ \forall\ j \in \{1, ..., N\}$, $j \neq i$. Moreover, the Jacobian of system (8.2.1) with synthetic modification (8.2.2) is irreducible on $\mathbb{R}_+^N$. □

Cooperative systems are part of monotone dynamical systems and generate order preserving flows, as explained in chapter 3. From this property, many results about asymptotic behavior and stability have been stated [109]. Proposition 8.3.1 can be used in order to rewrite the proof of theorem 8.3.1 for the positive loop:

Proof. First, from proposition 8.3.1, system (8.2.1) with synthetic modification (8.2.2) is cooperative on $\mathbb{R}_+^N$. Second, from proposition 8.2.2, every forward semi-orbit has compact closure in $\mathbb{R}_+^N$. Third, from lemma 8.3.1, if $\theta < \bar{x}_1^+$ and $n \geq \tilde{n}^+$, then S_{1n}^+ has $\bar{x}_1^+$ as a unique fixed point. Moreover, as the fixed points of S_{1n}^+ are in a one-to-one correspondence with the steady states of system (8.2.1) with synthetic modification (8.2.2), then $\bar{x}^+$ is the unique steady state. Finally, all the conditions of theorem C stated in [72] are met: $\bar{x}^+$ is globally asymptotically stable. □

The theorem C stated in [72] is really convenient to prove global convergence and stability for cooperative systems. However, the controlled negative loop is not a cooperative system, and the methodology developed in chapter 4 is really interesting in this case.

Theorem 8.3.1 finally proves that it is possible to determine θ and n such that $\bar{x}^*$ becomes the unique globally asymptotically stable steady state of system (8.2.1) with synthetic modification (8.2.2). This result is illustrated for the negative loop in dimension 3 in figure 8.3.1 and for the positive loop in dimension 2 in figure 8.3.2. For the positive loop, the parameters were calibrated to the real Toggle Switch experiment presented in [80] as done in chapter 6. As predicted, all the trajectories converge towards $\bar{x}^*$. However, from assumption 8.3.1, α must be tightly fixed once θ and n are chosen. In the next section, biological uncertainties are taken into account for the positive loop in order to relax this constraint.

8.4 Global convergence towards an undifferentiated region for the positive loop

As already explained in chapter 7, for biological reasons, it seems irrelevant to consider the undifferentiated state as the precise steady state $\bar{x}^+$ of the uncontrolled system (3.2.1). Indeed, due to inherent stochasticity in cells, biological quantities are not likely to asymptotically converge towards steady states in a mathematical sense. Moreover, only partial knowledge of the system is available due to qualitative measurements in biology. For all these reasons, the undifferentiated state is more likely to be a small region around the unstable steady state $\bar{x}^+$. As a consequence, in this section, the synthetic feedback will be determined in order to obtain global convergence towards a small

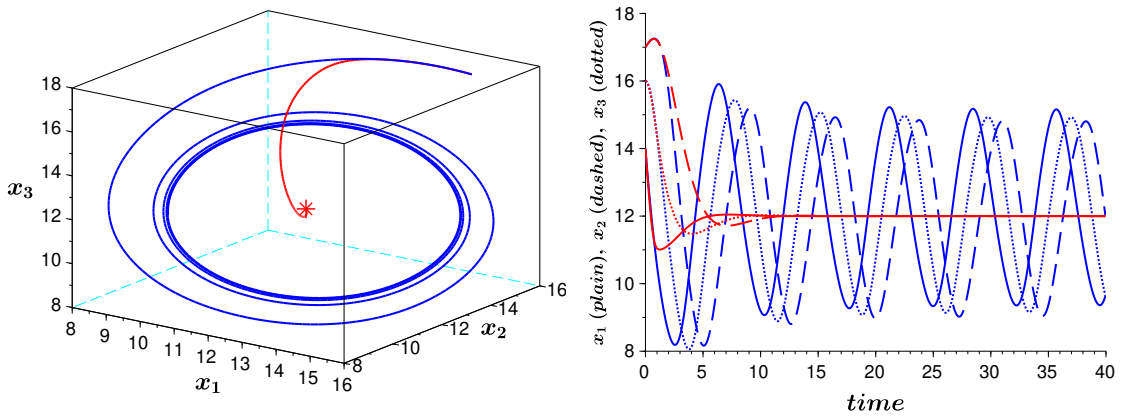

Figure 8.3.1: Simulation for the negative loop in dimension 3. For both figures, $\kappa_{0i} = 2$, $\kappa_i = 8$, $\gamma_i = 0.5$, $\theta_i = 12$, $n_i = 7$ for $i \in \{1, 2, 3\}$, leading to $\bar{x}^- = (12, 12, 12)$, and the initial condition is $x_0 = (14, 16, 17)$. The control parameters are $\theta = 2$, $n = 20$, and $\alpha \approx 3.65 \times 10^{15}$. Left: the blue line is the trajectory of the uncontrolled system (3.2.1). The red line is the trajectory of system (8.2.1) with synthetic modification (8.2.2), and $\bar{x}^-$ is represented by a red star. Right: same simulation with the trajectories plotted against time. The blue (resp. red) lines are the uncontrolled (resp. controlled) trajectories.

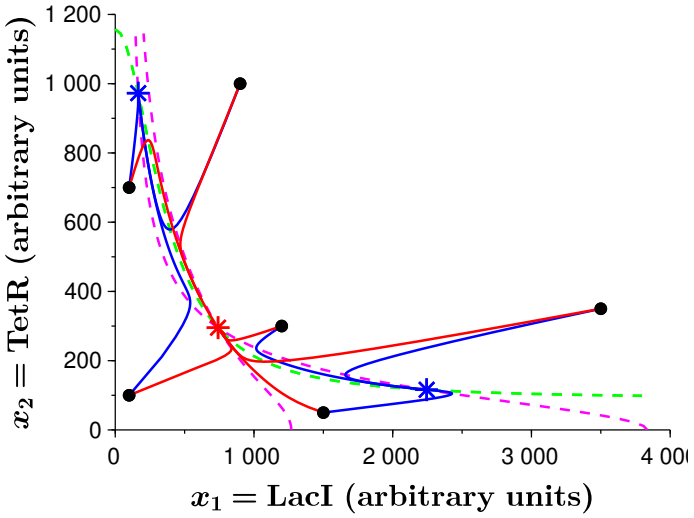

Figure 8.3.2: Simulation for the positive loop in dimension 2 with two inhibitions. The parameters are calibrated so that the three steady states of the uncontrolled system (3.2.1) are the same as in [80] for the Toggle Switch: $\kappa_{01} \approx 1.56$, $\kappa_{02} \approx 1.47$, $\kappa_1 \approx 61.7$, $\kappa_2 \approx 17.6$, $n_1 = n_2 = 2$, $\theta_1 \approx 362.7$, $\theta_2 \approx 134.9$, $\gamma_1 = \gamma_2 = 0.0165$ leading to $\bar{x}^+ = (741, 295.2)$. The green (resp. pink) dashed lines are the x_2 (resp x_1) nullclines. The blue stars are $\bar{x}^+_{inf}$ and $\bar{x}^+_{sup}$ and the red star is $\bar{x}^+$. The six initial conditions are depicted with black dots. The blue lines are the trajectories of the uncontrolled system (3.2.1). The red lines are the trajectories of system (8.2.1) under synthetic modification (8.2.2) with $\theta = 700$, $n = 3$, and $\alpha \approx 2.19$.

undifferentiated region instead of $\bar{x}^+$. This undifferentiated region is supposed to be an hypercube of side length $\delta > 0$ called $\mathcal{B}_\delta = \{x | \, ||x - \bar{x}^+||_\infty < \delta\}$. Obviously, the two stable steady states $\bar{x}^+_{inf}$ and $\bar{x}^+_{sup}$ of the canonical positive loop (3.2.1) must be outside $\mathcal{B}_\delta$. Thus, δ must satisfy the

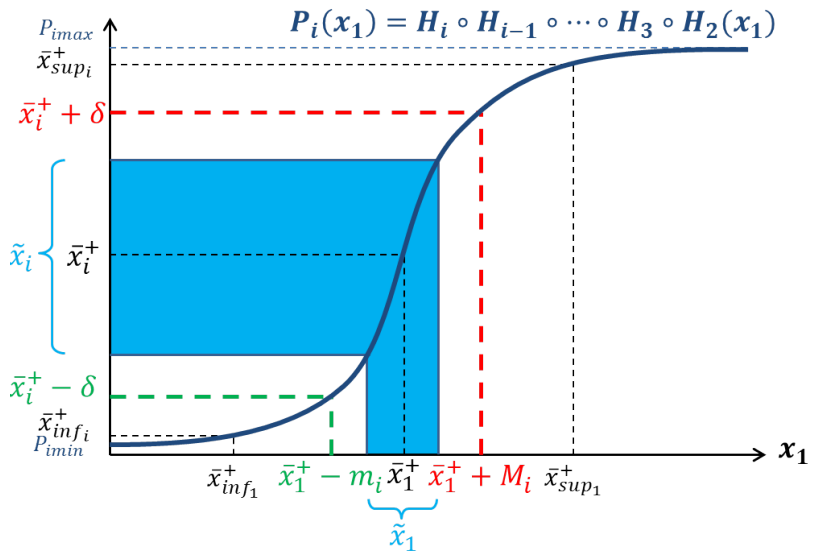

Figure 8.4.1: Illustration of definitions 8.4.1 and 8.4.2, and propositions 8.4.1 and 8.4.2.

following condition:

Assumption 8.4.1. $\delta < \min_{i\in\{1,...,N\}} \left\{ \bar{x}^+_i - \bar{x}^+_{inf_i}, \bar{x}^+_{sup_i} - \bar{x}^+_i \right\}$.

In what follows, the three auto-inhibition parameters θ, n, and α will be determined in order to contain all the possible steady states $\tilde{x}$ of the positive loop (8.2.1) with synthetic modification (8.2.2) inside the undifferentiated region $\mathcal{B}_\delta$ (there are possibly more than three steady states). Under these conditions, it will be shown that the cooperative properties of the positive loop (8.2.1) synthetically modified by (8.2.2) induce global convergence towards $\mathcal{B}_\delta$.

Definition 8.4.1. *$\forall\ i \in \{2, ..., N\}$, P_i is the composition of $(i-1)$ nullcline functions such that $P_i(x) = H_i \circ H_{i-1} \circ ... \circ H_3 \circ H_2(x)$. Their inverse functions are called $P_i^{-1}(x)$.*

These functions are positive and strictly increasing. Their bounds are called $P_i(0) = P_{imin} > 0$ and $\lim_{x\to+\infty} P_i(x) = P_{imax}$. Moreover, if $\tilde{x}$ is a steady state of the positive loop (8.2.1) with synthetic modification (8.2.2), then $\tilde{x}_i = P_i(\tilde{x}_1)$. Similarly, as the x_i-nullclines are the same for the canonical positive loop (3.2.1) and (8.2.1) modified by (8.2.2) $\forall\ i \in \{2, ..., N\}$, then $P_i(\bar{x}^+_{inf_1}) = \bar{x}^+_{inf_i}$, $P_i(\bar{x}^+_{sup_1}) = \bar{x}^+_{sup_i}$ and $P_i(\bar{x}^+_1) = \bar{x}^+_i$ (see figure 8.4.1). These functions allow the construction of bounds of the state space, included in $\mathcal{B}_\delta$:

Definition 8.4.2. *Under assumption 8.4.1, $\forall\ i \in \{2, ..., N\}$, $m_i = \bar{x}^+_1 - P_i^{-1}(\bar{x}^+_i - \delta)$ and $M_i = P_i^{-1}(\bar{x}^+_i + \delta) - \bar{x}^+_1$. From this, we define $m = \min_{i\in\{2,...,N\}} \{m_i\}$, $M = \min_{i\in\{2,...,N\}} \{M_i\}$, and $\epsilon = \min\{m, M, \delta\}$.*

It is possible to check that these parameters satisfy:

Proposition 8.4.1. *Under assumption 8.4.1, $\forall\ i \in \{2, ..., N\}$, $m_i > 0$, $M_i > 0$, $\bar{x}^+_1 - m_i > \bar{x}^+_{inf_1}$, and $\bar{x}^+_1 + M_i < \bar{x}^+_{sup_1}$. Moreover, $\bar{x}^+_1 - \epsilon > \bar{x}^+_{inf_1}$ and $\bar{x}^+_1 + \epsilon < \bar{x}^+_{sup_1}$.*

Proof. Let $i \in \{2, ..., N\}$. As $\delta > 0$, $\bar{x}^+_i - \delta < \bar{x}^+_i$. Moreover, from definition 8.4.2 and assumption 8.4.1, $P_{imin} < \bar{x}^+_{inf_i} < \bar{x}^+_i - \delta < \bar{x}^+_i$. As P_i^{-1} is strictly increasing, then the inequality becomes: $0 < \bar{x}^+_{inf_1} < P_i^{-1}(\bar{x}^+_i - \delta) < \bar{x}^+_1$, where $P_i^{-1}(P_{imin}) = 0$, $P_i^{-1}(\bar{x}^+_{inf_i}) = \bar{x}^+_{inf_1}$, and $P_i^{-1}(\bar{x}^+_i) = \bar{x}^+_1$ from definition 8.4.1. Then, $\bar{x}^+_1 - P_i^{-1}(\bar{x}^+_i - \delta) = m_i > 0$ and $\bar{x}^+_1 - m_i = P_i^{-1}(\bar{x}^+_i - \delta) > \bar{x}^+_{inf_1}$. Finally, as $\bar{x}^+_1 - m_i > \bar{x}^+_{inf_1}\ \forall\ i \in \{2, ..., N\}$, then $\bar{x}^+_1 - \min_{i\in\{2,...,N\}} \{m_i\} > \bar{x}^+_{inf_1}$, that implies that $\bar{x}^+_1 - m > \bar{x}^+_{inf_1}$. This induces that $\bar{x}^+_1 - \min\{m, M, \delta\} > \bar{x}^+_{inf_1}$, or in other words $\bar{x}^+_1 - \epsilon > \bar{x}^+_{inf_1}$.

The same is done for M_i: as $\delta > 0$, $\bar{x}_i^+ + \delta > \bar{x}_i^+$. Moreover, from definition 8.4.2 and assumption 8.4.1, $\bar{x}_i^+ < \bar{x}_i^+ + \delta < \bar{x}_{sup_i}^+ < P_{imax}$. As P_i^{-1} is strictly increasing, then the inequality becomes: $\bar{x}_1^+ < P_i^{-1}(\bar{x}_i + \delta) < \bar{x}_{sup_1}^+$, where $P_i^{-1}(\bar{x}_{sup_i}^+) = \bar{x}_{sup_1}^+$, and $P_i^{-1}(\bar{x}_i^+) = \bar{x}_1^+$ from definition 8.4.1. Then, $P_i^{-1}(\bar{x}_i^+ + \delta) - \bar{x}_1^+ = M_i > 0$ and $\bar{x}_1^+ + M_i = P_i^{-1}(\bar{x}_i^+ + \delta) < \bar{x}_{sup_1}^+$. Finally, as $\bar{x}_1^+ + M_i < \bar{x}_{sup_1}^+$ $\forall\ i \in \{2, ..., N\}$, then $\bar{x}_1^+ + \min_{i\in\{2,...,N\}}\{M_i\} < \bar{x}_{sup_1}^+$, that implies that $\bar{x}_1^+ + M < \bar{x}_{sup_1}^+$. This induces that $\bar{x}_1^+ + \min\{m, M, \delta\} < \bar{x}_{sup_1}^+$, or in other words $\bar{x}_1^+ + \epsilon < \bar{x}_{sup_1}^+$. □

The next proposition gives conditions on the position of the possible steady states $\tilde{x}$ of the positive loop (8.2.1) under synthetic modification (8.2.2).

Proposition 8.4.2. *Under assumption 8.4.1, if a steady state $\tilde{x}$ of the positive loop (8.2.1) with the synthetic modification (8.2.2) is such that $\bar{x}_{inf_1}^+ < \bar{x}_1^+ - \epsilon < \tilde{x}_1 < \bar{x}_1^+ + \epsilon < \bar{x}_{sup_1}^+$, then $\bar{x}_i^+ - \delta < \tilde{x}_i < \bar{x}_i^+ + \delta\ \forall\ i \in \{1, ..., N\}$.*

Proof. For $i = 1$, from definition 8.4.2 and the conditions of proposition 8.4.2, the result is straightforward $\bar{x}_1^+ - \delta < \bar{x}_1^+ - \epsilon < \tilde{x}_1 < \bar{x}_1^+ + \epsilon < \bar{x}_1^+ + \delta$. For $i \in \{2, ..., N\}$, if $\tilde{x}$ is such that $\bar{x}_{inf_1}^+ < \bar{x}_1^+ - \epsilon < \tilde{x}_1 < \bar{x}_1^+ + \epsilon < \bar{x}_{sup_1}^+$, then as P_i is positive and strictly increasing, the inequality becomes: $\bar{x}_{inf_i}^+ < P_i(\bar{x}_1^+ - \epsilon) < \tilde{x}_i < P_i(\bar{x}_1^+ + \epsilon) < \bar{x}_{sup_i}^+$ where $P_i(\bar{x}_{inf_1}^+) = \bar{x}_{inf_i}^+$, $P_i(\tilde{x}_1) = \tilde{x}_i$, and $P_i(\bar{x}_{sup_1}^+) = \bar{x}_{sup_i}^+$. Moreover, from definition 8.4.2, $\bar{x}_1^+ + \epsilon \leq \bar{x}_1^+ + M_i = P_i^{-1}(\bar{x}_i^+ + \delta)$, then $P_i(\bar{x}_1^+ + \epsilon) \leq P_i\left(P_i^{-1}(\bar{x}_i^+ + \delta)\right) = \bar{x}_i^+ + \delta$. In the same way, from definition 8.4.2, $\bar{x}_1^+ - \epsilon \geq \bar{x}_1^+ - m_i = P_i^{-1}(\bar{x}_i^+ - \delta)$, then $P_i(\bar{x}_1^+ - \epsilon) \geq P_i\left(P_i^{-1}(\bar{x}_i^+ - \delta)\right) = \bar{x}_i^+ - \delta$. Hence, the inequality becomes $\bar{x}_{inf_i}^+ < \bar{x}_i^+ - \delta \leq P_i(\bar{x}_1^+ - \epsilon) < \tilde{x}_i < P_i(\bar{x}_1^+ + \epsilon) \leq \bar{x}_i^+ + \delta < \bar{x}_{sup_i}^+\ \forall\ i \in \{2, ..., N\}$. □

These propositions are illustrated in figure 8.4.1 and allow the statement of the following lemma:

Lemma 8.4.1. *Under assumption 8.4.1, if $\bar{x}_1^+ - \epsilon < \theta < \bar{x}_1^+ + \epsilon$, it is possible to find $\tilde{n} \geq 2$ and $\tilde{\alpha} > 1$ such that $\forall\ n \geq \tilde{n}$ and $\forall\ \alpha \geq \tilde{\alpha}$, all the steady states $\tilde{x}$ of the positive loop (8.2.1) synthetically modified by (8.2.2) satisfy $\bar{x}_i^+ - \delta < \tilde{x}_i < \bar{x}_i^+ + \delta\ \forall\ i \in \{1, ..., N\}$.*

Proof. The equation for the steady states $\tilde{x}$ of system (8.2.1) modified by (8.2.2) can reduce to $G(\tilde{x}_1) = H_n(\tilde{x}_1)$ where $G(x) = \mathrm{h}^+(H_N \circ H_{N-1} \circ ... \circ H_3 \circ H_2(x), \theta_N, n_N)$ and $H_n(x)$ is defined in the proof of proposition 8.2.1. As $H_n(\theta) = 2\left(\gamma_1\theta - \kappa_{01}\right)/(\alpha\kappa_1)$, then $H_n(\theta)$ does not depend on n. Moreover, $\partial H_n/\partial n = \left((\gamma_1 x - \kappa_{01})x^n \ln(x/\theta)\right)/(\alpha\kappa_1\theta^n)$. For $x \geq \kappa_{01}/\gamma_1$, where the intersection between H_n and G can occur, $(\gamma_1 x - \kappa_{01})/\kappa_1 \geq 0$. Then, $\partial H_n/\partial n \geq 0 \Leftrightarrow x \geq \theta$. Hence, for $x \geq \kappa_{01}/\gamma_1$ and $x < \theta$, increasing n decreases H_n and for $x > \theta$, increasing n increases H_n.

It is possible to show that for $x > \theta$, $\lim_{n\to+\infty} H_n(x) = +\infty$. However, for $\kappa_{01}/\gamma_1 < x < \theta$, $\lim_{n\to+\infty} H_n(x) = (\gamma_1 x - \kappa_{01})/(\alpha\kappa_1)$. Hence, if $\alpha = 1$, the conditions for the steady states of the uncontrolled system (3.2.1) are recovered: this means that for $\kappa_{01}/\gamma_1 < x < \theta$ and $n \to +\infty$, there is an intersection between H_n and G at the point $\bar{x}_{inf_1}^+$. This must be prevented for a dedifferentiation objective. Hence, $\alpha > 1$ is fixed so that the limit function $(\gamma_1 x - \kappa_{01})/(\alpha\kappa_1)$ becomes smaller than $G(x)$ for $\kappa_{01}/\gamma_1 < x \leq \bar{x}_1^+ - \epsilon$. Besides, if $\bar{x}_1^+ - \epsilon < \theta < \bar{x}_1^+ + \epsilon$, then from proposition 3.2.8 and proposition 8.4.1, $\kappa_{01}/\gamma_1 \leq \bar{x}_{inf_1}^+ < \bar{x}_1^+ - \epsilon < \theta$. Once α is fixed as explained previously, it is possible to find $\tilde{n}$ such that $H_n(x) < G(x)$ for $\kappa_{01}/\gamma_1 < x \leq \bar{x}_1^+ - \epsilon$ and $H_n(x) > G(x)$ for $x \geq \bar{x}_1^+ + \epsilon$ (for an illustration, see figure 8.4.2). It follows that the intersection between H_n and G can only occur for $x \in]\bar{x}_1^+ - \epsilon, \bar{x}_1^+ + \epsilon[$. Hence, if $\bar{x}_1^+ - \epsilon < \theta < \bar{x}_1^+ + \epsilon$, then any steady state $\tilde{x}$ of system (8.2.1) with synthetic modification (8.2.2) verifies $\bar{x}_1^+ - \epsilon < \tilde{x}_1 < \bar{x}_1^+ + \epsilon$. Finally, from proposition 8.4.2, $\bar{x}_i^+ - \delta < \tilde{x}_i < \bar{x}_i^+ + \delta\ \forall\ i \in \{1, ..., N\}$. □

This lemma gives conditions on θ, n, and α such that all the steady states $\tilde{x}$ of the positive loop (8.2.1) modified by (8.2.2) are confined inside the undifferentiated region. From this result, the main theorem about global convergence is introduced:

Theorem 8.4.1. *Under assumption 8.4.1, if $\bar{x}_1^+ - \epsilon < \theta < \bar{x}_1^+ + \epsilon$, it is possible to find $\tilde{n} \geq 2$ and $\tilde{\alpha} > 1$ such that $\forall\ n \geq \tilde{n}$ and $\forall\ \alpha \geq \tilde{\alpha}$ the undifferentiated region $\mathcal{B}_\delta$ is globally attractive.*

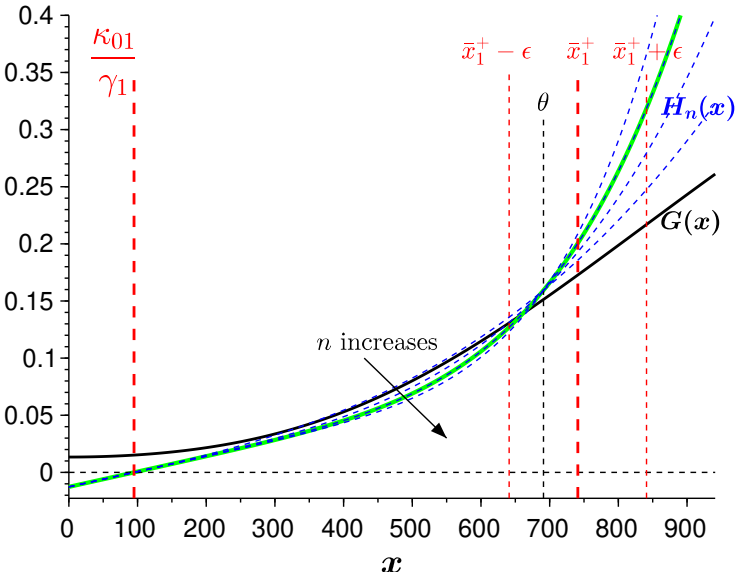

Figure 8.4.2: Illustration of the proof of lemma 8.4.1 with $N = 2$. The parameters are the same as in figure 8.3.2 with $\delta = 100$ leading to $\epsilon = \delta = 100$. The controlled parameters are fixed to: $\theta \approx 691$ and $\alpha = 2 > \tilde{\alpha}$. It is possible to determine $\tilde{n} = 4$. The black line is G. The blue dashed lines are different plots of H_n with different values of $n \in \{2, 3, 4, 5\}$. The plain green line is H_n with $n = \tilde{n}$.

Proof. First, from proposition 3.2.2, $\mathbb{R}_+^N$ is positively invariant. Furthermore, from proposition 8.3.1, the positive loop (8.2.1) modified by (8.2.2) is cooperative and irreducible in $\mathbb{R}_+^N$. It follows from the results in [109] or [34] that the flow is strongly monotone and there exist maximal and minimal steady states called respectively x_M and x_m such that any trajectory $x(t)$ of system (8.2.1) with synthetic modification (8.2.2) will be trapped between these two extreme steady states: $\lim_{t\to+\infty} x_i(t) \in [x_{mi}, x_{Mi}]\ \forall\ i \in \{1, ..., N\}$. On the other hand, from lemma 8.4.1, if $\bar{x}_1^+ - \epsilon < \theta < \bar{x}_1^+ + \epsilon$, it is possible to find $\tilde{n}$ and $\tilde{\alpha}$ such that $\forall\ n \geq \tilde{n}$ and $\forall\ \alpha \geq \tilde{\alpha}$, all the steady states $\tilde{x}$ of system (8.2.1) verify $\bar{x}_i^+ - \delta < \tilde{x}_i < \bar{x}_i^+ + \delta\ \forall\ i \in \{1, ..., N\}$. Hence, the extreme steady states x_M and x_m verify $\bar{x}_i^+ - \delta < x_{mi} < \bar{x}_i^+ + \delta$ and $\bar{x}_i^+ - \delta < x_{Mi} < \bar{x}_i^+ + \delta\ \forall\ i \in \{1, ..., N\}$. Finally, any trajectory $x(t)$ of system (8.2.1) with synthetic modification (8.2.2) will be trapped inside the undifferentiated region: $\lim_{t\to+\infty} x_i(t) \in [\bar{x}_i^+ - \delta, \bar{x}_i^+ + \delta]\ \forall\ i \in \{1, ..., N\}$. □

This theorem is illustrated in figure 8.4.3 for the Toggle Switch experimented in [80]. As analytically proved, it is possible to find conditions on n, θ, and α such that the undifferentiated region $\mathcal{B}_\delta$ becomes globally attractive. With these constraints, it is possible to observe that the new steady state $\tilde{x}$ of system (8.2.1) with synthetic modification (8.2.2) is contained in $\mathcal{B}_\delta$ and all the trajectories converge to it. With different parameters in the canonical loop (3.2.1), it might be possible to have multiple steady states all contained in the region $\mathcal{B}_\delta$. It would mean that the trajectories might not all converge towards the same steady state inside $\mathcal{B}_\delta$. However, they would all converge inside the undifferentiated region, as expected. Compared to the result presented in section 8.3, the constraints on the parameters are relaxed: θ can be chosen anywhere in a range, and n and α must be big enough. These constraints seem more realistic for biological applications. Moreover, as long as the parameters meet the right conditions, the result is valid even if they fluctuate in time. Importantly, this result is also valid if the undifferentiated region is not an hypercube: if the region has any shape around $\bar{x}^+$, it is always possible to define an hypercube included in the undifferentiated region that is globally attractive, with the same techniques as explained before.

This type of study could have been reproduced for the negative loop as well. Indeed, the same results can be achieved by limiting the fixed points of the function $F_{1n}^-(x)$ in a narrow region

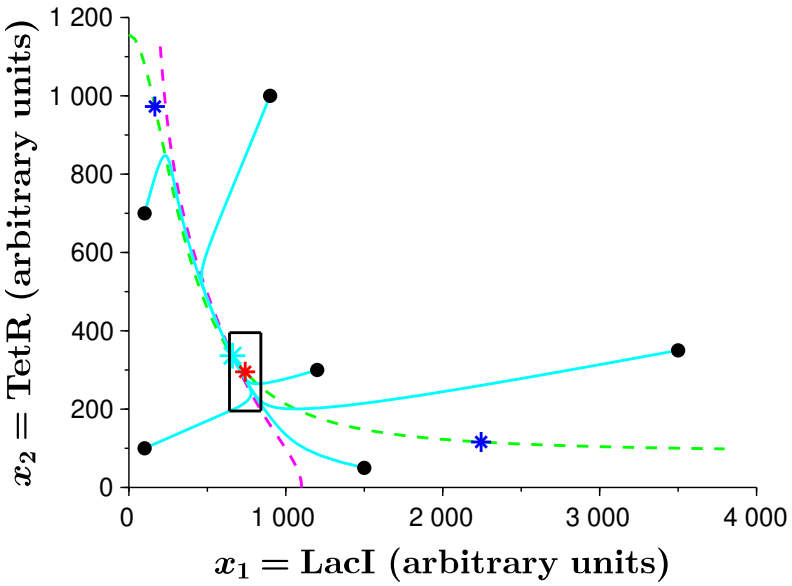

Figure 8.4.3: Simulation of the positive loop (8.2.1) under synthetic modification (8.2.2) with $N = 2$. The parameters are the same as in figure 8.4.2. With $n = 4$, system (8.2.1) modified by (8.2.2) has a unique steady state $\tilde{x} \approx (660.2, 336.4)$ represented by the light blue star. The undifferentiated region $\mathcal{B}_\delta$ is highlighted by the black square and contains $\tilde{x}$. The green (resp. pink) dashed line is the x_2 (resp x_1) nullcline of the modified system. The dark blue stars are $\bar{x}^+_{inf}$ and $\bar{x}^+_{sup}$ and the red star is $\bar{x}^+$. The six initial conditions are depicted with black dots. The light blue lines are the trajectories of system (8.2.1) synthetically modified by (8.2.2).

around $\bar{x}^-_1$, and by assuming that θ is in this narrow region $]\bar{x}^-_1 - \epsilon, \bar{x}^-_1 + \epsilon[$. By doing so, it is possible to construct a finite number of hyperrectangles as constructed in chapter 4, and show that the trajectories globally converge inside a small region around $\bar{x}^-$. However, the influence of n and α on $F^-_{1n}(x)$ can be challenging to determine when assumption 8.3.1 is not fulfilled.

8.5 Conclusion

In this chapter, it was shown that a simple synthetic modification of a biological feedback loop in any dimension N was able to globally stabilize the unstable state $\bar{x}^*$ of the system. First, for both the positive and negative loop, the parameters of the new synthetic self-inhibition were tightly fixed on order to ensure that $\bar{x}^*_1$ was the unique fixed point of the function $Z^*_{1n}(x)$ in order to apply the results presented in chapter 4. Moreover, thanks to the cooperative properties of the positive loop, these global results could be recovered with classical theorems of monotone dynamical systems. In a more relevant biological context, the undifferentiated state of the positive loop was then considered as a full region of the state space. The previous conditions on the self-inhibition parameters were relaxed in order to confine all the possible steady states of the positive loop in the undifferentiated region. Global convergence towards this region was finally proved thanks to cooperative properties.

From a biological point of view, this strategy may be a good alternative to classical biological control techniques as presented in [80]. Indeed, the intrinsic modification of the genetic motif avoids the use of measurements and control devices, that often lead to tedious experiments and generate uncertainties. Moreover, this synthetic modification is probably more adapted to inherent specificity and heterogeneity of each cell, and is hopefully more viable in the long-term thanks to replication machinery and cell division.

On the other hand, this persistence property may be a drawback if the natural behavior of the biological loop (oscillations for the negative loop and bistability for the positive loop) needs to be recovered for any reason. In this case, it may be interesting to study the synthetic modified circuit coupled with a classical biological control means, such as optogenetics for example, which is able to switch on or off the modified self-inhibition. This idea will probably lead to the study of hybrid systems, coupling piecewise constant control laws and synthetic modifications modeled by Hill functions, and seems an interesting extension of this work.

For the negative feedback loop, this type of study can also be applied for the reverse problem: recover sustained oscillations in a disrupted negative feedback loop that shows either homeostatic conditions or perturbed oscillations. The parameters of the synthetic modification may be tuned in order to fix the amplitude and the period of the clock. Chapter 9 focuses on this idea and on its application in the context of circadian rhythm disorders.

Chapter 9

A new problematic: the emergence of oscillations

9.1 Introduction

Many endogenous biological clocks have been brought to light recently such as the cell cycle and the circadian clock. This latter is essential for an organism to anticipate and adapt its behavior and its physiology to environmental perturbations. Importantly, it has been observed that many diseases such as cancers [76] or neurodegenerative disorders [91] can cause a disruption of the circadian clock. Alternatively, the synthetic generation of circadian rhythms in disrupted organisms has been proved to be effective for the slowdown of disease progression [76]. For these reasons, the circadian clock is now considered as a promising tool for therapeutic progress, and especially for cancer treatments. In this context, finding new strategies for the control of biological clocks seems of really high interest.

In this chapter, two different biologically relevant control strategies are designed in order to generate sustained oscillations in a disrupted clock that shows arrhythmic behavior. In section 9.2, the role and the disruptions of the circadian clock are summarized and give a concrete biological motivation for this work, and a reduced model of this biological oscillator is presented in section 9.2.1. A simple synthetic modification of the network is shown to generate sustained oscillations in section 9.3. The local results obtained with the analysis of the corresponding Routh table and the monotone properties of the controlled system allow one to show the emergence of global periodic orbits. In section 9.4, this modified system is proved to converge towards a switching system with discontinuous right-hand side, strengthening the conjecture that periodic orbits may emerge with a simple piecewise constant control strategy. To support this hypothesis, this qualitative control method is illustrated in section 9.5 with the disrupted circadian clock observed in human melanoma cells.

The content of this chapter has been submitted for the conference IFAC world congress 2020 (see the section “List of publications” in page 5).

9.2 A biological motivation: the circadian clock

Circadian rhythms are present in many organisms such as plants, molds, insects and mammals. From the macro-scale (human sleep-wake cycles, body temperature) to the micro-scale (genes, metabolism), these 24-hour self-sustained oscillations are observed everywhere and have been shown to be essential for the anticipation and adaption to environmental changes. In mammals, natural dark-light cycles generate circadian rhythms in a region of the brain called the Suprachiasmatic

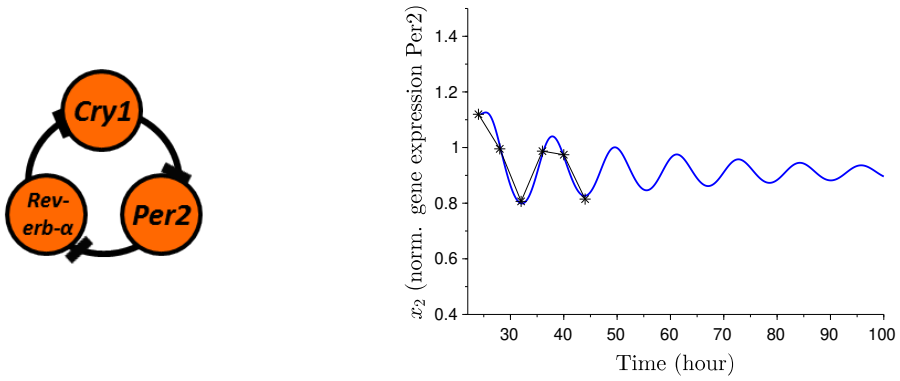

Figure 9.2.1: Left: directed graph of the reduced mammalian circadian clock model presented in [94]. With three inhibitions, this motif is fully equivalent to the canonical network (3.2.1). Right: calibration of model (9.2.1). The black star-plain line is the Per2 non-cycling data measured in melanoma cells provided by [76]. The blue curve is a simulation of the model where the parameters are calibrated with symmetrical hypothesis: $\kappa_{0i} = 0.18$, $\kappa_i = 5$, $\theta_i = 0.38$, $n_i = 4$, and $\gamma_i = 0.36$ $\forall\ i \in \{1, 2, 3\}$. The initial condition at $t_0 = 24.4$ is $x_0 = (0.81, 1.12, 1.015)$.

nucleus, and these oscillations are maintained in the whole organism by a group of genes referred as "clock genes" (see [7] for a review).

It is well known that several diseases, such as sleep disorders ([79]), cancers ([52, 84, 76]) and neurodegenerative diseases ([91]), lead to the disruption of circadian oscillations. Conversely, it has been shown more recently that an altered rhythmicity may have several harmful consequences at the metabolic ([112, 76]) and central nervous system level ([91, 17]). These two observations highlight the promising role of circadian rhythms in therapeutic research, especially for cancer treatments ([52]). In [76] for example, the authors have developed a new strategy based on the circadian clock to inhibit a tumor growth. Their experiments were based on the observation that clock genes (such as *cry1* or *per2*) show arrhythmic expression in human B16 melanoma cells, while they normally exhibit 24-hour oscillations in healthy cells. By enhancing these disrupted genes with different control strategies, such as heat shocks or Dexamethasone introductions, they have been able to restore their rhythmicity, which in turn induced a strong reduction of cancer cell proliferation.

This striking example emphasizes the importance of developing strategies for the control of disrupted biophysical clocks. For this purpose, next section presents a canonical model for biological oscillators.

9.2.1 A reduced circadian clock model

Quite a few models have been developed in order to explain and reproduce the oscillatory behavior of circadian clock genes. However, the huge number of elements and interactions involved in the network make their mathematical analyses difficult [77]. For this reason, an effort has been made to find reduced models composed of a minimal number of genes and interactions that accurately reproduce the 24-hour oscillations observed biologically (see for example [33] for mammals, or [100] for plants). In [94], a simple negative feedback loop composed of the three clock proteins Cry1, Per2 and Rev-erb-α, is shown to be essential for the emergence of periodic orbits in mammals (see the left sketch of figure 9.2.1). With three inhibitions, this network is equivalent to the canonical negative structure presented in section 3.2.2 of chapter 3 and can then be modeled by a generalization of system (3.2.1):

$$\begin{cases} \dot{x}_1 = \kappa_{01} + \kappa_1 \mathrm{h}^-(x_3, \theta_3, n_3) - \gamma_1 x_1, \\ \dot{x}_2 = \kappa_{02} + \kappa_2 \mathrm{h}^-(x_1, \theta_1, n_1) - \gamma_2 x_2, \\ \dot{x}_3 = \kappa_{03} + \kappa_3 \mathrm{h}^-(x_2, \theta_2, n_2) - \gamma_3 x_3, \end{cases} \tag{9.2.1}$$

where $x_1 = $ Cry1, $x_2 = $ Per2 and $x_3 = $ Rev-erb-α.

The parameters of model (9.2.1) are calibrated to the Per2 arrhythmic data points measured in B16 melanoma cells during the experiments conducted in [76]. For the sake of simplicity, the model is considered symmetric: the parameters κ_{0i}, κ_i, θ_i, n_i and γ_i are supposed to be equal for any $i \in \{1, 2, 3\}$. The classical cost function $J(p) = \sum_{i=1}^{m} \left(x_2(t_i, p) - y_i\right)^2$ is minimized using a least squares routine, where m is the number of time points, y_i is the fluorescence measurement of Per2 at time t_i provided by the data, and $x_2(t_i, p)$ is the evaluation of the second variable of system (9.2.1) with the vector of parameters p. The calibration must also assume that n_i are integers. The result is shown in the right sketch of figure 9.2.1: as observed biologically, the oscillations of protein Per2 are damped and converge towards a steady state. This calibration confirms that model (9.2.1) is able to capture the dynamics of a disrupted circadian clock.

In what follows, the analytical results will be illustrated with this calibrated model.

9.3 A synthetic modification of the loop

In the context of a disrupted clock as explained in section 3.5 of chapter 3, $\bar{x}^-$ is considered stable in the rest of this chapter such that the uncontrolled negative loop (3.2.1) generates undesired homeostasis. In sections 9.3 and 9.4, two biologically adapted control laws are designed in order to recover a functional biological clock that shows sustained oscillations. These strategies will be illustrated with the circadian clock in section 9.5.

In order to obtain sustained oscillations, the desired control law must at least destabilize the steady state $\bar{x}^-$. The first selected control leads to the following system:

$$\begin{cases} \dot{x}_1(x_1, x_N) = \kappa_{01} + \mathrm{u}(x_N)\kappa_1 \mathrm{h}^-(x_N, \theta_N, n_N) - \gamma_1 x_1, \\ \dot{x}_i(x_i, x_{i-1}) = \kappa_{0i} + \kappa_i \mathrm{h}^+(x_{i-1}, \theta_{i-1}, n_{i-1}) - \gamma_i x_i \quad \forall\ i \in \{2, ..., N\} \end{cases} \tag{9.3.1}$$

where

$$\mathrm{u}(x_N) = u_{min} + (u_{max} - u_{min})\mathrm{h}^-(x_N, \theta, n), \tag{9.3.2}$$

and

$$\theta = \left(\frac{1 - u_{min}}{u_{max} - 1}\right)^{1/n} \bar{x}_N^-,\ u_{min} < 1,\ u_{max} > 1. \tag{9.3.3}$$

For convenience, system (9.3.1) will also be denoted $\dot{x} = F(\mathrm{u}(x_N), x)$. For purposes of biological application and in order to facilitate the biological setups, the control law is kept as simple as possible: it only acts on the production of the first protein x_1 and only depends on the concentration of x_N. Moreover, $\mathrm{u}(x_N)$ stays positive and bounded as biologically required. Finally, this control can be interpreted as a synthetic modification of the genetic network. Indeed, the genetic regulation resulting from the multiplication of $\mathrm{u}(x_N) = u_{min} + (u_{max} - u_{min})\mathrm{h}^-(x_N, \theta, n)$ with the original decreasing interaction function $\kappa_1 \mathrm{h}^-(x_N, \theta_N, n_N)$ may be produced by multiple and close identical binding sites specific to the transcription factor x_N. These homotypic clusters are often present in cis-regulatory elements [41] and lead to a really rich regulation that may allow the implementation of control (9.3.2).

For the emergence of oscillations, the steady states of this new synthetic system are identified and analyzed.

Proposition 9.3.1. *The steady state $\bar{x}^-$ of the uncontrolled system (3.2.1) is also the unique steady state of system (9.3.1) under control law (9.3.2).*

Proof. From the condition (9.3.3) on θ, it is straightforward to check that $\mathrm{u}(\bar{x}^-) = 1$. Therefore, $\bar{x}^-$ is a steady state of system (9.3.1) under control law (9.3.2). For the uniqueness, it is possible to look at the nullclines of the system:

$$\begin{cases} \dot{x}_1 = 0 \iff x_1 = \left(\kappa_{01} + \kappa_1 \mathrm{u}(x_N)\mathrm{h}^-(x_N, \theta_N, n_N)\right)/\gamma_1 = H_{1u}(x_N), \\ \dot{x}_i = 0 \iff x_i = H_i(x_{i-1}) \quad \forall\, i \in \{2, ..., N\}\,, \end{cases}$$

where $H_i(x)$ have been introduced in definition 3.2.1. It follows that a steady state $\tilde{x} = (\tilde{x}_1, ..., \tilde{x}_N)$ satisfies $\tilde{x}_1 = H_{1u} \circ H_N \circ H_{N-1} \circ ... \circ H_2(\tilde{x}_1) = H(\tilde{x}_1)$. From the properties of Hill functions, H_i are monotonically increasing functions $\forall\, i \in \{2, ..., N\}$.
Moreover, $H'_{1u}(x_N) = (\kappa_1/\gamma_1)\left[\mathrm{u}'(x_N)\mathrm{h}^-(x_N, \theta_N, n_N) + \mathrm{u}(x_N)\mathrm{h}^{-\prime}(x_N, \theta_N, n_N)\right]$. As $\mathrm{u}'(x_N) \leq 0$ and $\mathrm{h}^{-\prime}(x_N, \theta_N, n_N) \leq 0$, H_{1u} is a monotonically decreasing function. It follows that H is a monotonically decreasing function, and the steady state of system (9.3.1) under control law (9.3.2) is unique. □

Remark 9.3.1. *From the properties of the nullclines, it is easy to check that system (9.3.1) under control (9.3.2) is a priori bounded: $x_1 \in]\kappa_{01}/\gamma_1, (\kappa_{01} + u_{max}\kappa_1)/\gamma_1]$ and $x_i \in [\kappa_{0i}/\gamma_i, (\kappa_{0i} + \kappa_i)/\gamma_i[$ $\forall\, i \in \{2, ..., N\}$.*

The local stability of $\bar{x}^-$ is investigated with the Jacobian matrix:

Definition 9.3.1. *As already explained in section 3.2.4 of chapter 3, the Jacobian matrix of the uncontrolled system (3.2.1) evaluated at $\bar{x}^-$ is:*

$$J^-(\bar{x}^-) = \begin{pmatrix} -\gamma_1 & 0 & \cdots & \cdots & \cdots & 0 & J_1^- \\ J_2^- & -\gamma_2 & 0 & \cdots & \cdots & \cdots & 0 \\ 0 & J_3^- & -\gamma_3 & 0 & \cdots & \cdots & 0 \\ \vdots & \ddots & \ddots & \ddots & \ddots & & \vdots \\ \vdots & & \ddots & \ddots & \ddots & \ddots & \vdots \\ \vdots & & & \ddots & \ddots & \ddots & 0 \\ 0 & \cdots & \cdots & \cdots & 0 & J_N^- & -\gamma_N \end{pmatrix}$$

where $J_1^- = \kappa_1 h^{-\prime}(\bar{x}_N^-, \theta_N, n_N) < 0$ and $J_i^- = \kappa_i h^{+\prime}(\bar{x}_{i-1}^-, \theta_{i-1}, n_{i-1}) > 0$ $\forall\, i \in \{2, ..., N\}$.

For system (9.3.1) under control (9.3.2), as $u(\bar{x}^-) = 1$, the Jacobian matrix evaluated at $\bar{x}^-$ is:

$$J_u^-(\bar{x}^-) = \begin{pmatrix} -\gamma_1 & 0 & \cdots & \cdots & \cdots & 0 & J_1^- + J_{1u}^- \\ J_2^- & -\gamma_2 & 0 & \cdots & \cdots & \cdots & 0 \\ 0 & J_3^- & -\gamma_3 & 0 & \cdots & \cdots & 0 \\ \vdots & \ddots & \ddots & \ddots & \ddots & & \vdots \\ \vdots & & \ddots & \ddots & \ddots & \ddots & \vdots \\ \vdots & & & \ddots & \ddots & \ddots & 0 \\ 0 & \cdots & \cdots & \cdots & 0 & J_N^- & -\gamma_N \end{pmatrix}$$

where $J_{1u}^- = \kappa_1 \mathrm{u}'(\bar{x}^-) h^-(\bar{x}_N^-, \theta_N, n_N) < 0$.

Proposition 9.3.2. *The characteristic polynomial associated with $J^-(\bar{x}^-)$ is:*

$$P^-(X) = \prod_{i=1}^{N}(X + \gamma_i) - \prod_{i=1}^{N} J_i^-,$$

while the one associated with $J_u^-(\bar{x}^-)$ *is:*

$$P_u^-(X) = P^-(X) - J_{1u}^- \prod_{i=2}^{N} J_i^-,$$

where $J_{1u}^- \prod_{i=2}^{N} J_i^- < 0$.

Proof. From the proof of proposition 3.2.9 in chapter 3, it is possible to show that:

$$P^-(X) = \prod_{i=1}^{N}(X + \gamma_i) - \prod_{i=1}^{N} J_i^-$$

As $J_u^-(\bar{x}^-)$ has the same structure as $J^-(\bar{x}^-)$, then:

$$\begin{aligned} P_u^-(X) = \det(X\mathrm{I}_N - J_u^-(\bar{x}^-)) &= \prod_{i=1}^{N}(X + \gamma_i) - (J_1^- + J_{1u}^-)\prod_{i=2}^{N} J_i^- \\ &= \prod_{i=1}^{N}(X + \gamma_i) - \prod_{i=1}^{N} J_i^- - J_{1u}^- \prod_{i=2}^{N} J_i^- \\ &= P^-(X) - J_{1u}^- \prod_{i=2}^{N} J_i^-. \end{aligned}$$

□

When the control parameters u_{min}, u_{max}, and n are fixed, the polynomial $P_u^-(X)$ is shifted up with respect to $P^-(X)$. This observation will greatly simplify the determination of the eigenvalues of $P_u^-(X)$: indeed, the addition of the positive term $-J_{1u}^- \prod_{i=2}^{N} J_i^-$ to $P^-(X)$ provokes the propagation of a perturbation in its Routh table, which is investigated in what follows.

From the hypothesis of a disrupted biological clock, the steady state $\bar{x}^-$ of the uncontrolled system (3.2.1) is supposed to be stable as explained previously. As a consequence, $P^-(X)$ has only eigenvalues with negative real part. Moreover, all the coefficients of $P^-(X)$ are positive, leading to the following proposition:

Proposition 9.3.3. *All the terms in the first column of the Routh table of* $P^-(X)$ *are strictly positive.*

This proposition is a classical result of control theory for localization of the roots of a characteristic polynomial. See for example [35] for more details.

From this proposition, a first lemma can be stated:

Lemma 9.3.1. *There exists* $\tilde{A} > 0$ *such that* $\forall\ A > \tilde{A}$*, the first column in the Routh table of the polynomial* $R(X) = P^-(X) + A$ *changes at least once in sign.*

The proof of this lemma can be found in appendix E.1, and this first lemma easily induces a second lemma:

Lemma 9.3.2. *There exists* $\tilde{n} > 0$ *such that* $\forall\ n > \tilde{n}$*, system (9.3.1) under control (9.3.2) has at least two complex conjugate eigenvalues with positive real part.*

Proof. From proposition 9.3.2, $P_u^-(X) = P^-(X) + A$ where $A = -J_{1u}^- \prod_{i=2}^{N} J_i^- > 0$. By developing:

$$
\begin{aligned}
A &= -\kappa_1 \mathrm{u}'(\bar{x}^-)\mathrm{h}^-(\bar{x}_N^-, \theta_N, n_N)\prod_{i=2}^{N} J_i^- \\
&= -(u_{max}-u_{min})\mathrm{h}^{-\prime}(\bar{x}_N^-, \theta, n)\kappa_1 \mathrm{h}^-(\bar{x}_N^-, \theta_N, n_N)\prod_{i=2}^{N} J_i^- \\
&= (u_{max}-u_{min})\frac{n\theta^n(\bar{x}_N^-)^{n-1}}{((\bar{x}_N^-)^n+\theta^n)^2}C
\end{aligned}
$$

where $C = \kappa_1 \mathrm{h}^-(\bar{x}_N^-, \theta_N, n_N)\prod_{i=2}^{N} J_i^- > 0$.
From the properties of $\mathrm{u}(x_N)$, $\theta = \left((1-u_{min})\,/\,(u_{max}-1)\right)^{1/n}\bar{x}_N^-$. Hence:

$$
\begin{aligned}
A &= (u_{max}-u_{min})\frac{n\left(\frac{1-u_{min}}{u_{max}-1}\right)(\bar{x}_N^-)^n(\bar{x}_N^-)^{n-1}}{\left((\bar{x}_N^-)^n+\left(\frac{1-u_{min}}{u_{max}-1}\right)(\bar{x}_N^-)^n\right)^2}C \\
&= (u_{max}-u_{min})\frac{n\left(\frac{1-u_{min}}{u_{max}-1}\right)}{\left(1+\left(\frac{1-u_{min}}{u_{max}-1}\right)\right)^2\bar{x}_N^-}C \\
&= n\frac{(1-u_{min})(u_{max}-1)}{u_{max}-u_{min}}\frac{C}{\bar{x}_N^-}.
\end{aligned}
$$

It follows that for any $\tilde{A} > 0$, there exists $\tilde{n} > 0$ such that $\forall\ n > \tilde{n}$, $A > \tilde{A}$. Hence, from lemma 9.3.1, there exists $\tilde{n} > 0$ such that $\forall\ n > \tilde{n}$ the first column in the Routh table of the polynomial $P_u^-(X)$ changes at least once of sign. Moreover, as $P_u^-(X) = \prod_{i=1}^{N}(X+\gamma_i) - (J_1^- + J_{1u}^-)\prod_{i=2}^{N} J_i^-$ with $(J_1^- + J_{1u}^-)\prod_{i=2}^{N} J_i^- < 0$, it cannot have real positive eigenvalues. Finally from the Routh-Hurwitz criterion, $P_u^-(X)$ has at least two complex conjugate eigenvalues with positive real part as there is at least a change of sign in the first column of its Routh table. □

Importantly, this synthetically modified network is part of monotone dynamical systems as defined in [83], for which strong global dynamical results can be inferred from these two lemmas.

Lemma 9.3.3. *System (9.3.1) under control (9.3.2) is an analytic monotone negative cyclic feedback system as defined in [83].*

Proof. With the notations of [83], system (9.3.1) under control (9.3.2) can be rewritten:

$$
\dot{x}_i = f^i(x_i, x_{i-1}),\ i \in \{1, ..., N\} \tag{9.3.4}
$$

where $x_0 = x_N$. From the expression of the vector field, it is easy to check that:

$$
\delta_i \frac{\partial f^i(x_i, x_{i-1})}{\partial x_{i-1}} \geq 0 \quad i \in \{1, ..., N\},
$$

with $\delta_1 = -1$, $\delta_i = +1$ otherwise, and the product $\Delta = \delta_1\delta_2...\delta_N$ verifies $\Delta = -1$. Moreover, the functions f^i are only composed of polynomials and rational functions that do not vanish on $\mathbb{R}^+$. It follows that system (9.3.1) under control (9.3.2) is an analytic monotone negative cyclic feedback system. □

Finally, these three lemmas allow the statement of the main result of this section:

Theorem 9.3.1. *There exists $\tilde{n} > 0$ such that $\forall\ n > \tilde{n}$, system (9.3.1) under control (9.3.2) has one orbitally asymptotically stable non trivial periodic orbit.*

Proof. The theorem stated below can be found in [83] as "Theorem 4.3" and consists in the core of this proof:
"Let (9.3.4) be an analytic monotone cyclic feedback system with $\Delta = -1$ in ${\mathbb{R}_N}^+$ which possesses a compact attractor $B \subset {\mathbb{R}_N}^+$. Suppose that B contains a single equilibrium x_* and that the Jacobian $Df(x_*)$ satisfies $\Delta \det(-Df(x_*)) < 0$ and has at least two eigenvalues with positive real part. Then (9.3.4) has at least one, but no more than a finite number of nontrivial periodic orbits. Moreover, at least one of these is orbitally asymptotically stable".

This theorem can be applied to system (9.3.1) under control (9.3.2). First, from lemma 9.3.3, this system is an analytic monotone cyclic feedback system with $\Delta = -1$ in ${\mathbb{R}_N}^+$. Moreover, from remark 9.3.1, this modified system possesses a compact attractor:
$B = \{x | x_1 \in]\kappa_{01}/\gamma_1, (\kappa_{01} + u_{max}\kappa_1)/\gamma_1], x_i \in [\kappa_{0i}/\gamma_i, (\kappa_{0i} + \kappa_i)/\gamma_i[\ \forall \ i \in \{2, ..., N\}\} \subset {\mathbb{R}_N}^+$.
From proposition 9.3.1, B contains a single equilibrium $\bar{x}^-$ and $-\det(-J_u^-(\bar{x}^-)) = -P_u^-(0) = -\prod_{i=1}^N \gamma_i + (J_{1u}^- + J_1^-)\prod_{i=2}^N J_i^- < 0$ from proposition 9.3.2. Finally, from lemma 9.3.2, there exists $\tilde{n} > 0$ such that $\forall \ n > \tilde{n}$, system (9.3.1) under control (9.3.2) has at least two complex conjugate eigenvalues with positive real part. Hence, from "Theorem 4.3" introduced in [83], theorem 9.3.1 is proved. □

This theorem is convenient as it mainly needs local results on the eigenvalues to deduce global dynamics. Due to the properties of the characteristic polynomial $P_u^-(X)$, the local existence of periodic orbits could have been inferred easily through the emergence of a Hopf bifurcation, but the monotone properties of the modified system greatly improve this result and justify the global emergence of periodic orbits. However, theorem 9.3.1 does not state whether the limit cycle is unique or not. This may be proved with the results presented in [99] by replacing Hill functions in system (9.3.1) with appropriate saturated functions, and assuming restrictions on the parameters, such as $\gamma_i = \gamma \ \forall \ i \in \{1, ..., N\}$.

From a biological point of view, this result suggests that an appropriate synthetic modification of the first gene promoter may be a good strategy in order to induce oscillations in a disrupted biological clock. However, due to the tight constraints on the control parameters such as θ, this strategy may be difficult to implement in practice. For this purpose, an extension and a generalization of this result, more adapted for a biological application, is presented in next section.

9.4 A PWC control strategy

In order to comply with experimental measurements and inputs constraints, the switching properties of Hill functions are exploited:

Proposition 9.4.1. *For $n \to +\infty$, control law (9.3.2) tends to the following PWC control strategy:*

$$\begin{cases} \mathrm{u}(x_N) = u_{max} \ \forall \ x_N < \bar{x}_N, \\ \mathrm{u}(x_N) = u_{min} \ \forall \ x_N > \bar{x}_N. \end{cases} \tag{9.4.1}$$

Proof. Control law (9.3.2) verifies:

$$\mathrm{u}(x_N) = u_{min} + (u_{max} - u_{min})\frac{\theta^n}{\theta^n + x_N^n}.$$

By replacing the expression of θ, the control becomes:

$$\begin{aligned} \mathrm{u}(x_N) &= u_{min} + (u_{max} - u_{min})\frac{\left(\frac{1-u_{min}}{u_{max}-1}\right)(\bar{x}_N^-)^n}{\left(\frac{1-u_{min}}{u_{max}-1}\right)(\bar{x}_N^-)^n + x_N^n} \\ &= u_{min} + (u_{max} - u_{min})\frac{1}{1 + \left(\frac{u_{max}-1}{1-u_{min}}\right)\left(\frac{x_N}{\bar{x}_N^-}\right)^n}. \end{aligned}$$

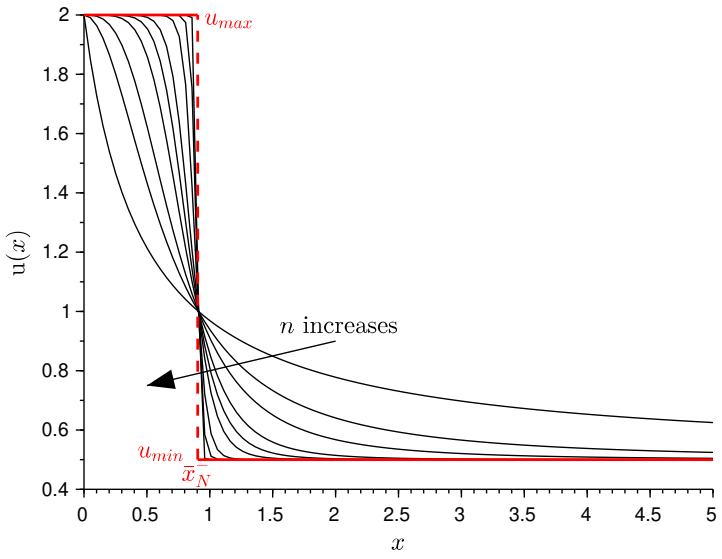

Figure 9.4.1: The black lines represent the smooth control law (9.3.2) with $u_{min} = 0.5$, $u_{max} = 2$, and different values of $n = \{1, 2, 3, 5, 7, 10, 20, 40, 100\}$. This control tends to the PWC control (9.4.1) depicted in red when $n \to +\infty$.

If follows that $\forall\ x_N < \bar{x}_N^-$ $\lim\limits_{n\to+\infty}$ u$(x_N) = u_{max}$, $\forall\ x_N > \bar{x}_N^-$ $\lim\limits_{n\to+\infty}$ u$(x_N) = u_{min}$ and for $x_N = \bar{x}_N^-$, u$(x_N) = 1$. □

This property is illustrated in figure 9.4.1. System (9.3.1) under control law (9.4.1) is part of differential systems with discontinuous right-hand side for which solutions are defined as the solutions of the following differential inclusion [47]:

$$\dot{x} \in H(x)$$

such that $H(x) = F(u_{max}, x)$ when $x_N < \bar{x}_N^-$, $H(x) = F(u_{min}, x)$ when $x_N > \bar{x}_N^-$, and on the switching domain $x_N = \bar{x}_N^-$, $H(x) = \bar{co}\{F(u_{min}, x), F(u_{max}, x)\}$, where $\bar{co}$ is the closed convex hull of the set of vector field. The properties of these types of systems are different from classical smooth dynamical systems as explained in the previous sections and must be analyzed carefully with adapted tools and theory.

Theorem 9.3.1 proves that the trajectories of system (9.3.1) under control (9.3.2) oscillate even when the control parameter n is arbitrarily large. Hence, with $n \to +\infty$, it sounds reasonable to infer that control (9.4.1) induces oscillations as well, leading to the following conjecture:

Conjecture 9.4.1. *With $u_{max} > 1$ and $u_{min} < 1$, the trajectories of system (9.3.1) under control law (9.4.1) converge towards a periodic orbit.*

From a biological point of view, this PWC control strategy seems promising and adapted to different biological constraints as explained in chapters 6 and 7. Indeed, the measurements of x_N are considered to be of qualitative nature: x_N can either be detected as weakly expressed ($x_N \leq \bar{x}_N$) or highly expressed ($x_N \geq \bar{x}_N$). Moreover, the two inputs u_{min} and u_{max} are relevant for the nature of the synthetic control means available in biology that often lead to constant inputs.

9.5 Application to the circadian clock

This PWC strategy is illustrated with the calibrated circadian clock model presented in section 9.2.1. Without control the trajectories globally converge towards $\bar{x}^-$, which is consistent with

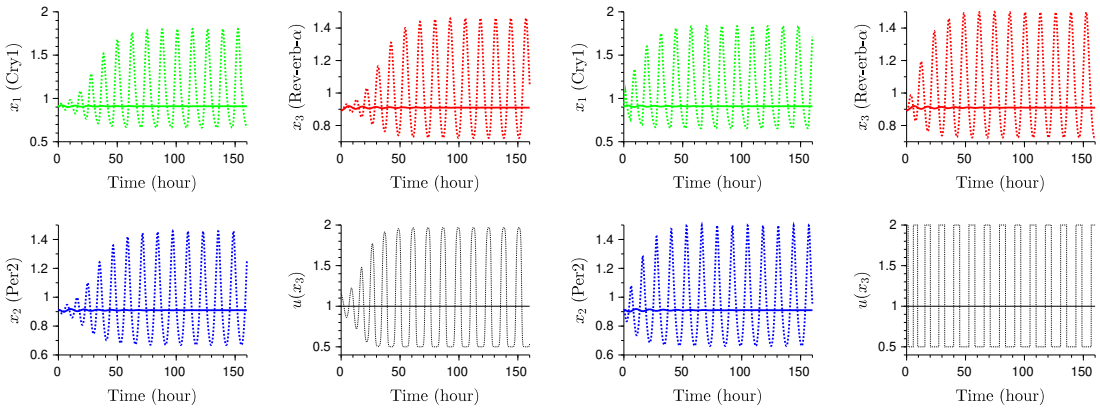

Figure 9.4.2: For all plots, the parameters are the same as in figure 9.2.1 and the initial condition is $x_0 = (0.9, 0.91, 0.89)$. Without control (depicted by plain lines), the three clock genes $x_1 =$ Cry1 (in green), $x_2 =$ Per2 (in blue), and $x_3 =$ Rev-erb-α (in red) of system (9.2.1) show a constant non-cycling expression as expected in the context of a disrupted clock: the system globally converges towards its unique steady state $\bar{x}^- = (0.91, 0.91, 0.91)$. With control, the trajectories are depicted by dashed lines. Four left plots: simulation of system (9.2.1) under control (9.3.2) with $n = 20$, $u_{max} = 2$ and $u_{min} = 0.5$. Four right plots: simulation of system (9.2.1) under control (9.4.1) with $u_{max} = 2$ and $u_{min} = 0.5$. As expected from conjecture 9.4.1, the three clock genes start to oscillate around their steady state, and the control u(x_N) switches between u_{max} and u_{min} as soon as $x_3 =$ Rev-erb-α crosses its steady state value $\bar{x}_3^- = 0.91$.

arrhythmic behaviors observed in B16 melanoma cells. With either the Hill control law (9.3.2) or the simple PWC control strategy (9.4.1), oscillations emerge as proved in theorem 9.3.1 and suspected in conjecture 9.4.1. When n is large enough, the trajectories of system (9.2.1) under control (9.3.2) (four left plots of figure 9.4.2) are numerically very similar to the ones emerging under control (9.4.1) (four right plots of figure 9.4.2), corresponding to the following simple control method: if the gene Rev-erb-α is detected highly expressed (resp. weakly expressed), its inhibition on Cry1 must be decreased (resp. increased).

The influence of u_{min} and u_{max} on the characteristics of the oscillations, namely the amplitude and the period, is an interesting open problem. Intuitively, as the parameter u_{max} increases (resp. u_{min} decreases), the x_1-nullcline is shifted up (resp. down): this may induce an increase in the maximum value (resp. a decrease in the minimum value) of the x_1-oscillations, and an increase of the period. This prediction is illustrated in figure 9.5.1. It is interesting to note that couples of u_{min} and u_{max} can be determined in order to generate 24-hour oscillations, as desired for circadian rhythms.

9.6 Conclusion

In the context of a disrupted biological clock, a simple synthetic modification of a negative feedback loop has been formulated for the emergence of sustained oscillations. From the local instability of the steady state, the existence of global limit cycles has been inferred with monotone properties. In a limit case, this synthetic strategy has been shown to be equivalent to a PWC control strategy, resulting in a differential system with discontinuous right-hand side. It has been conjectured that this qualitative method, nicely adapted to biological constraints, is indeed able to generate sustained oscillations in the N-dimensional disrupted negative feedback loop. This method has been shown to be efficient in melanoma mammalian cells that exhibit arrhythmic clock genes expression.

The control strategies presented in this chapter were designed in order to stabilize specifically the unstable steady state of the differential system, inducing tight constraints on the control parameters.

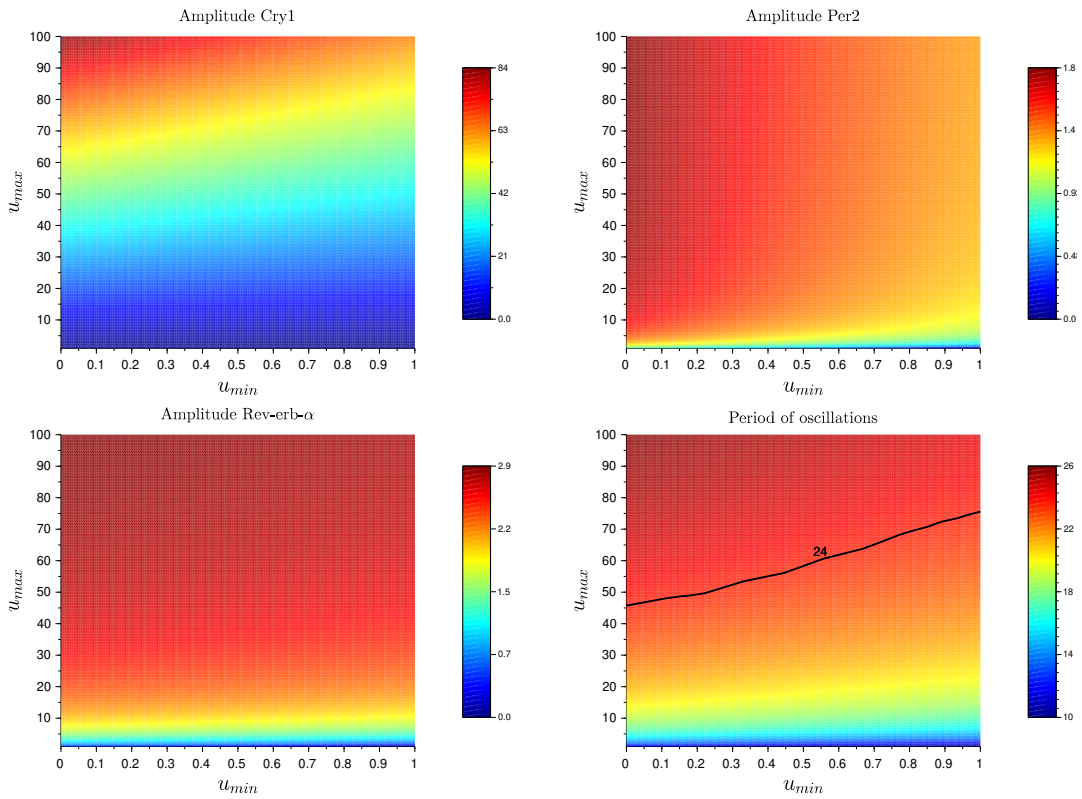

Figure 9.5.1: Influence of the control parameters u_{min} and u_{max} on the amplitude and the period of the oscillations in model (9.2.1) with control (9.4.1). For all plots, the parameters are the same as in figure 9.2.1. On the two upper plots and the first bottom plot, it is possible to observe that an increase of u_{max} (resp. u_{min}) increases (resp. decreases) the amplitude of the three variables. On the bottom right figure, it is possible to observe that an increase of u_{max} (resp. u_{min}) increases (resp. decreases) the period of the oscillations. The influence of u_{min} seems really limited compared to u_{max} probably due to the fact that u_{max} can be chosen in an unbounded range while $u_{min} \in [0, 1[$. Couples of u_{min} and u_{max} can be obtained such that the period of the oscillations reaches 24 hours (the 24 hours level curve is depicted by the dark line).

It is important to note that these constraints may be relaxed by considering the stabilization of other points, which may not be necessarily the steady state.

Another extension of this work may be to rigorously show that theorem 9.3.1, proved for the synthetically modified system, applies to the differential system with discontinuous right-hand side. Moreover, it may be interesting to demonstrate that the periodic orbit is unique, and to find an explicit relation between the control parameters and the properties of the orbit, namely its amplitude and its period. Due to the key roles of biological clocks in therapy, it may be really useful to find a simple control strategy capable of independently tuning these two oscillatory properties.

Finally, this study may also apply to different types of biological clocks, such as the cell cycle for example. Just as the circadian clock, this oscillator has been shown to be highly perturbed in the case of various diseases (for example in many cancers) and conversely, its disruption often induces severe damage: its control may be really promising from a therapeutic perspective.

Chapter 10

Conclusions and perspectives

In this manuscript, different strategies have been designed for the control of two key gene regulatory motifs, namely the negative and the positive feedback loops.

From chapter 4 to chapter 8, the main objective has consisted in globally stabilizing the unstable steady state of both loops. From a biological point of view, this purpose sounds promising regarding disease treatments and conception of new therapies: concerning the negative loop, such a control objective may allow us to better understand and cure diseases induced by a dyshomeostasis, while for the positive loop, these strategies may help in grasping and conceiving cell dedifferentiation processes.

With this underlying biological aspiration in mind, the control strategies have been successively improved in order to take into account more and more biological constraints and comply with biological implementations. To reflect this progression in the manuscript, different strategies from classical industrial to original switched control have been introduced.

First, a classical affine control strategy has been presented in chapter 4. An original and qualitative methodology based on the construction of successive repelling and invariant hyperrectangles has been developed for the proof of global results. In order to prevent extreme positive or negative values possibly attained by the controller, the affine law has been saturated in chapter 5. This saturation is essential from a biological perspective due to the nature of the inputs such as inducer molecules, that may be harmful in high dosage and cannot take negative values by definition. This non-trivial control problem has also been solved with the methodology developed in chapter 4, supporting the idea that this qualitative methodology is general enough to be applied for a large number of biological loop control problems. Finally, the partial and uncertain nature of biological measurements have been additionally considered in chapters 6 and 7 with the simplification of the saturated law by a partially undetermined switch-like control strategy. This qualitative feedback only depends on discrete levels of gene expression, well adapted to measurement tools outputs such as fluorescence microscopy, and only allows constant inputs such as doses of molecules or light intensity. The qualitative dynamics of these resulting hybrid systems have been determined by highlighting successive repelling regions of the state space.

These control strategies have induced different non-trivial highly non-linear dynamical systems in high dimension, with sometimes non-continuous and switched vector field. For this reason, qualitative methodologies based on the construction of successive repelling regions have been developed in chapters 4, 5, 6 and 7 in order to determine the dynamics of the resulting controlled systems. It turns out that this qualitative nature of the analytical techniques precisely opens new perspectives.

First, all the results presented for the canonical form of biological loops (3.2.1) may easily be extended for similar systems for which the interactions differ from Hill functions:

$$\begin{cases} \dot{x}_1(x_1, x_N) = \kappa_{01} + \kappa_1 \mathrm{f}_1(x_N) - \gamma_1 x_1, \\ \dot{x}_i(x_i, x_{i-1}) = \kappa_{0i} + \kappa_i \mathrm{f}_i(x_{i-1}) - \gamma_i x_i \quad \forall\ i \in \{2, ..., N\}\,. \end{cases}$$

These interaction functions f_i may be of any type as long as they are bounded and monotonic. If these two properties are satisfied, the majority of the qualitative methodologies developed in this manuscript for the analysis of the systems dynamics hold. In particular, Michaelis-Menten or Heaviside functions (introduced in chapter 3) may be used.

More generally, the qualitative methods for dynamics analysis may easily be applied in the following more general context:

$$\begin{cases} \dot{x}_1 = f_1(x_1, x_N), \\ \dot{x}_i = f_i(x_i, x_{i-1}) \quad \forall\ i \in \{2, ..., N\}\,, \end{cases} \tag{10.0.1}$$

such that the nullclines of the system satisfy:

$$\begin{cases} x_1 = F_1(x_N), \\ x_i = F_i(x_{i-1}) \quad \forall\ i \in \{2, ..., N\}\,, \end{cases}$$

where the nullcline functions F_i are positive, strictly monotonic, bounded and partition the space in two distinct regions in which the vector field has opposite sign. The function $Z(x)$ is defined as $Z(x) = F(x) = F_1 \circ F_N \circ F_{N-1} \circ ... \circ F_3 \circ F_2(x)$ if the number of strictly monotonically decreasing functions among $F_i(x)$ is even, and $Z(x) = F(x) \circ F(x)$ if the number of strictly monotonically decreasing functions among $F_i(x)$ is odd. Then, if $Z(x)$ has a unique fixed point, system (10.0.1) has a unique globally asymptotically stable steady state. The proof can be constructed in the same way as in chapter 4, with nested balls that are invariant and successively repellent. Obviously, this is a sufficient condition only. If $Z(x)$ does not have a unique fixed point, the global convergence may still happen. However, if system (10.0.1) does not present global convergence, then $Z(x)$ has more than a unique fixed point. Interestingly, this methodology obtains similar results to cooperative dynamical systems, introduced in chapter 3. Indeed, for these monotone systems, it has been proved under appropriate boundedness properties that if the system has a unique steady state, then it is globally asymptotically stable [72]. In chapter 4, the same theorem has been established for the following non-cooperative dynamical system with monotonic nullclines:

$$\begin{cases} \dot{x}_1(x_1, x_N) = \kappa_{01} + (1 - \alpha(x_1 - \bar{x}_1^+))\kappa_1 \mathrm{h}^+(x_N, \theta_N, n_N) - \gamma_1 x_1, \\ \dot{x}_i(x_i, x_{i-1}) = \kappa_{0i} + \kappa_i \mathrm{h}^+(x_{i-1}, \theta_{i-1}, n_{i-1}) - \gamma_i x_i \quad \forall\ i \in \{2, ..., N\}\,. \end{cases}$$

Similarly, the qualitative methodologies may be applied to more general networks that may not be loops. In general, these systems may be of the form:

$$\dot{x}_i = f_i(x_1, x_2, ..., x_N) \quad \forall\ i \in \{1, ..., N\}\,. \tag{10.0.2}$$

If for example the nullcline functions can be written in the form:

$$x_i = F_i(x_1, x_2, ..., x_{i-1}, x_{i+1}, ..., x_N) \quad \forall\ i \in \{1, ..., N\}\,, \tag{10.0.3}$$

where the functions F_i are monotonic with respect to all the variables, then successive repelling regions may be constructed (see figure 10.0.1 for an example in dimension 3 of a generalized positive circuit). As an illustration, the following system in dimension 3 satisfies these properties:

$$\begin{cases} \dot{x}_1 = \kappa_{01} + \kappa_1 \mathrm{h}^+(x_3, \theta_3, n_3) - \gamma_1 x_1, \\ \dot{x}_2 = \kappa_{02} + \kappa_2 \mathrm{h}^+(x_1, \theta_1, n_1) - \gamma_2 x_2, \\ \dot{x}_3 = \kappa_{03} + \kappa_3 \mathrm{h}^+(x_1, \theta_1, n_1)\mathrm{h}^+(x_2, \theta_2, n_2) - \gamma_3 x_3. \end{cases} \tag{10.0.4}$$

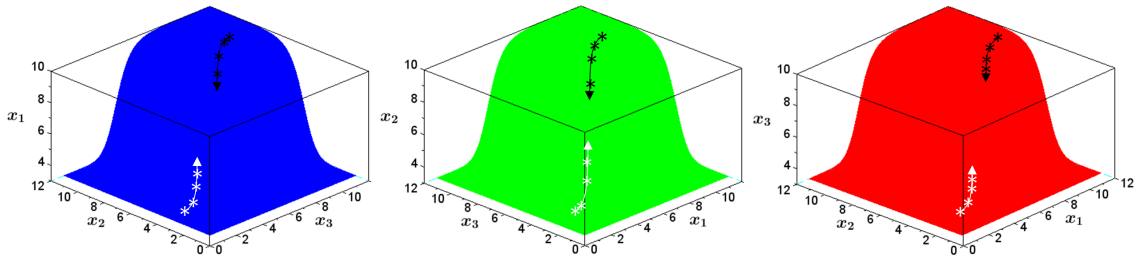

Figure 10.0.1: Nullcline surfaces $F_1(x_2, x_3)$ (left), $F_2(x_1, x_3)$ (middle) and $F_3(x_1, x_2)$ (right) for the generalized system (10.0.2) in dimension 3 for which nullclines satisfy (10.0.3). From the monotonic and boundedness properties of the three surfaces, it is possible to define decreasing sequences (in black) and increasing sequences (in white) for the construction of repulsive regions.

This system does not have a positive ring pattern as the production of the last protein x_3 is activated by both the first and the second genes (see the left sketch in figure 10.0.2). However, this system has monotonically increasing nullclines and hence successive repelling regions may be constructed. As for the canonical positive loop, system (10.0.4) can have several steady states, and a control strategy may be designed for the stabilization of one of its unstable steady state $\bar{x}^+$. In the right sketch of figure 10.0.2, the following controlled system

$$\begin{cases} \dot{x}_1 = \kappa_{01} + \mathrm{u}(x_1)\kappa_1 \mathrm{h}^+(x_3, \theta_3, n_3) - \gamma_1 x_1, \\ \dot{x}_2 = \kappa_{02} + \kappa_2 \mathrm{h}^+(x_1, \theta_1, n_1) - \gamma_2 x_2, \\ \dot{x}_3 = \kappa_{03} + \kappa_3 \mathrm{h}^+(x_1, \theta_1, n_1)\mathrm{h}^+(x_2, \theta_2, n_2) - \gamma_3 x_3, \end{cases} \tag{10.0.5}$$

under affine control law

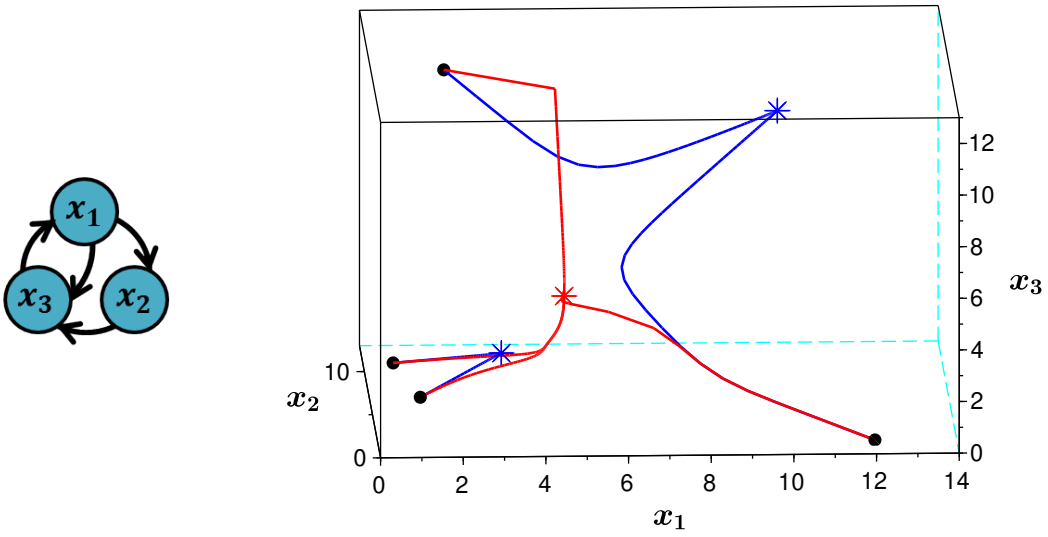

Figure 10.0.2: Left: Interaction network of the generalized motif (10.0.4). Right: Simulation of system (10.0.4) (blue lines) and system (10.0.5) under control (10.0.6) (red lines) with $\kappa_{0i} = 3$, $\kappa_i = 7$, $n_i = 10$, $\theta_i = 5$, $\gamma_i = 1\ \forall\ i \in \{1, 2, 3\}$ and $\alpha = 50$. Without control, system (10.0.4) has three steady states, two stable $\bar{x}^+_{inf} = (3.04, 3.04, 3)$ and $\bar{x}^+_{sup} = (9.99, 9.99, 9.98)$ depicted by blue stars and one unstable $\bar{x}^+ = (4.65, 5.28, 4.44)$ depicted by the red star. With control (10.0.6), the trajectories globally converge towards $\bar{x}^+$.

$$\mathrm{u}(x_1) = 1 - \alpha(x_1 - \bar{x}_1^+), \tag{10.0.6}$$

converges globally towards the unstable steady state if α is large enough. For the proof of global convergence, it may be shown that the unstable steady state $\bar{x}^+$ becomes the unique steady state under appropriate conditions on the control inputs. Hence, it may be possible to construct regions whose bounds are defined by monotonic sequences that converge towards $\bar{x}^+$. However, in this case, the monotonic sequences are defined through the multi-variable function:

$$(x_1, x_2, x_3) \to (F_1(x_3), F_2(x_1), F_3(x_1, x_2)),$$

where F_i are the nullclines. In this case, their convergence properties may be harder to determine.

These generalizations also allow one to include different biological control types. Indeed, this manuscript has only focused on strategies for the control of production rates, but it is easy to imagine that other parameters may be controlled as discussed in chapter 2. For example, some techniques have been developed for the control of protein degradation rates [117]. All these techniques often use a portion of a protein called a degron, that is involved in the regulation of protein degradation rates, and control it whether by heat shocks, inducer molecules or even optogenetics. The results developed in this manuscript may be easily generalized in this new context. As an illustration, the degradation rate of the first protein in a negative loop of dimension 3 may be controlled by a PWC control strategy for the global stabilization of its unique steady state $\bar{x}^-$, leading to the following system:

$$\begin{cases} \dot{x}_1 = \kappa_{01} + \kappa_1 \mathrm{h}^-(x_3, \theta_3, n_3) - \mathrm{u}(x_1)\gamma_1 x_1, \\ \dot{x}_2 = \kappa_{02} + \kappa_2 \mathrm{h}^+(x_1, \theta_1, n_1) - \gamma_2 x_2, \\ \dot{x}_3 = \kappa_{03} + \kappa_3 \mathrm{h}^+(x_2, \theta_2, n_2) - \gamma_3 x_3, \end{cases} \tag{10.0.7}$$

under control

$$\begin{cases} \mathrm{u}(x_1) = u_{max} \text{ when } x_1 \geq \bar{x}_1^-, \\ \mathrm{u}(x_1) = u_{min} \text{ when } x_1 \leq \bar{x}_1^-. \end{cases} \tag{10.0.8}$$

With the qualitative techniques developed, it is easy to demonstrate that if u_{max} is large enough and u_{min} small enough, then the system globally converges towards $\bar{x}_1^-$. This result is illustrated in figure 10.0.3.

Importantly, the qualitative nature of the methodologies developed also allows one to include a form of stochastic variations in the dynamical system. In chapter 7, the uncertainties emerging from measurement techniques in biology have been taken into account by defining zones in the state space in which the control input is uncertain. Similarly, it seems reasonable to consider that the dynamical system modeling the behavior of the biological loop is not perfectly known and may even vary with time, due to inherent stochasticities found in biological systems. To take this into account, one classical method may be to study stochastic differential equations. However, it may also be interesting to consider that some of the parameters that describe the ordinary differential system are partially known and may even vary with time, by defining ranges of uncertainties for each of them. This assumption may lead to the following framework:

$$\begin{cases} \dot{x}_1(x_1, x_N) = \kappa_{01}(t) + \kappa_1(t)\mathrm{h}^*\left(x_N, \theta_N(t), n_N(t)\right) - \gamma_1(t)x_1, \\ \dot{x}_i(x_i, x_{i-1}) = \kappa_{0i}(t) + \kappa_i(t)\mathrm{h}^+\left(x_{i-1}, \theta_{i-1}(t), n_{i-1}(t)\right) - \gamma_i(t)x_i \quad \forall\, i \in \{2, ..., N\}, \end{cases}$$

such that $p_i(t) \in [\bar{p}_i - \epsilon_{p_i}, \bar{p}_i + \epsilon_{p_i}]$ $\forall\ i \in \{1, ..., N\}$ where p_i stands for any parameter in the loop: κ_{0i}, κ_i, θ_i, n_i or γ_i. Basically, each parameter p_i is considered to vary in a range of length $2\epsilon_{p_i}$. These types of uncertain models have been already used for biological systems [61] and may be studied with the theory of interval analysis [70]. This new framework may also validate the methodologies that have been developed and the results that have been stated in this manuscript

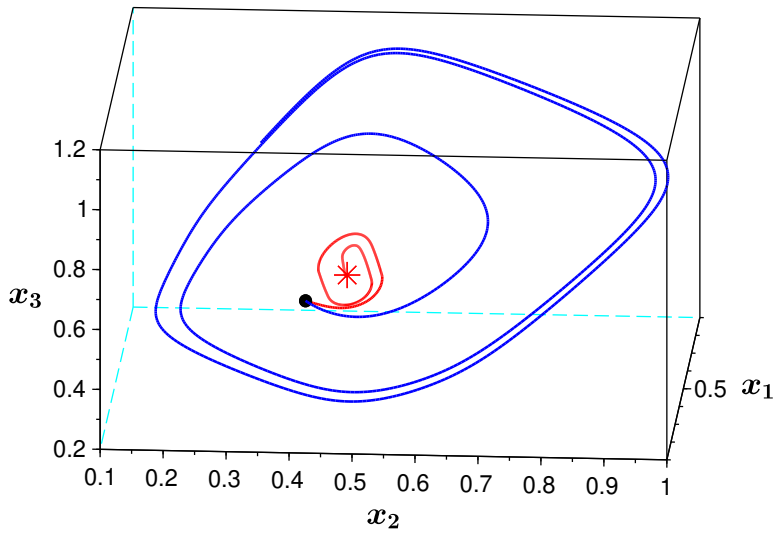

Figure 10.0.3: Simulation of an uncontrolled negative loop (in blue) and system (10.0.7) under control (10.0.8) (in red) with parameters: $\kappa_{0i} = 0.001$, $\kappa_i = 0.95$, $n_i = 10$, $\gamma_i = 0.65$, $\theta_i = 0.49$ $\forall\ i \in \{1, 2, 3\}$, $u_{max} = 2$ and $u_{min} = 0.3$. As expected, the controlled system converges towards the unique steady state $\bar{x}^- = (0.45, 0.46, 0.53)$.

in the more general and realistic case of stochastic systems. To illustrate this claim with a simple example, some results are presented below for a bistable canonical positive feedback loop for which parameters κ_i are considered uncertain:

$$\begin{cases} \dot{x}_1(x_1, x_N) = \kappa_{01} + \kappa_1(t)\mathrm{h}^+\left(x_N, \theta_N, n_N\right) - \gamma_1 x_1, \\ \dot{x}_i(x_i, x_{i-1}) = \kappa_{0i} + \kappa_i(t)\mathrm{h}^+\left(x_{i-1}, \theta_{i-1}, n_{i-1}\right) - \gamma_i x_i \quad \forall\ i \in \{2, ..., N\}\,. \end{cases}$$

In this case, the nullclines are now varying with time:

$$\begin{cases} x_1 = H_1(x_N, t), \\ x_i = H_i(x_{i-1}, t) \quad \forall\ i \in \{2, ..., N\}\,. \end{cases}$$

For the full set of parameters $\{\kappa_1, ..., \kappa_N\}$ in their uncertainty ranges, it is possible to define a family of nullclines contained between an upper and lower envelope. Indeed, the variation of a parameter κ_i in its uncertainty range has the effect of shifting up or down the nullcline. It follows that the functions S_i defined as the compositions of nullclines (see chapter 3) also form a family of curves contained between an upper and lower envelope (see the left plot in figure 10.0.4). It seems reasonable to consider that for any set of parameters, the dynamical behavior of the positive loop stays bistable. From this hypothesis, the uncertainties ϵ_{κ_i} are considered small enough so that the set of functions S_i have three fixed points. The set of these fixed points define two differentiated and one undifferentiated region (see the left plot in figure 10.0.4). Each of these three regions of steady states is centered around its mean steady state: $\bar{x}^+$, $\bar{x}^+_{inf}$ or $\bar{x}^+_{sup}$, defined for the mean parameters set $\{\bar{\kappa}_1, ..., \bar{\kappa}_N\}$. Let us assume that the control objective is to globally stabilize this stochastic system around its mean unstable steady state $\bar{x}^+$. In this case, it is easy to generalize the qualitative methodologies developed in the manuscript. For example, with a PWC control strategy, the system becomes:

$$\begin{cases} \dot{x}_1(x_1, x_N) = \kappa_{01} + \mathrm{u}(x_1)\kappa_1(t)\mathrm{h}^+\left(x_N, \theta_N, n_N\right) - \gamma_1 x_1, \\ \dot{x}_i(x_i, x_{i-1}) = \kappa_{0i} + \kappa_i(t)\mathrm{h}^+\left(x_{i-1}, \theta_{i-1}, n_{i-1}\right) - \gamma_i x_i \quad \forall\ i \in \{2, ..., N\}\,, \end{cases} \tag{10.0.9}$$

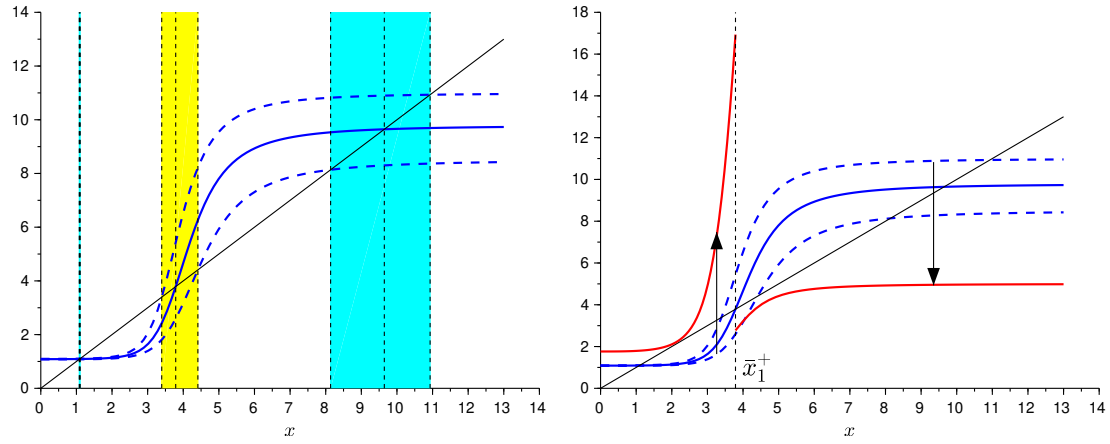

Figure 10.0.4: Left: The plain blue line is the function S_1, composed of nullcline functions with $\kappa_i = \bar{\kappa}_i \ \forall \ i \in \{1, ..., N\}$. Both dashed blue lines represent upper and lower envelope for the whole set of parameters $(\kappa_1(t), ..., \kappa_N(t))$. From these envelopes, the two differentiated regions (depicted by light blue regions) and the undifferentiated region (depicted by the yellow region) can be defined by seeking upper and lower fixed points. Right: $y = x$ is depicted by the black line. With a control parameter u_{max} large enough, the lower envelop becomes greater than $y = x$ in the region $x_1 \leq \bar{x}_1^+$ (red curve), while with u_{min} small enough, the upper envelop becomes smaller than $y = x$ in the region $x_1 \geq \bar{x}_1^+$ (red curve).

with

$$\begin{cases} \mathrm{u}(x_1) = u_{max} \text{ when } x_1 \leq \bar{x}_1^+, \\ \mathrm{u}(x_1) = u_{min} \text{ when } x_1 \geq \bar{x}_1^+. \end{cases} \tag{10.0.10}$$

The input u_{max} must be defined large enough so that the lower envelop of the function S_1 becomes greater than $y = x$ for $x_1 \leq \bar{x}_1^+$, and the input u_{min} must be defined small enough so that the upper envelop of S_1 becomes smaller than $y = x$ for $x_1 \geq \bar{x}_1^+$ (see the right plot of figure 10.0.4). In this case, sequences of repulsive regions can be determined, and it is possible to show that the system globally converges towards $\bar{x}^+$ even "in the worst case scenario" in which some parameters κ_i would stay close to their upper or lower bounds. This convergence result is illustrated in figure 10.0.5 for a positive loop of dimension 3. For the simulation, the parameters $\kappa_i(t)$ have been generated by a uniform distribution, with a change speed 1000 times slower than the controller speed. However, the choice of this probabilistic distribution does not change the convergence results.

Besides external control strategies, this manuscript has also presented a few examples of intrinsic motif modifications in chapter 8 for the global stabilization of both positive and negative loops. These strategies that consist in the internal redesign of biological networks are really promising for synthetic biology. The association of different motifs may allow construction of genetic networks with really specific behaviors. In [15] for example, a positive and a negative feedback loop are coupled and are shown to be able to generate damped oscillations, sustained oscillations and bistability, and these results have been analytically studied in [95]. It has also been stated in [118] that the addition of an auto-activation in a negative feedback loop induces more robust oscillations for which the amplitude is almost decorrelated from the frequency. Finally, in [59], two negative feedback loops have been coupled for the emergence of complex behaviors such as birithmicity and chaos. These examples provide evidence that intrinsically modifying or coupling simple motifs may be a nice solution for their control.

Finally, either internal or external control strategies for biological loops may be also motivated by other convergence objectives than global stabilization of unstable steady states. As a first simple example, control strategies may be designed for the global stabilization of one of the two stable

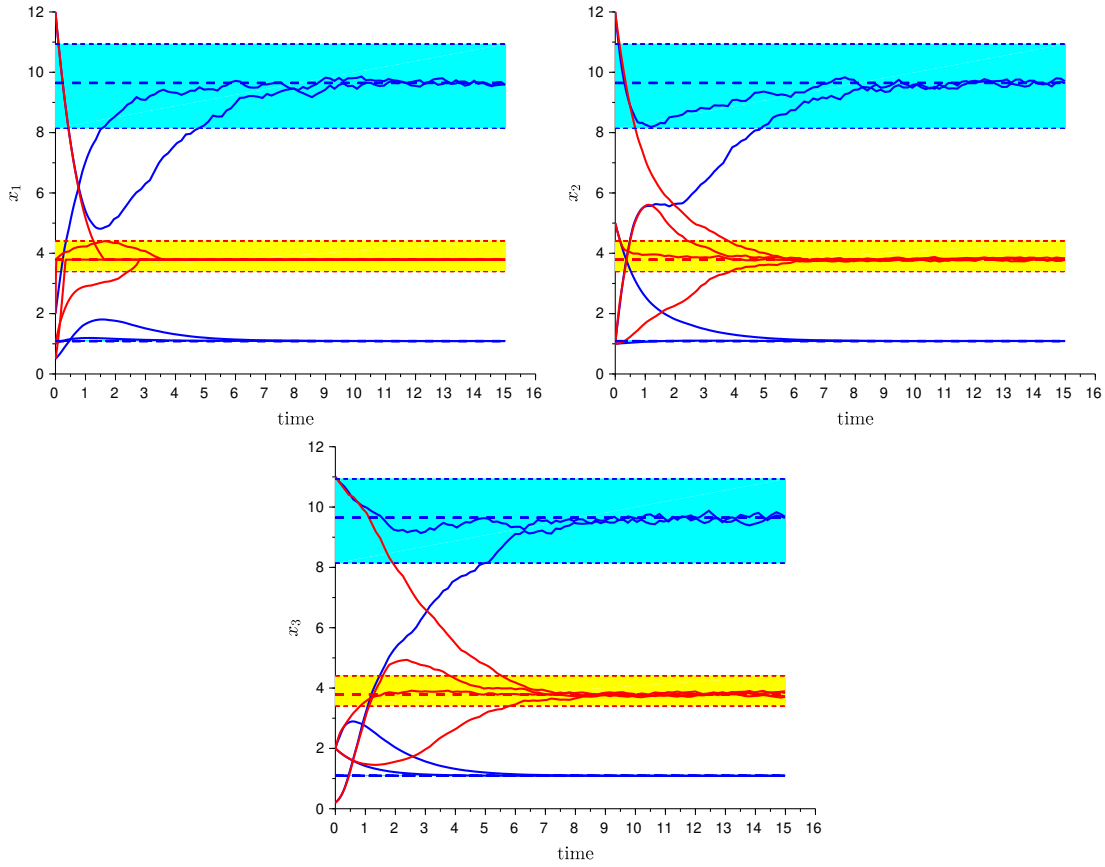

Figure 10.0.5: Simulation of system (10.0.9) under control (10.0.10) with parameters: $\kappa_{0i} = 1$, $\bar{\kappa}_i = 10$, $n_i = 3$, $\theta_i = 5.2$, $\gamma_i = 1$, $\epsilon_{\kappa_i} = 1 \ \forall \ i \in \{1, 2, 3\}$, $u_{max} = 10$ and $u_{min} = 0.4$. The plain blue lines represent the trajectories for the three variables without control (top left plot for x_1, top right plot for x_2 and bottom plot for x_3) and converge towards one of the two differentiated regions highlighted by light blue bands. The dashed blue lines in the middle of the differentiated regions are the steady states $\bar{x}^+_{inf}$ and $\bar{x}^+_{sup}$ of the mean dynamical system with $\kappa_i = \bar{\kappa}_i \ \forall \ i \in \{1, 2, 3\}$. Under control (10.0.10), the trajectories depicted by plain red lines converge towards the mean unstable steady state $\bar{x}^+ = (3.79, 3.79, 3.79)$ represented by the dashed red line in the middle of the undifferentiated yellow region.

steady states of positive feedback loops in order to force a cell to differentiate into one particular type. This may be interesting in the context of tissue regeneration for example, where a great amount of specialized cells is needed. In chapter 9, the interesting problem of creating sustained oscillations in disrupted negative loops has been introduced. Due to their importance, and especially their role in many diseases and disorders, being able to control the main characteristics of biological clocks is of really high interest. The results presented in chapter 9 may be strengthened in order to be able to fine tune both the period and the amplitude of the oscillations.

In summary, the qualitative nature of analytic methodologies developed in this manuscript seems really convenient for many biological networks and various controlled problems. Obviously, for complicated systems, analytical results may be hard to obtain "by hand". However, the detection of the successive invariant or repellent regions may be easily done by a computer. A nice extension of this work would consist in building a general framework with automated rules and computer assistance.

Unfortunately, the theoretical results presented in this manuscript have not been tested with con-

crete biological experiments. This practical step may be essential in order to validate the strategies developed. Moreover, this experimental feedback may give relevant information about limitations and improvements, and may allow the additon of new constraints to the control law that have not been considered previously or that have even not been thought of before. Thankfully, some successful previous experiments strengthen our belief that the mathematical control strategies developed in this manuscript may work in real conditions. The most striking example is probably the control method applied to the Toggle Switch done by [80]. As explained in chapters 6 and 7, the model that has been used in this manuscript is really similar to the model used for the calibration of their control strategy, and the bang-bang controller applied in their experiment works as the PWC strategy developed in chapters 6 and 7. Obviously, controlling genetic systems in general remains a hard task that brings a lot of theoretical problems. In this manuscript, non-linear, qualitative or uncertain constraints have been considered, and inherent stochasticities seem manageable as explained in this conclusion. However, still a lot of improvements in control strategies are needed in order to cope with additional implementation constraints such as growing aspects, communication in cells or even mutations that may arise in genetic systems, to name but a few.

Appendix A

Supplementary material of chapter 3

A.1 Schwarzian derivative

Schwarzian derivative is a shape-indicator that allows to characterize sigmoid functions:

Definition A.1.1. *The Schwarzian derivative of a function $f(x)$, denoted by $\mathrm{S}(f(x))$, is equal to:*

$$\begin{cases} \mathrm{S}(f(x)) = -\infty & \text{if} \quad f'(x) = 0 \\ \mathrm{S}(f(x)) = \dfrac{f^{(3)}(x)}{f'(x)} - \dfrac{3}{2}\left(\dfrac{f''(x)}{f'(x)}\right)^2 & \text{if} \quad f'(x) \neq 0. \end{cases}$$

Important properties of Schwarzian derivatives are presented below:

Property A.1.1. *Let $f(x)$ and $g(x)$ two functions, and $f \circ g(x)$ well defined. Assume that $f'(x) \neq 0$ $\forall\ x \in\ ]0, +\infty[$, then: $\mathrm{S}(f \circ g(x)) = \mathrm{S}(f(g(x)))\, g'(x)^2 + \mathrm{S}(g(x))$. It follows from this result that if $f(x)$ and $g(x)$ have a negative Schwarzian derivative, then the composition $\mathrm{S}(f \circ g(x))$ has a negative Schwarzian derivative as well.*

Property A.1.2. *Let $f(x)$ a function, and two constants $a \in \mathbb{R}$, $b \in \mathbb{R}^*$, then $\mathrm{S}(f(x) + a) = \mathrm{S}(f(x))$ and $\mathrm{S}(bf(x)) = \mathrm{S}(f(x))$.*

The details of these properties can be found in [5]. Basically, a function with a negative Schwarzian derivative is a sigmoid function under a few supplementary appropriate conditions.

A.2 Proof of proposition 3.2.8

Proof. From proposition 3.2.2, the steady state $\tilde{x}$ is also a priori contained in $\mathcal{A}^*$. With a little bit more of work, it is possible to conclude that the steady state $\tilde{x}$ is strictly contained in $\mathcal{A}^*$.

Let us start with the first coordinate $\tilde{x}_1$ for the negative loop: suppose that $\tilde{x}_1 = (\kappa_{01} + \kappa_1)/\gamma_1$, then as $\tilde{x}_1 = (\kappa_{01} + \kappa_1 \mathrm{h}^-(\tilde{x}_N, \theta_N, n_N))/\gamma_1$ and $\kappa_1 > 0$ by hypothesis, we must have $\tilde{x}_N = 0$. Then, by induction it is possible to show that $\kappa_{0i} = 0$ for $i \in \{N, ..., 2\}$ and $\tilde{x}_i = 0$ for $i \in \{N, ..., 1\}$. Finally, as $\tilde{x}_1 = 0$, we must have $\kappa_{01} = 0$ and $\kappa_1 = 0$ as well, which is not possible. Hence $\tilde{x}_1 = (\kappa_{01} + \kappa_1)/\gamma_1$ is not possible.

Concerning the lower bound for $\tilde{x}_i$ when $i \neq 1$, assume that there exists $j \in \{2, ..., N\}$ such that $\tilde{x}_j = \kappa_{0j}/\gamma_j$. As $\tilde{x}_j = (\kappa_{0j} + \kappa_j \mathrm{h}^+(\tilde{x}_{j-1}, \theta_{j-1}, n_{j-1}))/\gamma_j$ and $\kappa_j > 0$ by hypothesis, this induces that $\tilde{x}_{j-1} = 0$. Then, by induction it is possible to show that $\kappa_{0i} = 0$ for $i \in \{j-1, ..., 2\}$ and $\tilde{x}_i = 0$ for $i \in \{j-1, ..., 1\}$. Finally, as $\tilde{x}_1 = 0$ and $\mathrm{h}^-(\tilde{x}_N, \theta_N, n_N) > 0$, we must have $\kappa_{01} = 0$ and $\kappa_1 = 0$, that is not possible. Hence, it does not exist $i \in \{2, ..., N\}$ such that $\tilde{x}_i = \kappa_{0i}/\gamma_i$.

For the positive loop, assume that there exists $j \in \{1, ..., N\}$ such that $\tilde{x}_j = \kappa_{0j}/\gamma_j$. As $\tilde{x}_j = (\kappa_{0j} + \kappa_j \mathrm{h}^+(\tilde{x}_{j-1}, \theta_{j-1}, n_{j-1}))/\gamma_j$ and $\kappa_j > 0$ by hypothesis, this induces that $\tilde{x}_{j-1} = 0$. Then, by induction it is possible to show that $\kappa_{0i} = 0$ for $i \in \{j-1, ..., 2\}$ and $\tilde{x}_i = 0$ for $i \in \{j-1, ..., 1\}$. Finally, as $\tilde{x}_1 = 0$ then $\kappa_{01} = 0$ and $\tilde{x}_N = 0$. With the same steps, by induction it is possible to show that $\kappa_{0i} = 0$ for $i \in \{N, ..., j+1\}$ and $\tilde{x}_i = 0$ for $i \in \{N, ..., j\}$. Hence, as $\tilde{x}_j = 0$ and by hypothesis $\tilde{x}_j = \kappa_{0j}/\gamma_j$, then $\kappa_{0j} = 0$. Finally, in order to have the existence of $j \in \{1, ..., N\}$ such that $\tilde{x}_j = \kappa_{0j}/\gamma_j$, we must have $\kappa_{0i} = 0 \ \forall \ i \in \{1, ..., N\}$. However, from the conditions on the parameters given at the beginning of section 3.2.2, there exists at least one $i \in \{1, ..., N\}$ such that $\kappa_{0i} \neq 0$. Hence, it does not exist $i \in \{1, ..., N\}$ such that $\tilde{x}_i = \kappa_{0i}/\gamma_i$. □

A.3 Proof of proposition 3.2.9

Proof. From the structure of $J^*(\tilde{x})$ it is possible to show that if N is even

$$\begin{aligned} P^*(X) = \det(X\mathrm{I}_N - J^*(\tilde{x})) &= -\prod_{i=1}^{N}(-J_i^*) + \prod_{i=1}^{N}(X + \gamma_i) \\ &= (-1)^{N+1}\prod_{i=1}^{N} J_i^* + \prod_{i=1}^{N}(X + \gamma_i) \\ &= \prod_{i=1}^{N}(X + \gamma_i) - \prod_{i=1}^{N} J_i^* \end{aligned}$$

while if N is odd

$$\begin{aligned} P^*(X) = \det(X\mathrm{I}_N - J^*(\tilde{x})) &= \prod_{i=1}^{N}(-J_i^*) + \prod_{i=1}^{N}(X + \gamma_i) \\ &= (-1)^{N}\prod_{i=1}^{N} J_i^* + \prod_{i=1}^{N}(X + \gamma_i) \\ &= \prod_{i=1}^{N}(X + \gamma_i) - \prod_{i=1}^{N} J_i^*. \end{aligned}$$

□

Appendix B

Supplementary material of chapter 4

B.1 Proof of proposition 4.3.2

Proof. Let us start with $S^*_{j\alpha}(x)$: it is easy to show that $S^*_{j\alpha}(x)$ and $S^*_{(j+1)\alpha}(x)$ have the same number of fixed points for any $j \in \{1, ..., N\}$. To show that, suppose first that $\tilde{x}$ is a fixed point of $S^*_{j\alpha}(x)$, then:

$$\tilde{x} = \left(H_j \circ H_{j-1} \circ ... \circ H^*_{1\alpha} \circ H_N \circ ... \circ H_{j+2} \circ H_{j+1}\right)(\tilde{x}).$$

It is possible to compose on both sides by H_{j+1} and shift the parenthesis, leading to:

$$H_{j+1}(\tilde{x}) = \left(H_{j+1} \circ H_j \circ H_{j-1} \circ ... \circ H^*_{1\alpha} \circ H_N \circ ... \circ H_{j+2}\right)\left(H_{j+1}(\tilde{x})\right)$$

or in other words $S^*_{(j+1)\alpha}\left(H_{j+1}(\tilde{x})\right) = H_{j+1}(\tilde{x})$. Then $H_{j+1}(\tilde{x})$ is a fixed point of $S^*_{(j+1)\alpha}(x)$.

For the equivalence, suppose that $\tilde{x}$ is a fixed point of $S^*_{(j+1)\alpha}(x)$, then:

$$\tilde{x} = \left(H_{j+1} \circ H_j \circ ... \circ H^*_{1\alpha} \circ H_N \circ ... \circ H_{j+3} \circ H_{j+2}\right)(\tilde{x}).$$

It is possible to compose on both sides by $H_j \circ H_{j-1} \circ ... \circ H^*_{1\alpha} \circ H_N \circ ... \circ H_{j+2}$ and shift the parenthesis, leading to:

$$\begin{aligned}\left(H_j \circ H_{j-1} \circ ... \circ H^*_{1\alpha} \circ H_N \circ ... \circ H_{j+2}\right)(\tilde{x}) = &\left(H_j \circ H_{j-1} \circ ... \circ H^*_{1\alpha} \circ H_N \circ ... \circ H_{j+2} \circ H_{j+1}\right) \circ \\ &\left(H_j \circ H_{j-1} \circ ... \circ H^*_{1\alpha} \circ H_N \circ ... \circ H_{j+2}\right)(\tilde{x}),\end{aligned}$$

or in other words:

$$S^*_{j\alpha}\left(H_j \circ H_{j-1} \circ ... \circ H^*_{1\alpha} \circ H_N \circ ... \circ H_{j+2}(\tilde{x})\right) = H_j \circ H_{j-1} \circ ... \circ H^*_{1\alpha} \circ H_N \circ ... \circ H_{j+2}(\tilde{x}).$$

Then $H_j \circ H_{j-1} \circ ... \circ H^*_{1\alpha} \circ H_N \circ ... \circ H_{j+2}(\tilde{x})$ is a fixed point of $S^*_{j\alpha}(x)$.

Finally, $S^*_{j\alpha}(x)$ and $S^*_{(j+1)\alpha}(x)$ have the same number of fixed points for any $j \in \{1, ..., N\}$. Hence, by induction all the functions $S^*_{i\alpha}(x)$ have the same number of fixed points $\forall\ i \in \{1, ..., N\}$. Finally, if there exists $j \in \{1, ..., N\}$ such that $S^*_{j\alpha}(x)$ has a unique fixed point, then $\forall\ i \in \{1, ..., N\}$ $S^*_{i\alpha}(x)$ has a unique fixed point as well. From proposition 4.3.1, this fixed point is $\bar{x}^*_i\ \forall\ i \in \{1, ..., N\}$.

For $F^*_{j\alpha}(x)$, the same thing can be done: it is easy to show that $F^*_{j\alpha}(x)$ and $F^*_{(j+1)\alpha}(x)$ have the same number of fixed points for any $j \in \{1, ..., N\}$. To show that, suppose first that $\tilde{x}$ is a fixed point of $F^*_{j\alpha}(x)$, then:

$$\begin{aligned}\tilde{x} = &\left(H_j \circ H_{j-1} \circ ... \circ H^*_{1\alpha} \circ H_N \circ ... \circ H_{j+2} \circ H_{j+1}\right) \circ \\ &\left(H_j \circ H_{j-1} \circ ... \circ H^*_{1\alpha} \circ H_N \circ ... \circ H_{j+2} \circ H_{j+1}\right)(\tilde{x}).\end{aligned}$$

It is possible to compose on both sides by H_{j+1} and shift the parenthesis, leading to:

$$\begin{aligned} H_{j+1}(\tilde{x}) = &(H_{j+1} \circ H_j \circ H_{j-1} \circ ... \circ H^*_{1\alpha} \circ H_N \circ ... \circ H_{j+2}) \circ \\ &(H_{j+1} \circ H_j \circ H_{j-1} \circ ... \circ H^*_{1\alpha} \circ H_N \circ ... \circ H_{j+2}) \circ (H_{j+1}(\tilde{x})), \end{aligned}$$

or in other words $S^*_{(j+1)\alpha} \circ S^*_{(j+1)\alpha}(H_{j+1}(\tilde{x})) = H_{j+1}(\tilde{x})$. Then $H_{j+1}(\tilde{x})$ is a fixed point of $F^*_{(j+1)\alpha}(x)$.

For the equivalence, suppose that $\tilde{x}$ is a fixed point of $F^*_{(j+1)\alpha}(x)$, then:

$$\begin{aligned} \tilde{x} = &(H_{j+1} \circ H_j \circ ... \circ H^*_{1\alpha} \circ H_N \circ ... \circ H_{j+3} \circ H_{j+2}) \circ \\ &(H_{j+1} \circ H_j \circ ... \circ H^*_{1\alpha} \circ H_N \circ ... \circ H_{j+3} \circ H_{j+2})(\tilde{x}). \end{aligned}$$

It is possible to compose on both sides by $H_j \circ H_{j-1} \circ ... \circ H^*_{1\alpha} \circ H_N \circ ... \circ H_{j+2}$ and shift the parenthesis, leading to:

$$\begin{aligned} (H_j \circ H_{j-1} \circ ... \circ H^*_{1\alpha} \circ H_N \circ ... \circ H_{j+2})(\tilde{x}) = &(H_j \circ H_{j-1} \circ ... \circ H^*_{1\alpha} \circ H_N \circ ... \circ H_{j+2} \circ H_{j+1}) \circ \\ &(H_j \circ H_{j-1} \circ ... \circ H^*_{1\alpha} \circ H_N \circ ... \circ H_{j+2} \circ H_{j+1}) \circ \\ &(H_j \circ H_{j-1} \circ ... \circ H^*_{1\alpha} \circ H_N \circ ... \circ H_{j+2})(\tilde{x}), \end{aligned}$$

or in other words:

$$S^*_{j\alpha} \circ S^*_{j\alpha}(H_j \circ H_{j-1} \circ ... \circ H^*_{1\alpha} \circ H_N \circ ... \circ H_{j+2}(\tilde{x})) = H_j \circ H_{j-1} \circ ... \circ H^*_{1\alpha} \circ H_N \circ ... \circ H_{j+2}(\tilde{x}).$$

Then $H_j \circ H_{j-1} \circ ... \circ H^*_{1\alpha} \circ H_N \circ ... \circ H_{j+2}(\tilde{x})$ is a fixed point of $F^*_{j\alpha}(x)$.

Finally, $F^*_{j\alpha}(x)$ and $F^*_{(j+1)\alpha}(x)$ have the same number of fixed points for any $j \in \{1, ..., N\}$. Hence, by induction all the functions $F^*_{i\alpha}(x)$ have the same number of fixed points $\forall\, i \in \{1, ..., N\}$. Finally, if there exists $j \in \{1, ..., N\}$ such that $F^*_{j\alpha}(x)$ has a unique fixed point, then $\forall\, i \in \{1, ..., N\}$ $F^*_{i\alpha}(x)$ has a unique fixed point as well. From proposition 4.3.1, this fixed point is $\bar{x}^*_i\ \forall\, i \in \{1, ..., N\}$. □

B.2 Proof of proposition 4.3.3

Proof. **The negative loop is first investigated:**

For $i = 1$ and $j \in \mathbb{N}^*$, $x^{-(j+1)}_{1max} = H^-_{1\alpha}(x^{-j}_{Nmin})$ by definition. Hence by induction:

$$x^{-(j+1)}_{1max} = H^-_{1\alpha} \circ H_N \circ ... \circ H_2(x^{-j}_{1min}),$$

and by definition $x^{-j}_{1min} = H^-_{1\alpha}(x^{-j}_{Nmax})$, hence by induction:

$$\begin{aligned} x^{-(j+1)}_{1max} &= H^-_{1\alpha} \circ H_N \circ ... \circ H_2 \circ H^-_{1\alpha}(x^{-j}_{Nmax}) \\ &= H^-_{1\alpha} \circ H_N \circ ... \circ H_2 \circ H^-_{1\alpha} \circ H_N \circ ... \circ H_2(x^{-j}_{1max}). \end{aligned}$$

Hence, $x^{-(j+1)}_{1max} = S^-_{1\alpha} \circ S^-_{1\alpha}(x^{-j}_{1max}) = F^-_{1\alpha}(x^{-j}_{1max})$.

For $i \in \{2, ..., N\}$ and $j \in \mathbb{N}^*$, $x^{-(j+1)}_{imax} = H_i(x^{-(j+1)}_{i-1max})$ then by induction:

$$x^{-(j+1)}_{imax} = H_i \circ H_{i-1} \circ ... \circ H_2(x^{-(j+1)}_{1max}),$$

and by definition $x^{-(j+1)}_{1max} = H^-_{1\alpha}(x^{-j}_{Nmin})$. Hence, by induction:

$$\begin{aligned} x_{imax}^{-(j+1)} &= H_i \circ H_{i-1} \circ ... \circ H_2 \circ H_{1\alpha}^-(x_{Nmin}^{-j}) \\ &= H_i \circ H_{i-1} \circ ... \circ H_2 \circ H_{1\alpha}^- \circ H_N \circ ... \circ H_{i+1}(x_{imin}^{-j}). \end{aligned}$$

With a new induction:

$$\begin{aligned} x_{imax}^{-(j+1)} &= H_i \circ H_{i-1} \circ ... \circ H_2 \circ H_{1\alpha}^- \circ H_N \circ ... \circ H_{i+1}(x_{imin}^{-j}) \\ &= H_i \circ H_{i-1} \circ ... \circ H_2 \circ H_{1\alpha}^- \circ H_N \circ ... \circ H_{i+1} \circ H_i \circ H_{i-1} \circ ... \circ H_2(x_{1min}^{-j}), \end{aligned}$$

and by definition $x_{1min}^{-j} = H_{1\alpha}^-(x_{Nmax}^{-j})$. Then by induction:

$$\begin{aligned} &x_{imax}^{-(j+1)} = H_i \circ H_{i-1} \circ ... \circ H_2 \circ H_{1\alpha}^- \circ H_N \circ ... \circ H_{i+1} \circ H_i \circ H_{i-1} \circ ... \circ H_2 \circ H_{1\alpha}^-(x_{Nmax}^{-j}) \\ &= H_i \circ H_{i-1} \circ ... \circ H_2 \circ H_{1\alpha}^- \circ H_N \circ ... \circ H_{i+1} \circ H_i \circ H_{i-1} \circ ... \circ H_2 \circ H_{1\alpha}^- \circ H_N \circ ... \circ H_{i+1}(x_{imax}^{-j}). \end{aligned}$$

Hence, $x_{imax}^{-(j+1)} = S_{i\alpha}^- \circ S_{i\alpha}^-(x_{imax}^{-j}) = F_{i\alpha}^-(x_{imax}^{-j}) \ \forall \ i \in \{1, ..., N\}$.

The same steps can be followed to prove $x_{imin}^{-(j+1)} = F_{i\alpha}^-(x_{imin}^{-j}) \ \forall \ i \in \{1, ..., N\}$ by switching all the x_{imax} and x_{imin} in the proof.

For the positive loop, the proof is easier:

For $i = 1$ and $j \in \mathbb{N}^*$, $x_{1max}^{+(j+1)} = H_{1\alpha}^+(x_{Nmax}^{+j})$ by definition. Hence by induction:

$$x_{1max}^{+(j+1)} = H_{1\alpha}^+ \circ H_N \circ ... \circ H_2(x_{1max}^{+j}).$$

Hence, $x_{1max}^{+(j+1)} = S_{1\alpha}^+(x_{1max}^{+j})$.

For $i \in \{2, ..., N\}$ and $j \in \mathbb{N}^*$, $x_{imax}^{+(j+1)} = H_i(x_{i-1max}^{+(j+1)})$ then by induction:

$$x_{imax}^{+(j+1)} = H_i \circ H_{i-1} \circ ... \circ H_2(x_{1max}^{+(j+1)}),$$

and by definition $x_{1max}^{+(j+1)} = H_{1\alpha}^+(x_{Nmax}^{+j})$. Hence, by induction:

$$\begin{aligned} x_{imax}^{+(j+1)} &= H_i \circ H_{i-1} \circ ... \circ H_2 \circ H_{1\alpha}^+(x_{Nmax}^{+j}) \\ &= H_i \circ H_{i-1} \circ ... \circ H_2 \circ H_{1\alpha}^+ \circ H_N \circ ... \circ H_{i+1}(x_{imax}^{+j}). \end{aligned}$$

Hence, $x_{imax}^{+(j+1)} = S_{i\alpha}^+(x_{imax}^{+j}) \ \forall \ i \in \{1, ..., N\}$.

The same steps can be followed to prove $x_{imin}^{+(j+1)} = F_{i\alpha}^+(x_{imin}^{+j}) \ \forall \ i \in \{1, ..., N\}$ by switching all the x_{imax} and x_{imin} in the proof. □

B.3 Proof of proposition 4.3.4

Proof. It is firstly proved that $x_{1max}^{*1} = (\kappa_{01} + \kappa_1(1 + \alpha\bar{x}_1^*))/(\gamma_1 + \alpha\kappa_1)$ is strictly greater than $\bar{x}_1^*$. Indeed $x_{1max}^{*1} - \bar{x}_1^* = (\kappa_{01} + \kappa_1(1 + \alpha\bar{x}_1^*)) / (\gamma_1 + \alpha\kappa_1) - \bar{x}_1^* = (\kappa_{01} + \kappa_1 - \gamma_1\bar{x}_1^*) / (\gamma_1 + \alpha\kappa_1)$. From proposition 3.2.8, $\bar{x}_1^* < (\kappa_{01} + \kappa_1)/\gamma_1$, then $x_{1max}^{*1} > \bar{x}_1^*$.

Suppose now that $x_{pmax}^{*1} > \bar{x}_p^*$ with $p \in \{1, ..., N-1\}$.

Then $x_{p+1max}^{*1} = H_{p+1}(x_{pmax}^{*1}) > H_{p+1}(\bar{x}_p^*)$ as $H_{p+1}(x)$ is a strictly monotonically increasing function. Moreover $H_{p+1}(\bar{x}_p^*) = \bar{x}_{p+1}^*$. Hence $x_{p+1max}^{*1} > \bar{x}_{p+1}^*$. Finally by induction, $\forall \ i \in \{1, ..., N\}$, all the initial terms x_{imax}^{*1} are such that $x_{imax}^{*1} > \bar{x}_i^*$.

Secondly, for the negative loop $x^{-1}_{1min} = H^-_{1\alpha}(x^{-1}_{Nmax})$. As just proved $x^{-1}_{Nmax} > \bar{x}^-_N$. Hence, as $H^-_{1\alpha}(x)$ is a strictly monotonically decreasing function, $H^-_{1\alpha}(x^{-1}_{Nmax}) < H^-_{1\alpha}(\bar{x}^-_N) = \bar{x}^-_1$ by definition. Then $x^{-1}_{1min} < \bar{x}^-_1$. For the positive loop, $x^{+1}_{1min} = \kappa_{01}/\gamma_1$. From proposition 3.2.8, $\bar{x}^+_1 > \kappa_{01}/\gamma_1$, then $x^{+1}_{1min} < \bar{x}^+_1$. Hence, $x^{*1}_{1min} < \bar{x}^*_1$.

Suppose now that $x^{*1}_{pmin} < \bar{x}^*_p$ with $p \in \{1, ..., N-1\}$.

Then $x^{*1}_{p+1min} = H_{p+1}(x^{*1}_{pmin}) < H_{p+1}(\bar{x}^*_p)$ as $H_{p+1}(x)$ is a strictly monotonically increasing function. Moreover $H_{p+1}(\bar{x}^*_p) = \bar{x}^*_{p+1}$. Hence $x^{*1}_{p+1min} < \bar{x}^*_{p+1}$. Finally by induction, $\forall\ i \in \{1, ..., N\}$, all the initial terms x^{*1}_{imin} are such that $x^{*1}_{imin} < \bar{x}^*_i$.

Now, for $i \in \{1, ..., N\}$, if $Z^*_{i\alpha}(x)$ has a unique fixed point, this fixed point is $\bar{x}^*_i$ from proposition 4.3.2. Moreover, $Z^*_{i\alpha}(x)$ is a strictly monotonically increasing function, $Z^*_{i\alpha}(0) > 0$ and $x^{*1}_{imax} > \bar{x}^*_i$. Hence, the sequence $x^{*(j+1)}_{imax} = Z^*_{i\alpha}(x^{*j}_{imax})$ with initial term x^{*1}_{imax} is strictly monotonically decreasing and converges towards $\bar{x}^*_i$. As a consequence, $\forall\ i \in \{1, ..., N\}$, $x^{*j}_{imax} > \bar{x}^*_i\ \forall\ j \in \mathbb{N}^*$. Similarly, as $x^{*1}_{imin} < \bar{x}^*_i$, then the sequence $x^{*(j+1)}_{imin} = Z^*_{i\alpha}(x^{*j}_{imin})$ with initial term x^{*1}_{imin} is strictly monotonically increasing and converges towards $\bar{x}^*_i$. As a consequence, $\forall\ i \in \{1, ..., N\}$, $x^{*j}_{imin} < \bar{x}^*_i$ $\forall\ j \in \mathbb{N}^*$. □

B.4 Proof of proposition 4.3.7

Proof. **Firstly, the case j = 0 is investigated.** The x_1-vector field at the border $x_1 = 0$ is equal to: $\dot{x}_1(x_1 = 0, x_N) = \kappa_{01} + \kappa_1 \mathrm{h}^*(x_N, \theta_N, n_N)(1 + \alpha\bar{x}^*_1) \geq 0$. For $i \in \{2, ..., N\}$, the x_i-vector field at the border $x_i = 0$ is equal to $\dot{x}_i(x_i = 0, x_{i-1}) = \kappa_{0i} + \kappa_i \mathrm{h}^*(x_{i-1}, \theta_{i-1}, n_{i-1}) \geq 0$. Hence, $\mathcal{R}^*_0$ is invariant.

Secondly, let j ∈ N*. In order to prove invariance, we must show that $\forall\ i \in \{1, ..., N\}$:

- $\dot{x}_i(x^{*j}_{imax}, x_{i-1}) \leq 0\ \forall\ x_{i-1} \in [x^{*j}_{i-1min}, x^{*j}_{i-1max}]$,
- $\dot{x}_i(x^{*j}_{imin}, x_{i-1}) \geq 0\ \forall\ x_{i-1} \in [x^{*j}_{i-1min}, x^{*j}_{i-1max}]$.

Let us start with i = 1. For the negative loop, the x_1-vector field is evaluated when $x_1 = x^{-j}_{1max}$: $\dot{x}_1(x^{-j}_{1max}, x_N) = \dot{x}_1\left(H^-_{1\alpha}(x^{-(j-1)}_{Nmin}), x_N\right)$ from definition 4.3.2. Then:

$$
\begin{aligned}
\dot{x}_1(x^{-j}_{1max}, x_N) &= \dot{x}_1\left(\frac{\kappa_{01} + \kappa_1 \mathrm{h}^-(x^{-(j-1)}_{Nmin}, \theta_N, n_N)(1 + \alpha\bar{x}^-_1)}{\gamma_1 + \alpha\kappa_1 \mathrm{h}^-(x^{-(j-1)}_{Nmin}, \theta_N, n_N)}, x_N\right) \\
&= \kappa_{01} - \gamma_1 \frac{\kappa_{01} + \kappa_1 \mathrm{h}^-(x^{-(j-1)}_{Nmin}, \theta_N, n_N)(1 + \alpha\bar{x}^-_1)}{\gamma_1 + \alpha\kappa_1 \mathrm{h}^-(x^{-(j-1)}_{Nmin}, \theta_N, n_N)} \\
&+ \left(-\alpha\left(\frac{\kappa_{01} + \kappa_1 \mathrm{h}^-(x^{-(j-1)}_{Nmin}, \theta_N, n_N)(1 + \alpha\bar{x}^-_1)}{\gamma_1 + \alpha\kappa_1 \mathrm{h}^-(x^{-(j-1)}_{Nmin}, \theta_N, n_N)} - \bar{x}^-_1\right) + 1\right)\kappa_1 \mathrm{h}^-(x_N, \theta_N, n_N) \\
&= -\kappa_1 \mathrm{h}^-(x^{-(j-1)}_{Nmin}, \theta_N, n_N)\left[\frac{\gamma_1 + \alpha(\gamma_1\bar{x}^-_1 - \kappa_{01})}{\gamma_1 + \alpha\kappa_1 \mathrm{h}^-(x^{-(j-1)}_{Nmin}, \theta_N, n_N)}\right] \\
&+ \kappa_1 \mathrm{h}^-(x_N, \theta_N, n_N)\left[1 - \alpha\left(\frac{\kappa_{01} + \kappa_1 \mathrm{h}^-(x^{-(j-1)}_{Nmin}, \theta_N, n_N) - \gamma_1\bar{x}^-_1}{\gamma_1 + \alpha\kappa_1 \mathrm{h}^-(x^{-(j-1)}_{Nmin}, \theta_N, n_N)}\right)\right] \\
&= -\kappa_1 \mathrm{h}^-(x^{-(j-1)}_{Nmin}, \theta_N, n_N)\left[\frac{\gamma_1 + \alpha(\gamma_1\bar{x}^-_1 - \kappa_{01})}{\gamma_1 + \alpha\kappa_1 \mathrm{h}^-(x^{-(j-1)}_{Nmin}, \theta_N, n_N)}\right] \\
&+ \kappa_1 \mathrm{h}^-(x_N, \theta_N, n_N)\left[\frac{\gamma_1 + \alpha(\gamma_1\bar{x}^-_1 - \kappa_{01})}{\gamma_1 + \alpha\kappa_1 \mathrm{h}^-(x^{-(j-1)}_{Nmin}, \theta_N, n_N)}\right]
\end{aligned}
$$

$$= \kappa_1 \left[\frac{\gamma_1 + \alpha(\gamma_1 \bar{x}_1^- - \kappa_{01})}{\gamma_1 + \alpha\kappa_1 \mathrm{h}^-(x_{Nmin}^{-(j-1)}, \theta_N, n_N)} \right] \left(\mathrm{h}^-(x_N, \theta_N, n_N) - \mathrm{h}^-(x_{Nmin}^{-(j-1)}, \theta_N, n_N) \right).$$

Here, $x_{Nmin}^{-(j-1)} = 0$ for $j = 1$ by convention, from the expression of x_{1max}^{-1} in definition 4.3.2. Then, $\dot{x}_1(x_{1max}^{-j}, x_{Nmin}^{-(j-1)}) = 0$. Moreover, as $\gamma_1 \bar{x}_1^- - \kappa_{01} > 0$ from proposition 3.2.8 and as $\mathrm{h}^-(x_N, \theta_N, n_N)$ is a strictly monotonically decreasing function, $\dot{x}_1(x_{1max}^{-j}, x_N) \leq 0 \ \forall \ x_N \geq x_{Nmin}^{-(j-1)}$. From proposition 4.3.4, $x_{Nmin}^{-(j-1)} < x_{Nmin}^{-j} < x_{Nmax}^{-j}$. Then, $\dot{x}_1(x_{1max}^{-j}, x_N) < 0 \ \forall \ x_N \in [x_{Nmin}^{-j}, x_{Nmax}^{-j}]$.

Now the x_1-vector field is evaluated at a precise point of the lower bound of $\mathcal{R}_j^-$:
$\dot{x}_1(x_{1min}^{-j}, x_{Nmax}^{-j}) = \dot{x}_1(H_{1\alpha}^-(x_{Nmax}^{-j}), x_{Nmax}^{-j})$ from definition 4.3.2. Then $\dot{x}_1(x_{1min}^{-j}, x_{Nmax}^{-j}) = 0$ because from section 4.2, $\dot{x}_1(x_1, x_N) = 0 \iff x_1 = H_{1\alpha}^-(x_N)$.
Let $x_N \leq x_{Nmax}^{-j}$. From the proof of proposition 4.3.4, $x_{1min}^{-j} < \bar{x}_1^-$. Then, the control term $-\alpha(x_{1min}^{-j} - \bar{x}_1^-) + 1 > 0$. Hence, $\kappa_{01} + (-\alpha(x_{1min}^{-j} - \bar{x}_1^-) + 1)\kappa_1 \mathrm{h}^-(x_N, \theta_N, n_N) - \gamma_1 x_{1min}^{-j} \geq \kappa_{01} + (-\alpha(x_{1min}^{-j} - \bar{x}_1^-) + 1)\kappa_1 \mathrm{h}^-(x_{Nmax}^{-j}, \theta_N, n_N) - \gamma_1 x_{1min}^{-j} = 0$.
Then, $\dot{x}_1(x_{1min}^{-j}, x_N) \geq \dot{x}_1(x_{1min}^{-j}, x_{Nmax}^{-j}) = 0 \ \forall \ x_N \leq x_{Nmax}^{-j}$. From proposition 4.3.4, $x_{Nmin}^{-j} < x_{Nmax}^{-j}$. Then, $\dot{x}_1(x_{1min}^{-j}, x_N) \geq 0 \ \forall \ x_N \in [x_{Nmin}^{-j}, x_{Nmax}^{-j}]$.

The same thing can be done easily for the positive loop.
The x_1-vector field is evaluated when $x_1 = x_{1max}^{+j}$: $\dot{x}_1(x_{1max}^{+j}, x_N) = \dot{x}_1\left(H_{1\alpha}^+(x_{Nmax}^{+(j-1)}), x_N\right)$ from definition 4.3.2. Then:

$$\begin{aligned}
\dot{x}_1(x_{1max}^{+j}, x_N) &= \dot{x}_1 \left(\frac{\kappa_{01} + \kappa_1 \mathrm{h}^+(x_{Nmax}^{+(j-1)}, \theta_N, n_N)(1 + \alpha \bar{x}_1^+)}{\gamma_1 + \alpha\kappa_1 \mathrm{h}^+(x_{Nmax}^{+(j-1)}, \theta_N, n_N)}, x_N \right) \\
&= \kappa_{01} - \gamma_1 \frac{\kappa_{01} + \kappa_1 \mathrm{h}^+(x_{Nmax}^{+(j-1)}, \theta_N, n_N)(1 + \alpha \bar{x}_1^+)}{\gamma_1 + \alpha\kappa_1 \mathrm{h}^+(x_{Nmax}^{+(j-1)}, \theta_N, n_N)} \\
&+ \left(-\alpha \left(\frac{\kappa_{01} + \kappa_1 \mathrm{h}^+(x_{Nmax}^{+(j-1)}, \theta_N, n_N)(1 + \alpha \bar{x}_1^+)}{\gamma_1 + \alpha\kappa_1 \mathrm{h}^+(x_{Nmax}^{+(j-1)}, \theta_N, n_N)} - \bar{x}_1^+ \right) + 1 \right) \kappa_1 \mathrm{h}^+(x_N, \theta_N, n_N) \\
&= -\kappa_1 \mathrm{h}^+(x_{Nmax}^{+(j-1)}, \theta_N, n_N) \left[\frac{\gamma_1 + \alpha(\gamma_1 \bar{x}_1^+ - \kappa_{01})}{\gamma_1 + \alpha\kappa_1 \mathrm{h}^+(x_{Nmax}^{+(j-1)}, \theta_N, n_N)} \right] \\
&+ \kappa_1 \mathrm{h}^+(x_N, \theta_N, n_N) \left[1 - \alpha \left(\frac{\kappa_{01} + \kappa_1 \mathrm{h}^+(x_{Nmax}^{+(j-1)}, \theta_N, n_N) - \gamma_1 \bar{x}_1^+}{\gamma_1 + \alpha\kappa_1 \mathrm{h}^+(x_{Nmax}^{+(j-1)}, \theta_N, n_N)} \right) \right] \\
&= -\kappa_1 \mathrm{h}^+(x_{Nmax}^{+(j-1)}, \theta_N, n_N) \left[\frac{\gamma_1 + \alpha(\gamma_1 \bar{x}_1^+ - \kappa_{01})}{\gamma_1 + \alpha\kappa_1 \mathrm{h}^+(x_{Nmax}^{+(j-1)}, \theta_N, n_N)} \right] \\
&+ \kappa_1 \mathrm{h}^+(x_N, \theta_N, n_N) \left[\frac{\gamma_1 + \alpha(\gamma_1 \bar{x}_1^+ - \kappa_{01})}{\gamma_1 + \alpha\kappa_1 \mathrm{h}^+(x_{Nmax}^{+(j-1)}, \theta_N, n_N)} \right] \\
&= \kappa_1 \left[\frac{\gamma_1 + \alpha(\gamma_1 \bar{x}_1^+ - \kappa_{01})}{\gamma_1 + \alpha\kappa_1 \mathrm{h}^+(x_{Nmax}^{+(j-1)}, \theta_N, n_N)} \right] \left(\mathrm{h}^+(x_N, \theta_N, n_N) - \mathrm{h}^+(x_{Nmax}^{+(j-1)}, \theta_N, n_N) \right).
\end{aligned}$$

Here, $x_{Nmax}^{+(j-1)} = +\infty$ for $j = 1$ by convention, from the expression of x_{1max}^{+1} in definition 4.3.2. Then, $\dot{x}_1(x_{1max}^{+j}, x_{Nmax}^{+(j-1)}) = 0$. Moreover, as $\gamma_1 \bar{x}_1^+ - \kappa_{01} > 0$ from proposition 3.2.8 and as $\mathrm{h}^+(x_N, \theta_N, n_N)$ is a strictly monotonically increasing function, $\dot{x}_1(x_{1max}^{+j}, x_N) \leq 0 \ \forall \ x_N \leq x_{Nmax}^{+(j-1)}$. From proposition 4.3.4 $x_{Nmax}^{+(j-1)} > x_{Nmax}^{+j} > x_{Nmin}^{+j}$. Then, $\dot{x}_1(x_{1max}^{+j}, x_N) < 0 \ \forall \ x_N \in [x_{Nmin}^{+j}, x_{Nmax}^{+j}]$.

The x_1-vector field is evaluated when $x_1 = x_{1min}^{+j}$: $\dot{x}_1(x_{1min}^{+j}, x_N) = \dot{x}_1\left(H_{1\alpha}^+(x_{Nmin}^{+(j-1)}), x_N\right)$ from definition 4.3.2. Then by the same calculation as previously:

$$\dot{x}_1(x_{1min}^{+j}, x_N) = \kappa_1 \left[\frac{\gamma_1 + \alpha(\gamma_1 \bar{x}_1^+ - \kappa_{01})}{\gamma_1 + \alpha\kappa_1 \mathrm{h}^+(x_{Nmin}^{+(j-1)}, \theta_N, n_N)} \right] \left(\mathrm{h}^+(x_N, \theta_N, n_N) - \mathrm{h}^+(x_{Nmin}^{+(j-1)}, \theta_N, n_N) \right).$$

Here, $x_{Nmin}^{+(j-1)} = 0$ for $j = 1$ by convention, from the expression of x_{1min}^{+1} in definition 4.3.2. Then, $\dot{x}_1(x_{1min}^{+j}, x_{Nmin}^{+(j-1)}) = 0$. Moreover, as $\gamma_1 \bar{x}_1^+ - \kappa_{01} > 0$ from proposition 3.2.8 and as $\mathrm{h}^+(x_N, \theta_N, n_N)$ is a strictly monotonically increasing function, $\dot{x}_1(x_{1min}^{+j}, x_N) \geq 0 \; \forall \; x_N \geq x_{Nmin}^{+(j-1)}$. From proposition 4.3.4 $x_{Nmin}^{+(j-1)} < x_{Nmin}^{+j} < x_{Nmax}^{+j}$. Then, $\dot{x}_1(x_{1min}^{+j}, x_N) > 0 \; \forall \; x_N \in [x_{Nmin}^{+j}, x_{Nmax}^{+j}]$.

We finally conclude that $\dot{x}_1(x_{1max}^{*j}, x_N) \leq 0 \; \forall \; x_N \in [x_{Nmin}^{*j}, x_{Nmax}^{*j}]$, and $\dot{x}_1(x_{1min}^{*j}, x_N) \geq 0 \; \forall \; x_N \in [x_{Nmin}^{*j}, x_{Nmax}^{*j}]$.

The vector field in the other directions can now be investigated:

Assume that $i \in \{2, ..., N\}$. The x_i-vector field is evaluated at a precise point of the upper bound of $\mathcal{R}_j^*$: $\dot{x}_i(x_{imax}^{*j}, x_{i-1max}^{*j}) = \dot{x}_1(H_i(x_{i-1max}^{*j}), x_{i-1max}^{*j})$ from definition 4.3.2.

Then $\dot{x}_i(x_{imax}^{*j}, x_{i-1max}^{*j}) = 0$ because from section 4.2, $\dot{x}_i(x_i, x_{i-1}) = 0 \iff x_i = H_i(x_{i-1})$. Let $x_{i-1} \leq x_{i-1max}^{*j}$, then $\kappa_{0i} + \kappa_i \mathrm{h}^+(x_{i-1}, \theta_{i-1}, n_{i-1}) - \gamma_i x_{imax}^{*j} \leq \kappa_{0i} + \kappa_i \mathrm{h}^+(x_{i-1max}^{*j}, \theta_{i-1}, n_{i-1}) - \gamma_i x_{imax}^{*j} = 0$. Hence, $\dot{x}_i(x_{imax}^{*j}, x_{i-1}) \leq \dot{x}_i(x_{imax}^{*j}, x_{i-1max}^{*j}) = 0 \; \forall \; x_{i-1} \leq x_{i-1max}^{*j}$. From proposition 4.3.4 $x_{i-1min}^{*j} < x_{i-1max}^{*j}$. Then, $\dot{x}_i(x_{imax}^{*j}, x_{i-1}) \leq 0 \; \forall \; x_{i-1} \in [x_{i-1min}^{*j}, x_{i-1max}^{*j}]$.

Finally, the x_i-vector field is evaluated at a precise point of the lower bound of $\mathcal{R}_j^*$: $\dot{x}_i(x_{1min}^{*j}, x_{i-1min}^{*j}) = \dot{x}_1(H_i(x_{i-1min}^{*j}), x_{i-1min}^{*j})$ from definition 4.3.2. Then $\dot{x}_i(x_{imin}^{*j}, x_{i-1min}^{*j}) = 0$. Let $x_{i-1} \geq x_{i-1min}^{*j}$, then $\kappa_{0i} + \kappa_i \mathrm{h}^+(x_{i-1}, \theta_{i-1}, n_{i-1}) - \gamma_i x_{imin}^{*j} \geq \kappa_{0i} + \kappa_i \mathrm{h}^+(x_{i-1min}^{*j}, \theta_{i-1}, n_{i-1}) - \gamma_i x_{imin}^{*j} = 0$.

Hence, $\dot{x}_i(x_{imin}^{*j}, x_{i-1}) \geq \dot{x}_i(x_{imin}^{*j}, x_{i-1min}^{*j}) = 0 \; \forall \; x_{i-1} \geq x_{i-1min}^{*j}$. From proposition 4.3.4 $x_{i-1min}^{*j} < x_{i-1max}^{*j}$. Then, $\dot{x}_i(x_{imin}^{*j}, x_{i-1}) \geq 0 \; \forall \; x_{i-1} \in [x_{i-1min}^{*j}, x_{i-1max}^{*j}]$. □

B.5 Proof of proposition 4.3.8

Proof. It is first obvious to observe that, from proposition 4.3.7, $\forall \; j \in \mathbb{N}$, for all initial condition $x_0 = x(t = 0) \in \mathcal{R}_j^*$, $x(t) \in \mathcal{R}_j^* \; \forall \; t \geq 0$.

Let $x_0 \in \mathcal{R}_j^*$ with $j \in \mathbb{N}$.

Base case 1 for the negative loop: From the proof of proposition 4.3.7, $\dot{x}_1(x_{1max}^{-(j+1)}, x_{Nmin}^{-j}) = 0$ and $\forall \; x_N \geq x_{Nmin}^{-j}$, $\dot{x}_1(x_{1max}^{-(j+1)}, x_N) \leq 0$ (where $x_{Nmin}^{-j} = 0$ if $j = 0$). Assume now that $x_N \geq x_{Nmin}^{-j}$ is fixed, and $x_1 > x_{1max}^{-(j+1)}$: from the degradation term $-(\alpha\kappa_1 \mathrm{h}^-(x_N, \theta_N, n_N) + \gamma_1)x_1$ in the x_1-vector field, $\dot{x}_1(x_1, x_N) < \dot{x}_1(x_{1max}^{-(j+1)}, x_N) \leq 0$. Hence, $\dot{x}_1(x_1, x_N) < 0 \; \forall \; x_N \geq x_{Nmin}^{-j}$ and $\forall \; x_1 > x_{1max}^{-(j+1)}$. As $x_0 \in \mathcal{R}_j^-$, then $x_{Nmin}^{-j} \leq x_N(t) \leq x_{Nmax}^{-j} \; \forall \; t \geq 0$. In other words, $\exists \; 0 \leq t_{1max}^- < +\infty$ such that $x_1(t) \leq x_{1max}^{-(j+1)} \; \forall \; t \geq t_{1max}^-$.

Base case 1 for the positive loop: From the proof of proposition 4.3.7, $\dot{x}_1(x_{1max}^{+(j+1)}, x_{Nmax}^{+j}) = 0$ and $\forall \; x_N \leq x_{Nmax}^{+j}$, $\dot{x}_1(x_{1max}^{+(j+1)}, x_N) \leq 0$ (where $x_{Nmax}^{+j} = +\infty$ if $j = 0$). Assume now that $x_N \leq x_{Nmax}^{+j}$ is fixed, and $x_1 > x_{1max}^{+(j+1)}$: from the degradation term $-(\alpha\kappa_1 \mathrm{h}^+(x_N, \theta_N, n_N) + \gamma_1)x_1$ in the x_1-vector field, $\dot{x}_1(x_1, x_N) < \dot{x}_1(x_{1max}^{+(j+1)}, x_N) \leq 0$. Hence, $\dot{x}_1(x_1, x_N) < 0 \; \forall \; x_N \leq x_{Nmax}^{+j}$ and $\forall \; x_1 > x_{1max}^{+(j+1)}$. As $x_0 \in \mathcal{R}_j^+$, then $x_{Nmin}^{+j} \leq x_N(t) \leq x_{Nmax}^{+j} \; \forall \; t \geq 0$. In other words, $\exists \; 0 \leq t_{1max}^+ < +\infty$ such that $x_1(t) \leq x_{1max}^{+(j+1)} \; \forall \; t \geq t_{1max}^+$.

Induction hypothesis 1: Let $1 \leq i-1 < N$, it is assumed that $\exists\ 0 \leq T^*_{i-1max} < +\infty$ such that for all $1 \leq p \leq i-1$, $x_p(t) \leq x^{*(j+1)}_{pmax}\ \forall\ t \geq T^*_{i-1max}$.

Induction step 1: From the proof of proposition 4.3.7, $\dot{x}_i(x^{*(j+1)}_{imax}, x^{*(j+1)}_{i-1max}) = 0$ and $\forall\ x_{i-1} \leq x^{*(j+1)}_{i-1max}$, $\dot{x}_i(x^{*(j+1)}_{imax}, x_{i-1}) \leq 0$. Assume now that $x_{i-1} \leq x^{*(j+1)}_{i-1max}$ is fixed, and $x_i > x^{*(j+1)}_{imax}$: from the degradation term $-\gamma_i x_i$ in the x_i-vector field, $\dot{x}_i(x_i, x_{i-1}) < \dot{x}_i(x^{*(j+1)}_{imax}, x_{i-1}) \leq 0$. Hence, $\dot{x}_i(x_i, x_{i-1}) < 0\ \forall\ x_{i-1} \leq x^{*(j+1)}_{i-1max}$ and $\forall\ x_i > x^{*(j+1)}_{imax}$. Moreover, from "Induction hypothesis 1", $x_{i-1}(t) \leq x^{*(j+1)}_{i-1max}\ \forall\ t \geq T^*_{i-1max}$. Hence, $\forall\ t \geq T^*_{i-1max}$, $\dot{x}_i(x_i, x_{i-1}(t)) < 0\ \forall\ x_i > x^{*(j+1)}_{imax}$. In other words, $\exists\ 0 \leq t^*_{imax} < +\infty$ such that $x_i(t) \leq x^{*(j+1)}_{imax}\ \forall\ t \geq T^*_{i-1max} + t^*_{imax}$. The new time $T^*_{imax} = T^*_{i-1max} + t^*_{imax}$ is such that: for all $1 \leq p \leq i$, $x_p(t) \leq x^{*(j+1)}_{pmax}\ \forall\ t \geq T^*_{imax}$.

Conclusion 1: By induction, $\exists\ 0 \leq T^*_{Nmax} < +\infty$ such that for all $1 \leq p \leq N$, $x_p(t) \leq x^{*(j+1)}_{pmax}$ $\forall\ t \geq T^*_{Nmax}$.

Base case 2 for the negative loop: From the proof of proposition 4.3.7, $\dot{x}_1(x^{-(j+1)}_{1min}, x^{-(j+1)}_{Nmax}) = 0$ and $\forall\ x_N \leq x^{-(j+1)}_{Nmax}$, $\dot{x}_1(x^{-(j+1)}_{1min}, x_N) \geq 0$. Assume now that $x_N \leq x^{-(j+1)}_{Nmax}$ is fixed, and $x_1 < x^{-(j+1)}_{1min}$: from the degradation term $-(\alpha\kappa_1 \mathrm{h}^-(x_N, \theta_N, n_N) + \gamma_1)x_1$ in the x_1-vector field, $\dot{x}_1(x_1, x_N) > \dot{x}_1(x^{-(j+1)}_{1min}, x_N) \geq 0$. Hence, $\dot{x}_1(x_1, x_N) > 0\ \forall\ x_N \leq x^{-(j+1)}_{Nmax}$ and $\forall\ x_1 < x^{-(j+1)}_{1min}$. Moreover, from "Conclusion 1", $x_N(t) \leq x^{-(j+1)}_{Nmax}\ \forall\ t \geq T^-_{Nmax}$.
Hence, $\forall\ t \geq T^-_{Nmax}$, $\dot{x}_1(x_1, x_N(t)) > 0\ \forall\ x_1 < x^{-(j+1)}_{1min}$. In other words, $\exists\ 0 \leq t^-_{1min} < +\infty$ such that $x_1(t) \geq x^{-(j+1)}_{1min}\ \forall\ t \geq T^-_{Nmax} + t^-_{1min}$. The new time $T^-_{1min} = T^-_{Nmax} + t^-_{1min}$ is such that: $x^{-(j+1)}_{1min} \leq x_1(t) \leq x^{-(j+1)}_{1max}$ and for all $1 < p \leq N$, $x_p(t) \leq x^{-(j+1)}_{pmax}\ \forall\ t \geq T^-_{1min}$.

Base case 2 for the positive loop: From the proof of proposition 4.3.7, $\dot{x}_1(x^{+(j+1)}_{1min}, x^{+j}_{Nmin}) = 0$ and $\forall\, x_N \geq x^{+j}_{Nmin}$, $\dot{x}_1(x^{+(j+1)}_{1min}, x_N) \geq 0$ (where $x^{+j}_{Nmin} = 0$ if $j = 0$). Assume now that $x_N \geq x^{+j}_{Nmin}$ is fixed, and $x_1 < x^{+(j+1)}_{1min}$: from the degradation term $-(\alpha\kappa_1 \mathrm{h}^+(x_N, \theta_N, n_N) + \gamma_1)x_1$ in the x_1-vector field, $\dot{x}_1(x_1, x_N) > \dot{x}_1(x^{+(j+1)}_{1min}, x_N) \geq 0$. Hence, $\dot{x}_1(x_1, x_N) > 0\ \forall\ x_N \geq x^{+j}_{Nmin}$ and $\forall\ x_1 < x^{+(j+1)}_{1min}$. As $x_0 \in \mathcal{R}^+_j$, then $x^{+j}_{Nmin} \leq x_N(t) \leq x^{+j}_{Nmax}\ \forall\ t \geq 0$. In other words, $\exists\ 0 \leq t^+_{1min} < +\infty$ such that $x_1(t) \geq x^{+(j+1)}_{1min}\ \forall\ t \geq t^+_{1min}$. Moreover, from "Conclusion 1", $\exists\ 0 \leq T^+_{Nmax} < +\infty$ such that for all $1 \leq p \leq N$, $x_p(t) \leq x^{+(j+1)}_{pmax}\ \forall\ t \geq T^+_{Nmax}$. The new time $T^+_{1min} = T^+_{Nmax} + t^+_{1min}$ is such that: $x^{+(j+1)}_{1min} \leq x_1(t) \leq x^{+(j+1)}_{1max}$ and for all $1 < p \leq N$, $x_p(t) \leq x^{+(j+1)}_{pmax}\ \forall\ t \geq T^+_{1min}$.

Induction hypothesis 2: Let $1 \leq i-1 < N$, it is assumed that $\exists\ 0 \leq T^*_{i-1min} < +\infty$ such that for all $1 \leq p \leq i-1$, $x^{*(j+1)}_{pmin} \leq x_p(t) \leq x^{*(j+1)}_{pmax}$ and for all $i-1 < p \leq N$, $x_p(t) \leq x^{*(j+1)}_{pmax}$ $\forall\ t \geq T^*_{i-1min}$.

Induction step 2: From the proof of proposition 4.3.7, $\dot{x}_i(x^{*(j+1)}_{imin}, x^{*(j+1)}_{i-1min}) = 0$ and $\forall\ x_{i-1} \geq x^{*(j+1)}_{i-1min}$, $\dot{x}_i(x^{*(j+1)}_{imin}, x_{i-1}) \geq 0$. Assume now that $x_{i-1} \geq x^{*(j+1)}_{i-1min}$ is fixed, and $x_i < x^{*(j+1)}_{imin}$: from the degradation term $-\gamma_i x_i$ in the x_i-vector field, $\dot{x}_i(x_i, x_{i-1}) > \dot{x}_i(x^{*(j+1)}_{imin}, x_{i-1}) \geq 0$. Hence, $\dot{x}_i(x_i, x_{i-1}) > 0\ \forall\ x_{i-1} \geq x^{*(j+1)}_{i-1min}$ and $\forall\ x_i < x^{*(j+1)}_{imin}$. Moreover, from "Induction hypothesis 2", $x_{i-1}(t) \geq x^{*(j+1)}_{i-1min}\ \forall\ t \geq T^*_{i-1min}$. Hence, $\forall\ t \geq T^*_{i-1min}$, $\dot{x}_i(x_i, x_{i-1}(t)) > 0\ \forall\ x_i < x^{*(j+1)}_{imin}$. In other words, $\exists\ 0 \leq t^*_{imin} < +\infty$ such that $x_i(t) \geq x^{*(j+1)}_{imin}\ \forall\ t \geq T^*_{i-1min} + t^*_{imin}$. The new time $T^*_{imin} = T^*_{i-1min} + t^*_{imin}$ is such that: for all $1 \leq p \leq i$, $x^{*(j+1)}_{pmin} \leq x_p(t) \leq x^{*(j+1)}_{pmax}$ and for all $i < p \leq N$, $x_p(t) \leq x^{*(j+1)}_{pmax}\ \forall\ t \geq T^*_{imin}$.

Conclusion 2: By induction, $\exists\ 0 \leq T^*_{Nmin} < +\infty$ such that for all $1 \leq p \leq N$, $x^{*(j+1)}_{pmin} \leq x_p(t) \leq x^{*(j+1)}_{pmax}\ \forall\ t \geq T^*_{Nmin}$. Let $T^*_j = T^*_{Nmin}$, then proposition 4.3.8 is proved $\forall\ j \in \mathbb{N}$. □

B.6 Proof of proposition 4.4.1

Proof. By definition, $Z_{1\alpha}^{+}(x) = S_{1\alpha}^{+}(x)$ where $S_{1\alpha}^{+}(x) = H_{1\alpha}^{+} \circ H_N \circ H_{N-1} \circ ... \circ H_3 \circ H_2(x)$. From property A.1.1 in appendix A.1, if all the functions in this composition have a negative Schwarzian derivative, then the composed function $Z_{1\alpha}^{+}(x)$ will also have a negative Schwarzian derivative. From the previous calculations given in the proof of proposition 3.2.4, $\mathrm{S}(H_i(x)) < 0 \; \forall \; i \in \{2, ..., N\}$ and:

$$\begin{aligned}\mathrm{S}(H_{1\alpha}^{+}(x)) &= \mathrm{S}\left(\frac{\kappa_{01} + \kappa_1 \mathrm{h}^{+}(x, \theta_N, n_N)(1 + \alpha \bar{x}_1^{+})}{\gamma_1 + \alpha\kappa_1 \mathrm{h}^{+}(x, \theta_N, n_N)}\right) \\ &= \mathrm{S}(f \circ g(x)),\end{aligned}$$

where $f(x) = \left(\kappa_{01} + \kappa_1 x(1 + \alpha \bar{x}_1^{+})\right) / \left(\gamma_1 + \alpha\kappa_1 x\right)$ and $g(x) = \mathrm{h}^{+}(x, \theta_N, n_N)$. By the calculations in the proof of proposition 3.2.4:

$$\mathrm{S}\left(g(x)\right) = -\frac{n_N^2 - 1}{2x^2} < 0.$$

In order to calculate the Schwarzian derivative of $f(x)$, the three first derivatives of $f(x)$ are necessary:

$$\begin{aligned}f'(x) &= \frac{\kappa_1 \left[\gamma_1 + \alpha\left(\gamma \bar{x}_1^{+} - \kappa_{01}\right)\right]}{\left(\gamma_1 + \alpha\kappa_1 x\right)^2}, \\ f''(x) &= \frac{-2\kappa_1^2 \alpha \left[\gamma_1 + \alpha\left(\gamma \bar{x}_1^{+} - \kappa_{01}\right)\right]}{\left(\gamma_1 + \alpha\kappa_1 x\right)^3}, \\ f^{(3)}(x) &= \frac{6\kappa_1^3 \alpha^2 \left[\gamma_1 + \alpha\left(\gamma \bar{x}_1^{+} - \kappa_{01}\right)\right]}{\left(\gamma_1 + \alpha\kappa_1 x\right)^4}.\end{aligned}$$

After simplifications, $\mathrm{S}(f(x)) = 0$. Hence, with property A.1.1 in appendix A.1, $\mathrm{S}(H_{1\alpha}^{+}(x)) = \mathrm{S}(g(x)) = -\left(n_N^2 - 1\right)/2x^2 < 0$. Hence, $\mathrm{S}(S_{1\alpha}^{+}(x)) = \mathrm{S}(H_{1\alpha}^{+} \circ H_N \circ H_{N-1} \circ ... \circ H_3 \circ H_2(x)) < 0$. It follows that $Z_{1\alpha}^{+}(x)$ has a negative Schwarzian derivative.

For $Z_{1\alpha}^{-}(x)$, as $Z_{1\alpha}^{-}(x) = S_{1\alpha}^{-} \circ S_{1\alpha}^{-}(x)$ where $S_{1\alpha}^{-}(x) = H_{1\alpha}^{-} \circ H_N \circ H_{N-1} \circ ... \circ H_3 \circ H_2(x)$, if $S_{1\alpha}^{-}(x)$ has a negative Schwarzian derivative, then the composed function $Z_{1\alpha}^{-}(x)$ will also have a negative Schwarzian derivative. Again, $\mathrm{S}(H_i(x)) < 0 \; \forall \; i \in \{2, ..., N\}$ and:

$$\begin{aligned}\mathrm{S}(H_{1\alpha}^{-}(x)) &= \mathrm{S}\left(\frac{\kappa_{01} + \kappa_1 \mathrm{h}^{-}(x, \theta_N, n_N)(1 + \alpha \bar{x}_1^{-})}{\gamma_1 + \alpha\kappa_1 \mathrm{h}^{-}(x, \theta_N, n_N)}\right) \\ &= \mathrm{S}(f \circ g(x)),\end{aligned}$$

where $f(x) = \left(\kappa_{01} + \kappa_1 x(1 + \alpha \bar{x}_1^{-})\right) / \left(\gamma_1 + \alpha\kappa_1 x\right)$ and $g(x) = \mathrm{h}^{-}(x, \theta_N, n_N) =$. Again:

$$\mathrm{S}\left(g(x)\right) = -\frac{n_N^2 - 1}{2x^2} < 0,$$

and as previously, $\mathrm{S}(f(x)) = 0$. Hence, with property A.1.1 in appendix A.1, $\mathrm{S}(H_{1\alpha}^{-}(x)) = \mathrm{S}(g(x)) = -\left(n_N^2 - 1\right)/2x^2 < 0$. Hence, $\mathrm{S}(S_{1\alpha}^{-}(x)) = \mathrm{S}(H_{1\alpha}^{-} \circ H_N \circ H_{N-1} \circ ... \circ H_3 \circ H_2(x)) < 0$. Finally, as $Z_{1\alpha}^{-}(x) = S_{1\alpha}^{-} \circ S_{1\alpha}^{-}(x)$, from property A.1.1 in appendix A.1, $Z_{1\alpha}^{-}(x)$ has a negative Schwarzian derivative. □

Appendix C

Supplementary material of chapter 6

C.1 Proof of proposition 6.4.1

Proof. The proof is built with two mathematical inductions:

As a first base case, $\mu_N = \delta > 0$ and $m_N = \mu_N$ with definition 6.4.3. Then $\bar{x}_N^- - \mu_N < \bar{x}_N^-$ and under assumption 6.4.1, $\bar{x}_N^- - m_N = \bar{x}_N^- - \delta > \kappa_{0N}/\gamma_N$. Finally $\kappa_{0N}/\gamma_N < \bar{x}_N^- - m_N < \bar{x}_N^-$.

Assume that the property $\mu_{j+1} > 0$ and $\kappa_{0j+1}/\gamma_{j+1} < \bar{x}_{j+1}^- - m_{j+1} < \bar{x}_{j+1}^-$ holds for one natural number $j+1 \in \{2, ..., N\}$. Then from proposition 3.2.8, $\kappa_{0j+1}/\gamma_{j+1} < \bar{x}_{j+1}^- - m_{j+1} < \bar{x}_{j+1}^- < (\kappa_{0j+1} + \kappa_{j+1})/\gamma_{j+1}$ implies that:
$0 < \left(\gamma_{j+1}(\bar{x}_{j+1}^- - m_{j+1}) - \kappa_{0j+1}\right)/\kappa_{j+1} < \left(\gamma_{j+1}\bar{x}_{j+1}^- - \kappa_{0j+1}\right)/\kappa_{j+1} < 1$. From property 6.4.1, the use of the monotonically increasing function ϕ_{j+1} in the inequality gives:
$\phi_{j+1}(0) < \phi_{j+1}\left(\left(\gamma_{j+1}(\bar{x}_{j+1}^- - m_{j+1}) - \kappa_{0j+1}\right)/\kappa_{j+1}\right) < \phi_{j+1}\left(\left(\gamma_{j+1}\bar{x}_{j+1}^- - \kappa_{0j+1}\right)/\kappa_{j+1}\right)$. With $\phi_{j+1}(0) = 0$ and $\phi_{j+1}\left(\left(\gamma_{j+1}\bar{x}_{j+1}^- - \kappa_{0j+1}\right)/\kappa_{j+1}\right) = \bar{x}_j^-$, this implies:
$0 < \phi_{j+1}\left(\left(\gamma_{j+1}(\bar{x}_{j+1}^- - m_{j+1}) - \kappa_{0j+1}\right)/\kappa_{j+1}\right) < \bar{x}_j^-$.
Then, $\bar{x}_j^- - \phi_{j+1}\left(\left(\gamma_{j+1}(\bar{x}_{j+1}^- - m_{j+1}) - \kappa_{0j+1}\right)/\kappa_{j+1}\right) > 0$. Finally, from the definition 6.4.3, $\mu_j > 0$. As a consequence, $\bar{x}_j^- - \mu_j < \bar{x}_j^-$ and under assumption 6.4.1, $\kappa_{0j}/\gamma_j < \bar{x}_j^- - \delta < \bar{x}_j^-$. As $m_j = \min(\delta, \mu_j)$, the desired inequality $\kappa_{0j}/\gamma_j < \bar{x}_j^- - m_j < \bar{x}_j^-$ holds.

Then, if the property holds for one natural number $j+1 \in \{2, ..., N\}$, it also holds for j. By a mathematical induction, $\mu_i > 0$ and $\kappa_{0i}/\gamma_i < \bar{x}_i^- - m_i < \bar{x}_i^-$ for all $i \in \{N, ..., 1\}$.

As a second base case, $\kappa_{01}/\gamma_1 < \bar{x}_1^- - m_1 < \bar{x}_1^-$. Then from proposition 3.2.8, $\kappa_{01}/\gamma_1 < \bar{x}_1^- - m_1 \leq \bar{x}_1^- \leq (\kappa_{01} + \kappa_1)/\gamma_1$ implies that $0 < \left(\gamma_1(\bar{x}_1^- - m_1) - \kappa_{01}\right)/\kappa_1 < \left(\gamma_1\bar{x}_1^- - \kappa_{01}\right)/\kappa_1 \leq 1$. From property 6.4.1, the use of the monotonically decreasing function ϕ_1^- in the inequality gives: $\phi_1^-\left(\left(\gamma_1(\bar{x}_1^- - m_1) - \kappa_{01}\right)/\kappa_1\right) > \phi_1^-\left(\left(\gamma_1\bar{x}_1^- - \kappa_{01}\right)/\kappa_1\right) \geq \phi_1^-(1)$. With $\phi_1^-(1) = 0$ and $\phi_1^-\left(\left(\gamma_1\bar{x}_1^- - \kappa_{01}\right)/\kappa_1\right) = \bar{x}_N^-$, this implies:
$\phi_1^-\left(\left(\gamma_1(\bar{x}_1^- - m_1) - \kappa_{01}\right)/\kappa_1\right) > \bar{x}_N^- \geq 0$. Then, $\phi_1^-\left(\left(\gamma_1(\bar{x}_1^- - m_1) - \kappa_{01}\right)/\kappa_1\right) - \bar{x}_N^- > 0$. Finally, from the definition 6.4.3, $\alpha_N > 0$. As a consequence, $\bar{x}_N^- + \alpha_N > \bar{x}_N^-$ and under assumption 6.4.1, $\bar{x}_N^- < \bar{x}_N^- + \delta < (\kappa_{0N} + \kappa_N)/\gamma_N$. As $M_N = \min(\delta, \alpha_N)$, the desired inequality $\bar{x}_N^- < \bar{x}_N^- + M_N < (\kappa_{0N} + \kappa_N)/\gamma_N$ holds.

Assume that the property $\alpha_{j+1} > 0$ and $\bar{x}_{j+1}^- < \bar{x}_{j+1}^- + M_{j+1} < (\kappa_{0j+1} + \kappa_{j+1})/\gamma_{j+1}$ holds for one natural number $j+1 \in \{3, ..., N\}$. Then from proposition 3.2.8, $\kappa_{0j+1}/\gamma_{j+1} \leq \bar{x}_{j+1}^- < \bar{x}_{j+1}^- + M_{j+1} < (\kappa_{0j+1} + \kappa_{j+1})/\gamma_{j+1}$ implies that:

$0 \leq \left(\gamma_{j+1}\bar{x}_{j+1}^{-} - \kappa_{0j+1}\right)/\kappa_{j+1} < \left(\gamma_{j+1}(\bar{x}_{j+1}^{-} + M_{j+1}) - \kappa_{0j+1}\right)/\kappa_{j+1} < 1$. From property 6.4.1, the use of the monotonically increasing function ϕ_{j+1} in the inequality gives:
$\phi_{j+1}(0) \leq \phi_{j+1}\left(\left(\gamma_{j+1}\bar{x}_{j+1}^{-} - \kappa_{0j+1}\right)/\kappa_{j+1}\right) < \phi_{j+1}\left(\left(\gamma_{j+1}(\bar{x}_{j+1}^{-} + M_{j+1}) - \kappa_{0j+1}\right)/\kappa_{j+1}\right)$. With $\phi_{j+1}(0) = 0$ and $\phi_{j+1}\left(\left(\gamma_{j+1}\bar{x}_{j+1}^{-} - \kappa_{0j+1}\right)/\kappa_{j+1}\right) = \bar{x}_{j}^{-}$, this implies:
$0 \leq \bar{x}_{j}^{-} < \phi_{j+1}\left(\left(\gamma_{j+1}(\bar{x}_{j+1}^{-} + M_{j+1}) - \kappa_{0j+1}\right)/\kappa_{j+1}\right)$.
Then, $\phi_{j+1}\left(\left(\gamma_{j+1}(\bar{x}_{j+1}^{-} + M_{j+1}) - \kappa_{0j+1}\right)/\kappa_{j+1}\right) - \bar{x}_{j}^{-} > 0$. Finally, from definition 6.4.3, $\alpha_j > 0$. As a consequence, $\bar{x}_{j}^{-} + \alpha_j > \bar{x}_{j}^{-}$ and under assumption 6.4.1, $\bar{x}_{j}^{-} < \bar{x}_{j}^{-} + \delta < (\kappa_{0j} + \kappa_j)/\gamma_j$. As $M_j = \min(\delta, \alpha_j)$, the desired inequality $\bar{x}_{j}^{-} < \bar{x}_{j}^{-} + M_j < (\kappa_{0j} + \kappa_j)/\gamma_j$ holds.

Then, if the property holds for one natural number $j+1 \in \{3, ..., N\}$, it also holds for j. By a mathematical induction, $\alpha_i > 0$ and $\bar{x}_{i}^{-} < \bar{x}_{i}^{-} + M_i < (\kappa_{0i} + \kappa_i)/\gamma_i$ for all $i \in \{N, ..., 2\}$.

For i = 1, the same steps are followed. The inequality $\kappa_{02}/\gamma_2 \leq \bar{x}_{2}^{-} < \bar{x}_{2}^{-} + M_2 < (\kappa_{02} + \kappa_2)/\gamma_2$ implies that $0 \leq \left(\gamma_2\bar{x}_{2}^{-} - \kappa_{02}\right)/\kappa_2 < \left(\gamma_2(\bar{x}_{2}^{-} + M_2) - \kappa_{02}\right)/\kappa_2 < 1$. From property 6.4.1, the use of the monotonically increasing function ϕ_2 in the inequality gives: $\phi_2(0) \leq \phi_2\left(\left(\gamma_2\bar{x}_{2}^{-} - \kappa_{02}\right)/\kappa_2\right) < \phi_2\left(\left(\gamma_2(\bar{x}_{2}^{-} + M_2) - \kappa_{02}\right)/\kappa_2\right)$. With $\phi_2(0) = 0$ and $\phi_2\left(\left(\gamma_2\bar{x}_{2}^{-} - \kappa_{02}\right)/\kappa_2\right) = \bar{x}_{1}^{-}$, this implies: $0 \leq \bar{x}_{1}^{-} < \phi_2\left(\left(\gamma_2(\bar{x}_{2}^{-} + M_2) - \kappa_{02}\right)/\kappa_2\right)$. Then, $\phi_2\left(\left(\gamma_2(\bar{x}_{2}^{-} + M_2) - \kappa_{02}\right)/\kappa_2\right) - \bar{x}_{1}^{-} > 0$. Finally, from the definition 6.4.3, $\alpha_1 > 0$. As a consequence, $\bar{x}_{1}^{-} + \alpha_1 > \bar{x}_{1}^{-}$ and under assumption 6.4.1, $\bar{x}_{1}^{-} < \bar{x}_{1}^{-} + \delta$. As $M_1 = \min(\delta, \alpha_1)$, the desired inequality $\bar{x}_{1}^{-} < \bar{x}_{1}^{-} + M_1$ holds. □

C.2 Proof of lemma 6.4.1

Proof. To prove this lemma, it is shown that the boundaries of the region $\mathcal{B}^{-}$ are repellent, i.e.:

- $\dot{x}_i(\bar{x}_{i}^{-} - m_i, x_{i-1}) \geq 0 \ \forall \ x_{i-1} \in [\bar{x}_{i-1}^{-} - m_{i-1}, \bar{x}_{i-1}^{-} + M_{i-1}] \ \forall \ i \in \{1, ..., N\}$,
- $\dot{x}_i(\bar{x}_{i}^{-} + M_i, x_{i-1}) \leq 0 \ \forall \ x_{i-1} \in [\bar{x}_{i-1}^{-} - m_{i-1}, \bar{x}_{i-1}^{-} + M_{i-1}] \ \forall \ i \in \{1, ..., N\}$.

First, for all $i \in \{2, ..., N\}$, $\dot{x}_i(x_i, x_{i-1}) = \kappa_{0i} + \kappa_i \mathrm{h}^{+}(x_{i-1}, \theta_{i-1}, n_{i-1}) - \gamma_i x_i$. Then, when evaluating this expression at the point $(\bar{x}_{i}^{-} - m_i, \bar{x}_{i-1}^{-} - \mu_{i-1})$, which is well defined as proved by proposition 6.4.1, the x_i-vector field becomes: $\dot{x}_i(\bar{x}_{i}^{-} - m_i, \bar{x}_{i-1}^{-} - \mu_{i-1}) = \kappa_{0i} + \kappa_i \mathrm{h}^{+}(\bar{x}_{i-1}^{-} - \mu_{i-1}, \theta_{i-1}, n_{i-1}) - \gamma_i(\bar{x}_{i}^{-} - m_i)$. With the definition of $\mu_{i-1} = \bar{x}_{i-1}^{-} - \phi_i\left(\left(\gamma_i(\bar{x}_{i}^{-} - m_i) - \kappa_{0i}\right)/\kappa_i\right)$, the x_i-vector field further becomes: $\dot{x}_i(\bar{x}_{i}^{-} - m_i, \bar{x}_{i-1}^{-} - \mu_{i-1}) = \kappa_{0i} + \kappa_i \mathrm{h}^{+}\left(\phi_i\left(\left(\gamma_i(\bar{x}_{i}^{-} - m_i) - \kappa_{0i}\right)/\kappa_i\right), \theta_{i-1}, n_{i-1}\right) - \gamma_i(\bar{x}_{i}^{-} - m_i)$. From property 6.4.1 and proposition 6.4.1:
$\dot{x}_i(\bar{x}_{i}^{-} - m_i, \bar{x}_{i-1}^{-} - \mu_{i-1}) = \kappa_{0i} + \kappa_i\left(\left(\gamma_i(\bar{x}_{i}^{-} - m_i) - \kappa_{0i}\right)/\kappa_i\right) - \gamma_i(\bar{x}_{i}^{-} - m_i)$. Then $\dot{x}_i(\bar{x}_{i}^{-} - m_i, \bar{x}_{i-1}^{-} - \mu_{i-1}) = 0$. Now, the strictly monotonic property of the increasing Hill function implies that for all $x_{i-1} \geq \bar{x}_{i-1}^{-} - \mu_{i-1}$, $\mathrm{h}^{+}(x_{i-1}, \theta_{i-1}, n_{i-1}) \geq \mathrm{h}^{+}(\bar{x}_{i-1}^{-} - \mu_{i-1}, \theta_{i-1}, n_{i-1}) \geq 0$. In the x_i-vector field, for x_i fixed, this property induces $\dot{x}_i(\bar{x}_{i}^{-} - m_i, x_{i-1}) \geq \dot{x}_i(\bar{x}_{i}^{-} - m_i, \bar{x}_{i-1}^{-} - \mu_{i-1}) = 0$ for all $x_{i-1} \geq \bar{x}_{i-1}^{-} - \mu_{i-1}$. In particular, as $\bar{x}_{i-1}^{-} - m_{i-1} \geq \bar{x}_{i-1}^{-} - \mu_{i-1}$, then for all $x_{i-1} \in [\bar{x}_{i-1}^{-} - m_{i-1}, \bar{x}_{i-1}^{-} + M_{i-1}]$, the x_i-vector field is positive: $\dot{x}_i(\bar{x}_{i}^{-} - m_i, x_{i-1}) \geq 0$. This inequality means that a trajectory that starts in the region $\mathcal{B}^{-}$ cannot leave the region through the boundary $x_i = \bar{x}_{i}^{-} - m_i$.

Second, for all $i \in \{2, ..., N\}$, $\dot{x}_i(x_i, x_{i-1}) = \kappa_{0i} + \kappa_i \mathrm{h}^{+}(x_{i-1}, \theta_{i-1}, n_{i-1}) - \gamma_i x_i$. Then, when evaluating this expression at the point $(\bar{x}_{i}^{-} + M_i, \bar{x}_{i-1}^{-} + \alpha_{i-1})$, which is well defined as proved by the proposition 6.4.1, the x_i-vector field becomes: $\dot{x}_i(\bar{x}_{i}^{-} + M_i, \bar{x}_{i-1}^{-} + \alpha_{i-1}) = \kappa_{0i} + \kappa_i \mathrm{h}^{+}(\bar{x}_{i-1}^{-} + \alpha_{i-1}, \theta_{i-1}, n_{i-1}) - \gamma_i(\bar{x}_{i}^{-} + M_i)$. With the definition of $\alpha_{i-1} = \phi_i\left(\left(\gamma_i(\bar{x}_{i}^{-} + M_i) - \kappa_{0i}\right)/\kappa_i\right) - \bar{x}_{i-1}^{-}$, the x_i-vector field further becomes:
$\dot{x}_i(\bar{x}_{i}^{-} + M_i, \bar{x}_{i-1}^{-} + \alpha_{i-1}) = \kappa_{0i} + \kappa_i \mathrm{h}^{+}\left(\phi_i\left(\left(\gamma_i(\bar{x}_{i}^{-} + M_i) - \kappa_{0i}\right)/\kappa_i\right), \theta_{i-1}, n_{i-1}\right) - \gamma_i(\bar{x}_{i}^{-} + M_i)$. From property 6.4.1 and proposition 6.4.1: $\dot{x}_i(\bar{x}_{i}^{-} + M_i, \bar{x}_{i-1}^{-} + \alpha_{i-1}) = \kappa_{0i} + \kappa_i\left(\left(\gamma_i(\bar{x}_{i}^{-} + M_i) - \kappa_{0i}\right)/\kappa_i\right) - \gamma_i(\bar{x}_{i}^{-} + M_i)$. Then $\dot{x}_i(\bar{x}_{i}^{-} + M_i, \bar{x}_{i-1}^{-} + \alpha_{i-1}) = 0$. Now, the strictly monotonic property of the

increasing Hill function implies that for all $0 \leq x_{i-1} \leq \bar{x}_{i-1}^- + \alpha_{i-1}$, $0 \leq \mathrm{h}^+(x_{i-1}, \theta_{i-1}, n_{i-1}) \leq \mathrm{h}^+(\bar{x}_{i-1}^- + \alpha_{i-1}, \theta_{i-1}, n_{i-1})$. In the x_i-vector field, for x_i fixed, this property induces $\dot{x}_i(\bar{x}_i^- + M_i, x_{i-1}) \leq \dot{x}_i(\bar{x}_i^- + M_i, \bar{x}_{i-1}^- + \alpha_{i-1}) = 0$ for all $0 \leq x_{i-1} \leq \bar{x}_{i-1}^- + \alpha_{i-1}$. In particular, as $\bar{x}_{i-1}^- + M_{i-1} \leq \bar{x}_{i-1}^- + \alpha_{i-1}$, then for all $x_{i-1} \in [\bar{x}_{i-1}^- - m_{i-1}, \bar{x}_{i-1}^- + M_{i-1}]$ the x_i-vector field is negative: $\dot{x}_i(\bar{x}_i^- + M_i, x_{i-1}) \leq 0$. This inequality means that a trajectory that starts in the region $\mathcal{B}^-$ cannot leave the region through the boundary $x_i = \bar{x}_i^- + M_i$.

Third, when $x_1 = \bar{x}_1^- + M_1 > \bar{x}_1^-$, the x_1-vector field is defined as: $\dot{x}_1(\bar{x}_1^- + M_1, x_N) = \kappa_{01} + u_{min}\kappa_1 \mathrm{h}^-(x_N, \theta_N, n_N) - \gamma_1(\bar{x}_1^- + M_1)$. With the condition on u_{min} given in assumption 6.3.1, namely $u_{min} \leq (\gamma_1 \bar{x}_1^- - \kappa_{01})/\kappa_1$, then:
$\dot{x}_1(\bar{x}_1^- + M_1, x_N) \leq \kappa_{01} + \left(\gamma_1 \bar{x}_1^- - \kappa_{01}\right)/\kappa_1) \kappa_1 \mathrm{h}^-(x_N, \theta_N, n_N) - \gamma_1(\bar{x}_1^- + M_1)$, leading to $\dot{x}_1(\bar{x}_1^- + M_1, x_N) \leq (\gamma_1 \bar{x}_1^- - \kappa_{01}) \left(\mathrm{h}^-(x_N, \theta_N, n_N) - 1\right) - \gamma_1 M_1$. From proposition 3.2.8, $\gamma_1 \bar{x}_1^- - \kappa_{01} > 0$, moreover $\mathrm{h}^-(x_N, \theta_N, n_N) - 1 \leq 0$, and $-\gamma_1 M_1 < 0$. Then, the x_1-vector field is strictly negative: $\dot{x}_1(\bar{x}_1^- + M_1, x_N) < 0$ for all $x_N \geq 0$. In particular, for all $x_N \in [\bar{x}_N^- - m_N, \bar{x}_N^- + M_N]$, the x_1-vector field is strictly negative: $\dot{x}_1(\bar{x}_1^- + M_1, x_N) < 0$. This inequality means that a trajectory that starts in the region $\mathcal{B}^-$ cannot leave the region through the boundary $x_1 = \bar{x}_1^- + M_1$.

Fourth, when $x_1 = \bar{x}_1^- - m_1 < \bar{x}_1^-$, the x_1-vector field is defined as: $\dot{x}_1(\bar{x}_1^- - m_1, x_N) = \kappa_{01} + \kappa_1 \mathrm{h}^-(x_N, \theta_N, n_N) - \gamma_1(\bar{x}_1^- - m_1)$. Then, when evaluating this expression at the point $(\bar{x}_1^- - m_1, \bar{x}_N^- + \alpha_N)$, which is well defined as proved by the proposition 6.4.1, the x_1-vector field becomes: $\dot{x}_i(\bar{x}_1^- - m_1, \bar{x}_N^- + \alpha_N) = \kappa_{01} + \kappa_1 \mathrm{h}^-(\bar{x}_N^- + \alpha_N, \theta_N, n_N) - \gamma_1(\bar{x}_1^- - m_1)$. With the definition of $\alpha_N = \phi_1^- \left(\left(\gamma_1(\bar{x}_1^- - m_1) - \kappa_{01}\right)/\kappa_1\right) - \bar{x}_N^-$, the x_1-vector field further becomes: $\dot{x}_1(\bar{x}_1^- - m_1, \bar{x}_N^- + \alpha_N) = \kappa_{01} + \kappa_1 \mathrm{h}^- \left(\phi_1^- \left(\left(\gamma_1(\bar{x}_1^- - m_1) - \kappa_{01}\right)/\kappa_1\right), \theta_N, n_N\right) - \gamma_1(\bar{x}_1^- - m_1)$. From property 6.4.1 and proposition 6.4.1, $\dot{x}_1(\bar{x}_1^- - m_1, \bar{x}_N^- + \alpha_N) = \kappa_{01} + \kappa_1 \left(\left(\gamma_1(\bar{x}_1^- - m_1) - \kappa_{01}\right)/\kappa_1\right) - \gamma_1(\bar{x}_1^- - m_1)$. Then $\dot{x}_1(\bar{x}_1^- - m_1, \bar{x}_N^- + \alpha_N) = 0$. Now, the strictly monotonic property of the decreasing Hill function implies that for all $0 \leq x_N \leq \bar{x}_N^- + \alpha_N$, $\mathrm{h}^-(x_N, \theta_N, n_N) \geq \mathrm{h}^-(\bar{x}_N^- + \alpha_N, \theta_N, n_N) > 0$. In the x_1-vector field, for x_1 fixed, this property induces $\dot{x}_1(\bar{x}_1^- - m_1, x_N) \geq \dot{x}_1(\bar{x}_1^- - m_1, \bar{x}_N^- + \alpha_N) = 0$ for all $0 \leq x_N \leq \bar{x}_N^- + \alpha_N$. In particular, as $\bar{x}_N^- + M_N \leq \bar{x}_N^- + \alpha_N$, then for all $x_N \in [\bar{x}_N^- - m_N, \bar{x}_N^- + M_N]$ the x_1-vector field is positive: $\dot{x}_1(\bar{x}_1^- - m_1, x_N) \geq 0$. This inequality means that a trajectory that starts in the region $\mathcal{B}^-$ cannot leave the region through the boundary $x_1 = \bar{x}_1^- - m_1$.

Finally, if $x(0) \in \mathcal{B}^-$ then $x(t) \in \mathcal{B}^- \ \forall\ t \geq 0$. The region $\mathcal{B}^-$ is invariant. □

C.3 Proof of proposition 6.4.3

Proof. The proof is built with two mathematical inductions:

As a first base case, $\mu_N = \min\left(\delta, \bar{x}_N^+ - x_{Nmin}\right) > 0$ and $m_N = \mu_N$ with definition 6.4.6. From definition 6.4.5, $\bar{x}_N^+ - \mu_N < \bar{x}_N^+$. Moreover, under assumption 6.4.3, $\bar{x}_N^+ - \mu_N \geq \bar{x}_N^+ - \delta > \kappa_{0N}/\gamma_N$. Finally $\kappa_{0N}/\gamma_N < \bar{x}_N^+ - m_N < \bar{x}_N^+$.

Assume that the property $\mu_{j+1} > 0$ and $\kappa_{0j+1}/\gamma_{j+1} < \bar{x}_{j+1}^+ - m_{j+1} < \bar{x}_{j+1}^+$ holds for one natural number $j+1 \in \{2, ..., N\}$. Then from proposition 3.2.8, $\kappa_{0j+1}/\gamma_{j+1} < \bar{x}_{j+1}^+ - m_{j+1} < \bar{x}_{j+1}^+ < (\kappa_{0j+1} + \kappa_{j+1})/\gamma_{j+1}$ implies that:
$0 < \left(\gamma_{j+1}(\bar{x}_{j+1}^+ - m_{j+1}) - \kappa_{0j+1}\right)/\kappa_{j+1} < \left(\gamma_{j+1}\bar{x}_{j+1}^+ - \kappa_{0j+1}\right)/\kappa_{j+1} < 1$. From property 6.4.1, the use of the monotonically increasing function ϕ_{j+1} in the inequality gives:
$\phi_{j+1}(0) < \phi_{j+1}\left(\left(\gamma_{j+1}(\bar{x}_{j+1}^+ - m_{j+1}) - \kappa_{0j+1}\right)/\kappa_{j+1}\right) < \phi_{j+1}\left(\left(\gamma_{j+1}\bar{x}_{j+1}^+ - \kappa_{0j+1}\right)/\kappa_{j+1}\right)$. With $\phi_{j+1}(0) = 0$ and $\phi_{j+1}\left(\left(\gamma_{j+1}\bar{x}_{j+1}^+ - \kappa_{0j+1}\right)/\kappa_{j+1}\right) = \bar{x}_j^+$, this implies:
$0 < \phi_{j+1}\left(\left(\gamma_{j+1}(\bar{x}_{j+1}^+ - m_{j+1}) - \kappa_{0j+1}\right)/\kappa_{j+1}\right) < \bar{x}_j^+$.
Then, $\bar{x}_j^+ - \phi_{j+1}\left(\left(\gamma_{j+1}(\bar{x}_{j+1}^+ - m_{j+1}) - \kappa_{0j+1}\right)/\kappa_{j+1}\right) > 0$. Finally, from definition 6.4.6, $\mu_j > 0$. As a consequence, $\bar{x}_j^+ - \mu_j < \bar{x}_j^+$ and under assumption 6.4.3, $\kappa_{0j}/\gamma_j < \bar{x}_j^+ - \delta < \bar{x}_j^+$. As $m_j = \min(\delta, \mu_j)$, the desired inequality $\kappa_{0j}/\gamma_j < \bar{x}_j^+ - m_j < \bar{x}_j^+$ holds.

Then, if the property holds for one natural number $j+1 \in \{2,...,N\}$, it also holds for j. By a mathematical induction, $\mu_i > 0$ and $\kappa_{0i}/\gamma_i < \bar{x}_i^+ - m_i < \bar{x}_i^+$ for all $i \in \{N,...,1\}$.

As a second base case, $\alpha_N = \min\left(\delta, x_{Nmax} - \bar{x}_N^+\right) > 0$ and $M_N = \alpha_N$ with definition 6.4.6. From definition 6.4.5, $\bar{x}_N^+ + \alpha_N > \bar{x}_N^+$. Moreover, under assumption 6.4.3, $\bar{x}_N^+ + \alpha_N \leq \bar{x}_N^+ + \delta < (\kappa_{0N} + \kappa_N)/\gamma_N$. Finally $\bar{x}_N^+ < \bar{x}_N^+ + M_N < (\kappa_{0N} + \kappa_N)/\gamma_N$.

Assume that the property $\alpha_{j+1} > 0$ and $\bar{x}_{j+1}^+ < \bar{x}_{j+1}^+ + M_{j+1} < (\kappa_{0j+1} + \kappa_{j+1})/\gamma_{j+1}$ holds for one natural number $j+1 \in \{3,...,N\}$. Then from proposition 3.2.8, $\kappa_{0j+1}/\gamma_{j+1} \leq \bar{x}_{j+1}^+ < \bar{x}_{j+1}^+ + M_{j+1} < (\kappa_{0j+1} + \kappa_{j+1})/\gamma_{j+1}$ implies that:
$0 \leq \left(\gamma_{j+1}\bar{x}_{j+1}^+ - \kappa_{0j+1}\right)/\kappa_{j+1} < \left(\gamma_{j+1}(\bar{x}_{j+1}^+ + M_{j+1}) - \kappa_{0j+1}\right)/\kappa_{j+1} < 1$. From property 6.4.1, the use of the monotonically increasing function ϕ_{j+1} in the inequality gives:
$\phi_{j+1}(0) \leq \phi_{j+1}\left(\left(\gamma_{j+1}\bar{x}_{j+1}^+ - \kappa_{0j+1}\right)/\kappa_{j+1}\right) < \phi_{j+1}\left(\left(\gamma_{j+1}(\bar{x}_{j+1}^+ + M_{j+1}) - \kappa_{0j+1}\right)/\kappa_{j+1}\right)$. With $\phi_{j+1}(0) = 0$ and $\phi_{j+1}\left(\left(\gamma_{j+1}\bar{x}_{j+1}^+ - \kappa_{0j+1}\right)/\kappa_{j+1}\right) = \bar{x}_j^+$, this implies:
$0 \leq \bar{x}_j^+ < \phi_{j+1}\left(\left(\gamma_{j+1}(\bar{x}_{j+1}^+ + M_{j+1}) - \kappa_{0j+1}\right)/\kappa_{j+1}\right)$.
Then, $\phi_{j+1}\left(\left(\gamma_{j+1}(\bar{x}_{j+1}^+ + M_{j+1}) - \kappa_{0j+1}\right)/\kappa_{j+1}\right) - \bar{x}_j^+ > 0$. Finally, from the definition 6.4.6, $\alpha_j > 0$. As a consequence, $\bar{x}_j^+ + \alpha_j > \bar{x}_j^+$ and under assumption 6.4.3, $\bar{x}_j^+ < \bar{x}_j^+ + \delta < (\kappa_{0j} + \kappa_j)/\gamma_j$. As $M_j = \min(\delta, \alpha_j)$, the desired inequality $\bar{x}_j^+ < \bar{x}_j^+ + M_j < (\kappa_{0j} + \kappa_j)/\gamma_j$ holds.

Then, if the property holds for one natural number $j+1 \in \{3,...,N\}$, it also holds for j. By a mathematical induction, $\alpha_i > 0$ and $\bar{x}_i^+ < \bar{x}_i^+ + M_i < (\kappa_{0i} + \kappa_i)/\gamma_i$ for all $i \in \{N,...,2\}$.

For $\mathbf{i = 1}$, the same steps are followed. The inequality $\kappa_{02}/\gamma_2 \leq \bar{x}_2^+ < \bar{x}_2^+ + M_2 < (\kappa_{02} + \kappa_2)/\gamma_2$ implies that $0 \leq \left(\gamma_2\bar{x}_2^+ - \kappa_{02}\right)/\kappa_2 < \left(\gamma_2(\bar{x}_2^+ + M_2) - \kappa_{02}\right)/\kappa_2 < 1$. From property 6.4.1, the use of the monotonically increasing function ϕ_2 in the inequality gives: $\phi_2(0) \leq \phi_2\left(\left(\gamma_2\bar{x}_2^+ - \kappa_{02}\right)/\kappa_2\right) < \phi_2\left(\left(\gamma_2(\bar{x}_2^+ + M_2) - \kappa_{02}\right)/\kappa_2\right)$. With $\phi_2(0) = 0$ and $\phi_2\left(\left(\gamma_2\bar{x}_2^+ - \kappa_{02}\right)/\kappa_2\right) = \bar{x}_1^+$, this implies: $0 \leq \bar{x}_1^+ < \phi_2\left(\left(\gamma_2(\bar{x}_2^+ + M_2) - \kappa_{02}\right)/\kappa_2\right)$. Then, $\phi_2\left(\left(\gamma_2(\bar{x}_2^+ + M_2) - \kappa_{02}\right)/\kappa_2\right) - \bar{x}_1^+ > 0$. Finally, from the definition 6.4.6, $\alpha_1 > 0$. As a consequence, $\bar{x}_1^+ + \alpha_1 > \bar{x}_1^+$ and under assumption 6.4.3, $\bar{x}_1^+ < \bar{x}_1^+ + \delta$. As $M_1 = \min(\delta, \alpha_1)$, then $\bar{x}_1^+ < \bar{x}_1^+ + M_1$ holds. Moreover, if $1 > u_{min} > (\gamma_1\bar{x}_1^+ - \kappa_{01})/\kappa_1$, then from assumption 6.4.3, $\bar{x}_1^+ < \bar{x}_1^+ + \delta < (\kappa_{01} + u_{min}\kappa_1)/\gamma_1$, and it follows that $\bar{x}_1^+ < \bar{x}_1^+ + M_1 < (\kappa_{01} + u_{min}\kappa_1)/\gamma_1$. □

C.4 Proof of lemma 6.4.3

Proof. The proof of this lemma is really similar to the equivalent proof for the negative loop in appendix C.2. It is shown that the boundaries of the region $\mathcal{B}^+$ are repellent, i.e.:

- $\dot{x}_i(\bar{x}_i^+ - m_i, x_{i-1}) \geq 0 \ \forall \ x_{i-1} \in [\bar{x}_{i-1}^+ - m_{i-1}, \bar{x}_{i-1}^+ + M_{i-1}] \ \forall \ i \in \{1,...,N\}$,
- $\dot{x}_i(\bar{x}_i^+ + M_i, x_{i-1}) \leq 0 \ \forall \ x_{i-1} \in [\bar{x}_{i-1}^+ - m_{i-1}, \bar{x}_{i-1}^+ + M_{i-1}] \ \forall \ i \in \{1,...,N\}$.

In order to prove that $\dot{x}_i(\bar{x}_i^+ - m_i, x_{i-1}) \geq 0 \ \forall \ x_{i-1} \in [\bar{x}_{i-1}^+ - m_{i-1}, \bar{x}_{i-1}^+ + M_{i-1}] \ \forall \ i \in \{2,...,N\}$, and $\dot{x}_i(\bar{x}_i^+ + M_i, x_{i-1}) \leq 0 \ \forall \ x_{i-1} \in [\bar{x}_{i-1}^+ - m_{i-1}, \bar{x}_{i-1}^+ + M_{i-1}] \ \forall \ i \in \{2,...,N\}$, then the same steps explained for the negative loop in the proof of lemma 6.4.1 can be reproduced by replacing all $\bar{x}^-$ by $\bar{x}^+$.

When $x_1 = \bar{x}_1^+ + M_1 > \bar{x}_1^+$, the x_1-vector field is defined as:
$\dot{x}_1(\bar{x}_1^+ + M_1, x_N) = \kappa_{01} + u_{min}\kappa_1 \mathrm{h}^+(x_N, \theta_N, n_N) - \gamma_1(\bar{x}_1^+ + M_1)$. Then, when evaluating this expression at the point $(\bar{x}_1^+ + M_1, x_{Nmax})$, the x_1-vector field becomes: $\dot{x}_1(\bar{x}_1^+ + M_1, x_{Nmax}) = \kappa_{01} + u_{min}\kappa_1 \mathrm{h}^+(x_{Nmax}, \theta_N, n_N) - \gamma_1(\bar{x}_1^+ + M_1)$. Two cases appear now depending on the value of u_{min}.

First case, if $1 > u_{min} > (\gamma_1 \bar{x}_1^+ - \kappa_{01})/\kappa_1$ then $x_{Nmax} = \phi_1^+\left((\gamma_1 \bar{x}_1^+ - \kappa_{01})/(u_{min}\kappa_1)\right)$. In this case, the x_1-vector field further becomes:
$\dot{x}_1(\bar{x}_1^+ + M_1, x_{Nmax}) = \kappa_{01} + u_{min}\kappa_1 \mathrm{h}^+(\phi_1^+\left((\gamma_1 \bar{x}_1^+ - \kappa_{01})/(u_{min}\kappa_1)\right), \theta_N, n_N) - \gamma_1(\bar{x}_1^+ + M_1)$. From property 6.4.1 and proposition 6.4.3, $\dot{x}_1(\bar{x}_1^+ + M_1, x_{Nmax}) = \kappa_{01} + u_{min}\kappa_1\left((\gamma_1 \bar{x}_1^+ - \kappa_{01})/(u_{min}\kappa_1)\right) - \gamma_1(\bar{x}_1^+ + M_1)$. Then, $\dot{x}_1(\bar{x}_1^+ + M_1, x_{Nmax}) = -\gamma_1 M_1 < 0$. Now, the strictly monotonic property of the increasing Hill function implies that for all $x_N \leq x_{Nmax}$, $\mathrm{h}^+(x_N, \theta_N, n_N) \leq \mathrm{h}^+(x_{Nmax}, \theta_N, n_N) \leq 0$. In the x_1-vector field, for x_1 fixed, this property induces $\dot{x}_1(\bar{x}_1^+ + M_1, x_N) \leq \dot{x}_1(\bar{x}_1^+ + M_1, x_{Nmax}) < 0$ for all $x_N \leq x_{Nmax}$. In particular, as $\bar{x}_N^+ + M_N \leq x_{Nmax}$, then for all $x_N \in [\bar{x}_N^+ - m_N, \bar{x}_N^+ + M_N]$ the x_1-vector field is negative: $\dot{x}_1(\bar{x}_1^+ + M_1, x_N) \leq 0$. This inequality means that a trajectory that starts in the region $\mathcal{B}^+$ cannot leave the region through the boundary $x_1 = \bar{x}_1^+ + M_1$ in the first case.

Second case, $u_{min} \leq (\gamma_1 \bar{x}_1^+ - \kappa_{01})/\kappa_1$. In this case, the x_1-vector field becomes: $\dot{x}_1(x_1, x_N) = \kappa_{01} + u_{min}\kappa_1 \mathrm{h}^+(x_N, \theta_N, n_N) - \gamma_1(\bar{x}_1^+ + M_1)$. By evaluating this expression on the wall $x_1 = \bar{x}_1^+$ and using the condition on u_{min}, the following inequality comes up: $\dot{x}_1(\bar{x}_1^+, x_N) \leq (\kappa_{01} - \gamma_1 \bar{x_1})\left(1 - \mathrm{h}^+(x_N, \theta_N, n_N)\right)$. The properties of the system explained in proposition 3.2.8 gives $\bar{x}_1^+ \in [\kappa_{01}/\gamma_1, (\kappa_{01} + \kappa_1)/\gamma_1[$ and the increasing Hill function meets the condition $\mathrm{h}^+(x_N, \theta_N, n_N) \in [0, 1[$. This induces $\dot{x}_1(\bar{x}_1^+, x_N) \leq 0$. Moreover, for x_N fixed and $x_1 > \bar{x}_1^+$, the linear degradation term $-\gamma_1 x_1$ in the x_1-vector field expression gives: $\dot{x}_1(x_1, x_N) < \dot{x}_1(\bar{x}_1^+, x_N) \leq 0$. Hence, $\dot{x}_1(x_1, x_N) < 0$ $\forall\ x_N \geq 0$ and $\forall\ x_1 > \bar{x}_1^+$. In particular, for all $x_N \in [\bar{x}_N^+ - m_N, \bar{x}_N^+ + M_N]$ the x_1-vector field is negative: $\dot{x}_1(\bar{x}_1^+ + M_1, x_N) \leq 0$. This inequality means that a trajectory that starts in the region $\mathcal{B}^+$ cannot leave the region through the boundary $x_1 = \bar{x}_1^+ + M_1$ in the second case.

When $x_1 = \bar{x}_1^+ - m_1 < \bar{x}_1^+$, the x_1-vector field is defined as:
$\dot{x}_1(\bar{x}_1^+ - m_1, x_N) = \kappa_{01} + u_{max}\kappa_1 \mathrm{h}^+(x_N, \theta_N, n_N) - \gamma_1(\bar{x}_1^+ - m_1)$. Then, when evaluating this expression at the point $(\bar{x}_1^+ - m_1, x_{Nmin})$, the x_1-vector field becomes: $\dot{x}_1(\bar{x}_1^+ - m_1, x_{Nmin}) = \kappa_{01} + u_{max}\kappa_1 \mathrm{h}^+(x_{Nmin}, \theta_N, n_N) - \gamma_1(\bar{x}_1^+ - m_1)$.
With the definition of $x_{Nmin} = \phi_1^+\left((\gamma_1 \bar{x}_1^+ - \kappa_{01})/(u_{max}\kappa_1)\right)$, the x_1-vector field further becomes $\dot{x}_1(\bar{x}_1^+ - m_1, x_{Nmin}) = \kappa_{01} + u_{max}\kappa_1 \mathrm{h}^+(\phi_1^+\left((\gamma_1 \bar{x}_1^+ - \kappa_{01})/(u_{max}\kappa_1)\right), \theta_N, n_N) - \gamma_1(\bar{x}_1^+ - m_1)$. From property 6.4.1 and proposition 6.4.3, $\dot{x}_1(\bar{x}_1^+ - m_1, x_{Nmin}) = \kappa_{01} + u_{max}\kappa_1\left((\gamma_1 \bar{x}_1^+ - \kappa_{01})/(u_{max}\kappa_1)\right) - \gamma_1(\bar{x}_1^+ - m_1)$. Then, $\dot{x}_1(\bar{x}_1^+ - m_1, x_{Nmin}) = \gamma_1 m_1 > 0$. Now, the strictly monotonic property of the increasing Hill function implies that for all $x_N \geq x_{Nmin}$, $\mathrm{h}^+(x_N, \theta_N, n_N) \geq \mathrm{h}^+(x_{Nmin}, \theta_N, n_N) \geq 0$. In the x_1-vector field, for x_1 fixed, this property induces $\dot{x}_1(\bar{x}_1^+ - m_1, x_N) \geq \dot{x}_1(\bar{x}_1^+ - m_1, x_{Nmin}) > 0$ for all $x_N \geq x_{Nmin}$. In particular, as $\bar{x}_N^+ - m_N \geq x_{Nmin}$, then for all $x_N \in [\bar{x}_N^+ - m_N, \bar{x}_N^+ + M_N]$ the x_1-vector field is positive: $\dot{x}_1(\bar{x}_1^+ - m_1, x_N) \geq 0$. This inequality means that a trajectory that starts in the region $\mathcal{B}^+$ cannot leave the region through the boundary $x_1 = \bar{x}_1^+ - m_1$.

Finally, if $x(0) \in \mathcal{B}^+$ then $x(t) \in \mathcal{B}^+\ \forall\ t \geq 0$. The region $\mathcal{B}^+$ is invariant. □

Appendix D

Supplementary material of chapter 8

D.1 Proof of lemma 8.3.1

Proof. For the proof if this lemma, the influence of n on the function Z^*_{1n} is investigated.

First, as a reminder, from the proof of proposition 8.2.1, $H_n(x) \geq 0 \iff x \geq \kappa_{01}/\gamma_1$ and $H_n(\kappa_{01}/\gamma_1) = 0$. Moreover, for $x \geq \kappa_{01}/\gamma_1$, H_n is strictly increasing. From assumption 8.3.1, $\alpha = 1/\mathrm{h}^-(\bar{x}^*_1, \theta, n) = (\theta^n + (\bar{x}^*_1)^n)/\theta^n$, leading to $H_n(\bar{x}^*_1) = (\gamma_1 \bar{x}^*_1 - \kappa_{01})/\kappa_1 = \mathrm{h}^*(\bar{x}^*_N, \theta_N, n_N)$. This implies that $H_n(\bar{x}^*_1)$ and $H_n(\kappa_{01}/\gamma_1)$ neither depend on θ nor n. The influence of the parameter n on H_n is investigated:

$$\frac{\partial H_n}{\partial n}(x) = \frac{(\gamma_1 x - \kappa_{01})}{\kappa_1} \left[\frac{\theta^n (\bar{x}^*_1)^n \ln(\frac{\theta}{\bar{x}^*_1}) + x^n \theta^n \ln(\frac{x}{\theta}) + x^n (\bar{x}^*_1)^n \ln(\frac{x}{\bar{x}^*_1})}{(\theta^n + (\bar{x}^*_1)^n)^2} \right].$$

Again, the study of this dependence is important for $x \geq \kappa_{01}/\gamma_1$, leading to $(\gamma_1 x - \kappa_{01})/\kappa_1 \geq 0$. With these conditions, $\partial H_n/\partial n \geq 0 \Leftrightarrow [\theta^n (\bar{x}^*_1)^n \ln(\theta/\bar{x}^*_1) + x^n \theta^n \ln(x/\theta) + x^n (\bar{x}^*_1)^n \ln(x/\bar{x}^*_1)] \geq 0 \Leftrightarrow h(x) \geq \theta^n (\bar{x}^*_1)^n \ln(\bar{x}^*_1/\theta)$, where $h(x) = x^n \theta^n \ln(x/\theta) + x^n (\bar{x}^*_1)^n \ln(x/\bar{x}^*_1)$. This new function h can be studied:

$$\frac{\partial h}{\partial x} = x^{n-1} \left[n\theta^n \ln(\frac{x}{\theta}) + (\bar{x}^*_1)^n n \ln(\frac{x}{\bar{x}^*_1}) + \theta^n + (\bar{x}^*_1)^n \right].$$

From this expression it is possible to deduce that:

$$\begin{aligned} \frac{\partial h}{\partial x} \geq 0 &\Leftrightarrow n\theta^n \ln(\frac{x}{\theta}) + n(\bar{x}^*_1)^n \ln(\frac{x}{\bar{x}^*_1}) + \theta^n + (\bar{x}^*_1)^n \geq 0 \\ &\Leftrightarrow x \geq \exp\left(\frac{\theta^n \ln(\theta) + (\bar{x}^*_1)^n \ln(\bar{x}^*_1)}{\theta^n + (\bar{x}^*_1)^n} - \frac{1}{n} \right) = X_1 \end{aligned}$$

The function h also satisfies: $h(0) = 0$, $\lim\limits_{x \to +\infty} h(x) = +\infty$ and $h(\bar{x}^*_1) = \theta^n (\bar{x}^*_1)^n \ln(\bar{x}^*_1/\theta)$. The function h is decreasing and negative until $x = X_1$ and then starts increasing for $x > X_1$, and eventually becomes positive .

Now, the hypothesis $\theta < \bar{x}^*_1$ on lemma 8.3.1 gives: $h(\bar{x}^*_1) = \theta^n (\bar{x}^*_1)^n \ln(\bar{x}^*_1/\theta) > 0$, leading to $h(x) \geq \theta^n (\bar{x}^*_1)^n \ln(\bar{x}^*_1/\theta) \Leftrightarrow x \geq \bar{x}^*_1$. Hence, for $x \geq \kappa_{01}/\gamma_1$, from the previous equivalence $\partial H_n/\partial n \geq 0 \Leftrightarrow h(x) \geq \theta^n (\bar{x}^*_1)^n \ln(\bar{x}^*_1/\theta)$, it is possible to conclude that $\partial H_n/\partial n > 0 \Leftrightarrow x > \bar{x}^*_1$. Consequently, for $\kappa_{01}/\gamma_1 < x < \bar{x}^*_1$, $\partial H_n/\partial n < 0$.

In the end, with $\theta < \bar{x}^*_1$, an increase of parameter n decreases the function H_n for $\kappa_{01}/\gamma_1 < x < \bar{x}^*_1$ and increases H_n for $x > \bar{x}^*_1$. Moreover, it is possible to check that for $\kappa_{01}/\gamma_1 < x < \bar{x}^*_1$,

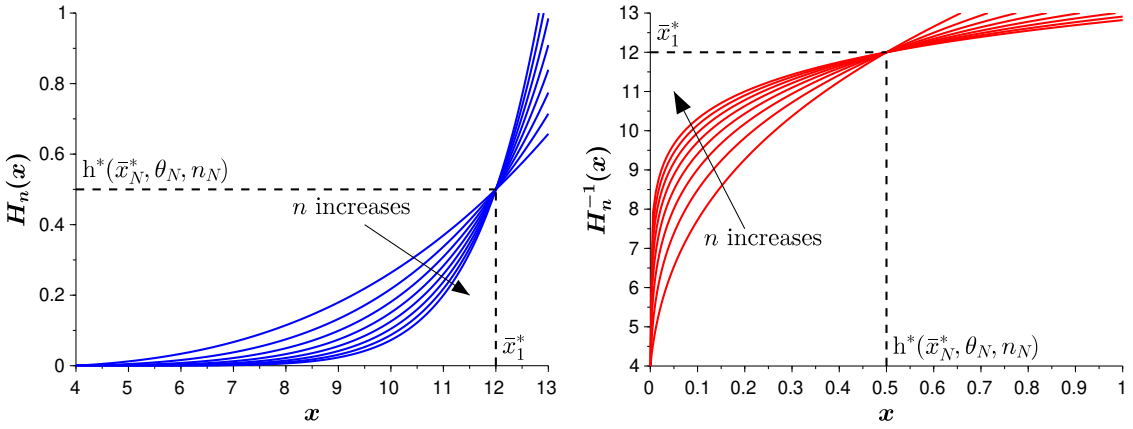

Figure D.1.1: Left: influence of n on the function $H_n(x)$. As explained in the proof, when n increases, the function decreases if $x < \bar{x}_1^*$ and increases if $x > \bar{x}_1^*$. Right: influence of n on the function $H_n^{-1}(x)$. The variation is deduced from that of $H_n(x)$.

$H_n(x) \underset{n\to+\infty}{\longrightarrow} 0$ and for $x > \bar{x}_1^*$, $H_n(x) \underset{n\to+\infty}{\longrightarrow} +\infty$. An illustration of this is shown in the left plot of figure D.1.1.

Now from this result on H_n, the influence of n on its inverse H_n^{-1} and on H_{1n}^* can be investigated. For more clarity, the notations $H_n(x,n)$ and $H_n^{-1}(x,n)$ will be used. By definition of the inverse function: $H_n^{-1}\left(H_n(x,n),n\right) = G(x,n) = x$. Hence:

$$\frac{\partial G}{\partial n}(x,n) = 0.$$

At the same time, the definition of partial derivatives for a function with several variables can be applied:

$$\frac{\partial G}{\partial n}(x,n) = \frac{\partial H_n^{-1}}{\partial x}\left(H_n(x,n),n\right) \times \frac{\partial H_n}{\partial n}(x,n) + \frac{\partial H_n^{-1}}{\partial n}\left(H_n(x,n),n\right) = 0.$$

It follows that:

$$\frac{\partial H_n^{-1}}{\partial n}\left(H_n(x,n),n\right) = -\frac{\partial H_n^{-1}}{\partial x}\left(H_n(x,n),n\right) \times \frac{\partial H_n}{\partial n}(x,n).$$

As H_n^{-1} and H_n are increasing functions, $\partial H_n^{-1}/\partial x\left(H(x,n),n\right) \geq 0$.

For any $\kappa_{01}/\gamma_1 < x < \bar{x}_1^*$, $H_n(x,n) < H_n(\bar{x}_1^*,n) = \mathrm{h}^*(\bar{x}_N^*,\theta_N,n_N)$, and $\partial H_n/\partial n\,(x,n) < 0$ from the previous calculations. Hence $\forall\ y < \mathrm{h}^*(\bar{x}_N^*,\theta_N,n_N)$, $\partial H_n^{-1}/\partial n\,(y,n) > 0$.

Similarly, for any $x > \bar{x}_1^*$, $H_n(x,n) > H_n(\bar{x}_1^*,n) = \mathrm{h}^*(\bar{x}_N^*,\theta_N,n_N)$, and $\partial H_n/\partial n\,(x,n) > 0$ from the previous calculations. Hence $\forall\ y > \mathrm{h}^*(\bar{x}_N^*,\theta_N,n_N)$, $\partial H_n^{-1}/\partial n\,(y,n) < 0$.

It follows that $H_n^{-1}(x)$ increases with n when $x < \mathrm{h}^*(\bar{x}_N^*,\theta_N,n_N)$ and $H_n^{-1}(x)$ decreases with n when $x > \mathrm{h}^*(\bar{x}_N^*,\theta_N,n_N)$. Moreover, from the limits of H_n when n tends to infinity, it is possible to conclude that for $x > 0$ and $x \neq \mathrm{h}^*(\bar{x}_N^*,\theta_N,n_N)$, $H_n^{-1}(x) \underset{n\to+\infty}{\longrightarrow} \bar{x}_1^*$, and $H_n^{-1}(\mathrm{h}^*(\bar{x}_N^*,\theta_N,n_N)) = \bar{x}_1^*$. An illustration of this is shown in the right plot of figure D.1.1.

These results about the influence of n on H_n^{-1} are essential in order to determine the influence of n on the nullcline H_{1n}^*. Indeed, $\partial H_{1n}^*/\partial n(x) = \partial H_n^{-1}/\partial n(\mathrm{h}^*(x,\theta_N,n_N))$. Two cases appear depending on the loop:

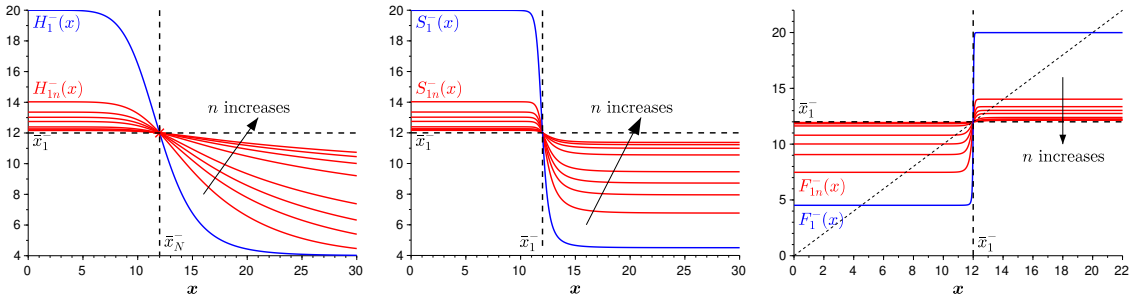

Figure D.1.2: The three plots concern the negative feedback loop. The functions of the uncontrolled system are depicted in blue, and for system (8.2.1) with synthetic modification (8.2.2) the functions are depicted in red. Left: influence of n on the x_1-nullcline H_{1n}^-. Middle: influence of n on the composition of nullclines S_{1n}^-. Right: influence of n on F_{1n}^-. For n large enough, $\bar{x}_1^-$ is the unique fixed point.

- For the positive loop, for any $x < \bar{x}_N^+$, $\mathrm{h}^+(x, \theta_N, n_N) < \mathrm{h}^+(\bar{x}_N^+, \theta_N, n_N)$.
  Hence, $\partial H_n^{-1}/\partial n \left(\mathrm{h}^+(x, \theta_N, n_N), n\right) > 0$. Finally, for any $x < \bar{x}_N^+$, $\partial H_{1n}^+/\partial n(x) > 0$. Similarly, for any $x > \bar{x}_N^+$, $\mathrm{h}^+(x, \theta_N, n_N) > \mathrm{h}^+(\bar{x}_N^+, \theta_N, n_N)$.

  Hence, $\partial H_n^{-1}/\partial n \left(\mathrm{h}^+(x, \theta_N, n_N), n\right) < 0$. Finally, for any $x > \bar{x}_N^+$, $\partial H_{1n}^+/\partial n(x) < 0$. It follows that $H_{1n}^+(x)$ increases with n when $x < \bar{x}_N^+$ and $H_{1n}^+(x)$ decreases with n when $x > \bar{x}_N^+$. The x_1-nullcline converges towards to fixed point $\bar{x}_1^+$ when n increases.

- For the negative loop, for any $x < \bar{x}_N^-$, $\mathrm{h}^-(x, \theta_N, n_N) > \mathrm{h}^-(\bar{x}_N^-, \theta_N, n_N)$.
  Hence, $\partial H_n^{-1}/\partial n \left(\mathrm{h}^-(x, \theta_N, n_N), n\right) < 0$. Finally, for any $x < \bar{x}_N^-$, $\partial H_{1n}^-/\partial n(x) < 0$. Similarly, for any $x > \bar{x}_N^-$, $\mathrm{h}^-(x, \theta_N, n_N) < \mathrm{h}^-(\bar{x}_N^-, \theta_N, n_N)$.

  Hence, $\partial H_n^{-1}/\partial n \left(\mathrm{h}^-(x, \theta_N, n_N), n\right) > 0$. Finally, for any $x > \bar{x}_N^-$, $\partial H_{1n}^-/\partial n(x) > 0$. It follows that $H_{1n}^-(x)$ decreases with n when $x < \bar{x}_N^-$ and $H_{1n}^-(x)$ increases with n when $x > \bar{x}_N^+$. The x_1-nullcline converges towards to fixed point $\bar{x}_1^-$ when n increases.

An illustration of these results for the negative loop are shown in the left plot of figure D.1.2. For the positive loop, the illustrations are exactly the same with increasing functions.

It is straightforward to see that $\partial S_{1n}^*/\partial n(x) = \partial H_{1n}^*/\partial n \left(H_N \circ ... \circ H_2(x)\right)$ from the definition of S_{1n}^*. From the dependence of H_{1n}^* on n, the influence of n on S_{1n}^* is easily induced for both loops:

- For the positive loop, for any $x < \bar{x}_1^+$, $H_N \circ ... \circ H_2(x) < H_N \circ ... \circ H_2(\bar{x}_1^+) = \bar{x}_N^+$.
  Hence, $\partial H_{1n}^+/\partial n \left(H_N \circ ... \circ H_2(x)\right) > 0$. Finally, for any $x < \bar{x}_1^+$, $\partial S_{1n}^+/\partial n(x) > 0$. Similarly, for any $x > \bar{x}_1^+$, $H_N \circ ... \circ H_2(x) > H_N \circ ... \circ H_2(\bar{x}_1^+) = \bar{x}_N^+$.
  Hence, $\partial H_{1n}^+/\partial n \left(H_N \circ ... \circ H_2(x)\right) < 0$. Finally, for any $x > \bar{x}_1^+$, $\partial S_{1n}^+/\partial n(x) < 0$. It follows that $S_{1n}^+(x)$ increases with n when $x < \bar{x}_1^+$ and $S_{1n}^+(x)$ decreases with n when $x > \bar{x}_1^+$. The increasing function S_{1n}^+ converges towards the fixed point $\bar{x}_1^+$ when n increases.

- For the negative loop, for any $x < \bar{x}_1^-$, $H_N \circ ... \circ H_2(x) < H_N \circ ... \circ H_2(\bar{x}_1^-) = \bar{x}_N^-$.
  Hence, $\partial H_{1n}^-/\partial n \left(H_N \circ ... \circ H_2(x)\right) < 0$. Finally, for any $x < \bar{x}_1^-$, $\partial S_{1n}^-/\partial n(x) < 0$. Similarly, for any $x > \bar{x}_1^-$, $H_N \circ ... \circ H_2(x) > H_N \circ ... \circ H_2(\bar{x}_1^-) = \bar{x}_N^-$.
  Hence, $\partial H_{1n}^-/\partial n \left(H_N \circ ... \circ H_2(x)\right) > 0$. Finally, for any $x > \bar{x}_1^-$, $\partial S_{1n}^-/\partial n(x) > 0$. It follows that $S_{1n}^-(x)$ decreases with n when $x < \bar{x}_1^-$ and $S_{1n}^-(x)$ increases with n when $x > \bar{x}_1^-$. The decreasing function S_{1n}^- converges towards the fixed point $\bar{x}_1^-$ when n increases.

An illustration of these results for the negative loop are shown in the middle plot of figure D.1.2. For the positive loop, the illustrations are the same with increasing functions.

At this point, it is possible to conclude that if assumption 8.3.1 holds and with the condition $\theta < \bar{x}_1^+$, then there exists $\tilde{n}^+$ such that for any $n > \tilde{n}^+$, the function S_{1n}^+ verifies: $S_{1n}^+(x) > x$ for any $x < \bar{x}_1^+$, $S_{1n}^+(x) < x$ for any $x > \bar{x}_1^+$, and $S_{1n}^+(\bar{x}_1^+) = \bar{x}_1^+$. Hence, lemma 8.3.1 is proved for the positive loop.

For the negative loop, the influence of n on F_{1n}^- must be investigated. The notation $F_{1n}^-(x,n) = S_{1n}^-\left(S_{1n}^-(x,n),n\right)$ will be used for more clarity. The definition of partial derivatives for functions with several variables is used:

$$\frac{\partial F_{1n}^-}{\partial n}(x,n) = \frac{\partial S_{1n}^-}{\partial x}\left(S_{1n}^-(x,n),n\right) \times \frac{\partial S_{1n}^-}{\partial n}(x,n) + \frac{\partial S_{1n}^-}{\partial n}\left(S_{1n}^-(x,n),n\right).$$

As a reminder, for any $x \geq 0$, S_{1n}^- is a decreasing function, hence: $\partial S_{1n}^-/\partial x\left(S_{1n}^-(x,n),n\right) < 0$ for any $x > 0$. Now, assume that $x < \bar{x}_1^-$, then from the definition of S_{1n}^-, $S_{1n}^-(x) > \bar{x}_1^-$. From the previous results, it follows that $\partial S_{1n}^-/\partial n\,(x,n) < 0$ and $\partial S_{1n}^-/\partial n\left(S_{1n}^-(x,n),n\right) > 0$. Hence, $\partial F_{1n}^-/\partial n(x,n)$ =(-)×(-)+(+). Finally, for any $x < \bar{x}_1^-$, $\partial F_{1n}^-/\partial n(x,n) > 0$. Similarly, assume that $x > \bar{x}_1^-$, then from the definition of S_{1n}^-, $S_{1n}^-(x) < \bar{x}_1^-$. From the previous results, it follows that $\partial S_{1n}^-/\partial n\,(x,n) > 0$ and $\partial S_{1n}^-/\partial n\left(S_{1n}^-(x,n),n\right) < 0$. Hence, $\partial F_{1n}^-/\partial n(x,n)$ =(-)×(+)+(-). Finally, for any $x > \bar{x}_1^-$, $\partial F_{1n}^-/\partial n(x,n) < 0$. It follows that $F_{1n}^-(x)$ increases with n when $x < \bar{x}_1^-$ and $F_{1n}^-(x)$ decreases with n when $x > \bar{x}_1^-$. In conclusion, the increasing function F_{1n}^- converges towards the fixed point $\bar{x}_1^-$ when n increases.

An illustration of this result is presented in the right plot of figure D.1.2. Finally, it is possible to conclude that if assumption 8.3.1 holds and with the condition $\theta < \bar{x}_1^-$, then there exists $\tilde{n}^-$ such that for any $n > \tilde{n}^-$, the function F_{1n}^- satisfies: $F_{1n}^-(x) > x$ for any $x < \bar{x}_1^-$, $F_{1n}^-(x) < x$ for any $x > \bar{x}_1^-$, and $F_{1n}^-(\bar{x}_1^-) = \bar{x}_1^-$. Hence, lemma 8.3.1 is proved for the negative loop. □

Appendix E

Supplementary material of chapter 9

E.1 Proof of lemma 9.3.1

Proof. **Four cases will be treated separately:**

- Case 1A: $P^-(X)$ has even degree $2n$ and n is even,
- Case 1B: $P^-(X)$ has even degree $2n$ and n is odd,
- Case 2A: $P^-(X)$ has odd degree $2n+1$ and n is odd,
- Case 2B: $P^-(X)$ has odd degree $2n+1$ and n is even.

It is first assumed that $\mathbf{P^-(X)}$ has even degree 2n. The polynomial $P^-(X)$ is developed:

$$P^-(X) = a_{1,1}X^{2n} + a_{2,1}X^{2n-1} + a_{1,2}X^{2n-2} + a_{2,2}X^{2n-3} + ... + a_{1,n}X^2 + a_{2,n}X + a_{1,n+1}.$$

Its associated Routh table is:

$a_{1,1}$	$a_{1,2}$	$a_{1,3}$	$\cdots$	$\cdots$	$\cdots$	$a_{1,n-1}$	$a_{1,n}$	$a_{1,n+1}$
$a_{2,1}$	$a_{2,2}$	$a_{2,3}$	$\cdots$	$\cdots$	$\cdots$	$a_{2,n-1}$	$a_{2,n}$	0
$a_{3,1}$	$a_{3,2}$	$a_{3,3}$	$\cdots$	$\cdots$	$\cdots$	$a_{3,n-1}$	$a_{3,n}$	0
$a_{4,1}$	$a_{4,2}$	$a_{4,3}$	$\cdots$	$\cdots$	$\cdots$	$a_{4,n-1}$	0	
$a_{5,1}$	$a_{5,2}$	$a_{5,3}$	$\cdots$	$\cdots$	$a_{5,n-2}$	$a_{5,n-1}$	0	
$a_{6,1}$	$a_{6,2}$	$a_{6,3}$	$\cdots$	$a_{6,n-3}$	$a_{6,n-2}$	0		
$\vdots$	$\vdots$							
$a_{2n,1}$	0							
$a_{2n+1,1}$	0							

Similarly, the polynomial $R(X) = P^-(X) + A$, with $A \geq 0$ can be developed:

$$R(X) = a_{1,1}X^{2n} + a_{2,1}X^{2n-1} + a_{1,2}X^{2n-2} + a_{2,2}X^{2n-3} + ... + a_{1,n}X^2 + a_{2,n}X + a_{1,n+1} + A.$$

With $a_{i,j} = (-1/a_{i-1,1})\left[a_{i-2,1}a_{i-1,j+1} - a_{i-1,1}a_{i-2,j+1}\right] \forall\, i \in \{3, ..., 2n+1\}$ and $\forall\, j \in \{1, ..., n+1\}$, its associated Routh table can be inferred from that of $P^-(X)$:

$a_{1,1}$	$a_{1,2}$	$a_{1,3}$	$\cdots$	$\cdots$	$\cdots$	$a_{1,n-1}$	$a_{1,n}$	$\boldsymbol{a_{1,n+1}+A}$
$a_{2,1}$	$a_{2,2}$	$a_{2,3}$	$\cdots$	$\cdots$	$\cdots$	$a_{2,n-1}$	$a_{2,n}$	0
$a_{3,1}$	$a_{3,2}$	$a_{3,3}$	$\cdots$	$\cdots$	$\cdots$	$a_{3,n-1}$	$\boldsymbol{\tilde{a}_{3,n}}$	0
$a_{4,1}$	$a_{4,2}$	$a_{4,3}$	$\cdots$	$\cdots$	$\cdots$	$\boldsymbol{\tilde{a}_{4,n-1}}$	0	
$a_{5,1}$	$a_{5,2}$	$a_{5,3}$	$\cdots$	$\cdots$	$\boldsymbol{\tilde{a}_{5,n-2}}$	$\boldsymbol{\tilde{a}_{5,n-1}}$	0	
$a_{6,1}$	$a_{6,2}$	$a_{6,3}$	$\cdots$	$\boldsymbol{\tilde{a}_{6,n-3}}$	$\boldsymbol{\tilde{a}_{6,n-2}}$	0		
$\vdots$	$\vdots$							
$\boldsymbol{\tilde{a}_{2n,1}}$	0							
$\boldsymbol{\tilde{a}_{2n+1,1}}$	0							

where the terms in bold are those that are perturbed from the addition of A, and are therefore different from the equivalent term in the Routh table of $P^-(X)$. It is possible to observe that from the row $i = 3$, the perturbation shifts left at each new row. It means that n rows are needed before the perturbation reaches the first term in the first column, which is $\tilde{a}_{n+2,1}$.

Moreover, it is possible to show by induction the following property:

"**H1**: if $i \leq n+2$, any term in the i-th row of the Routh table of $R(X)$ can be expressed as: $\tilde{a}_{i,j} = a_{i,j} - \alpha_{i,j}A$ if i is even, and $\tilde{a}_{i,j} = a_{i,j} + \alpha_{i,j}A$ if i is odd, with $\alpha_{i,j} \geq 0$. When $\alpha_{i,j} = 0$, the term is not perturbed."

Indeed, as a base case, $\tilde{a}_{3,n} = (-1/a_{2,1})\left[a_{1,1}0 - a_{2,1}(a_{1,n+1}+A)\right] = (-1/a_{2,1})\left[a_{1,1}0 - a_{2,1}a_{1,n+1}\right] + A = a_{3,n} + \alpha_{3,n}A$, with $\alpha_{3,n} = 1 > 0$. All the other terms in the row $i = 3$ are not perturbed. It is assumed that **H1** is true until row $3 < i \leq n+2$. Then any term in this row verifies: $\tilde{a}_{i,j} = (-1/a_{i-1,1})\left[a_{i-2,1}\tilde{a}_{i-1,j+1} - a_{i-1,1}\tilde{a}_{i-2,j+1}\right]$ (the terms $a_{*,1}$ are not perturbed because $i \leq n+2$). Then, from **H1**, two cases appear:

- if i is even: $\tilde{a}_{i,j} = (-1/a_{i-1,1})\left[a_{i-2,1}(a_{i-1,j+1} + \alpha_{i-1,j+1}A) - a_{i-1,1}(a_{i-2,j+1} - \alpha_{i-2,j+1}A)\right]$, and then by developing $\tilde{a}_{i,j} = a_{i,j} - (1/a_{i-1,1})\left[a_{i-2,1}\alpha_{i-1,j+1} + a_{i-1,1}\alpha_{i-2,j+1}\right]A = a_{i,j} - \alpha_{i,j}A$. From proposition 9.3.3, $\alpha_{i,j} \geq 0$.
- if i is odd: $\tilde{a}_{i,j} = (-1/a_{i-1,1})\left[a_{i-2,1}(a_{i-1,j+1} - \alpha_{i-1,j+1}A) - a_{i-1,1}(a_{i-2,j+1} + \alpha_{i-2,j+1}A)\right]$, and then by developing $\tilde{a}_{i,j} = a_{i,j} + (1/a_{i-1,1})\left[a_{i-2,1}\alpha_{i-1,j+1} + a_{i-1,1}\alpha_{i-2,j+1}\right]A = a_{i,j} + \alpha_{i,j}A$. From proposition 9.3.3, $\alpha_{i,j} \geq 0$.

By induction, **H1** is proved.

Now, it is possible to distinguish the two cases 1A and 1B. First, it is assumed that n is even. In this case, the line $i = n+2$ for which the perturbation reaches the first column is even. It follows from **H1** that $\tilde{a}_{n+2,1} = a_{n+2,1} - \alpha_{n+2,1}A$. In this case, it is straightforward to see that there exists $\tilde{A} > 0$ such that $\forall\ A > \tilde{A}$, $\tilde{a}_{n+2,1} < 0$. Hence, there is a change of sign in the first column of the Routh table of $R(X)$, and lemma 9.3.1 is proved in case 1A.

If n is odd, the line $i = n+2$ for which the perturbation reaches the first column is odd. It follows from **H1** that $\tilde{a}_{n+2,1} = a_{n+2,1} + \alpha_{n+2,1}A$. Hence, $\tilde{a}_{n+2,1}$ will never change sign, no matter the value of A. In this case, the bottom term $\tilde{a}_{n+3,1}$ in the first column is investigated: $\tilde{a}_{n+3,1} = (-1/\tilde{a}_{n+2,1})\left[a_{n+1,1}\tilde{a}_{n+2,2} - \tilde{a}_{n+2,1}\tilde{a}_{n+1,2}\right]$.
From **H1**, $\tilde{a}_{n+3,1} = (-1/(a_{n+2,1} + \alpha_{n+2,1}A))\left[a_{n+1,1}(a_{n+2,2} + \alpha_{n+2,2}A) - (a_{n+2,1} + \alpha_{n+2,1}A)(a_{n+1,2} - \alpha_{n+1,2}A)\right]$. By developing and using $\left[a_{n+1,1}a_{n+2,2} - a_{n+2,1}a_{n+1,2}\right] = -a_{n+3,1}a_{n+2,1} < 0$, the perturbed term becomes: $\tilde{a}_{n+3,1} = (-1/(a_{n+2,1} + \alpha_{n+2,1}A)) \times \left[A^2c_1 + Ac_2 + c_3\right]$, where $c_1 = \alpha_{n+2,1}\alpha_{n+1,2} > 0$, $c_3 = -a_{n+3,1}a_{n+2,1} < 0$ from proposition 9.3.3, and $c_2 = a_{n+1,1}\alpha_{n+2,2} + a_{n+2,1}\alpha_{n+1,2} - \alpha_{n+2,1}a_{n+1,2}$. Then, there exists $\tilde{A} > 0$ such that $\forall\ 0 < A < \tilde{A}$, $A^2c_1 + Ac_2 + c_3 < 0$, $\tilde{A}^2c_1 + \tilde{A}c_2 + c_3 = 0$ and $\forall\ A > \tilde{A} > 0$, $A^2c_1 + Ac_2 + c_3 > 0$. As $(-1/(a_{n+2,1} + \alpha_{n+2,1}A)) < 0$, $\forall\ A > \tilde{A}$, $\tilde{a}_{n+3,1} < 0$. Finally, there is a change of sign in the first column of the Routh table of $R(X)$, and lemma 9.3.1 is proved in case 1B.

It is now assumed that $\mathbf{P^-(X)}$ has odd degree $\mathbf{2n+1}$. The polynomial $P^-(X)$ is developed:

$$P^-(X) = a_{1,1}X^{2n+1} + a_{2,1}X^{2n} + a_{1,2}X^{2n-1} + a_{2,2}X^{2n-2} + ... + a_{2,n}X^2 + a_{1,n+1}X + a_{2,n+1}.$$

Its associated Routh table is:

$a_{1,1}$	$a_{1,2}$	$a_{1,3}$	$\cdots$	$\cdots$	$\cdots$	$\cdots$	$a_{1,n}$	$a_{1,n+1}$
$a_{2,1}$	$a_{2,2}$	$a_{2,3}$	$\cdots$	$\cdots$	$\cdots$	$\cdots$	$a_{2,n}$	$a_{2,n+1}$
$a_{3,1}$	$a_{3,2}$	$a_{3,3}$	$\cdots$	$\cdots$	$\cdots$	$\cdots$	$a_{3,n}$	0
$a_{4,1}$	$a_{4,2}$	$a_{4,3}$	$\cdots$	$\cdots$	$\cdots$	$a_{4,n-1}$	$a_{4,n}$	0
$a_{5,1}$	$a_{5,2}$	$a_{5,3}$	$\cdots$	$\cdots$	$a_{5,n-2}$	$a_{5,n-1}$	0	
$a_{6,1}$	$a_{6,2}$	$a_{6,3}$	$\cdots$	$a_{6,n-3}$	$a_{6,n-2}$	$a_{6,n-1}$	0	
$\vdots$	$\vdots$							
$a_{2n,1}$	0							
$a_{2n+1,1}$	0							

The polynomial $R(X) = P^-(X) + A$, with $A \geq 0$ can be developed:

$$R(X) = a_{1,1}X^{2n+1} + a_{2,1}X^{2n} + a_{1,2}X^{2n-1} + a_{2,2}X^{2n-2} + ... + a_{2,n}X^2 + a_{1,n+1}X + a_{2,n+1} + A,$$

and its associated Routh table can be inferred from that of $P^-(X)$, as done previously:

$a_{1,1}$	$a_{1,2}$	$a_{1,3}$	$\cdots$	$\cdots$	$\cdots$	$\cdots$	$a_{1,n}$	$a_{1,n+1}$
$a_{2,1}$	$a_{2,2}$	$a_{2,3}$	$\cdots$	$\cdots$	$\cdots$	$\cdots$	$a_{2,n}$	$\boldsymbol{a_{2,n+1} + A}$
$a_{3,1}$	$a_{3,2}$	$a_{3,3}$	$\cdots$	$\cdots$	$\cdots$	$\cdots$	$\boldsymbol{\tilde{a}_{3,n}}$	0
$a_{4,1}$	$a_{4,2}$	$a_{4,3}$	$\cdots$	$\cdots$	$\cdots$	$\boldsymbol{\tilde{a}_{4,n-1}}$	$\boldsymbol{\tilde{a}_{4,n}}$	0
$a_{5,1}$	$a_{5,2}$	$a_{5,3}$	$\cdots$	$\cdots$	$\boldsymbol{\tilde{a}_{5,n-2}}$	$\boldsymbol{\tilde{a}_{5,n-1}}$	0	
$a_{6,1}$	$a_{6,2}$	$a_{6,3}$	$\cdots$	$\boldsymbol{\tilde{a}_{6,n-3}}$	$\boldsymbol{\tilde{a}_{6,n-2}}$	$\boldsymbol{\tilde{a}_{6,n-1}}$	0	
$\vdots$	$\vdots$							
$\boldsymbol{\tilde{a}_{2n,1}}$	0							
$\boldsymbol{\tilde{a}_{2n+1,1}}$	0							

As for the case when $P^-(X)$ has degree $2n$, it is possible to observe that from the row $i = 3$, the perturbation shifts left at each new row. Once again, the first term perturbed in the first column is $\tilde{a}_{n+2,1}$.

It is also possible to show by induction the following property:

"**H2**: if $i \leq n+2$, any term in the row i of the Routh table of $R(X)$ can be expressed as: $\tilde{a}_{i,j} = a_{i,j} - \alpha_{i,j}A$ if i is odd, and $\tilde{a}_{i,j} = a_{i,j} + \alpha_{i,j}A$ if i is even, with $\alpha_{i,j} \geq 0$."

Indeed, as a base case, $\tilde{a}_{3,n} = (-1/a_{2,1})\left[a_{1,1}(a_{2,n+1} + A) - a_{2,1}a_{1,n+1}\right] = (-1/a_{2,1})\left[a_{1,1}a_{2,n+1} - a_{2,1}a_{1,n+1}\right] - (a_{1,1}/a_{2,1})\,A = a_{3,n} - \alpha_{3,n}A$, with $\alpha_{3,n} > 0$. All the other terms in the row $i = 3$ are not perturbed. It is assumed that **H2** is true until row $3 < i \leq n+2$. Then any term in this row verifies: $\tilde{a}_{i,j} = (-1/a_{i-1,1})\left[a_{i-2,1}\tilde{a}_{i-1,j+1} - a_{i-1,1}\tilde{a}_{i-2,j+1}\right]$ (the terms $a_{*,1}$ are not perturbed because $i \leq n+2$). Then, from **H2**, two cases appear:

- if i is even: $\tilde{a}_{i,j} = (-1/a_{i-1,1})\left[a_{i-2,1}(a_{i-1,j+1} - \alpha_{i-1,j+1}A) - a_{i-1,1}(a_{i-2,j+1} + \alpha_{i-2,j+1}A)\right]$, and then by developing $\tilde{a}_{i,j} = a_{i,j} + \alpha_{i,j}A$. From proposition 9.3.3, $\alpha_{i,j} \geq 0$.
- if i is odd: $\tilde{a}_{i,j} = (-1/a_{i-1,1})\left[a_{i-2,1}(a_{i-1,j+1} + \alpha_{i-1,j+1}A) - a_{i-1,1}(a_{i-2,j+1} - \alpha_{i-2,j+1}A)\right]$, and then by developing $\tilde{a}_{i,j} = a_{i,j} - \alpha_{i,j}A$. From proposition 9.3.3, $\alpha_{i,j} \geq 0$.

By induction, **H2** is proved.

Now, it is possible to distinguish the two cases 2A and 2B. First, it is assumed that n is odd. In this case, the line $i = n + 2$ for which the perturbation reaches the first column is odd. It follows from **H2** that $\tilde{a}_{n+2,1} = a_{n+2,1} - \alpha_{n+2,1}A$. In this case, it is straightforward to see that there exists $\tilde{A} > 0$ such that $\forall\ A > \tilde{A}$, $\tilde{a}_{n+2,1} < 0$. Hence, there is a change of sign in the first column of the Routh table of $R(X)$, and lemma 9.3.1 is proved in case 2A.

If n is even, the line $i = n + 2$ for which the perturbation reaches the first column is even. It follows from **H2** that $\tilde{a}_{n+2,1} = a_{n+2,1} + \alpha_{n+2,1}A$. Hence, $\tilde{a}_{n+2,1}$ will never change sign, no matter the value of A. In this case, the bottom term $\tilde{a}_{n+3,1}$ in the first column is investigated: $\tilde{a}_{n+3,1} = (-1/\tilde{a}_{n+2,1})\,[a_{n+1,1}\tilde{a}_{n+2,2} - \tilde{a}_{n+2,1}\tilde{a}_{n+1,2}]$.
From **H2**, $\tilde{a}_{n+3,1} = (-1/(a_{n+2,1} + \alpha_{n+2,1}A))\,[a_{n+1,1}(a_{n+2,2}+\alpha_{n+2,2}A)-(a_{n+2,1}+\alpha_{n+2,1}A)(a_{n+1,2}-\alpha_{n+1,2}A)]$. We recover the same situation as case 1B. Hence, lemma 9.3.1 is proved in case 2B. □

Bibliography

[1] https://www.nature.com/scitable/topicpage/translation-dna-to-mrna-to-protein-393/.

[2] https://sciencesnaturelles.ch/topics/synbio/what_is_synthetic_biology_/elements/gene_regulation.

[3] https://www.cusabio.com/c-20927.html.

[4] W. Abou-Jaoudé, D. A. Ouattara, and M. Kaufman. From structure to dynamics: frequency tuning in the p53–mdm2 network: I. logical approach. *Journal of theoretical biology*, 258(4):561–577, 2009.

[5] M. E. Ahsen, H. Özbay, and S. I. Niculescu. *Analysis of deterministic cyclic gene regulatory network models with delays*. Birkhäuser, 2015.

[6] B. Alberts, A. Johnson, J. Lewis, M. Raff, K. Roberts, and P. Walter. *Molecular biology of the cell: Fifth edition*. Garland Science, 2007.

[7] U. Albrecht. Invited review: regulation of mammalian circadian clock genes. *Journal of Applied Physiology*, 92(3):1348–1355, 2002.

[8] D. J. Allwright. A global stability criterion for simple control loops. *J. Math. Biology*, 4:363–373, 1977.

[9] U. Alon. *An introduction to systems biology: design principles of biological circuits*. Chapman and Hall/CRC, 2006.

[10] D. Angeli, J. E. Ferrell, and E. D. Sontag. Detection of multistability, bifurcations, and hysteresis in a large class of biological positive-feedback systems. *Proceedings of the National Academy of Sciences*, 101(7):1822–1827, 2004.

[11] D. Angeli and E. Sontag. Interconnections of monotone systems with steady-state characteristics. In *Optimal control, stabilization and nonsmooth analysis*, pages 135–154. Springer, 2004.

[12] D. Angeli and E. D. Sontag. Monotone control systems. *IEEE Transactions on automatic control*, 48(10):1684–1698, 2003.

[13] D. Angeli and E. D. Sontag. Multi-stability in monotone input/output systems. *Systems & Control Letters*, 51(3-4):185–202, 2004.

[14] J. Aracena. Maximum number of fixed points in regulatory boolean networks. *Bulletin of mathematical biology*, 70(5):1398, 2008.

[15] M. R. Atkinson, M. A. Savageau, J. T. Myers, and A. J. Ninfa. Development of genetic circuitry exhibiting toggle switch or oscillatory behavior in Escherichia coli. *Cell*, 113(5):597–607, 2003.

[16] A. Bacciotti and F. Ceragioli. Stability and stabilization of discontinuous systems and nonsmooth Lyapunov functions. *ESAIM: Control, Optimisation and Calculus of Variations*, 4:361–376, 1999.

[17] A. R. Barnard and P. M. Nolan. When clocks go bad: neurobehavioural consequences of disrupted circadian timing. *PLoS genetics*, 4(5):e1000040, 2008.

[18] A. Becskei and L. Serrano. Engineering stability in gene networks by autoregulation. *Nature*, 405(6786):590, 2000.

[19] O. Bernard and J. L. Gouzé. Transient behavior of biological loop models with application to the Droop model. *Mathematical Biosciences*, 127:19–43, 1995.

[20] O. Bernard and J. L. Gouzé. Global qualitative behavior of a class of nonlinear biological systems; application to the qualitative validation of phytoplankton growth models. 1998.

[21] C. A. Brady and L. D. Attardi. p53 at a glance. *J Cell Sci*, 123(15):2527–2532, 2010.

[22] R. Brette and W. Gerstner. Adaptive exponential integrate-and-fire model as an effective description of neuronal activity. *Journal of neurophysiology*, 94(5):3637–3642, 2005.

[23] C. L. Brooks and W. Gu. p53 ubiquitination: Mdm2 and beyond. *Molecular cell*, 21(3):307–315, 2006.

[24] S. Cai, X. Fu, and Z. Sheng. Dedifferentiation: a new approach in stem cell research. *Bioscience*, 57(8):655–662, 2007.

[25] R. Casey, H. De Jong, and J. L. Gouzé. Piecewise-linear models of genetic regulatory networks: equilibria and their stability. *Journal of mathematical biology*, 52(1):27–56, 2006.

[26] F. Cazals and P. Kornprobst. *Modeling in Computational Biology and Biomedicine: A Multidisciplinary Endeavor*. Springer Science & Business Media, 2012.

[27] R. Chait, J. Ruess, T. Bergmiller, G. Tkačik, and C. C. Guet. Shaping bacterial population behavior through computer-interfaced control of individual cells. *Nature communications*, 8(1):1535, 2017.

[28] M. Chaves and J. L. Gouzé. Exact control of genetic networks in a qualitative framework: The bistable switch example. *Automatica*, 47:1105–1112, 2011.

[29] M. Chaves and J. L. Gouzé. 2d piecewise affine models approximate real continuous dynamics up to invariant sets. *IFAC-PapersOnLine*, 49(18):1060–1065, 2016.

[30] M. Chaves, L. Tournier, and J. L. Gouzé. Comparing boolean and piecewise affine differential models for genetic networks. *Acta biotheoretica*, 58(2-3):217–232, 2010.

[31] D. Chen, E. S. Gibson, and M. J. Kennedy. A light-triggered protein secretion system. *J Cell Biol*, 201(4):631–640, 2013.

[32] J. L. Cherry and F. R. Adler. How to make a biological switch. *Journal of theoretical biology*, 203(2):117–133, 2000.

[33] J. P. Comet, G. Bernot, A. Das, F. Diener, C. Massot, and A. Cessieux. Simplified models for the mammalian circadian clock. *Procedia Computer Science*, 11:127–138, 2012.

[34] E. Dancer. Some remarks on a boundedness assumption for monotone dynamical systems. *Proceedings of the American Mathematical Society*, 126(3):801–807, 1998.

[35] B. d'Andréa Novel and M. De Lara. *Control theory for engineers*. Springer, 2013.

[36] H. De Jong. Modeling and simulation of genetic regulatory systems: a literature review. *Journal of computational biology*, 9(1):67–103, 2002.

[37] R. Edwards. Analysis of continuous-time switching networks. *Physica D: Nonlinear Phenomena*, 146(1-4):165–199, 2000.

[38] R. Edwards, S. Kim, and P. Van Den Driessche. Control design for sustained oscillation in a two-gene regulatory network. *Journal of mathematical biology*, 62(4):453–478, 2011.

[39] R. Edwards, P. Van Den Driessche, and L. Wang. Periodicity in piecewise-linear switching networks with delay. *Journal of mathematical biology*, 55(2):271–298, 2007.

[40] M. B. Elowitz and S. Leibler. A synthetic oscillatory network of transcriptional regulators. *Nature*, 403:335–338, 2000.

[41] D. Ezer, N. R. Zabet, and B. Adryan. Homotypic clusters of transcription factor binding sites: a model system for understanding the physical mechanics of gene expression. *Computational and structural biotechnology journal*, 10(17):63–69, 2014.

[42] E. Farcot and J. L. Gouzé. A mathematical framework for the control of piecewise-affine models of gene networks. *Automatica*, 44(9):2326–2332, 2008.

[43] E. Farcot and J. L. Gouzé. Periodic solutions of piecewise affine gene network models with non uniform decay rates: the case of a negative feedback loop. *Acta Biotheoretica*, 57:429–455, 2009.

[44] E. Farcot and J. L. Gouzé. Limit cycles in piecewise-affine gene network models with multiple interaction loops. *International Journal of Control*, 41(1):119–130, 2010.

[45] E. Farcot and J. L. Gouzé. Qualitative control of periodic solutions in piecewise affine models of genetic networks. *IFAC Proceedings Volumes*, 43(14):326–331, 2010.

[46] C. Feillet, G. T. J. Van Der Horst, F. Levi, D. A. Rand, and F. Delaunay. Coupling between the circadian clock and cell cycle oscillators: implication for healthy cells and malignant growth. *Frontiers in neurology*, 6:96, 2015.

[47] A.F. Filippov. *Differential Equations With Discontinuous Righthand Sides*. Kluwer, Dordrecht, The Netherlands, 1988.

[48] D. Fiore, A. Guarino, and M. di Bernardo. Analysis and control of genetic toggle switches subject to periodic multi-input stimulation. *IEEE control systems letters*, 3(2):278–283, 2018.

[49] G. Fiore, G. Perrino, M. Di Bernardo, and D. Di Bernardo. In-vivo real-time control of gene expression: a comparative analysis of feedback control strategies in yeast. *ACS synthetic biology*, 5(2):154–162, 2015.

[50] C. Fracassi, L. Postiglione, G. Fiore, and D. Di Bernardo. Automatic control of gene expression in mammalian cells. *ACS synthetic biology*, 5(4):296–302, 2015.

[51] F. Fröhlich, M. Bazhenov, and T. J. Sejnowski. Pathological effect of homeostatic synaptic scaling on network dynamics in diseases of the cortex. *Journal of Neuroscience*, 28(7):1709–1720, 2008.

[52] L. Fu and C. C. Lee. The circadian clock: pacemaker and tumour suppressor. *Nature Reviews Cancer*, 3(5):350–361, 2003.

[53] F. Gachon, P. Fonjallaz, F. Damiola, P. Gos, T. Kodama, J. Zakany, D. Duboule, B. Petit, M. Tafti, and U. Schibler. The loss of circadian PAR bZip transcription factors results in epilepsy. *Genes & development*, 18(12):1397–1412, 2004.

[54] T. S. Gardner, C. R. Cantor, and J. J. Collins. Construction of a genetic toggle switch in Escherichia coli. *Nature*, 403(6767):339, 2000.

[55] N. Geva-Zatorsky, N. Rosenfeld, S. Itzkovitz, R. Milo, A. Sigal, E. Dekel, T. Yarnitzky, Y. Liron, P. Polak, G. Lahav, and U. Alon. Oscillations and variability in the p53 system. *Molecular systems biology*, 2(1), 2006.

[56] L. Glass. Combinatorial and topological methods in nonlinear chemical kinetics. *The Journal of chemical physics*, 63(4):1325–1335, 1975.

[57] L. Glass and J. S. Pasternack. Prediction of limit cycles in mathematical models of biological oscillations. *Bulletin of Mathematical Biology*, 40:27–44, 1978.

[58] L. Glass and J. S. Pasternack. Stable oscillations in mathematical models of biological control systems. *Journal of Mathematical Biology*, 6(3):207, 1978.

[59] A. Goldbeter, D. Gonze, G. Houart, J. C. Leloup, J. Halloy, and G. Dupont. From simple to complex oscillatory behavior in metabolic and genetic control networks. *Chaos: An Interdisciplinary Journal of Nonlinear Science*, 11(1):247–260, 2001.

[60] J. L. Gouzé. Positive and negative circuits in dynamical systems. *Journal of Biological Systems*, 6(01):11–15, 1998.

[61] J. L. Gouzé, A. Rapaport, and M. Z. Hadj-Sadok. Interval observers for uncertain biological systems. *Ecological modelling*, 133(1-2):45–56, 2000.

[62] F. Grognard, J. Rault, and J. L. Gouzé. Positive control for global stabilization of predator-prey systems. *IFAC Proceedings Volumes*, 46(23):265–270, 2013.

[63] A. Guarino, D. Fiore, and M. Di Bernardo. In-silico feedback control of a mimo synthetic toggle switch via pulse-width modulation. In *2019 18th European Control Conference (ECC)*, pages 680–685. IEEE, 2019.

[64] A. Guarino, D. Fiore, D. Salzano, and M. di Bernardo. Balancing cell populations endowed with a synthetic toggle switch via adaptive pulsatile feedback control. *bioRxiv*, page 851212, 2019.

[65] D. Harnack, M. Pelko, A. Chaillet, Y. Chitour, and M. C.W. van Rossum. Stability of neuronal networks with homeostatic regulation. *PLoS computational biology*, 11(7):e1004357, 2015.

[66] S. Hastings, J. Tyson, and D. Webster. Existence of periodic solutions for negative feedback cellular control systems. *Journal of Differential Equations*, 25:39–64, 1977.

[67] M. W. Hirsch and H. Smith. Monotone dynamical systems. In *Handbook of differential equations: ordinary differential equations*, volume 2, pages 239–357. Elsevier, 2006.

[68] Y. P. Hung, C. Teragawa, N. Kosaisawe, T. E. Gillies, M. Pargett, M. Minguet, K. Distor, B. L. Rocha-Gregg, J. L. Coloff, M. A. Keibler, et al. Akt regulation of glycolysis mediates bioenergetic stability in epithelial cells. *Elife*, 6:e27293, 2017.

[69] J. Izard, C. D. C. Gomez Balderas, D. Ropers, S. Lacour, X. Song, Y. Yang, A. B. Lindner, J. Geiselmann, and H. de Jong. A synthetic growth switch based on controlled expression of rna polymerase. *Molecular systems biology*, 11(11), 2015.

[70] L. Jaulin, M. Kieffer, O. Didrit, and E. Walter. Interval analysis. In *Applied Interval Analysis*, pages 11–43. Springer, 2001.

[71] J. Ji-Fa. A Liapunov function for three-dimensional feedback systems. *Proceedings of the American Mathematical Society*, 114(4):1009–1013, 1992.

[72] J. Ji-Fa. On the global stability of cooperative systems. *Bulletin of the London Mathematical Society*, 26(5):455–458, 1994.

[73] E. R. Kastenhuber and S. W. Lowe. Putting p53 in context. *Cell*, 170(6):1062–1078, 2017.

[74] S. Kauffman. The large scale structure and dynamics of gene control circuits: an ensemble approach. *Journal of Theoretical Biology*, 44(1):167–190, 1974.

[75] H. K. Khalil. *Nonlinear systems*. Prentice-Hall, New Jersey, 1996.

[76] S. Kiessling, L. Beaulieu-Laroche, I. D. Blum, D. Landgraf, D. K. Welsh, K. F. Storch, N. Labrecque, and N. Cermakian. Enhancing circadian clock function in cancer cells inhibits tumor growth. *BMC biology*, 15(1):13, 2017.

[77] J. C. Leloup and A. Goldbeter. Toward a detailed computational model for the mammalian circadian clock. *Proceedings of the National Academy of Sciences*, 100(12):7051–7056, 2003.

[78] R. Lev Bar-Or, R. Maya, L. A. Segel, U. Alon, A. J. Levine, and M. Oren. Generation of oscillations by the p53-Mdm2 feedback loop: a theoretical and experimental study. *Proc Natl Acad Sci USA*, 97:11250–11255, 2000.

[79] J. Lippert, H. Halfter, A. Heidbreder, D. Röhr, B. Gess, M. Boentert, N. Osada, and P. Young. Altered dynamics in the circadian oscillation of clock genes in dermal fibroblasts of patients suffering from idiopathic hypersomnia. *PloS one*, 9(1):e85255, 2014.

[80] J. B. Lugagne, S. Sosa Carrillo, M. Kirch, A. Köhler, G. Batt, and P. Hersen. Balancing a genetic toggle switch by real-time feedback control and periodic forcing. *Nature Communications*, 8:1671, 2017.

[81] J. Lunze and F. Lamnabhi-Lagarrigue. *Handbook of hybrid systems control: theory, tools, applications*. Cambridge University Press, 2009.

[82] F. Mairet and J. L. Gouzé. Hybrid control of a bioreactor with quantized measurements. *IEEE Transactions on automatic control*, 61(5):1385–1390, May 2016.

[83] J. Mallet-Paret and H. L. Smith. The Poincare-Bendixson theorem for monotone cyclic feedback systems. *Journal of Dynamics and Differential Equations*, 2:367–421, 1990.

[84] T. Mannic, P. Meyer, F. Triponez, M. Pusztaszeri, G. Le Martelot, O. Mariani, D. Schmitter, D. Sage, J. Philippe, and C. Dibner. Circadian clock characteristics are altered in human thyroid malignant nodules. *The Journal of Clinical Endocrinology & Metabolism*, 98(11):4446–4456, 2013.

[85] M. Maroto and N. Monk. *Cellular oscillatory mechanisms*, volume 641. Springer Science & Business Media, 2008.

[86] A. I. Mees and P. E. Rapp. Periodic metabolic systems: Oscillations in multiple-loop negative feedback biochemical control networks. *J. Math Biology*, 5:99–114, 1978.

[87] F. Menolascina, G. Fiore, E. Orabona, L. De Stefano, M. Ferry, J. Hasty, M. Di Bernardo, and D. Di Bernardo. In-vivo real-time control of protein expression from endogenous and synthetic gene networks. *PLoS computational biology*, 10(5), 2014.

[88] A. Milias-Argeitis, M. Rullan, S. K. Aoki, P. Buchmann, and M. Khammash. Automated optogenetic feedback control for precise and robust regulation of gene expression and cell growth. *Nature communications*, 7:12546, 2016.

[89] A. Milias-Argeitis, S. Summers, J. Stewart-Ornstein, I. Zuleta, D. Pincus, H. El-Samad, M. Khammash, and J. Lygeros. In silico feedback for in vivo regulation of a gene expression circuit. *Nature biotechnology*, 29(12):1114–1116, 2011.

[90] R. Milo, S. Shen-Orr, S. Itzkovitz, N. Kashtan, D. Chklovskii, and U. Alon. Network motifs: Simple building blocks of complex networks. *Science*, 298:824–827, Oct 2002.

[91] E. S. Musiek. Circadian clock disruption in neurodegenerative diseases: cause and effect? *Frontiers in pharmacology*, 6:29, 2015.

[92] D. A. Ouattara, W. Abou-Jaoudé, and M. Kaufman. From structure to dynamics: Frequency tuning in the p53-mdm2 network. ii: Differential and stochastic approaches. *Journal of theoretical biology*, 264(4):1177–1189, 2010.

[93] K. M. Page and R. Perez-Carrasco. Degradation rate uniformity determines success of oscillations in repressive feedback regulatory networks. *Journal of The Royal Society Interface*, 15(142):20180157, 2018.

[94] J. P. Pett, A. Korenčič, F. Wesener, A. Kramer, and H. Herzel. Feedback loops of the mammalian circadian clock constitute repressilator. *PLoS computational biology*, 12(12):e1005266, 2016.

[95] B. Pfeuty and K. Kaneko. The combination of positive and negative feedback loops confers exquisite flexibility to biochemical switches. *Physical biology*, 6(4):046013, 2009.

[96] S. Pigolotti, S. Krishna, and M. H. Jensen. Oscillation patterns in negative feedback loops. *Proceedings of the National Academy of Sciences*, 104(16):6533–6537, April 2007.

[97] E. Plahte, T. Mestl, and S. W. Omholt. Global analysis of steady points for systems of differential equations with sigmoid interactions. *Dynamics and Stability of Systems*, 9(4):275–291, 1994.

[98] C. Poignard, M. Chaves, and J. L. Gouzé. Periodic oscillations for nonmonotonic smooth negative feedback circuits. *SIAM Journal on Applied Dynamical Systems*, 15(1):257–286, 2016.

[99] C. Poignard, M. Chaves, and J. L. Gouzé. A stability result for periodic solutions of nonmonotonic smooth negative feedback systems. *SIAM Journal on Applied Dynamical Systems*, 17(2):1091–1116, 2018.

[100] A. Pokhilko, A. P. Fernández, K. D. Edwards, M. M. Southern, K. J. Halliday, and A. J. Millar. The clock gene circuit in arabidopsis includes a repressilator with additional feedback loops. *Molecular systems biology*, 8(1), 2012.

[101] A. Polyakov and L. Fridman. Stability notions and Lyapunov functions for sliding mode control systems. *Journal of the Franklin Institute*, 351(4):1831–1865, 2014.

[102] A. Polynikis, S. J. Hogan, and M. Di Bernardo. Comparing different ode modelling approaches for gene regulatory networks. *Journal of theoretical biology*, 261(4):511–530, 2009.

[103] O. Purcell, N. J. Savery, C. S. Grierson, and M. Di Bernardo. A comparative analysis of synthetic genetic oscillators. *Journal of the Royal Society Interface*, 7:1503–1524, 2010.

[104] P. Ruoff, J. J. Loros, and J. C. Dunlap. The relationship between FRQ-protein stability and temperature compensation in the Neurospora circadian clock. *Proc Natl Acad Sci USA*, 102:17681–17686, 2005.

[105] L. A. Sanchez. Global asymptotic stability of the Goodwin system with repression. *Nonlinear Analysis: Real World Applications*, 10:2151–2156, 2009.

[106] V. C. Scanlon and T. Sanders. *Essentials of anatomy and physiology*. FA Davis, 2018.

[107] L. A. Segel and M. Slemrod. The quasi-steady-state assumption: a case study in perturbation. *SIAM review*, 31(3):446–477, 1989.

[108] H. L. Smith. Systems of ordinary differential equations which generate an order preserving flow. a survey of results. *SIAM review*, 30(1):87–113, 1988.

[109] H. L. Smith. *Monotone dynamical systems: an introduction to the theory of competitive and cooperative systems*. Number 41. American Mathematical Soc., 2008.

[110] E. D. Sontag. Molecular systems biology and control. *European journal of control*, 11(4-5):396–435, 2005.

[111] E. D. Sontag. Monotone and near-monotone biochemical networks. *Systems and synthetic biology*, 1(2):59–87, 2007.

[112] B. Staels. When the clock stops ticking, metabolic syndrome explodes. *Nature medicine*, 12(1):54, 2006.

[113] A. Szybińska and W. Leśniak. P53 dysfunction in neurodegenerative diseases-the cause or effect of pathological changes? *Aging and disease*, 8(4):506, 2017.

[114] R. Thomas and R. d'Ari. *Biological feedback*. CRC press, 1990.

[115] R. Thomas and J. Richelle. Positive feedback loops and multistationarity. *Discrete Applied Mathematics*, 19(1-3):381–396, 1988.

[116] J. E. Toettcher, D. Gong, W. A. Lim, and O. D. Weiner. Light-based feedback for controlling intracellular signaling dynamics. *Nature methods*, 8(10):837–839, 2011.

[117] J. Trauth, J. Scheffer, S. Hasenjäger, and C. Taxis. Synthetic control of protein degradation during cell proliferation and developmental processes. *ACS Omega*, 4(2):2766–2778, 2019.

[118] T. Y. C. Tsai, Y. S. Choi, W. Ma, J. R. Pomerening, C. Tang, and J. E. Ferrell. Robust, tunable biological oscillations from interlinked positive and negative feedback loops. *Science*, 321(5885):126–129, 2008.

[119] J. J. Tyson. On the existence of oscillatory solutions in negative feedback cellular control processes. *Journal of Mathematical Biology*, 1(4):311–315, 1975.

[120] J. Uhlendorf, A. Miermont, T. Delaveau, G. Charvin, F. Fages, S. Bottani, G. Batt, and P. Hersen. Long-term model predictive control of gene expression at the population and single-cell levels. *Proceedings of the National Academy of Sciences*, 109(35):14271–14276, August 2012.

[121] L. Wang, P. De Leenheer, and E. D. Sontag. Conditions for global stability of monotone tridiagonal systems with negative feedback. *Systems and Control Letters*, 59:130–138, 2010.

[122] K. B. Wee, U. Surana, and B. D. Aguda. Oscillations of the p53-akt network: implications on cell survival and death. *PloS one*, 4(2):e4407, 2009.